Title
Ring-Opening Alkyne Metathesis Methods For Functional Conjugated Polymer Synthesis

Author
von Kugelgen, Stephen Winthrop

Publication Date
2018

Peer reviewed|Thesis/dissertation

Ring-Opening Alkyne Metathesis Methods For Functional Conjugated Polymer Synthesis

by

Stephen W. von Kugelgen

A dissertation submitted in partial satisfaction of the

requirements for the degree of

Doctor of Philosophy

in

Chemistry

in the

Graduate Division

of the

University of California, Berkeley

Committee in charge:

Professor Felix R. Fischer, Chair
Professor Robert G. Bergman
Professor Phillip B. Messersmith

Fall 2018

Ring-Opening Alkyne Metathesis
Methods For Functional Conjugated Polymer Synthesis

Abstract

Ring-Opening Alkyne Metathesis
Methods For Functional Conjugated Polymer Synthesis

by

Stephen W. von Kugelgen

Doctor of Philosophy in Chemistry

University of California, Berkeley

Professor Felix R. Fischer, Chair

Since its discovery in the mid 20th century, most applications of alkyne metathesis have relied on thermodynamics to control product distributions. Ring-opening alkyne metathesis polymerization (ROAMP), in contrast, requires the kinetic product of metathesis of a strained, cyclic alkyne monomer to give a living, chain-growth polymerization (Chapter 1, Introduction). This living polymerization of conjugated alkyne-containing monomers has the potential to access a wide range of functional *poly*(arylene ethynylene) materials with exceptional control over length, dispersity, topology, and endgroups. To this end, we demonstrate the first ROAMP synthesis of conjugated *poly*(*ortho*-phenylene ethynylene) and elucidate a mechanistic description of the reaction to understand the enabling catalyst selectivity and unexpectely find that initiator sterics dictate endgroup fidelity and polymer topology (Chapter 2). To disentangle the role of steric and electronic factors in initiator performance, we describe a novel synthetic method that gives a series of isosteric benzylidyne catalysts which exhibit a strong, deterministic electronic effect on both ROAMP initiation rates and polymer endgroup fidelity (Chapter 3). Finally, we develop an extension of this methodology to leverage the alkynes from these living polymers to template the synthesis of telechelic graphene nanoribbons (GNRs) (Chapter 4). This work has not only uncovered mechanistic insights and design principles to improve ROAMP catalysts and facilitate access to hybrid polymer materials, but also demonstrated the potential of ROAMP to access other conjugated materials via post-polymerization modification of precision polymer templates.

For Eileen Rohmer and Margret Geselbracht

The two great teachers who got me hooked on chemistry.
I'm honored to be part of their legacy.

Contents

List of Figures

List of Schemes

List of Tables

Acknowledgments

Countless thanks are due to my advisor, Felix, for taking a risk on an extra student my year, for his seemingly endless patience for my wild ideas, and for keeping me on track whenever I pursued a few too many of them at once. I'm also indebted to my labmates and colleagues who got me up to speed, helped sustain me through the ups and downs, and tolerated (even welcomed) my endless desire to chat about chemistry. I'd like to thank my roommates, Anne and Christoph, for being amazing folks to live with through job changes and moves over the better part of a decade. And last but not least, a big thank you to my family for your ever-present love and support waiting just out of sight but never out of mind.

Chapter 1

Introduction

This chapter serves as an introduction to alkyne metathesis, homogenous alkyne metathesis catalysts, and synthetic and mechanistic aspects of their operation. A survey of four decades of homogenous catalyst development for equilibrium alkyne metathesis applications is provided for two periods: the organometallic-oriented era of the Schrock group and the applications-oriented period starting near the turn of the century. Ring-opening alkyne metathesis polymerization is introduced and its particular design challenges highlighted.

1.1 Alkyne Metathesis: Discovery and Early History

Alkyne metathesis was first described by Pannella, Banks, and Bailey in 1968, where they observed the "disproportionation" of alkynes over a tungsten oxide catalyst at high temperatures.[1] Four years later, Mortreux and Blanchard reported alkyne metathesis catalyzed by the molybdenum oxide analogue,[2] followed soon after by a homogenous system comprised of $Mo(CO)_6$/resorcinol in 1974.[3]

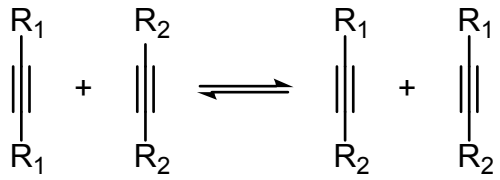

Scheme 1.1: Alkyne metathesis: the "disproportionation" of alkynes

Mechanistic investigations of alkyne metathesis revealed it exhibited many of the same characteristics as its alkene analogue, proceeding via scission and exchange of the carbon-carbon multiple bonds.[4] Woodward and Hoffman's contemporary work on orbital symmetry[5] highlighted problems with the simple "four-membered intermediate" put forth by Pannella, et. al. (Scheme 1.2A). While early studies of these systems identified factors critical for activity, they featured little in the way of proposed intermediates.[6,7] Presumably, the forbidden orbital symmetry of the [2+2] cycloaddition reaction could be overcome with a transition metal mediating the bond-forming and bond-breaking steps (Scheme 1.2B). Although metal cyclobutadiene complexes were well precedented, the lack of metathesis activity of existing examples left few good alternative structures for these organometallic metathesis intermediates.

That situation changed when E. O. Fischer reported the first metal carbyne complexes in 1973.[8] Shortly thereafter, Katz invoked this new class of organometallic complexes in a new mechanistic proposal for alkyne metathesis.[9] While subsequent solution-phase studies of Mortreux's $Mo(CO)_6$/phenol systems by Devarajan, et. al.[10] and gas-phase pyrolylsis work by Fritsch and Vollhardt breathed new life into the possible intermediacy of low-valent metal cyclobutadiene complexes,[11] Schrock's 1981 report of metathesis by well-defined tungsten carbyne complexes dispelled any doubt of the plausibility Katz's [2+2]/isomerization/retro[2+2] mechanism mediated by metal-carbon triple bonds,[12] at least insofar as high oxidation state systems were concerned.

1.2 The Schrock Era of Alkyne Metathesis

Over the next decade and a half, alkyne metathesis catalyst development was dominated by these new well-defined carbyne complexes of W, Mo, and Re pioneered by the Schrock group. Their new synthetic routes to Mo,[13–15] W,[13,16–18] and Re[19–23] carbyne complexes enabled the

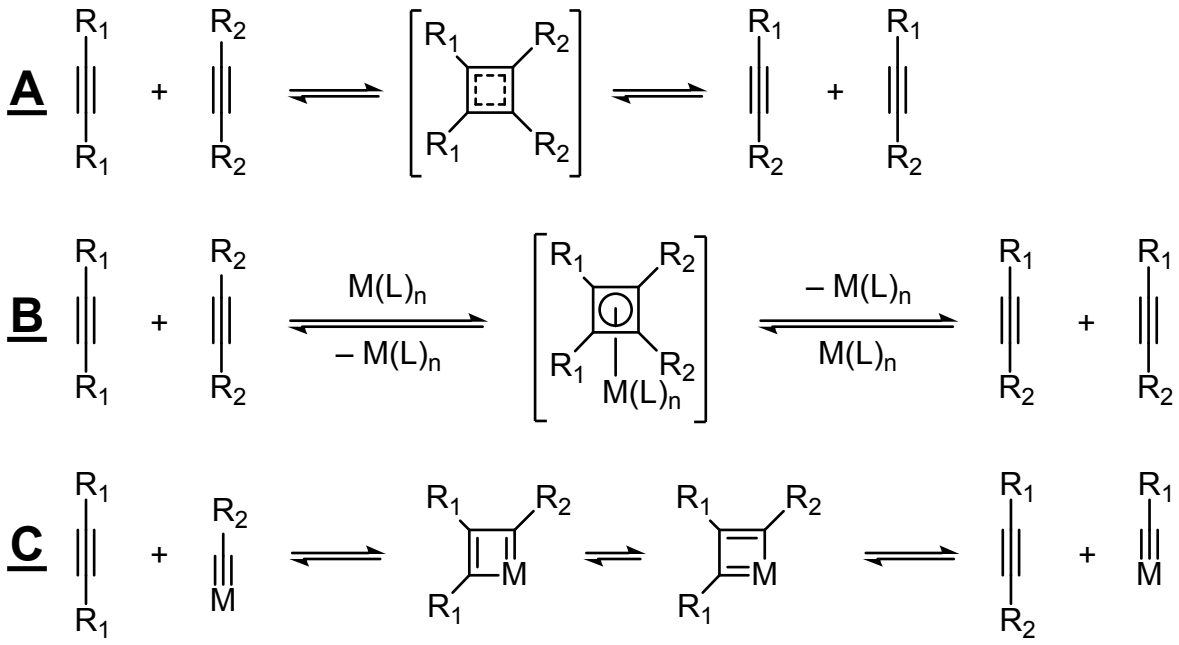

Scheme 1.2: Early mechanistic proposals for alkyne metathesis. **A.** Panella's "four-membered intermediate" proposal. **B.** A metal cyclobutadiene-mediated [2+2]/retro[2+2] reaction. **C.** The Katz mechanism, invoking metal carbyne complexes and metallacyclobutadiene intermediates

detailed study of many aspects of their structure, catalytic activity, substrate tolerance, and ligand scope. Perhaps just as significantly, their publications faithfully detailed many modifications and reactions that were detrimental to performance.

While tungsten carbyne complexes supported by bulky alkoxide[12,24] and aryloxide[24] ligands proved to be at least minimally competent metathesis catalysts, the more electron-rich alkyl,[12,13] amido,[25] or thiolato[26] complexes were completely inactive while the more electron-deficient chloride[27] or carboxylate[28] complexes reacted with alkynes to form other, inactive species. The reactivity trend indicated that an electrophilic, but not too electrophilic, metal center is required for productive reaction with alkynes. The use of bulky fluorinated alkoxides as weaker donor ligands generally led to more rapid metathesis;[24] this was especially true of the Mo carbynes which were generally found to be less active and required more electron deficient donor ligands to match the activities of their W analogs.[29]

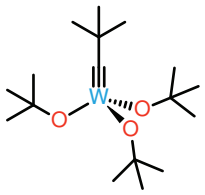

1

Figure 1.1: The "Schrock Catalyst," tris(tert-butoxy) tungsten neopentylidyne (**1**).

Generally, these early Mo and W complexes of the form $(CH_3)_3C{\equiv}M(OR)_3$ exhibited surprisingly broad functional group tolerance, at least in metathesis of simple substrates. In the absence of water, the prototypical Schrock catalyst, $(CH_3)_3C{\equiv}W(OC(CH_3)_3)_3$ (**1**, Fig-

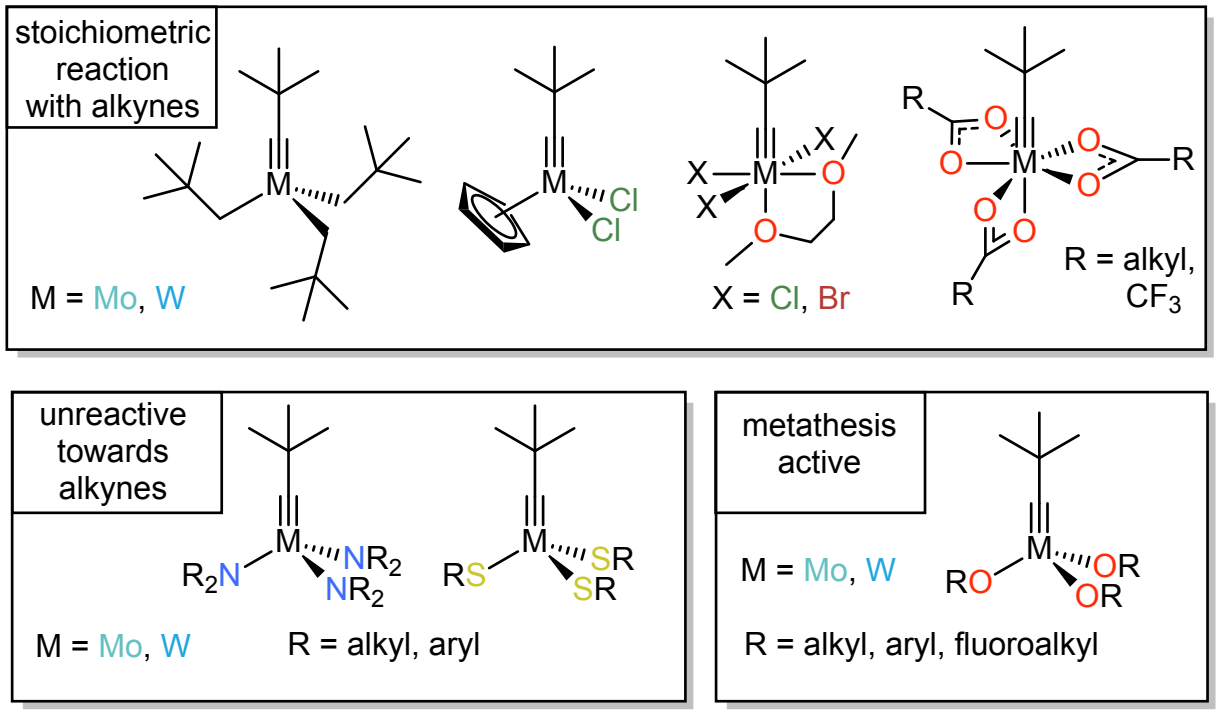

Figure 1.2: Early examples of W and Mo neopentylidyne complexes displaying strongly ligand-dependent reactivity towards alkynes.

ure 1.1) tolerates superstoichiometric alcohols, nitriles, tertiary amines, ethers, esters and leaves olefinic substrates untouched.[25] Terminal alkynes, however, posed a unique problem: while they could be metathesized, cycloaddition of a terminal alkyne to the metal-carbon triple bond could generate metallacyclobutadienes containing a hydrogen at the β position (Scheme 1.3A).[30] This acidic proton is lost, in some cases extremely rapidly, to give a deprotiometallacyclobutadiene complex as a thermodynamic dead-end.[31] Even in cases where metathesis is productive, the Chisholm group showed that bimolecular dimerization of terminal methylidynes to give an acetylene-bridged binuclear complex is facile (Scheme 1.3B).[32,33]

Increasing the electrophilicity of the metal center and decreasing the steric bulk of the ligand sphere by moving to smaller, weaker donor ligands like carboxylates or halides produces carbyne complexes that react with alkynes unproductively to give several different products. In the coordinatively saturated carboxylate systems, a "side-on" [2+2] reaction can occur (Scheme 1.3C), yielding a metallatetrahedrane or a metal cyclopropenyl complex.[28] Typical metallacylobutadienes with halide ligands do not readily dissociate into a carbyne and an alkyne, addition of a bulky ligand causes them to rearrange into these more compact structures (Scheme 1.3D).[27,34] While the carboxylate-supported tetrahedranes might form through rearrangement of an intermediate metallacyclobutadiene, orbital symmetry does not preclude direct tetrahedrane formation in cases where steric contraints or coordinative saturation might prevent the initial formation of a metallacyclobutadiene.

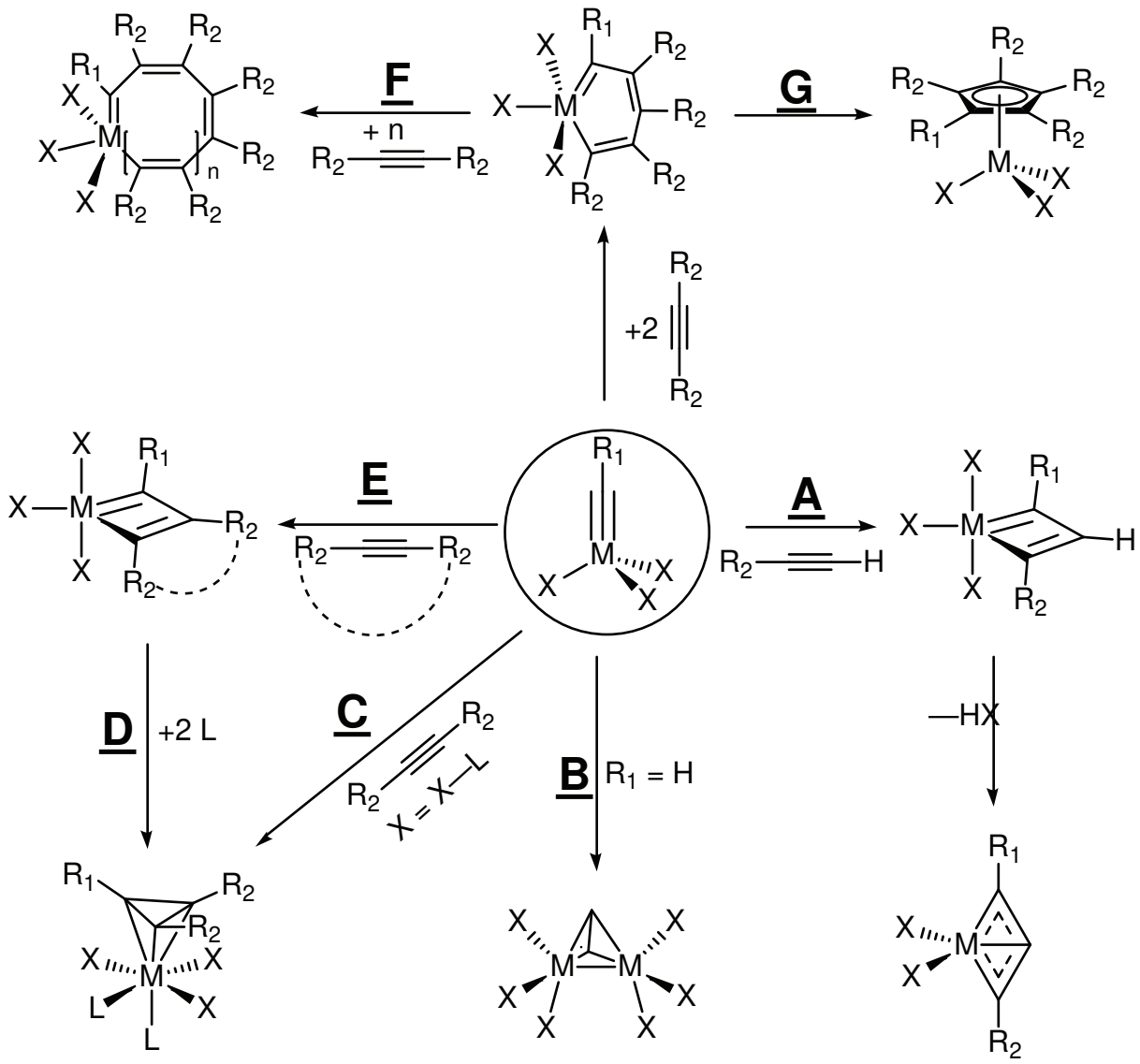

Scheme 1.3: Unproductive modes of reactivity between metal carbyne complexes and alkyne susbtrates. **A.** Deprotiometallacyclobutadiene formation (M = Mo, W, X = OR). **B.** Bimolecular decomposition of terminal methylidynes to dimetallatetrahedranes. **C.** Direct formation of (M = Mo, W, X = O_2CR) or **D.** metallacycle collapse into a metallatetrahedrane (M = W, X = Cl). **E.** Metallacyclobutadienes as thermodynamic traps (M = W, Re, X = Cl, Br, OR, =NR). **F.** Ring expansion of metallacyclobutadienes leading to alkyne polymerization (e.g. R = CH_3). **G.** Reductive elimination of metallacyclohexatrienes to give reduced cyclopentadienyl complexes (X = Cl, O_2CCF_3, OR (slowly))

Excessive stabilization of the metallacyclobutadiene intermediate can suppress metathesis activity if the cycloaddition is so exergonic that the cycloelimination is insurmountably

uphill (Scheme 1.3E). Small ligands like halides or bidentate diols with small bite angles lack the steric pressure to destabilize the metallacyclobutadiene and promote productive expulsion of the alkyne by [2+2] cycloelimination.[34–37] Relief of ring strain in cyclic alkynes like cyclooctyne drives cycloaddition still further downhill and traps the bicyclic intermediate by reducing the otherwise favorable entropy of the cycloelimination.[38] These metallacyclobutadiene problems are more common in carbyne complexes of 3rd row metals where the formation of stronger M-C σ bonds stabilizes those metallacyclobutadienes; many W and Re metallacyclobutadienes have been characterized, but only Mo complexes with highly electron withdrawing ligands form stable metallacyclobutadienes at room temperature.[39]

If the 5-coordinate metallacyclobutadiene intermediate is sufficiently electrophilic further alkyne insertion to give ring-expanded products can occur. The resulting metallacyclohexatriene can lead alkyne polymerization via consecutive insertions to form larger and larger metallacycles[37,40] (Scheme 1.3F) or can reductively eliminate to give a reduced metal cyclopentadienyl complex (Scheme 1.3G).[27,28,35]

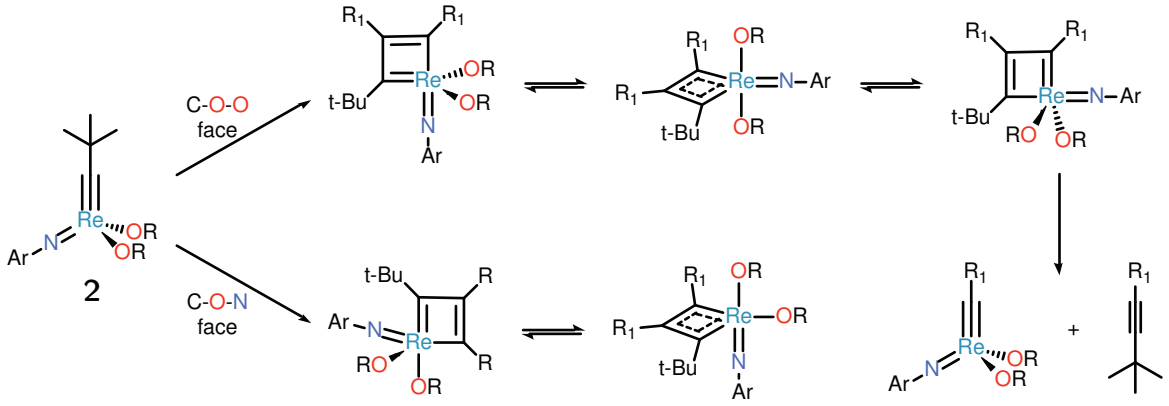

Scheme 1.4: Heteroleptic Re carbyne **2** leads to electronically distinct rhenacyclobutadienes. R = $C(CF_3)_2CH_3$, Ar = 2,6-diisopropylphenyl

The role of ligand electronics in metallacyclobutadiene stabilization is exaggerated in cases where the four-coordinate metal carbyne complex is not homoleptic, (e.g. Re imido carbyne complex **2**, Figure 1.4) [2+2] cycloaddition can occur at one of two different faces of the tetrahedral coordination sphere: the C-O-O face or the two C-O-N faces (Scheme 1.4). Unexpectedly, the former productively turns over to give metathesis products, while the latter is an unproductive thermodynamic sink.[41] This can be rationalized based on the two possible rhenacyclobutadienes, one in which the imido ligand can share the equatorial plane with the metallacycle and one in which the imido ligand is axial rendering the Re=N π bond orthogonal to the metallacycle π system. In the the C-O-O face adduct (Figure 1.4, top), the strong trans-effect of the imido ligand and the π loading competition between Re=C and Re=N bonds helps expel the alkyne during the [2+2] cycloelimination, while in the C-O-N face adduct (Figure 1.4, bottom) this same influence disfavors the necessary ligand sphere

rearrangement.[42] Upon successive turnovers, the remaining active **2** derivatives eventually partition completely into these nonproductive rhenacyclobutadienes.

These studies culminated in the core dogma of alkyne metathesis catalyst design principles that wouldn't be challenged until the 21st century:

1. The essential M≡C bond (M = Mo, W, Re, possibly others)
    a) weak enough to access [2+2] cycloadditions
    b) strong enough to reform from the metallacycle by [2+2] cycloelimination
2. An available coordination site to bind an alkyne substrate
3. A metal center supported by electron-poor X-type ligands
    a) electrophilic enough to promote [2+2] reactions with alkynes
    b) not so electrophilic that the metallacycle reacts further
4. A ligand sphere, preferably homoleptic, with a steric profile
    a) large enough to prevent dimerization and promote [2+2] cycloelimination
    b) small enough to avoid driving metallacycle collapse to a tetrahedrane

Despite the constant advancement of understanding of unproductive modes of reactivity, the Schrock catalyst **1** and the "instant" $Mo(CO)_6$/phenol systems developed by Mortreux were overwhelming favorites for applications of alkyne metathesis until the resurgence of alkyne metathesis catalyst development around the turn of the millennium.

1.3 Alkyne Metathesis Catalyst Development in the 21st Century

Alkyne metathesis applications experienced a renaissance in the late 1990s, with the synthetic power of ring-closing alkyne metathesis (RCAM)[43] and acyclic diyne metathesis (ADIMET)[44] driving new approaches to the synthesis of natural products[45] and polymer materials.[46] But the growing applications of age-old metathesis catalysts rapidly revealed their shortcomings and motivated a renewed interest in exploring new organometallic structures as potential metathesis catalysts.

The first truly new ligand motifs for alkyne metathesis grew out of the Cummins group's quest for trigonal planar Mo(III) species. Some of their more reactive analogues could be elaborated into Schrock-type trisalkoxy Mo(VI) carbyne complexes with reasonable activities in several steps.[47–49] But their prototypical trisamido complex, $Mo(N(t\text{-}Bu)(Ar))_3$ (Ar = 3,5-dimethylphenyl) (**3**) drew the interest of the Fürstner group, as it stoichiometrically activated dinitrogen,[50] which is tantalizingly isoelectronic to the C≡C bond of an alkyne.

While the parent complex **3** was inactive, when treated with halogenated compounds like CH_2Cl_2 or TMSCl a metathesis active mixture was created.[51] They identified that the products of the reaction with CH_2Cl_2 were the Mo(IV) chloro complex $ClMo(N(t\text{-}Bu)(Ar))_3$ (**4**) and the terminal methylidyne $HC{\equiv}Mo(N(t\text{-}Bu)(Ar))_3$ (**5**) (Scheme 1.5A.).[52] While both were reactive with internal alkynes, the methylidyne complex **5** was deactivated stoichiometrically, presumably either by reaction with the initial terminal alkyne product to make a deprotiometallacyclobutadiene or by formation of a new carbyne complex too bulky to react further. In contrast, the Mo(IV) chloro complex **4** was a competent metathesis precatalyst, and though the exact structure of the active species is still unknown, it is possible that it is further activated to give a mixed chloro-amido Mo(VI) carbyne; the Schrock group has referred several times to unpublished results indicating that $(CH_3)_3C{\equiv}M(NR_2)_3$ complexes prepared from the corresponding $(CH_3)_3C{\equiv}MCl_3$ complex contain a metathesis-active impurity presumably containing chloride, while those prepared from $(CH_3)_3C{\equiv}M(OR)_3$ do not.[53]

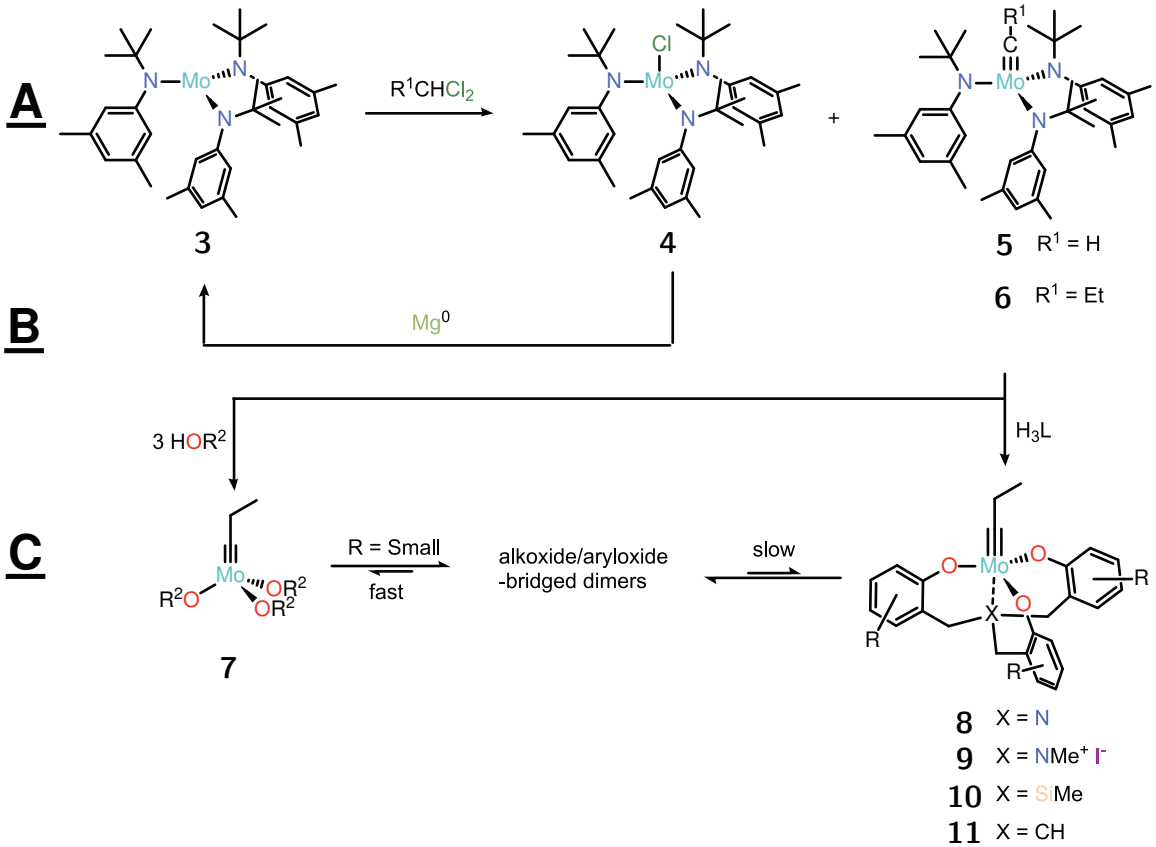

Scheme 1.5: Trisamido Mo(III) complex **3** as a precursor to alkyne metathesis catalysts

Due to the increased steric bulk and decreased electrophilicity, this new catalytic mixture demonstrated much improved functional group tolerance as compared to Schrock's catalyst.[52]

But the reactivity was not particularly tunable, presumably still based on the four-coordinate M(VI) carbyne architecture. Zhang and Moore came up with a clever adaptation of Fürstner's activation reaction to give a more versatile Mo(VI) carbyne platform. Reductively recycling the Mo(IV) chloro coproduct **4** formed during the reaction of a *gem*-dichloroalkane with **3** back into starting material, they could prepare RC≡Mo(N(t-Bu)(Ar))$_3$ (**6**) in high yield (Scheme 1.5B).[54] Upon addition of various alcohols, a library of related trisalkoxymolybdenum(VI) carbyne complexes (**7**) could be prepared *in situ*. This protonolysis strategy was leveraged by several groups to explore a much greater structural space for Mo(VI) metathesis catalysts (Scheme 1.5C, left).[55] Though few of these phenoxide complexes could be isolated without contamination by the liberated amine or by decomposition during concentration/recrystallization, especially through dimerization, some that could be generated cleanly also exhibited reasonable kinetic stability in solution.

Building off of this protonolysis strategy, the Zhang[56] (and later Fürstner[57]) group developed a series of podand ligands, which engendered their resulting Mo carbyne complexes with much lower propensity for alkyne polymerization (Scheme 1.5C, right). Initially attributing this stability to the trigonal bipyramidal coordination environment in **8** enforced by a C_3-symmetric tris(2-hydroxybenzyl)amine framework, the Zhang group found that quaternizing the axial nitrogen to give **9** or replacing it with with noncoordinating silyl (**8**) or alkyl (**11**) groups led to even better performance.[58,59] Their conclusion was that rather than enforcing a different ground-state coordination geometry, the reduced flexibility in the ligand sphere rendered non-metathetical side reactions less kinetically accessible and potential ligand protonolysis reactions less entropically favorable through the chelate effect.

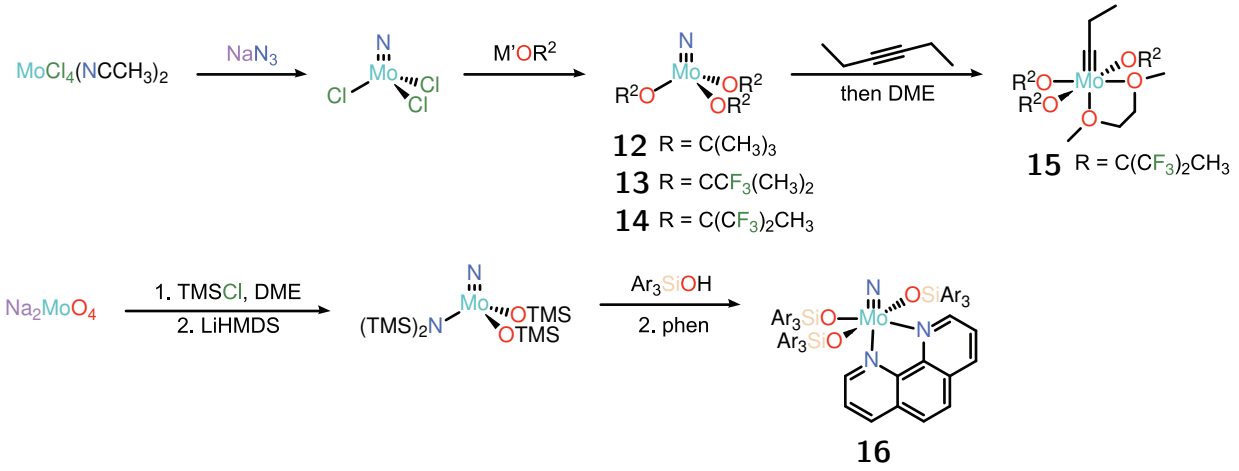

Scheme 1.6: Mo(VI) nitrides as precursors to active alkyne metathesis catalysts.

While these *in situ* systems were simple to prepare, their activity was dependent on their method of activation and the active species were often a fraction of the total. The return to well-defined, structurally-characterized metathesis catalysts was initiated by Marc Johnson's group in 2006.[60] They discovered that sufficiently electrophilic Mo nitride complexes

like $NMo(OC(CF_3)_2CH_3)_3$ (**14**) could undergo nitride-alkyne cross metathesis to give a Mo alkylidyne and a nitrile (Scheme 1.6, top).[61] Those with insufficiently electron-withdrawing ligands (**12** and **13**), that could not be activated stoichiometrically, could give metathesis-active mixtures by the addition of Lewis acids to assist in activation of the nitride.[62,63] While their ultimate goal of catalytic nitrile metathesis to give alkynes and dinitrogen was never achieved,[64] this new entry into Mo alkylidynes not only gave a much-needed alternative to the traditional Schrock αH-abstraction routes to Mo≡C bonds but also enabled the related development of much more robust, bench-stable Mo nitride alkyne metathesis precatalysts (**16**) by the Fürstner group using triarylsilanolates in lieu of fluoroalkoxide supporting ligands (Scheme 1.6, bottom).[65] The decomplexation of the bidentate ligand followed by the same nitride-alkyne cross metathesis activation process generates the active metathesis catalyst *in situ*.

Despite the promising role of Mo nitrides as metathesis precatalysts, the system able to stoichiometrically access the Mo alkylidyne **15** simply recapitulated the propagating species from Schrock's earlier fluoroalkoxide systems. The first true departures from the simple trisalkoxy carbyne motif in a well-defined, isolable system was put forth by Tamm's group in 2007 (Figure 1.3).[66] Derived from Schrock alkylidyne complexes by substitution of one alkoxide with a more electron-rich nitrogen donor, these heteroleptic complexes displayed admirable enhancements in activity compared to their homoleptic precursor **17**.[67] Surprisingly, unlike the isoelectronic Re system $(CH_3)_3C{\equiv}Re(OR)_2NAr$ (Ar = 2,6-diisopropylphenyl) (**2**),[42] these N,O,O-coordinated W carbynes did not manifest the same [2+2] face-selectivity problem, possibly because their imidazolin-2-iminato (**18** and **19**) or amido (**20**) ligands didn't quite replicate the electronic effects of the better π donating imido.

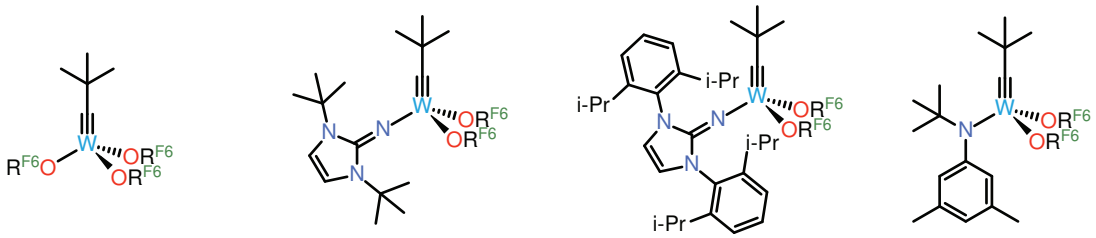

17 **18** **19** **20**

Figure 1.3: Heteroleptic, N,O,O-coordinated W carbynes (R^{F6} = $C(CF_3)_2CH_3$)

This work was rapidly eclipsed, however, by their subsequent work on benzylidyne complexes leveraging the pioneering but thereto underutilized route to trihalocarbyne complexes developed by Mayr and coworkers.[68,69] The so-called "Low-Valent Route" (Scheme 1.7) enabled the rapid access to well-defined W and Mo tribromobenzylidyne complexes (**21**) which could be elaborated into the corresponding trisalkoxycarbyne complexes (**22**). While the 2,4,6-trimethylbenzylidynes such as **23** from the Tamm group simply recapitulated the behavior of many neopentylidyne complexes prepared by the Schrock group, the Fürstner

group leveraged the approach to prepare the benzylidyne analogues of the active species derived from their silanolate-supported Mo nitride precatalysts **24** and their more stable bipyridine or phenanthroline adducts **25**. They found these exhibited higher molar activities but bypassing the nitride activation step also enabled the more facile optimization of ligand parameters for use in alkyne metathesis of highly functionalized substrates toward natural product syntheses.[70]

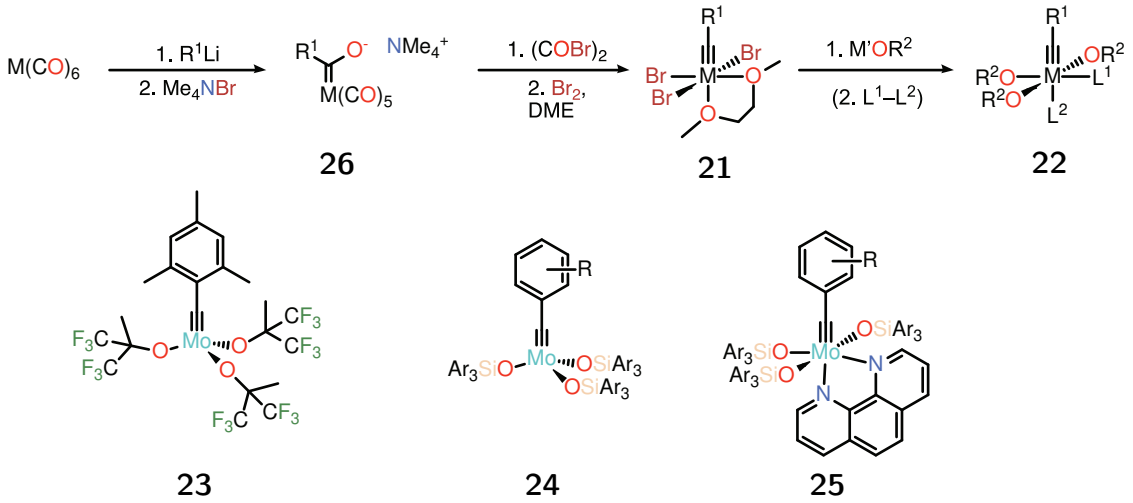

Scheme 1.7: The "Low-Valent" route to Mo(VI) and W(VI) carbyne complexes and selected examples of benzylidyne metathesis catalysts.

The dominant applications of alkyne metathesis, cross metathesis (ACM), ring-closing alkyne metathesis (RCAM), and acyclic diyne metathesis (ADIMET) share similar operational principles since they are all fundamentally thermodynamically-controlled processes. Advances in catalyst design toward these ends targeted and achieved improvements in substrate scope (functional group tolerance), turnover frequency (catalyst activity), and turnover numbers (catalyst longevity). In optimizing these parameters, these groups active in alkyne metathesis catalyst design were fundamentally searching for the most active, most indiscriminate metathesis catalysts that would enable a rapid approach to the thermodynamic equilibrium. In contrast, ring-opening alkyne metathesis polymerization (ROAMP) is the one alkyne metathesis application where the **kinetic** product is desired over the thermodynamic one.

1.4 Ring-Opening Alkyne Metathesis Polymerization

The Schrock group reported the first example of ROAMP in 1987, noting that cyclooctyne reacted extremely rapidly with their tungsten alkyne metathesis catalysts **1** or $[(tBuO)_3W]_2$ (**27**) to give a gelatinous precipitate of *poly*(octynamer) (Scheme 1.8) whose molecular weight increased with decreased catalyst loading.[71] Initially suspecting a living ring-opening alkyne

metathesis polymerization was occuring, subsequent analysis of the resulting polymers after hydrogenation to polyethylene revealed that the polymer molecular weights exhibited a broad distribution of cyclic polymers. These observations were consistent with nonselective alkyne cross metathesis reactions, since the propagating species can react either productively by reacting with more monomer to extend the polymer chain, or unproductively by attacking the alkynes of the polymer backbone. Reacting with its own polymer chain can extrude a cyclic oligomer/polymer while interchain metathesis leads to chain transfer and chain-termination events.

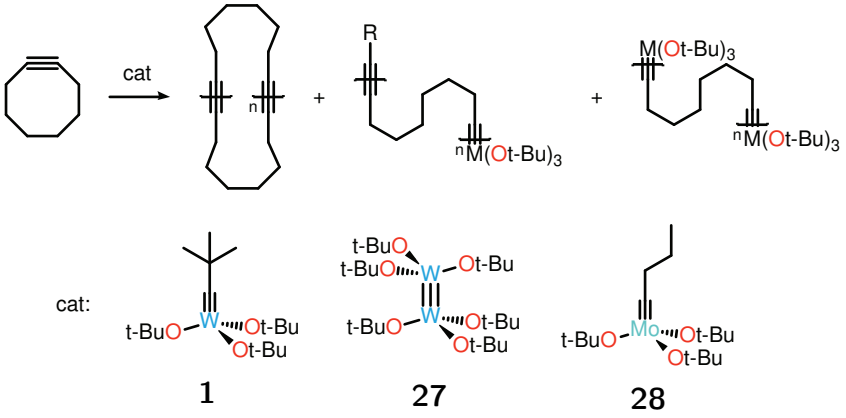

Scheme 1.8: Early examples of ROAMP exhibiting poor kinetic control leading predominantly to cyclic oliogmers.

The thermodynamic product of a ROAMP would exhibit heavy depolymerization to give the entropically favored maximum number of minimally strained cyclic oligomers, as predicted by Jacobson-Stockmayer (J-S) polycondensation theory.[72] While they found that reaching this J-S equilibrium could be delayed by using the less reactive, more selective Mo analogues such as **28** which attacked the internal alkynes of the polymer more slowly, they could not suppress this equilibration completely.[38] Even using more highly strained cyclooctynes, the Nuckolls group found that **1** was insufficiently selective and led to disperse polymer samples of uncontrollable molecular weight.[73] The Tamm group similarly found that **18** gave *poly*(octynamer) with J-S behavior, unable to discriminate between the alkynes of cyclooctyne and those of *poly*(octynamer).[74]

These ROAMP side reactions are fundamentally a problem of kinetic selectivity, a parameter of alkyne metathesis that had gone largely underappreciated for most of its history. A few groups noted some kinetic selectivities in alkyne cross-metathesis, e.g. that alkyl-alkynes react faster than aryl-alkynes[25,29,75] or that high steric congestion can almost completely suppress metathesis,[76] but aside from the observation that molybdenum species tended to react more selectively with activated alkynes than their tungsten congeners few strategies to leverage these kinetic preferences appeared.[77]

In 2010, Fischer and Nuckolls confronted this kinetic selectivity problem head on. They used the *in situ* method screen a wide range of Mo initiators to identify ones capable of

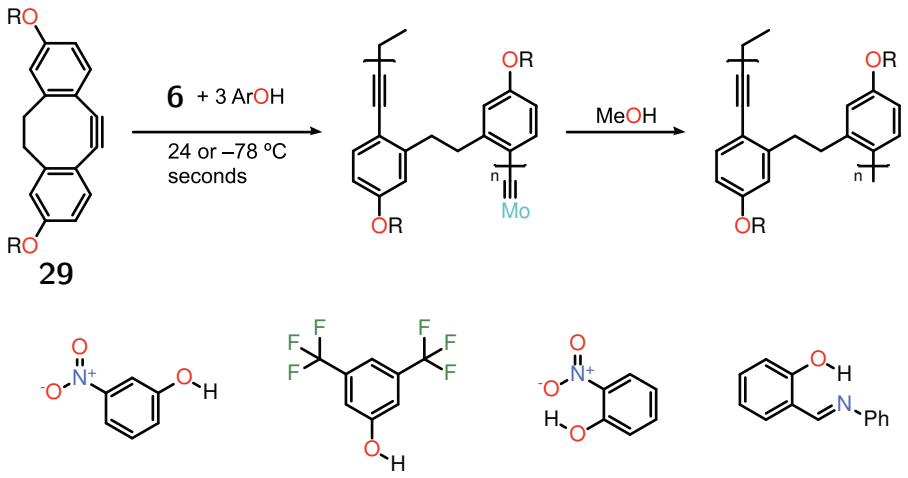

Scheme 1.9: First example of successful living ROAMP using catalysts generated *in-situ* from **6** (top) and top-performing phenol activators (bottom).

discriminating between a strained dibenzocyclooctyne substrate **29** and the resulting polymer backbone. Their efforts led to the first successful living ROAMP (Scheme 1.9).[78] Using phenols with electron withdrawing groups, they found that some generated sufficiently selective metathesis catalyst mixtures to give linear polymers with dispersities as low as 1.1. Bidentate phenols proved optimal activators, whose extra coordinating moiety restricted the coordination geometry about the active catalyst center and discouraged catalyst dimerization. The molecular weights they achieved, however, were much higher than predicted from the catalyst loading, indicating that only a small fraction of the molybdenum in solution was active in ROAMP and hampering any conclusive assignment of the structure of the catalytically active species. At cryogenic temperatures, however, bidentate phenol ligands such as 2-nitrophenol or 2-(phenyliminomethyl)phenol slowed chain propagation enough to allow all the catalysts to initiate, give predictable molecular weights with narrow dispersities.[79]

This problem was overcome in a more easily handled, well-defined system by stepping back from the orthodoxy of homoleptic Mo and W carbyne complexes. While Tamm's N,O,O-ligated systems such as **18** were *more* active, the Zhang group's podand motifs such as in **8** gave conformationally restricted catalysts only active at elevated temperature. Going even further in restricting the achievable coordination geometry about the metal center than the those in the arguably still rather flexible podand motifs of the Zhang group, Bellone and Fischer developed a Mo carbyne complex **30** featuring a bulky pyridine bis(phenol) ONO pincer ligand (Scheme 1.10). This rigid ligand framework maintained the additional pyridine ligand in the coordination sphere throughout the catalytic cycle, unlike the presumably hemilabile bidentate phenoxides of the *in situ* systems that required low temperatures to maintain persistent binding. Moreover, the rigid ligand prevented the catalyst from achieving the canonically-preferred, five-coordinate trigonal-bipyramidal metallacyclobutadiene geometry. This rendered the energetics of the initial cycloaddition (Scheme 1.10 **TS1**) and subsequent

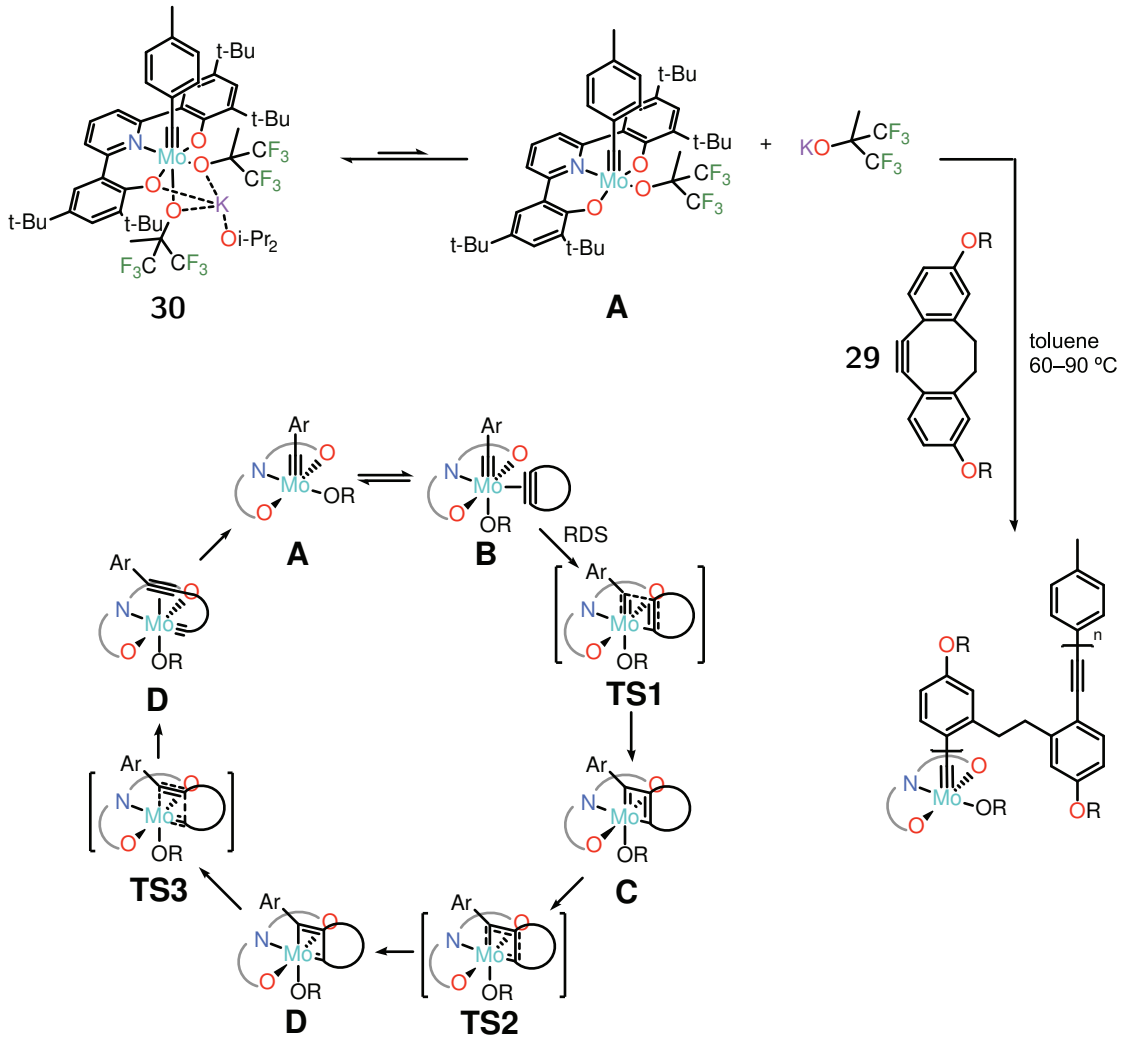

Scheme 1.10: Living ROAMP using an ONO pincer catalyst **30**. Top: dissociation equilibrium between inactive, octacoordinate **30** and its unsaturated active species. Bottom: proposed catalytic cycle highlighting the rate-determining [2+2] cycloaddition step; intermediates after the RDS are not observed. **A**. pentacoordinate active species in equilibrium with the ligand-isomerized, bound monomer complex **B** which undergoes turnover-limiting [2+2] cycloaddition through **TS1** to give initial molybdacyclobutadiene **C**. This isomerizes through **TS2** to the more preferred valence isomer **D** which places the weaker donor *trans* to the carbene carbon. Finally, ring-opening through **TS3** gives the ring-opened product **D** which rearranges to the pentacoordinate species **A** to close the cycle.

cycloelimination (Scheme 1.10 **TS3**) very different due to the different ligands *trans* to the forming (pyridinic N) and breaking (alkoxide O) Mo–C bond. This transition state- and intermediate-destabilizing strategy worked extremely well; not only did they succeed in rais-

ing the operating temperature of the catalyst without harming its selectivity, they also shut down side reactions such as catalyst dimerization that would otherwise terminate the living chain ends. NMR studies and density functional theory (DFT) suggest that the initial [2+2] cycloaddition is rate-determining, positioning the catalyst system to take optimal advantage of the transition-state preorganization of the strained alkyne, whose C–C≡C angle is much closer to the 120° ideal for the sp^2 carbons of the metallacyclobutadiene than the 180° ideal for an unstrained alkyne. Combined with the hindered steric profile of the alkynes of the polymer backbone, they observed exceptional selectivity giving essentially no backbiting even at elevated temperatures.

1.5 Conclusion

Alkyne metathesis has evolved considerably since its discovery in 1968. The early pioneering work in the Schrock group illustrated in great detail the potential pitfalls of this carefully orchestrated organometallic dance, and set up what would remain the orthodoxy of alkyne metathesis catalyst design for the better part of two decades. The turn of the century saw a boom in interest in the applications of alkyne metathesis in RCAM and ADIMET, leading to a new generation of alkyne metathesis catalysts for equilibrium alkyne metathesis processes. New synthetic routes to Mo carbyne complexes via Mo(III) amides, Mo(VI) nitrides, or Mo(0) acyl precursors greatly expanded the organometallic space over which metathesis catalysts could be studied and optimized. Other studies by the Nuckolls and Fischer groups demonstrated that the kinetically-controlled metathesis of strained alkynes needed for living ROAMP is possible, but the scope of polymer materials they could prepare remained small and of relatively little practical interest. Due to the low relative availability of strained alkynes compared to alkenes, collaborative feedback between design and synthesis of strained alkyne monomers and optimization of compatible metathesis catalysts will be critical to advance the scope of ROAMP into functional conjugated polymer materials.

Chapter 2

Poly(*ortho*-phenylene ethynylene)s by ROAMP

In this chapter, *poly*(phenylene ethynylene)s are introduced and motivations for their chain-growth synthesis by ROAMP discussed. The ROAMP synthesis of *poly*-(*ortho*-phenylene ethynylene) is described. A mechanistic description of the polymerization by multinuclear NMR kinetics is formulated. Lastly, potential termination reactions are discussed in the context of cyclic *versus* linear polymer synthesis and unproductive reactions of the propagating species. A preliminary structural assignment for the terminated organometallic species is developed, supported by model systems that react quantitatively to form catalytically-inactive molybdatetrahedranes.

2.1 *Poly*(phenylene ethynylene)s

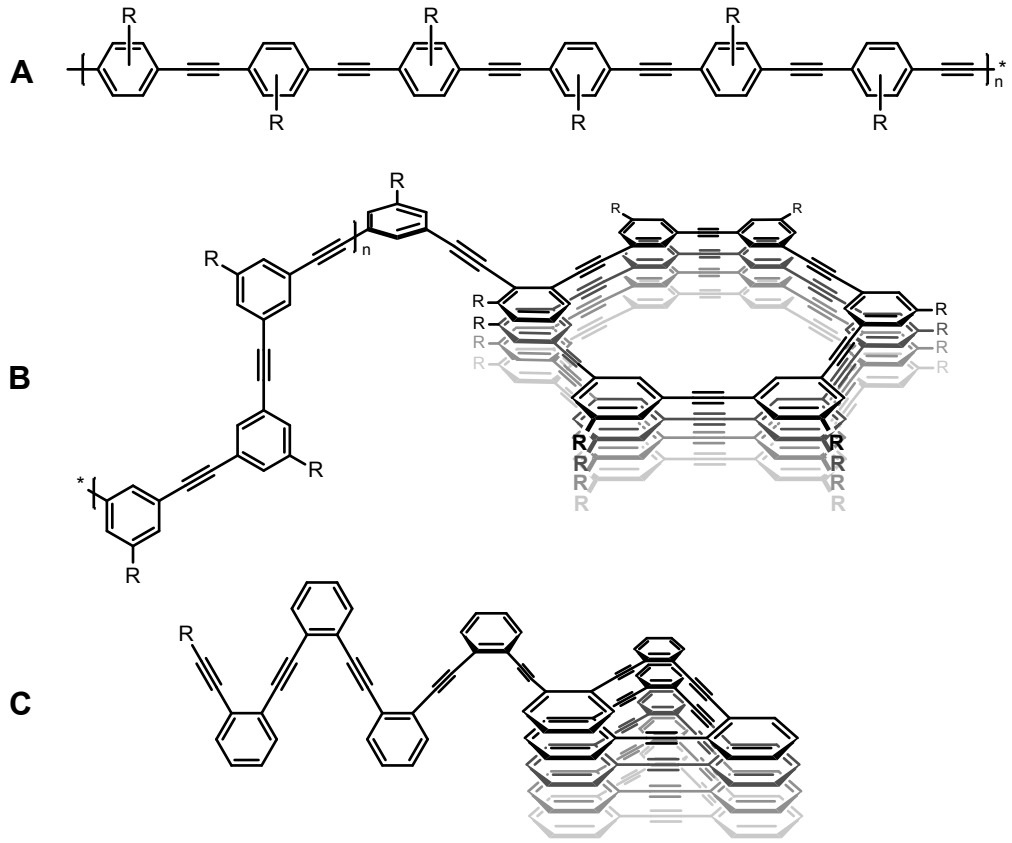

Figure 2.1: The three classes of PPEs. Rigid-rodlike PpPE (**A**), and flexible foldameric PmPE (**B**) and PoPEs (**C**) in their open chain (left) or helically folded (right) states.

Semiconducting, π-conjugated polymers have become a central part of many modern electronic materials. *Poly*(phenylene ethynylene)s (PPEs) are a class of these where phenyl rings are connected by alkyne units, and they have been used in a vast array of applications that leverage their fluorescence, thermochromism, solvatochromism, electroluminescence, and self assembly.[80,81] The connectivity of the phenyl linkages *ortho*, *meta*, or *para* leads to three different families of PPEs whose physical and electronic properties depend not only on their connectivity but also, due to the rotational flexibility of the alkyne linkage, their conformation. The rigid linear structures of *poly*-(*para*-phenylene ethynylene) (PpPE) give rise to long effective conjugation lengths and high fluorescence quantum yields which have been central to their applications from light-emitting diodes to fluorescent environmental sensors.[46,82] In contrast, *poly*-(*meta*-phenylene ethynylene) (PmPE) and *poly*-(*ortho*-phenylene ethynylene) (PoPE) have bent phenyl linkages, enabling them to adopt either a random chain or solvophobically-driven helically coiled conformation[83–87] (Figure 2.1B-C, right). This change in secondary structure also triggers changes in their properties; their optical bandgaps change

as a function of folding, and the potential electronic conduction mechanisms also change from through-chain conduction to hopping through intrachain π-π contacts.[88,89]

These conformationally dynamic classes of PPEs, however, have seen comparatively little development in part due to their more challenging syntheses. The rigid, linear PpPEs are easily synthesized by step-growth polymerizations, either by cross-coupling or by ADIMET.[82] The bent backbones of PmPE and PoPE lead to intramolecular cyclization of the active sites of polymerization under these conditions, severely limiting the achievable molecular weights. Targeting *poly*(phenylene ethynylene)s by ROAMP, in a chain-growth synthesis, would not only obviate this problem but enable the synthesis of PPE block copolymers which combine blocks featuring different backbones. These hybrid materials could form the core of new classes of stimulus-responsive electronic materials.

2.2 Strained Alkyne Monomers for PPEs

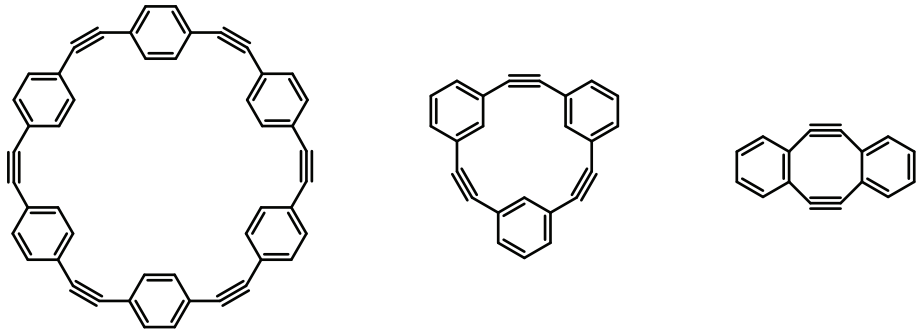

31 **32** **33**

Figure 2.2: Strained cyclo(phenylene ethynylene)s with potential as ROAMP monomers.

To prepare PPEs by ROAMP, the logical retrosynthetic disconnection would be to the smallest *oligo*(phenylene ethynylene) macrocycles that are stable. Theoretically, if the initial [2+2] cycloaddition is rate-determining as it was for the Bellone system,[90] the more strained the monomer, the larger the transition-state preorganization and the easier it should be to discriminate between it and the unstrained alkynes of the growing *poly*(phenylene ethynylene), up to the point where the thermal instability of the monomer or metallacyclobutadiene intermediates becomes prohibitive. For the *para* case, the resulting "cycloparaphenyleneacetylenes" or CPPAs are known only for n $\geq$ 5,[91] with the sextyne **31** being the smallest member that is stable at ambient temperature.[92] For *meta*(phenylene ethynylene)s, the dimer is too strained to be isolated, leaving the trimer **32**[93] as the logical choice. The *ortho*(phenylene ethynylene)s can logically be synthesized by the ROAMP of the small dialkyne **33**.

The unsubstituted *para* and *meta* monomers **31** and **32** were synthesized according to literature procedures by other Fischer group members, Nathan Usselman and Justin Bours

respectively, but the extreme insolubility of the resulting polymers led to precipitation of the active species after as little as one turnover. The *poly*-(*ortho*-phenylene ethynylene)s resulting from the ROAMP of **33**, however, are soluble enough to study.

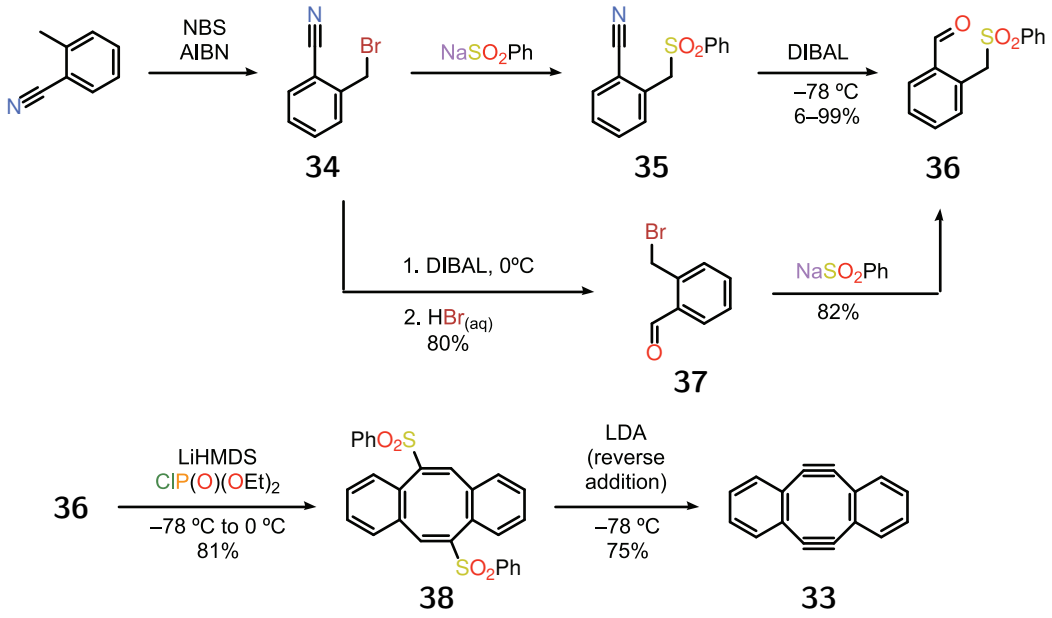

Scheme 2.1: Synthesis of strained *ortho*-dialkyne monomer **33**.

The diyne **33** was first reported by Wong and Sondheimer,[94] but subsequent syntheses reported greatly improved procedures.[95] The synthesis in Scheme 2.1 was adapted from the Otera group.[96] Starting from *o*-tolunitrile, radical bromination to **34** and subsequent sulfonylation with sodium benzenesulfinate gave nitrile **35**. The Otera route called for a DIBAL reduction of **35** to give aldehyde **36** in 78% yield, but this step was highly irreproducible giving yields between 6 and 99% and exhibiting poor scalability. The reaction fails to go to completion with a single equivalent of reductant even after prolonged reaction times, easily proceeds to the overreduced benzylamine if excess DIBAL is used, and **35** and **36** are chromatographically inseparable. Inverting the series of steps gave a much more readily scalable procedure. DIBAL reduction of **34** using the procedure of Zhang and Lippard gave **37** in 80% on a 25 mmol scale.[97] Sulfonylation of **37** proceeds smoothly to give **36** in 84% after recrystallization.

The remaining steps can be done in one pot, as Orita et. al. report but the scalability is poor, presumably due to the instability of the intermediate ene-yne that is formed as base is added slowly. Double Horner-Emmons-Wadsworth olefination gives a mixture of oligomeric material and bis(vinyl sulfone) dimer **38**, determined largely by the E to Z selectivity of the initial olefination. The oligomeric material is tedious to separate chromatographically from **38**, but a modification to the literature procedure makes purification much more straightforward: allowing the reaction to warm to room temperature and stirring until

all the color of the carbanion intermediates dissipates (typically 12-24 h) leads to step-growth of the polymeric material to much higher molecular weights. Subsequent chromatography or Soxhlet extraction with heptanes then readily separates **38** from the high molecular weight polymeric material. Reverse addition of **39** to excess base avoids buildup of the unstable mono-eliminated ene-yne intermediate and gives much more reproducible elimination to **33**. At large scales, the yield is substantially improved by avoiding chromatography; after aqueous workup and rotary evaporation, trituration of the crude material with cold (–40 °C) DCM/hexanes gives pure **33**.

2.3 Catalyst Design and Selectivity in ROAMP of PoPE

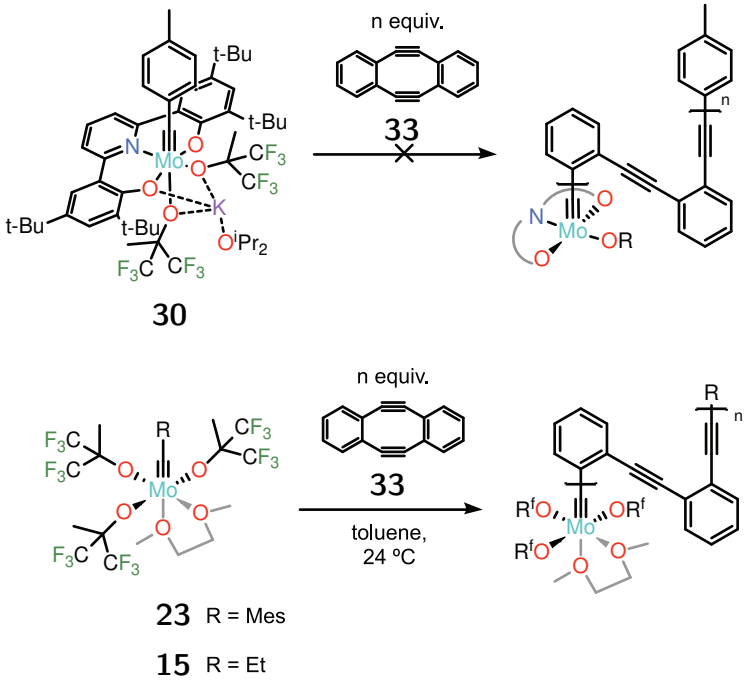

Scheme 2.2: ROAMP of **33** with Mo intitiators.

Initial attempts at ROAMP of **33** with Bellone's catalyst **30** immediately revealed how different **33** is from other cyclooctynes that had been studied. No polymerization was observed, but a stoichiometric adduct between **33** and **30** was formed. Heating to attempt to turn over the catalytic cycle led instead to decomposition of the organometallic intermediate. This was surprising, considering **33** is known to be stable under nitrogen to temperatures in excess of 100 °C.[98] One possible explanation is that this adduct is the molybdacyclobutadiene (Scheme 1.10C) where one triple bond of **33** has reacted to give two metallacycle sp^2 carbons, in which case the strained 8-membered ring should behave like its more highly

strained ene-yne cousin, which is known to decompose at far lower temperatures in both solution and the solid state.[94]

Clearly, the strategy of raising the barrier to the initial cycloaddition would not work for this highly reactive 8π, formally antiaromatic substrate for which cycloaddition chemistry is so facile. Initial experiments suggested that the cycloelimination would be the rate-determining step; to avoid decomposition of the metallacyclobutadiene, a more highly active alkyne metathesis catalyst would be necessary to enable turnover at a lower temperature. Returning to the more orthodox trisalkoxycarbyne motif, the highly active alkyne cross metathesis catalysts **23** and **15** were found to be competent to polymerize **33** (Scheme 2.2). According to Schrock the neopentylidyne analogue of these complexes "is one of the best acetylene metathesis catalysts containing molybdenum that [they] have prepared," so the fact that they do not simply cyclodepolymerize the resulting polymer by nonselective metathesis is surprising.[29]

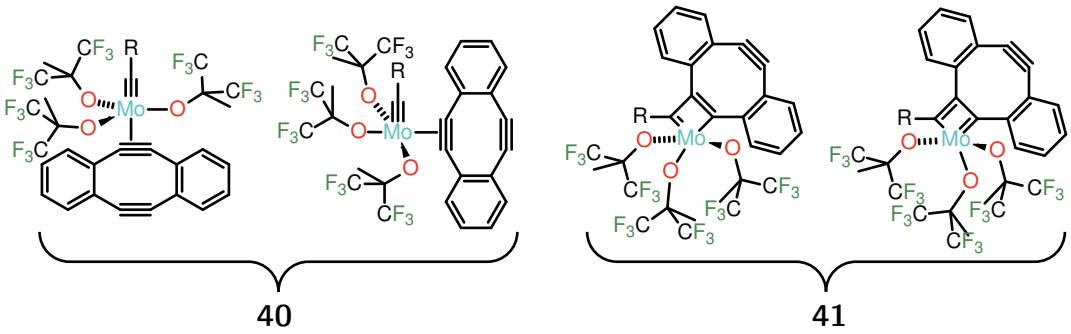

Figure 2.3: Potential catalyst resting states in the ROAMP of **33**.

Examining the polymerization *in situ* by ^{1}H, ^{19}F, and ^{13}C NMR spectroscopy was instrumental in understanding both the competence of these molybdenum catalysts and their unexpected selectivity for **33** over the unstrained polymer backbone. By ^{1}H NMR the initial Mo complex is completely consumed within 60s, giving a new organometallic species. The aromatic region is complex, limiting the structural information that can be gleaned, however the ^{19}F NMR clearly shows three broadened CF_3 resonances in a pseudo two-to-one ratio indicating lowered local symmetry on the NMR timescale consistent with a C_s symmetry or C_1 symmetry (if two CF_3 groups of the $OC(CF_3)_2CH_3$ ligands are coincidentally isochronous). The protons in DME from **15** resonate at the chemical shift of free DME, indicating it is not bound to the intermediate. This structure could be consistent with an axial or equatorial monomer adduct (**40**) of C_s symmetry or a molybdacyclobutadiene complex (**41**) of C_1 symmetry (Figure 2.3).

Using a ^{13}C-labeled **33** enables us to gain additional structural information. The ^{13}C NMR spectrum in Figure 2.4A shows that upon mixing, new downfield resonances appear around 134, 176, and 191 ppm. This is far downfield of the monomer **33** (110 ppm), but these chemical shifts are low compared to known Mo metallacyclobutadienes, where the carbons bound to Mo resonate at 220-270 ppm.[14,39,99] The carbons of formally d^2 alkyne complexes of

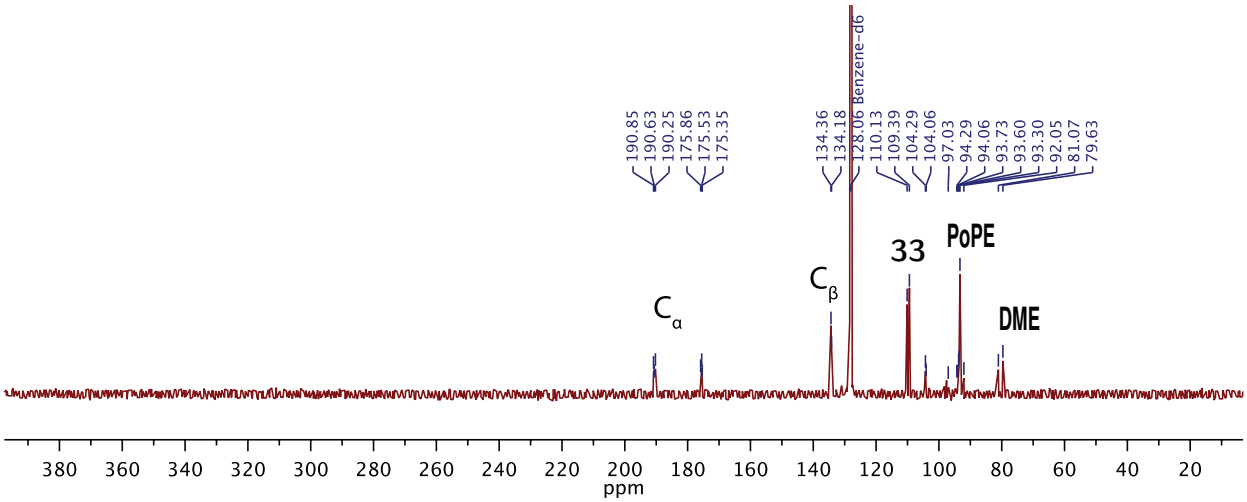

Figure 2.4: ^{13}C NMR of the catalyst resting state in the ROAMP of **33** using ^{13}C-labeled substrate.

Mo are known to resonate at 190-200 ppm, but this might not be a good point of comparison as this compound can be represented as Mo(IV) alkyne complex *or* a Mo(VI) complex of an alkyne ligand partially reduced by heavy π-backdonation.[100] Examples of unambiguously d^0 alkyne complexes are few; the downfield shift due to binding is much smaller.[101,102]

However, the appearance of *three* new carbon resonances, and the fact that upon catalyst turnover we don't observe a ^{13}C-labelled carbyne carbon resonance near 300 ppm, suggests that it is not simply the coordination complex **40**. Instead, the lower than expected chemical shifts of the resting state could be due to a combination of a paratropic ring current from the 8π system of **33** and a reversible [2+2] cycloaddition reaction that is fast on the NMR timescale (DFT modeling detailed in Chapter 3 suggests this is nearly barrierless), producing an averaged chemical shift between those two canonical bonding pictures. With this in mind, but not knowing the chemical shifts of each individual canonical form, we assigned the 176 and 191 ppm resonances to the time-averaged α carbons of **41** and the resonance at 134 ppm to the β carbon based on the chemical shift trends in metallacyclobutadienes. These resonances decay away once **33** is consumed and we see the formation of the ^{13}C-labelled carbyne carbon near 300 ppm.

With the catalyst resting state understood, it is clear why polymerization of **33** with a catalyst usually regarded as a highly active cross metathesis catalyst actually works: the cycloaddition is facile and the cycloelimination is turnover-limiting. The catalyst resting state is sequestered by the monomer and unable to engage in stochastic metathesis along the polymer backbone. We turned to multinuclear NMR kinetics to flesh out the remainder of the reaction scheme (Figure 2.5, left). First we observe that the consumption of **33** is zero-order in **33** and first-order in catalyst, consistent with our rate-determining cycloelimination from **41**. When **33** is consumed, an interesting difference between the polymerization with **23** and **43** appears. The active chain ends of **42** are stable in the presence of the mesityl

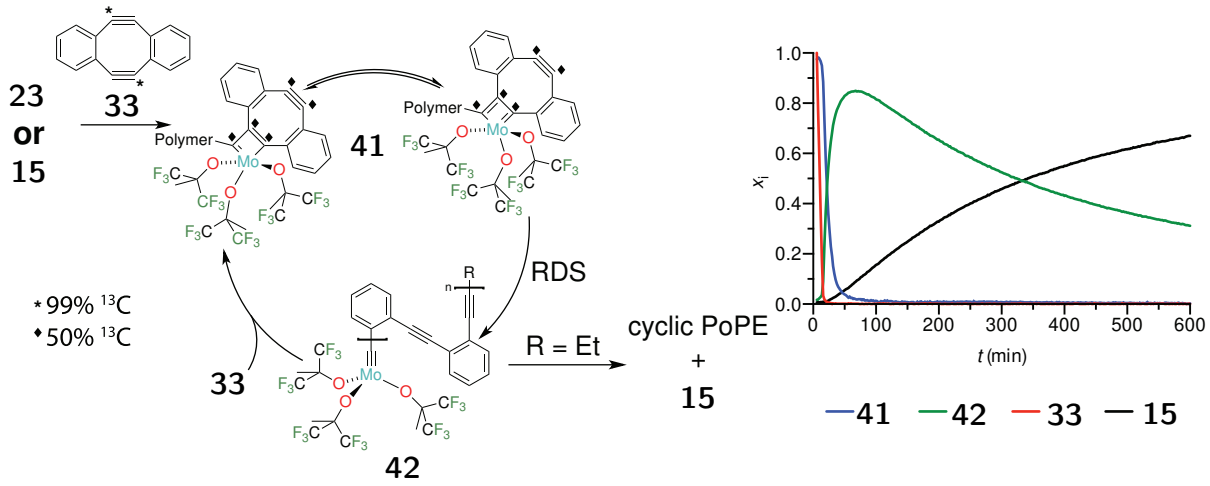

Figure 2.5: Proposed mechanism and speciation diagram during the ROAMP of **33**.

endgroup, but the sterically- and electronically-activated butynyl endgroups introduced by **15** are metathesized much more readily. This endgroup-directed metathesis regenerates the starting initiator **15** and extrudes a cyclic polymer (Figure 2.5, right). Matrix-assisted laser desorption time-of-flight mass spectrometry (MALDI-TOF MS) of these polymers cationized with silver nitrate exhibits only ions with an integer multiple of the monomer mass (200n+Ag^+, Figure 2.6). On the timescale of hours, we observe no ions with masses of 200n+100 that would be formed by random metathesis along the polymer backbone, indicating that random backbiting is slow.

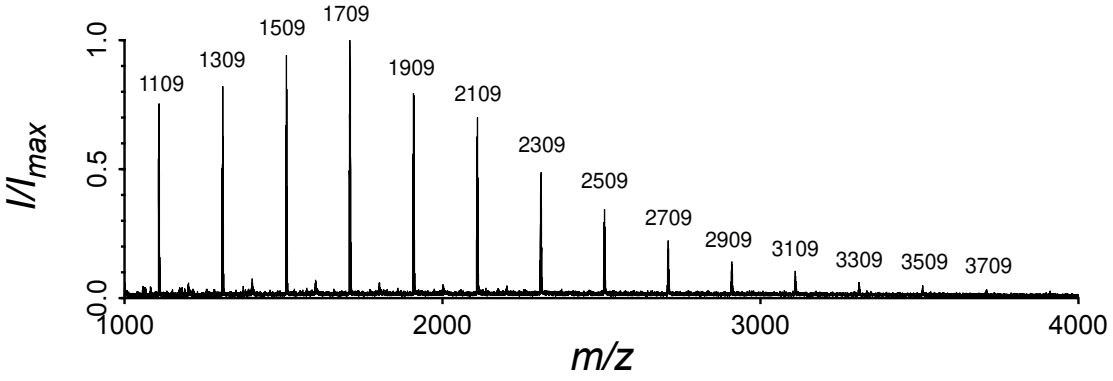

Figure 2.6: MALDI-TOF MS of cyclic *poly*(*ortho*-phenylene ethynylene)s exhibiting only 200n+109^+ $[M+Ag]^+$ ions lacking additional mass for endgroups. Minor peaks correspond to 200n ions $[M]^+$ without Ag.

Heating or leaving the reaction to run for days to weeks, however, leads to stochastic backbiting and depolymerization, forming cyclic polymers with random numbers of alkynes. This indicated that the origin of this selectivity is a kinetic one. We turned to **45** and

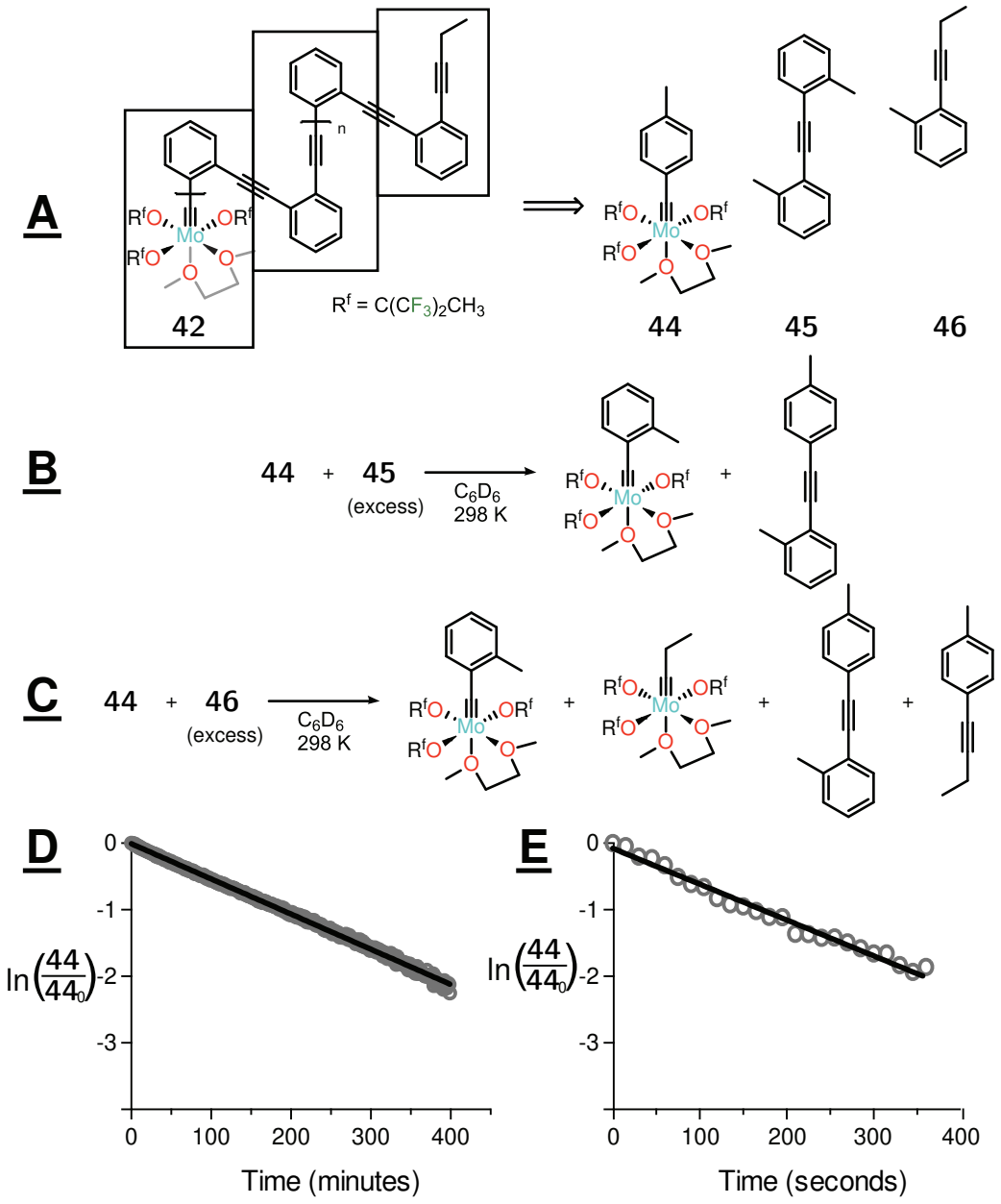

Figure 2.7: **A**. Kinetic models of nonselective backbiting at internal alkynes and macrocyclization by metathesis at the butynyl endgroup during ROAMP of **33** with **15**. Model reaction and kinetic experiments under pseudo-first-order conditions for metathesis at the internal (**B**,**D**) and engroup (**C**,**E**) alkynes.

Table 2.1: Concentration dependence of cyclic PoPE formation.
[**33**]/[**15**] = 5, T = 24 °C, t = 16 h.

[15] (mM)	**% cyclic PoPE**	$\mathbf{M}_n$	$\mathbf{M}_w$	**Đ**
10	86	370	840	2.2
5	91	330	660	2.0
2	92	280	550	1.9
1	93	280	530	1.8

46 as models for the internal alkynes of the polymer backbone and its butynyl endgroup, respectively, and **44** as a surrogate for the propagating species. Under pseudo-first-order conditions, we observe that metathesis at the hindered diaryl alkyne **45** is 180 times slower (k_{298} = 7.1(2) x 10^{-4} $M^{-1}s^{-1}$) than metathesis at the alkyl-aryl alkyne **46** (k_{298} = 1.3(4) x 10^{-1} $M^{-1}s^{-1}$) (Figure 2.7). The real selectivity of the propagating species, which is more hindered than **44**, is likely even higher. To examine the molecularity of the macrocylization process, we also measured the cyclic polymer yield as a function of concentration. Fortunately, the two polymer topologies have different ^{1}H NMR chemical shifts. Consistent with a unimolecular process, the fraction of cyclic polymers produced increases with decreasing concentration (Figure 2.8).

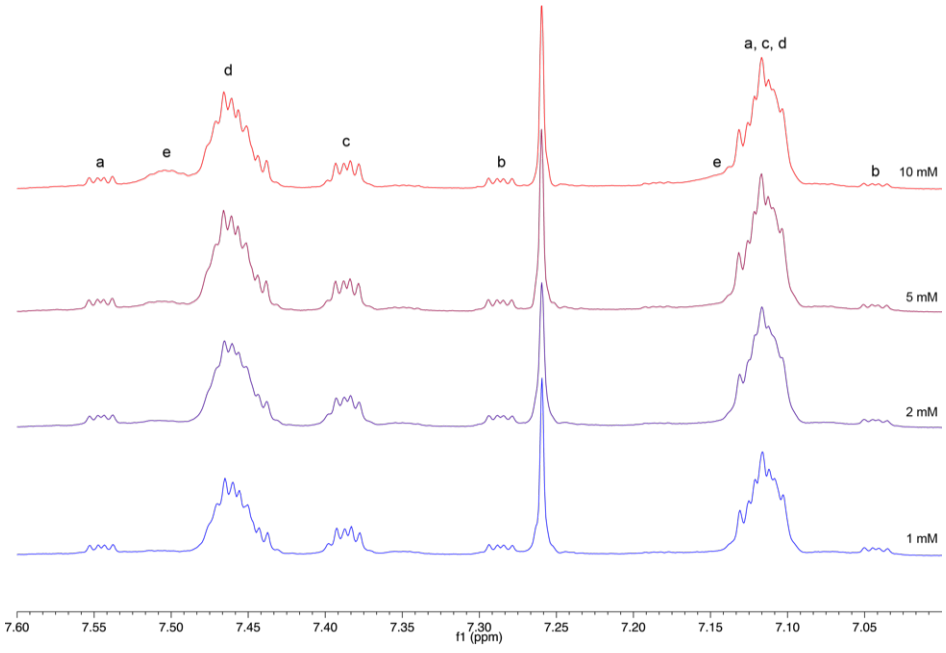

Figure 2.8: Cyclic PoPE yield as a function of concentration during endgroup-directed macrocyclization from ROAMP of **33** with **15**. With increasing dilution, signals from cyclic oligomers of **33** with n = 2 (a),[103] 3 (b),[104] 5 (c),[105] and > 5 (d) remain consistent, while less linear polymer (e) is formed.

2.4 Chain Termination During ROAMP of PoPEs

Careful inspection of the speciation diagram during the ROAMP of PoPE (Figure 2.5, right) reveals that the sum of Mo species is not quite unity. In fact some activity is lost over time to a self-termination reaction, which is more obvious at lower catalyst loadings. At low (e.g. <5%) catalyst loadings, we observe curvature develop in the concentration vs. time plot of monomer **33** consumption. Since it should be first-order in catalyst and zero-order in **33** giving a straight line with a slope equal to k[cat], this curvature implies a loss of catalyst. The rate of termination exactly corresponds to the rate of formation of a new, presumably deactivated catalyst species observed by NMR *in situ* (Figure 2.9).

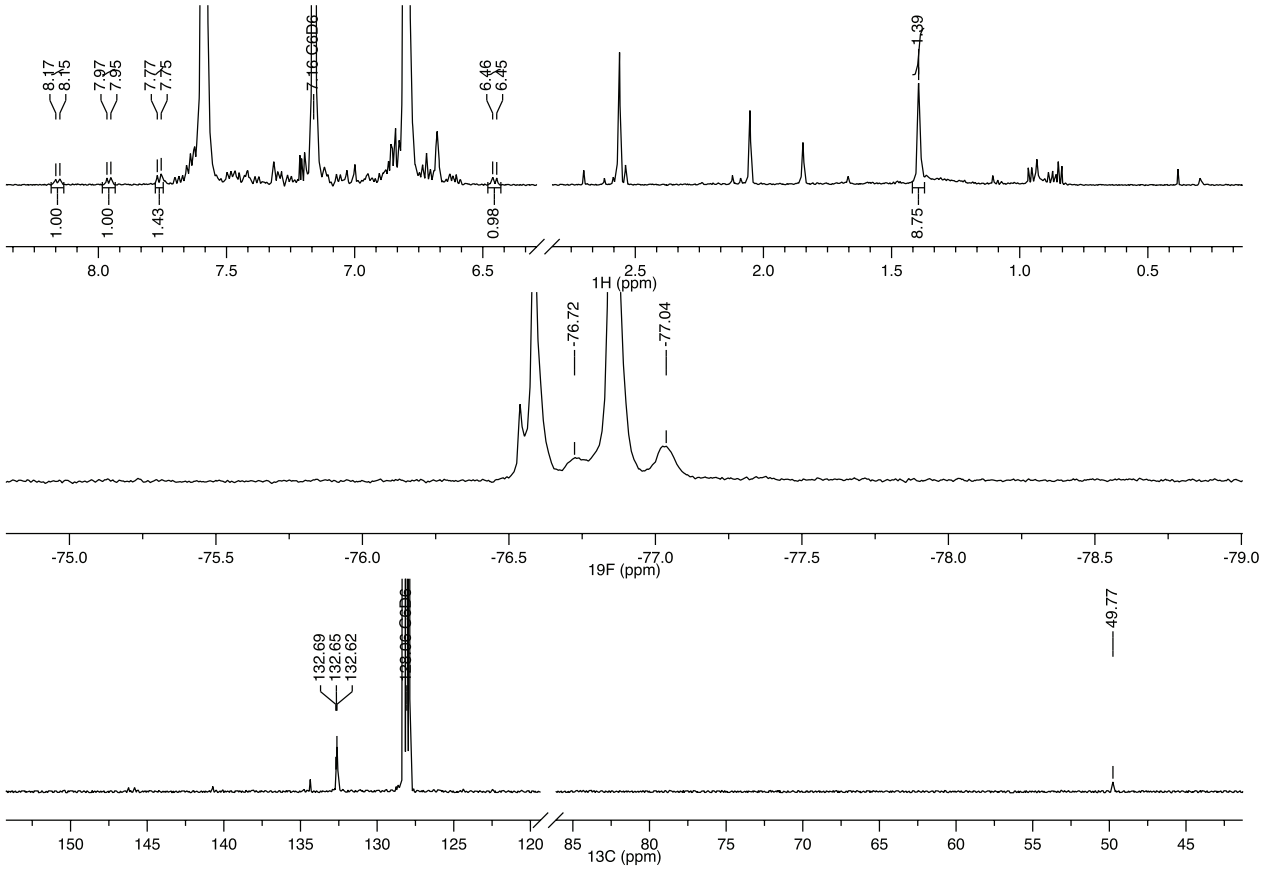

Figure 2.9: Partial NMR spectra (^{1}H, top, ^{19}F, center, ^{13}C, bottom) showing the NMR signatures of terminated Mo catalyst species in ROAMP of **33**.

This deactivated species exhibits three diagnostic spectroscopic signatures: a pseudo-2-to-1 bimodal ^{1}H NMR signal at 1.4 ppm in addition to some aromatic doublets from the monomer fragment (Figure 2.9, top), broad ^{19}F resonances at –76.7 and –77.0 ppm (Figure 2.9, center), and two ^{13}C labeled carbons from labeled **33** at 49.7 and 132.6 ppm (Figure 2.9, bottom). We know that this termination reaction is most likely a reaction of the molybdacy-

clobutadiene for three reasons: this species only grows in while the molybdacyclobutadiene **41** is present, the cycloeliminated carbyne species are stable in the absence of monomer, and we don't observe an equivalent of free $HOC(CF_3)_2CH_3$ by ^1H or ^{19}F NMR that would indicate a hydrolysis by adventitious water. While the rate of termination is not consistent from trial-to-trial, it is *independent* of the concentration of **33**, suggesting that it is not an unproductive reaction between **33** and the propagating species such as a further ring expansion to a molybdacyclohexatriene.

Considering that the resting state is, or at least has predominant character of, a metallacyclobutadiene, a plausible termination reaction would be the collapse of the metallacyclobutadiene into a metallatetrahedrane (see Figure 1.3D). Since we see this reaction in noncoordinating solvents and even in the absence of 1,2-dimethoxyethane (as is the case for **23**), it is possible that association of some other ligand (an alkyne of the polymer, the alkoxide of another Mo complex, etc.) triggers this reaction. Attempting to run this polymerization in THF or in the presence of excess PMe_3 does completely suppress productive polymerization but subsequent reactions of the terminated species led to a complex mixture of Mo- and F-containing products that are difficult to glean structural information from.

Tethering the additional ligand to the metal center could enable a high effective concentration of donor without needing more than a stoichiometric quantity. Scheme 2.3 shows the synthesis of a series of bidentate 1,1,1,3,3,3-hexafluoro-2-propanols featuring strongly donating pyridine (**47**), moderately donating ketone (**48**), and weakly donating ether (**50**) ancillary ligands. Lithiation of 2-picoline and quenching with hexafluoroacetone gave **47** in 12% yield. Ketone ligand **48** is prepared in 45% yield by the reaction of neat acetophenone and hexafluoroacetone trihydrate. Acylation of 1,3,5-trimethoxybenzene with trifluoroacetic anhydride gives trifluoromethyl ketone **49** in 77% yield, which under nucleophilic trifluoromethylation conditions gives 1,1,1,3,3,3-hexafluoro-2-(2,4,6-trimethoxyphenyl)-2-propanol **50** in 10% yield.

Metalation of these bidentate ligands with strong neutral donors is trivial; simply mixing **15** with the bidentate ligands **47** or **48** in toluene quantitatively forms the chelate complexes **51** and **52** which crystallize out of solution as loosely-bound, DME-bridged dimers. In solution, NMR indicates the pyridine complex **51** has six inequivalent CF_3 groups, indicating that it is a non-fluxional, square-pyramidal C_s geometry (or octahedral, if you consider the weakly associated DME). The single-crystal X-ray structure of **52** is shown in Figure 2.10, which mimics this square pyramidal conformation in the solid state; however in solution above 298 K it has C_2 symmetry on the NMR timescale, rapidly equilibrating the two enantiomers either by isomerization through a trigonal bipyramidal intermediate or by dissociation and re-coordination of the carbonyl oxygen.

The X-ray structure of **52** features the expected short Mo–C distance 1.743(2) Å and nearly linear Mo–C1–C2 angle (176.0(2)° for the triply bonded carbyne carbon, and typical Mo–$O_{alkoxide}$ distances of 1.946(1) and 1.923(1) for Mo–O3 and Mo–O4 *cis* and *trans* to the weaker carbonyl donor respectively. The chelating ligand alkoxide distance (Mo–O1) is significantly longer in order to accommodate the acute O1–Mo–O2 bite angle of 76.09(5)° created by the puckered 6-membered Mo–O1–C4–C7–C8–O2 ring. The ketone O2–Mo dis-

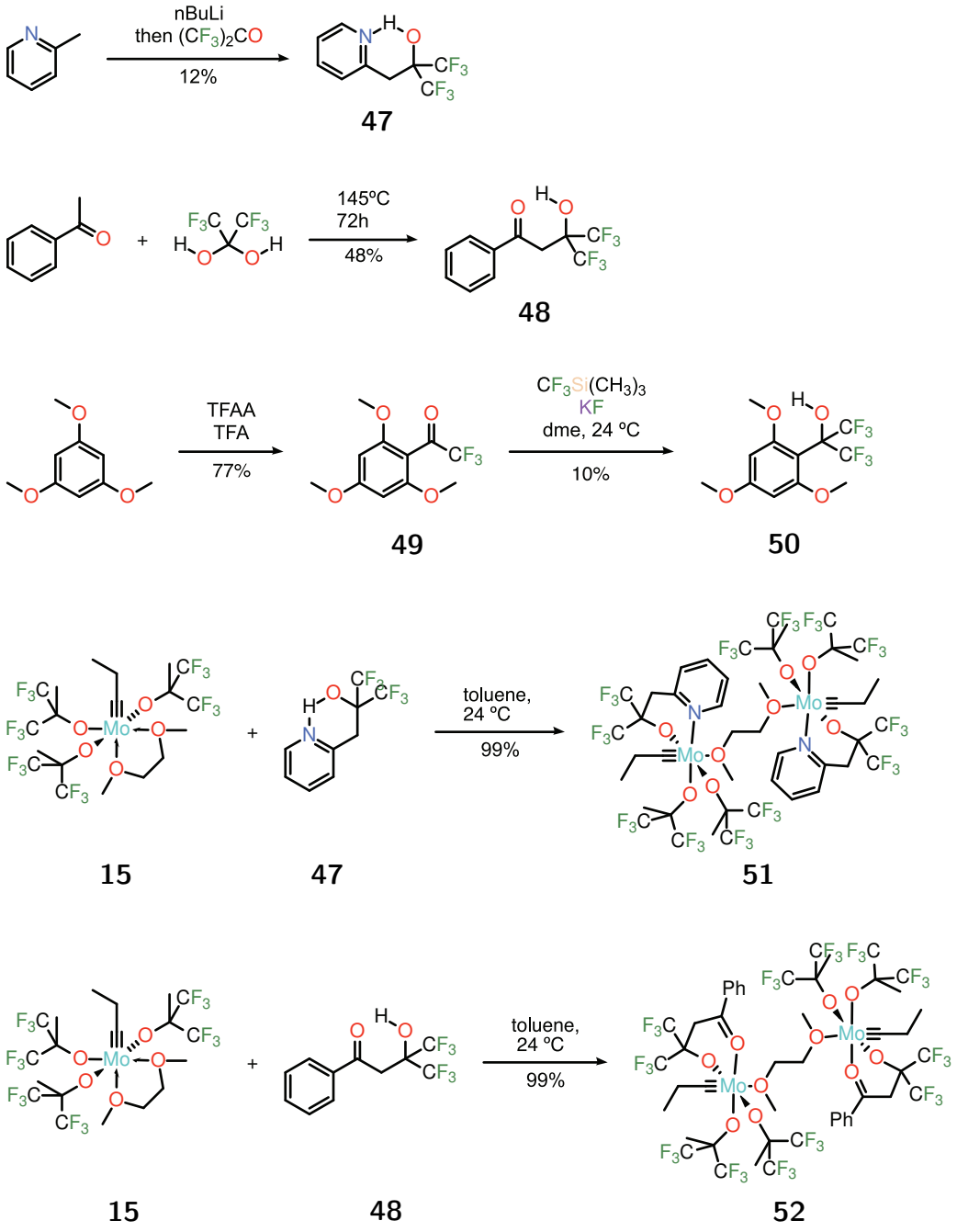

Scheme 2.3: Synthesis of bidentate 1,1,1,3,3,3-hexafluoro-2-propanol derivatives **47**, **48** and **50** and the chelated Mo propylidyne complexes **51** and **52**.

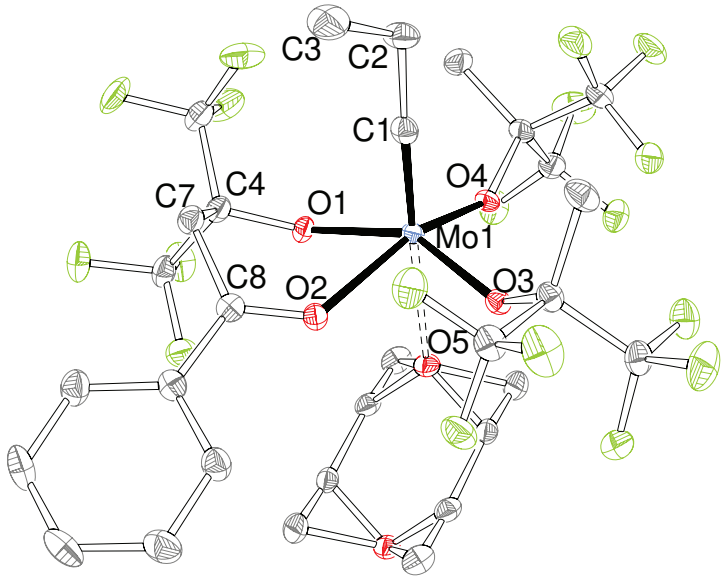

Figure 2.10: Single-crystal X-ray structure of O,O'-chelated propylidyne complex **52**. The bridging DME lies on an inversion center and is disordered over two positions. Hydrogen atoms and the rest of the other symmetry-equivalent complex are omitted for clarity. Thermal ellipsoids drawn at the 50% probability level. Color code: Mo (turquoise), C (gray), O (red), F (green).

tance is in the typical range for a dative Mo–O bond at 2.205(1) Å, but is noticeably shorter than the corresponding equatorial ethereal O–Mo distance in **15** (2.228(2) Å) reflecting its stronger Lewis basicity

Addition of **33** to an orange solution of **51** or **52** in benzene or toluene almost instantaneously forms a deep, virtually opaque blue-black solution containing a 1:1 adduct by ^{1}H NMR. Black prisms of **54** suitable for X-ray crystallography were grown by vapor diffusion of HMDSO into toluene at –30 °C. The structure of one of the two molecules in the assymmetric unit is depicted in Figure 2.11 (the other position exhibits whole-molecule disorder, as it is occupied by both enantiomers). The geometry about Mo is best described as a distorted trigonal bipyramid, with the C_3 ligand occupying one equatorial position and the chelating ligand spanning an axial and an equatorial position. The MoC_3 tetrahedron, being the key portion of the molecule, exhibits very close Mo–C contacts of 2.067(5) Å (Mo–C1), 2.159(5) Å (Mo–C4), and 2.126(6) Å (Mo–C19). These are substantially less than the Mo–C contacts to an η^3 cyclopropenyl cation as seen in $MoBr(CO)_2(\eta^3-C_3Ph_3)bpy$[106] of 2.193(17), 2.204(26), and 2.262(22) Å, and compares reasonably with the known W–C distances in tungstenatetrahedranes $W[C_3(C(CH_3)_3)Et_2](O_2CCH_3)_3$[28] (2.089(5) Å, 2.114(7) Å, and 2.134(6) Å) and $W[C_3(C(CH_3)_3)(CH_3)_2]Cl_3\bullet(TMEDA)$[34] (2.040(7) Å, 2.115(7) Å, and 2.133(7) Å). Like those tungstenatetrahedranes, the Mo–C_3 system does not appear to exhibit any rotation on the NMR timescale up to 60 °, suggesting a more localized σ-bonding motif.

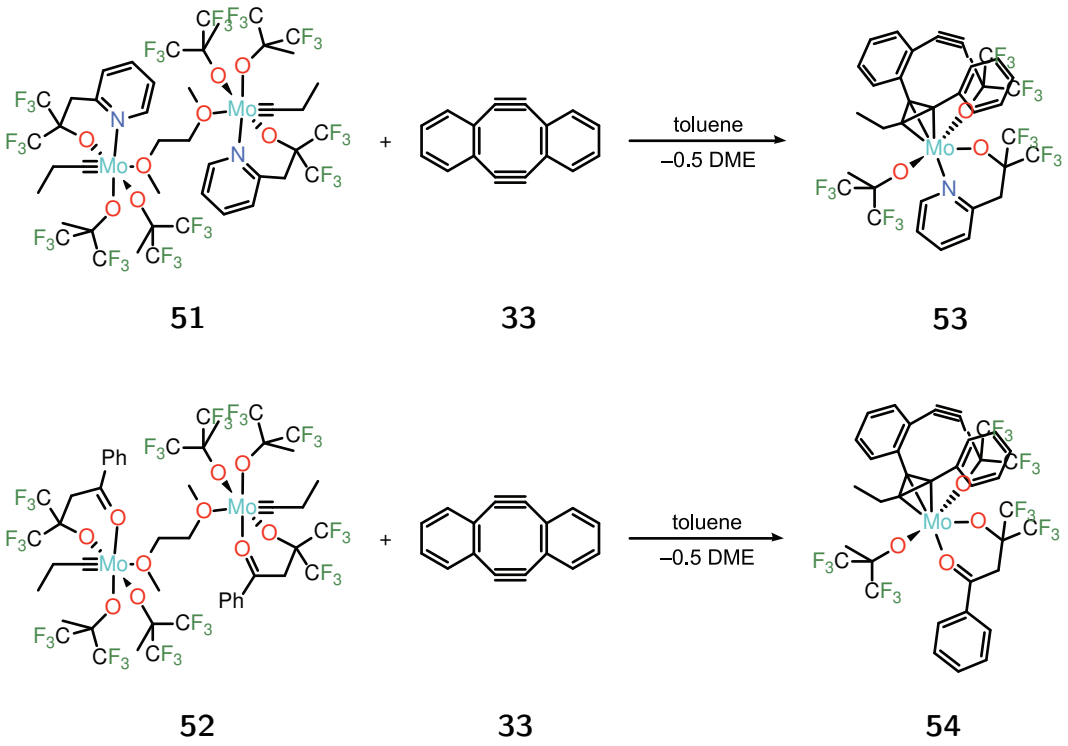

Scheme 2.4: Synthesis of molybdatetrahedranes from chelated carbyne complexes **51** and **52** and strained alkyne **33**.

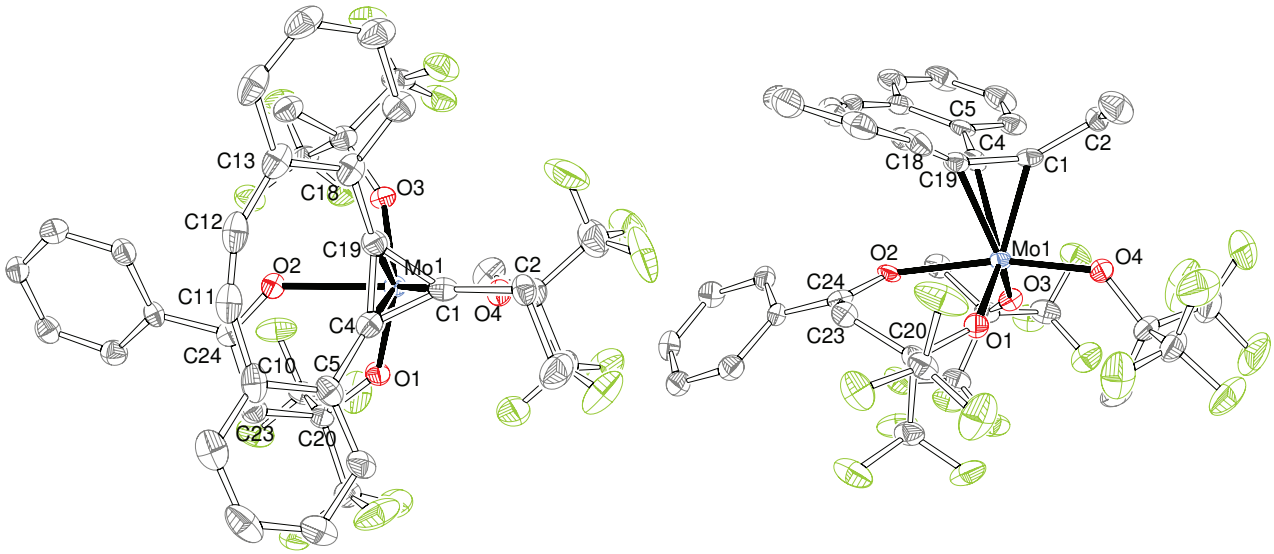

Figure 2.11: Single-crystal X-ray structure of O,O'-chelated molybdatetrahedrane **54** viewed along (left) and perpendicular to (right) the Mo–(C1–C4–C19) centroid axis. Hydrogen atoms have been omitted for clarity. Thermal ellipsoids drawn at the 50% probability level. Color code: Mo (turquoise), C (gray), O (red), F (green).

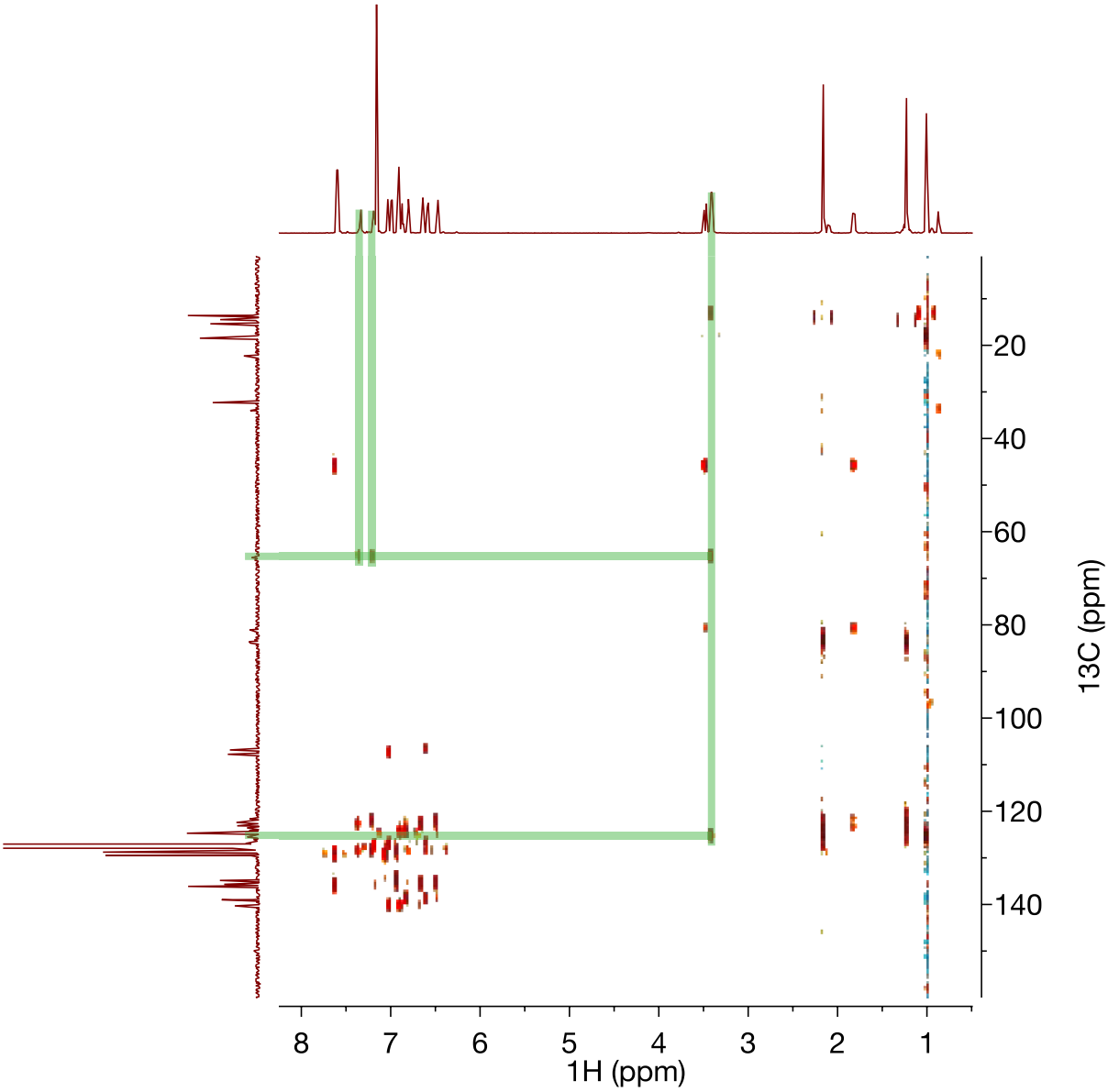

Figure 2.12: ^{1}H-^{13}C HMBC of molybdatetrahedrane **54** showing the 2- and 3-bond correlations to the carbon framework of the tetrahedrane.

To directly compare this tetrahedrane to the terminated species observed using ^{13}C-labeled **33**, an assignment of the carbon resonances of the molybdatetrahedrane core was required. Unfortunately, the sensitivity of carbons bonded to Mo are low, and due to the low symmetry of **54**, the six CF_3 groups of the three inequivalent 1,1,1,3,3,3-hexafluoro-2-propyl moieties crowd the 1D carbon spectrum with 9 quartets of quartets. Fortunately, the ethyl group from the propylidyne gives a convenient handle for indirect detection of the tetrahedrane carbons. The ^{1}H-^{13}C HMBC is depicted in Figure 2.12, clearly showing the 2- and 3-bond correlations between two carbons of the tetrahedrane at 65.6 and 125.4 ppm and the ethyl CH_2 at 3.41 ppm. Their identity can be further refined, seeing the 3-bond correlation to the *ortho*-CH on the fragment from **33** only to the upfield carbons indicating that the upfield carbons come from **33** and the downfield carbon originates as the carbyne carbon of **52**.

These chemical shifts agree reasonably well with the resonances of the labeled carbons observed in the terminated catalyst species at 49.7 and 132.6 ppm. Performing the same HMBC experiment on the propagating species with ^{13}C-labeled **33** at low temperature does not reveal any 3-bond correlations in this upfield region; correlation between the *ortho*-protons from **33** and the metallacycle carbons in the 170-200 ppm range are observed which is consistent with the metallacyclobutadiene resting state. These findings cement metallacyclobutadiene collapse into an inactive tetrahedrane as the overwhelmingly most likely candidate for the termination pathway during ROAMP of PoPE with this system.

2.5 Conclusion

The synthesis of *poly*(phenylene ethynylene)s by ROAMP opens up the possibility to incorporate these stimulus-responsive materials into more complex polymer architectures. The first member, *poly*-(*ortho*-phenylene ethynylene) PoPE, was prepared by polymerizatiion of **33** by a class of highly active alkyne metathesis catalysts supported by electron-deficient hexafluoro-tert-butoxide ligands. While these catalysts were expected to exhibit poor selectivity, multinuclear NMR, kinetic experiments, and ^{13}C-labelling studies revealed two monomer-controlled factors that enabled a successful ROAMP: catalyst sequestration by the monomer as a molybdacyclobutadiene in the resting state and slow metathesis along the polymer backbone largely due to steric hindrance. This steric preference could be exploited to give cyclic polymers by selective metathesis at a sterically- and electronically-activated butynyl endgroup.

The unusual reactivity of this monomer and catalyst system that make it such an interesting system to study also lead to its biggest failure. The achievable molecular weights of PoPE and the application of deliberate functional termination using this method is limited by a self-termination reaction. This non-hydrolytic reaction first-order in catalyst and zeroth-order in monomer leads to a catalytically-inactive organometallic species whose spectroscopic signatures are consistent with a molybdatetrahedrane. For comparison, two model systems were synthesized which would rapidly trigger the sterically-induced metallacycle

collapse by association of a tethered ligand, one of which was structurally characterized by X-ray crystallography. These model systems give spectroscopic signatures consistent with the species observed *in situ* and support its assignment as a four-coordinate analogue of these five-coordinate molybdatetrahedrane models. Future development of ROAMP systems for PoPEs would need to address this possibly fundamental instability of metallacyclobutadiene intermediates, perhaps by reducing their lifetime in solution or identifying the mechanism of their collapse.

Chapter 3

Electronic Control of Alkyne Metathesis

In this chapter, the effects of carbyne ligand and alkyne substrate electronics on alkyne metathesis are investigated. Strategies for introducing the carbyne ligand are discussed, and a kinetically-controlled method using (3,3,3-trifluoroprop-1-yn-1-yl)benzenes is developed. This late-stage installation is used to prepare a series of isosteric Mo benzylidynes to probe the effect of carbyne electronics on ROAMP initiation kinetics. The experimental results are rationalized by DFT modeling of the reaction coordinate and a general design rule for functionalized ROAMP initiators is formulated.

3.1 Structure-Property Relationships in ROAMP

The diverse applications of ring-opening olefin metathesis polymerization (ROMP) have been built upon a vast body of work that has given us a detailed understanding of each elementary step. This remarkable progress of the field from the early ill-defined catalysts to the high-performance initiators of today has been extensively reviewed.[107,108] Careful tuning of catalyst selectivity and monomer structure can control chain transfer[109] and termination, giving these chain-growth polymerizations exceptional control over polymer molecular weights and polydispersities. Yet higher order polymer structures also depend upon controlling the interface between monomer and polymer types; understanding initiation rates,[110–112] relative monomer reactivity,[113,114] and endgroup functionality[115] has enabled integration of ROMP monomers into novel block, alternating,[114,116] and gradient co-polymer structures.[117] While the control exerted by structural, electronic, and steric factors on olefin-metathesis initiators has been well studied,[112,118–120] our understanding of these effects on ROAMP is thus far anecdotal at best. For this method to tolerate a wide range of substrates and access more complex polymer architectures, it is crucial to understand how the catalyst's structure modulates initiation and propagation rates in more detail.

In contrast to its olefin metathesis relative, only in the last few years have similar developments of ROAMP begun to emerge. Early work by Fischer,[78] Bellone's pincer system,[90] and the ROAMP systems detailed in Chapter 2 have demonstrated largely substrate-controlled strategies to enable ROAMP (either by monomer/polymer steric or electronic properties). A more general understanding of factors dictating initiation/propagation rates and new strategies for the introduction of endgroup functionality both require a fundamental understanding of the reactivity of Mo carbyne complexes towards strained and unstrained alkynes. As both initiation rate and polymer endgroup are set by the first catalyst turnover, the way to improve both of these simultaneously is to modify the carbyne ligand. Understanding this behavior will dictate the catalyst and monomer design principles that lead to a successful ROAMP, especially when compensating for differential monomer reactivity in block copolymerizations.

3.2 Functional Mo Benzylidynes as Mechanistic Probes

Chapter 2 described the first ROAMP synthesis of fully-conjugated PoPE, using molybdenum carbyne complexes **15** and **23** bearing highly fluorinated alkoxides. While this ROAMP system showed that steric factors could control polymer topology by modulating the reactivity of polymer endgroups, it also highlighted the fact that the steric bulk of the carbyne substituent alone cannot modulate initiation rates without introducing other potential complications. These simple Mo carbynes bearing hydrocarbon substituents, while the most synthetically accessible, limited our ability to explore electronic effects. A late-stage installation of functional carbynes would be a much more general way to prepare an isosteric series of Mo benzylidynes as mechanistic probes.

By avoiding carrying any functionality through potentially harsh conditions during cat-

alyst synthesis (cf. Scheme 1.7), late-stage installation offers increased functional scope and can enable one-pot approaches that minimize handling and purifying sensitive organometallic complexes. Many ways to form new active olefin metathesis catalysts by transfer of functional carbenes to metals have been documented, ranging from simple cross metathesis to reaction of diazoalkanes[118] to elegant tandem ring-opening/ring-closing[121] or en-yne metathesis cascades.[122] In contrast to their carbene counterparts, very few methods of selective carbyne transfer have been reported; a method featuring both functional generality and high synthetic accessibility is to date unknown. To address this synthetic gap, we envisioned a more controlled carbyne transfer protocol. An ideal carbyne transfer agent would 1) selectively transfer the benzylidyne unit to the metal center 2) produce only volatile or insoluble co-products to facilitate removal from the desired complex, and 3) be mild enough to permit installation of sensitive functional groups.

3.3 Carbyne Transfer by Electronically-directed Alkyne Cross Metathesis

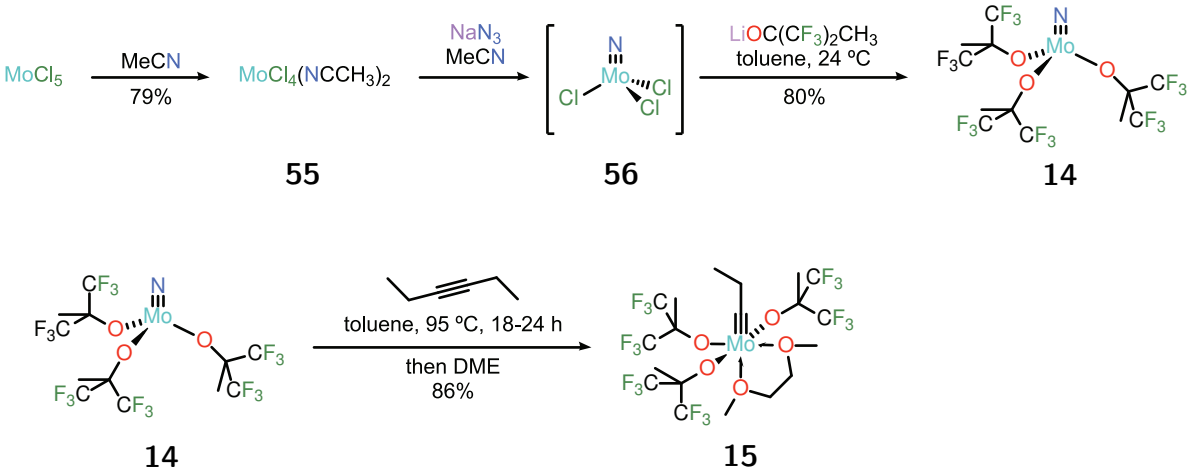

Scheme 3.1: Simple, high-valent synthesis Mo propylidyne complex **15**.

While cross metathesis of Schrock neopentylidynes such as $(CH_3)_3CMo(OC(CF_3)_2CH_3)_3$ (**57**) with internal alkynes is essentially irreversible due to the steric hindrance of the resulting ^{t}Bu-alkyne co-product, its synthesis is involved and the first step, the preparation of $(CH_3)_3CMo(CH_2C(CH_3)_3)_3$ (**58**), is highly irreproducible (even in the hands of the Schrock group itself) and represents a demanding organometallic preparation even in experienced hands.[29] Gdula and Johnson's route to propylidyne complex **15** is operationally trivial in comparison, even at multigram scales (Scheme 3.1). Starting from molybdenum pentachloride, reduction in acetonitrile gives $MoCl_4(NCCH_3)_2$ **55** in 79% yield. Installation of the

nitride by oxidation with sodium azide gives intermediate nitridotrichloride **56**, which is directly subjected to salt metathesis with $LiOC(CF_3)_2CH_3$ to give trisalkoxynitride **14** in 80% over two steps. This electron-deficient Mo nitride undergoes nitride-alkyne cross metathesis with excess 3-hexyne to give **15** in 86% yield.

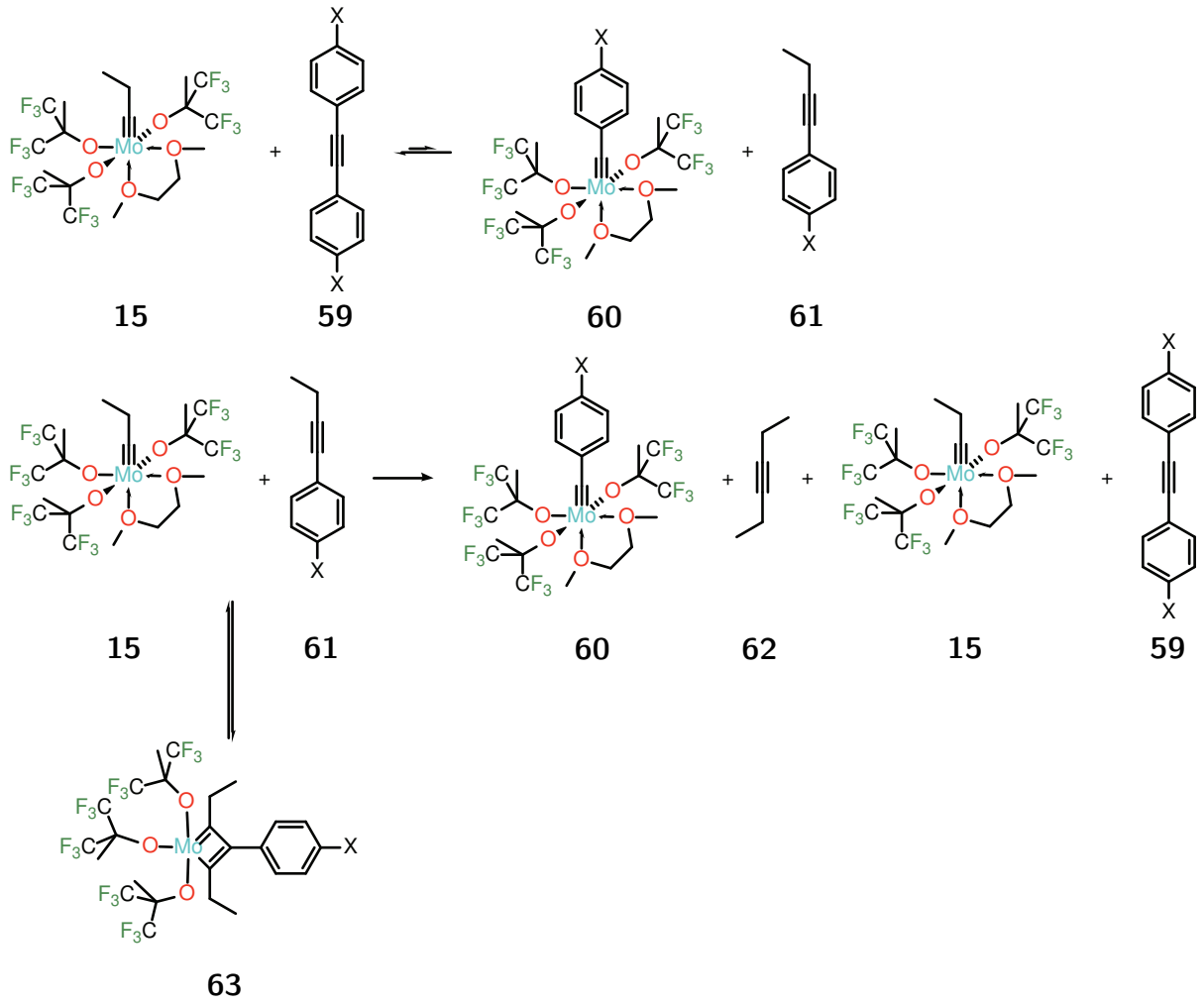

Scheme 3.2: Equilibrium metathesis strategies for functional carbyne installation. **A**. Cross metathesis with symmetrical alkynes requiring excess to drive the reaction to completion. **B**. Cross metathesis with alkyl-aryl acetylenes that is slow to approach due to degenerate metathesis through the sterically-favored metallacyclobutadiene **C**.

Initial attempts at preparing functional benzylidyne derivatives from **15** by simple cross-metathesis were complicated by selectivity and purification issues. Under equilibrium metathesis conditions (Scheme 3.2), high conversions to the desired benzylidyne by using symmetrically functionalized diarylacetylenes could only be reached by shifting the position of the equilibrium of this reversible process toward product by mass action. The desired Mo com-

plexes proved difficult to separate from the vast excess of alkyne in most cases. Cross metathesis with 1-aryl-1-propynes or 1-aryl-1-butynes led predominantly to Mo alkylidyne complexes and corresponding diarylacetylene as the thermodynamic product. Attempts to drive off the volatile dialkyl-alkynes or trap them in molecular sieves as they were formed were highly irreproducible, and led to significant decomposition or alkyne polymerization during prolonged heating.

This shouldn't have been surprising, as it has been well established that alkyl-alkynes kinetically outcompete aryl-alkynes.[25,29,75] The long reaction times needed to drive the reaction of **15** and 1-aryl-1-propynes or 1-aryl-1-butynes to completion by removing the volatile dialkyl-alkyne co-product **62** are due to the degenerate metathesis between the alkylidyne complexes and the alkyl-substituted alkynes via the sterically most accessible metallacyclobutadiene **63** (Scheme 3.2).

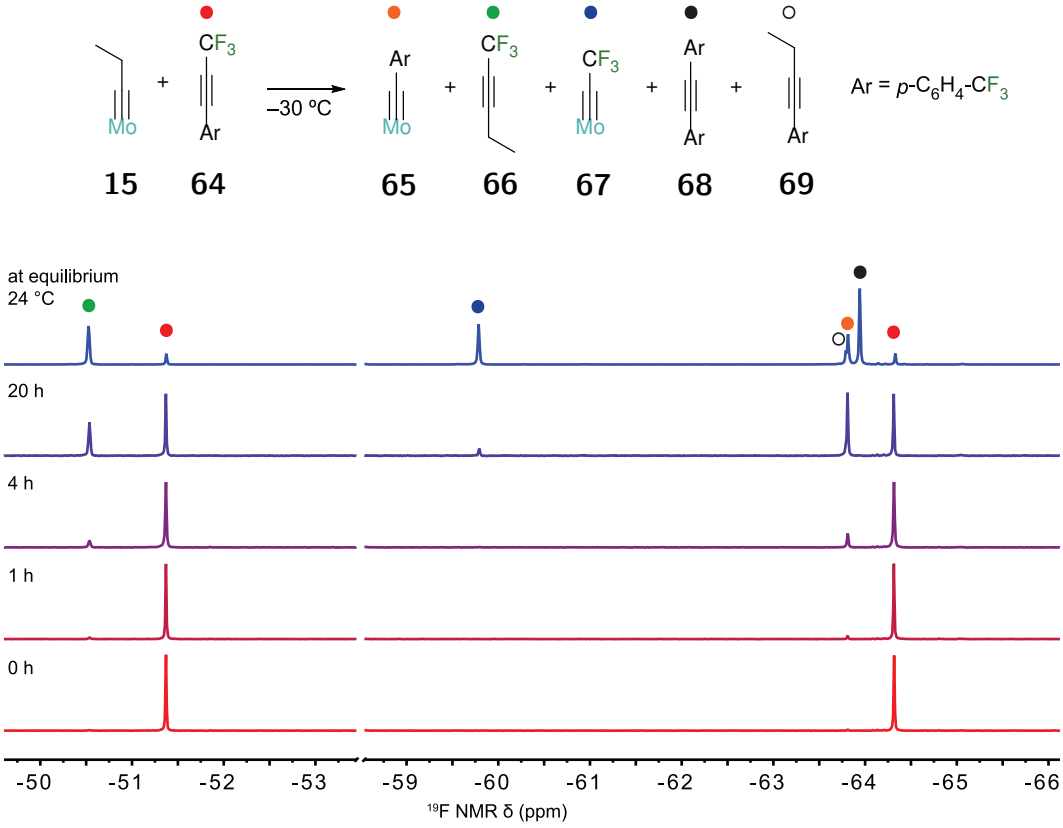

Figure 3.1: Time-resolved ^{19}F NMR spectroscopy of the carbyne transfer of **64** to **15** under kinetic control (–30 °C in $CDCl_3$). Aliquots were quenched at –30 °C with 2,2-bipyridine. The equilibrium mixture under thermodynamic control (24 °C in $CDCl_3$, top) shows the loss of selectivity due to favorable formation of the diaryl alkyne.

Cross metathesis with trifluoromethyl aryl acetylenes avoids all these problems. The electron withdrawing nature of the CF_3 group directs the orientation of cycloaddition to

favor transfer of the more donating benzylidyne to the metal. Second, the fluorinated alkyne co-product is highly volatile, allowing facile removal from the reaction mixture, and is deactivated towards further metathesis relative to dialkyl acetylenes. Finally, since the cross metathesis is mild and only one end of the alkyne is transferred, initiators bearing complex functional groups are easily prepared. As an added bonus, the ^{19}F NMR handle allows facile monitoring of the progress of the reaction.

Propylidyne complex **15** reacts with one equivalent of (3,3,3-trifluoroprop-1-yn-1-yl)benzenes rapidly at room temperature, eventually yielding a thermodynamic mixture of Mo-containing products within a few hours. Due to the electron-withdrawing nature of the CF_3 substituent, the metal center expresses a slight thermodynamic preference for the more electron-rich end of the alkyne. However, the favorable formation of diaryl acetylenes **59** ultimately drives the equilibrium backwards, away from the Mo benzylidyne. Thus, the principal Mo species at equilibrium are the more stable starting propylidyne complex and the undesired 2,2,2-trifluoroethylidyne complex **67**.

The kinetic preference for metathesis that forms the substituted Mo benzylidyne over the trifluoroethylidyne is more pronounced. The cross-metathesis of **64** at –30 °C is highly selective, as shown by ^{19}F NMR (Figure 3.1). Conservatively assuming that every trifluoroethylidyne complex **67** observed is formed by reaction with the substrate and not with the co-product **66**, the kinetic selectivity of this metathesis favors benzylidyne transfer by a factor of more than 8:1. More likely, this side product is caused in no small part from slow back reaction with **66** that builds up in solution.

We can rationalize this kinetic selectivity by considering the frontier molecular orbitals that need to overlap during the initial [2+2] cycloaddition. Figure 3.2A depicts DFT models of the Mo-C π^* orbital of an electron-rich Mo carbyne **70** supported by unfluorinated alkoxides and an electron-poor Mo carbyne **71** supported by fluorinated ligands. The electron-deficient Mo(VI) carbyne is more *electrophilic* at carbon, reflected in the larger carbon contribution to (and lower energy of) this unfilled molecular orbital. The alkyne C-Cπ HOMO is the logical compliment to them, and this orbital for 1-aryl-1-propynes and **72** are depicted in Figure 3.2B. The (3,3,3-trifluoroprop-1-yn-1-yl)benzene has a much larger π-HOMO contribution at the CF_3-bearing carbon when compared to the relatively symmetric π-HOMO of the unfluorinated analog.

This orbital asymmetry leads the [2+2] reaction with the fluorinated alkyne in the desired orientation to have much more bonding character much earlier, since the orbital interaction between the Mo-Cπ^* of **71** and the C-Cπ of **72** will be largest between the carbyne carbon and the CF_3-bearing carbon. This earlier bonding interaction lowers the overall barrier to the metathesis that leads to selective benzylidyne transfer.

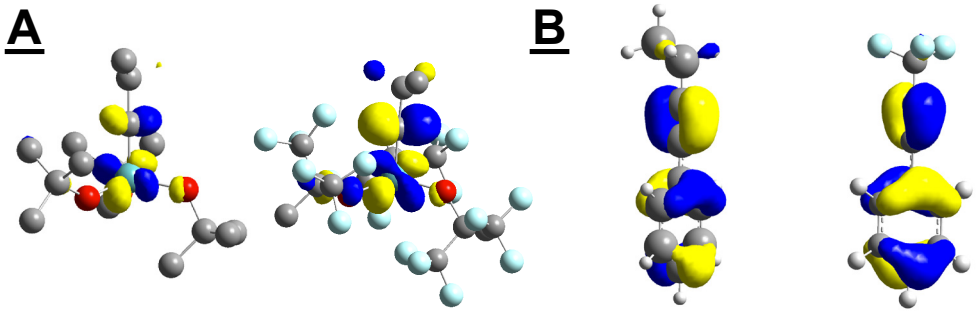

Figure 3.2: DFT models of frontier molecular orbitals involved in regioselective alkyne cross metathesis between electrophilic Mo carbyne complexes and (3,3,3-trifluoroprop-1-yn-1-yl)benzenes. **A**. Mo propylidyne complexes supported by $OC(CH_3)_3$ or $OC(CF_3)_2CH_3$ ligands showing larger Mo-Cπ^* character on the carbyne carbon in the more electron-deficient complex. **B**. Alkyne C-Cπ HOMO of 1-phenyl-1-propyne and (3,3,3-trifluoroprop-1-yn-1-yl)benzene showing the asymmetry induced by the electron-withdrawing CF_3 group.

3.4 ROAMP Initiator Synthesis by Benzylidyne Transfer to Mo Alkylidynes

There are several different synthetic routes to (3,3,3-trifluoroprop-1-yn-1-yl)benzenes. Scheme 3.3 highlights the three principal retrosynthetic disconnections used to prepare a library of these alkyne substrates: direct oxidative trifluoromethylation of terminal alkynes, "intramolecular Wittig" reactions of β-oxo ylides, and transition metal cross coupling reaction of an appropriate 3,3,3-trifluoropropynyl metal synthon. The Cu-mediated trifluoromethylation of terminal alkynes works efficiently only for electron-rich alkynes, and yields predominantly Glaser coupling for electron-deficient ones (except on small scales[123]). While the "intramolecular Wittig" gives the cleanest reaction, since the product distills or sublimes out of the reaction mixture, the temperature required increases with increasingly electron-rich substrates (reaction of methoxy substrate **76** is slow even at 300 °C). Cross coupling works on more sensitive substrates, with the *in situ* generation of 3,3,3-trifluoropropynyl zinc reagent **83** representing a convenient option.

This kinetic selectivity can be exploited to transfer a range of benzylidynes, from electron rich to very electron poor. By adding ~1 equivalent of substituted (3,3,3-trifluoroprop-1-yn-1-yl)benzene to **15** in toluene at –60 °C and warming to room temperature under vacuum to remove **66** as it is formed, the desired benzylidynes can be isolated in up to 95% yield by NMR, or 46–83% after recrystallization (Table 3.1).

Coordinating functional groups are tolerated along with basic, electrophilic, and oxidation- or reduction-prone functional groups that would otherwise be unstable to the traditional

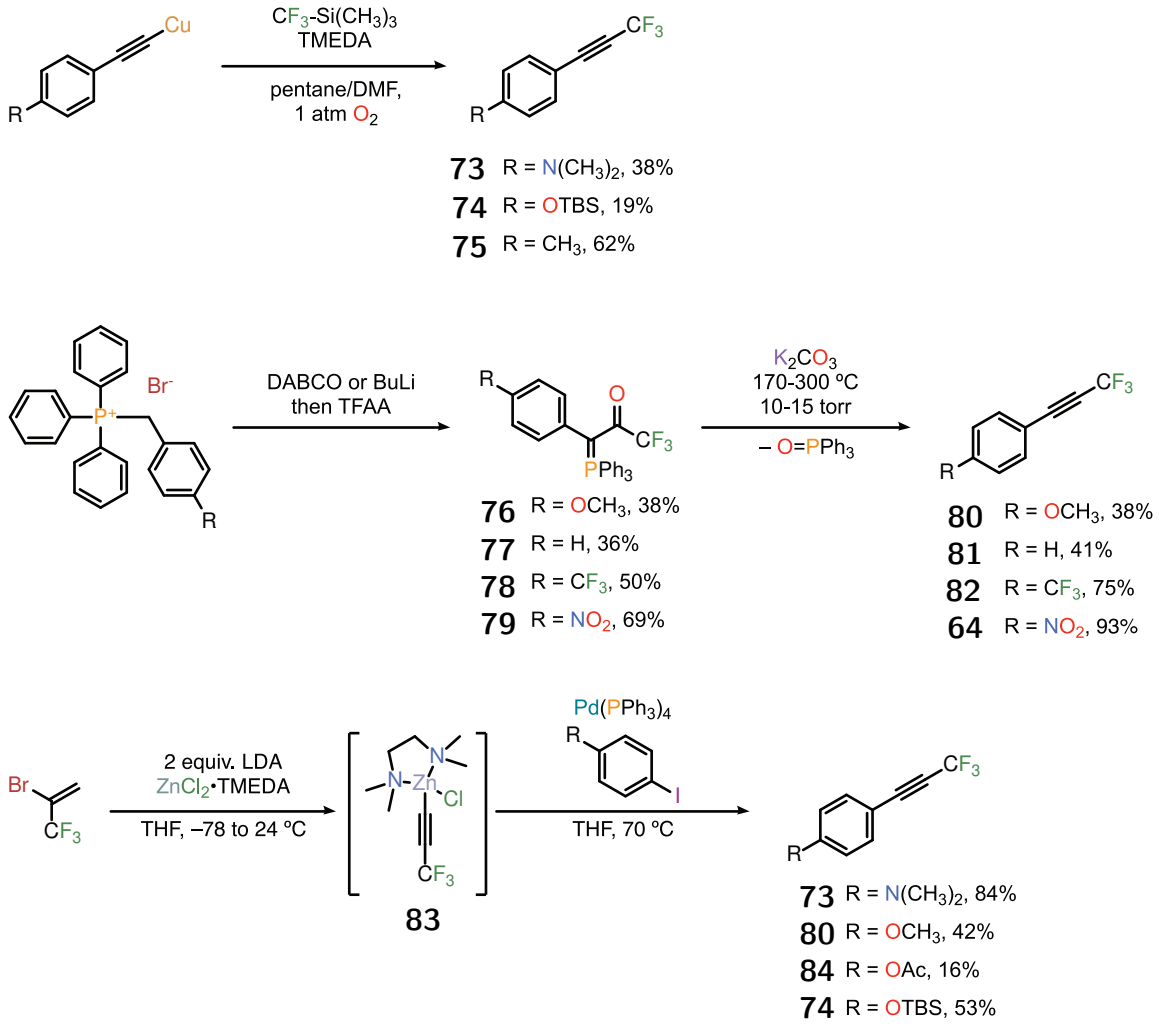

Scheme 3.3: Synthesis of (3,3,3-trifluoroprop-1-yn-1-yl)benzenes.

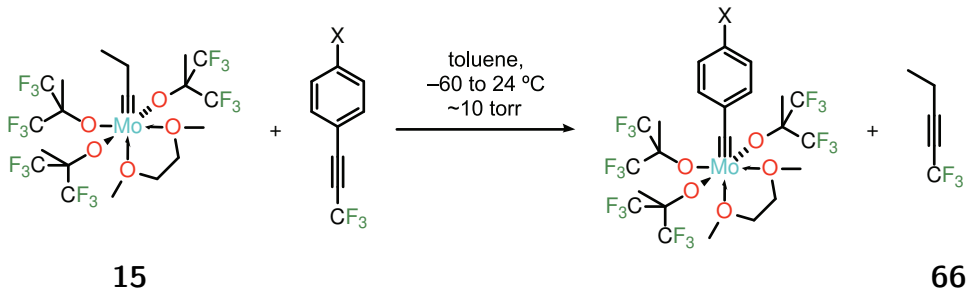

Scheme 3.4: Electronically-directed cross metathesis synthesis of a library of 4-substituted benzylidyne complexes.

Table 3.1: Functional benzylidynes synthesized by electronically-directed cross metathesis with (3,3,3-trifluoroprop-1-yn-1-yl)benzenes (Scheme 3.4). Yields are isolated yield after recrystallization; crude NMR yields in parentheses.

X =	Alkyne	Addition T (°C)	Benzylidyne	% Yield
$N(CH_3)_2$	**73**	24	**85**	48 (96)
OCH_3	**80**	0	**86**	66 (94)
CH_3	**75**	–20	**87**	83 (95)
H	**81**	–20	**88**	79
OAc	**84**	–60	**89**	77 (92)
CF_3	**64**	–60	**65**	74 (92)
NO_2	**82**	–60	**90**	62 (83)

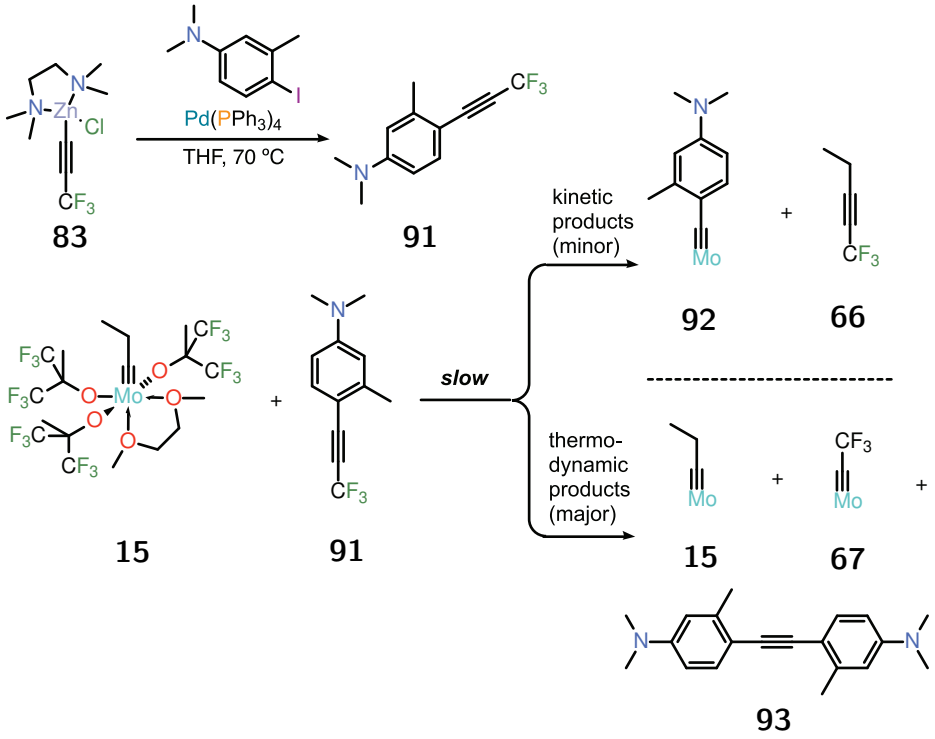

Scheme 3.5: Synthesis of and inefficient benzylidyne transfer from *ortho*-methyl-substituted substrate **91**, demonstrating that steric factors can hinder electronic control in cross metathesis.

"low-valent" route to these benzylidynes. Unfortunately, any steric perturbation to the system that slows the reaction leads to poor selectivity; even the simple addition of an ortho-methyl group to alkyne **73** to give alkyne **91** leads to a reaction that is so slow that it is challenging to perform under dynamic vacuum for the tens of hours it would require to go to completion. The kinetic selectivity for metathesis between **15** and **91** seems to remain, but the reaction to form the hindered benzylidyne is very slow compared to other metathesis reactions. Benzylidyne **92** only forms ~5 times faster than **93** which is presumably produced (at early reaction times) by the reaction of the desired product **92** with the starting alkyne **91**. As equilibrium is established, the formation of the highly hindered diarylalkyne **93** eventually drives the reaction away from the product by formation of **67**. This sterically-driven equilibrium might itself be useful for preparation of functionalized benzylidynes, if suitable substrates were developed.

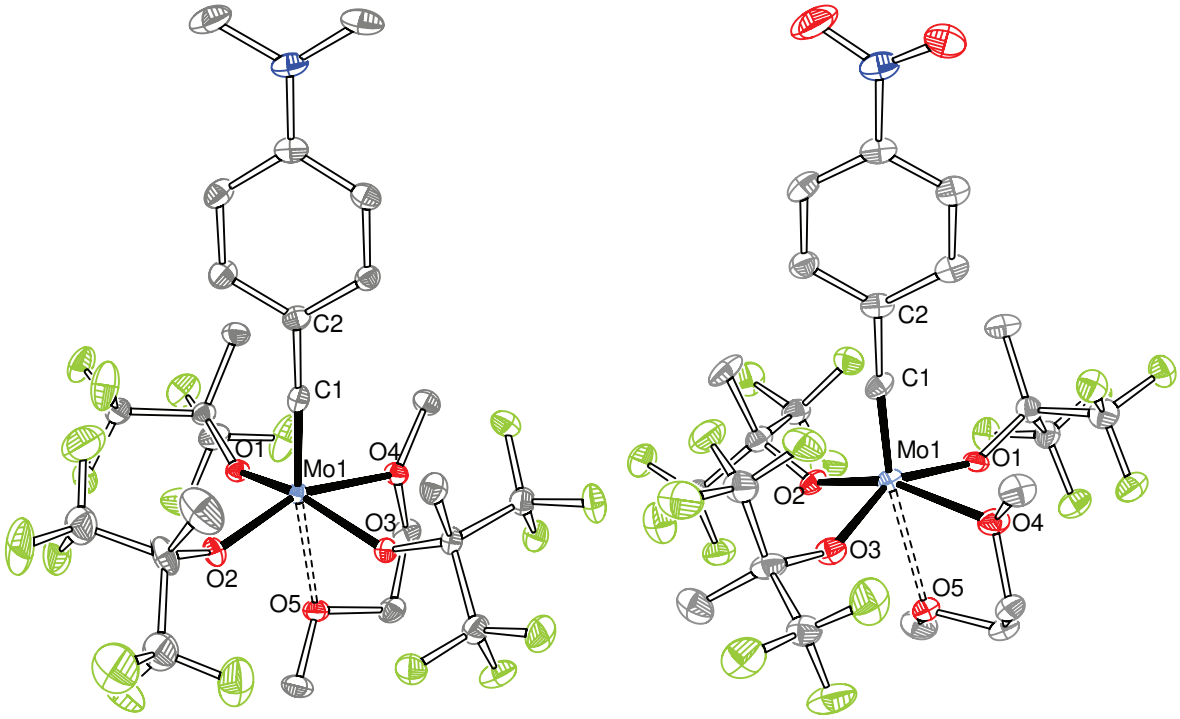

Figure 3.3: Single-crystal X-ray structures of the 4-substituted benzylidynes bearing electron-donating $N(CH_3)_2$ (**85**) (left) or electron-withdrawing NO_2 groups (**90**) (right). Hydrogen atoms are omitted for clarity. Thermal ellipsoids drawn at the 50% probability level. Color code: Mo (turquoise), C (gray), O (red), N (blue), F (green).

Spectroscopic evidence indicates that the molybdenum benzylidyne complexes prepared in this series are isostructural, in line with the crystallographic analysis of the series endpoints, complexes **85** and **90**. Dark green plates of **85** from Et_2O/pentane (1:1) and orange prisms of **90** from toluene/pentane (1:1) suitable for X-ray crystallography were obtained from saturated solutions at –35 °C. In both complexes the geometry at the Mo center is

pseudo-octahedral. X-ray crystallography of **85** (Figure 3.3, left) confirms the expected C(1)–Mo(1) triple bond with a short bond length of 1.761(3) Å and a C(2)–C(1)–Mo(1) angle of 177.3(2)°. Three hexafluoro-tert-butoxide ligands adopt a meridional conformation featuring Mo(1)–O(1), Mo(1)–O(2), and Mo(1)–O(3) distances of 1.968(2) Å, 1.928(2) Å, and 1.975(2) Å. One equiv of DME is coordinated to the Mo complex in the crystal. The bond distances are 2.226(2) Å and 2.415(2) Å for the Mo(1)–O(4) cis and Mo(1)–O(5) trans to the carbyne, respectively.

X-ray crystallography of **90** (Figure 3.3, right) shows that substitution of the electron donating $N(CH_3)_2$ group in **85** for an electron with-drawing NO_2 group in **90** has only a small effect on the C(1)–Mo(1) bond length (1.754(7) Å) and C(2)–C(1)–Mo(1) bond angle (174.8(6)°). More pronounced changes are observed for the bond lengths between the molybdenum and the three hexafluoro-tert-butoxide ligands. The weaker π-donating character of the carbyne in **90** is partially compensated by a contraction of the Mo(1)–O(1), Mo(1)–O(2), and Mo(1)–O(3) bond lengths, 1.958(4) Å, 1.922(4) Å, and 1.952(5) Å respectively.

3.5 Electronic Effects in ROAMP Initiation

In Chapter 2 we discussed the finding that in the polymerization of dialkyne **33**, the cycloaddition step is fast relative to the rate-determining ring-opening cycloelimination reaction (Scheme 3.6). This rate of ring-opening cycloelimination, k_{i}, limits the overall rate of initiation, $k_{\mathrm{i,obs}}$. Upon addition of **33** to an excess of a Mo benzylidyne, the monomer is consumed in less than 60 s at 25 °C to form the molybdacyclobutadienes **41**. By ^{19}F and ^{1}H NMR, these species decay in a first-order process to ring-open to the new initiated benzylidyne **94** (Figure 3.4). As the initial cycloaddition is practically instantaneous at 25 °C, the observed rate of initiation, $k_{\mathrm{i,obs}}$ can be approximated by the rate limiting step, k_{i}. Fitting the experimental data to a first-order exponential decay of the metallacyclobutadienes **41** gives a unique rate constant k_{i} for the cycloelimination step for each of the ROAMP initiators. The trend indicates that more electron-deficient benzylidynes initiate more rapidly.

As this isosteric benzylidyne series spans the Hammett parameter space, a linear free-energy relationship (LFER) analysis provides further insight into the structure of the rate determining transition state (Figure 3.5). A positive Hammett reaction constant $\rho = +0.36(6)$ is indicative of either the buildup of negative charge or the decrease of positive charge in the benzylic α-carbon in the rate-determining transition state. The significant rate acceleration of the ROAMP initiation step upon introducing electron withdrawing groups on the benzylidyne complex is unusual and has not been observed for the analogous ROMP with Mo or Ru carbene complexes.[118] This contrast is attributable to the extended π-conjugation of the metallacyclobutadiene that mediates resonance stabilization effects more efficiently than a saturated metallacyclobutane does.

To facilitate interpretation of the LFER analysis, we used theory to explore the potential energy surface associated with the ROAMP initiation reaction. Figure 3.6 summarizes the

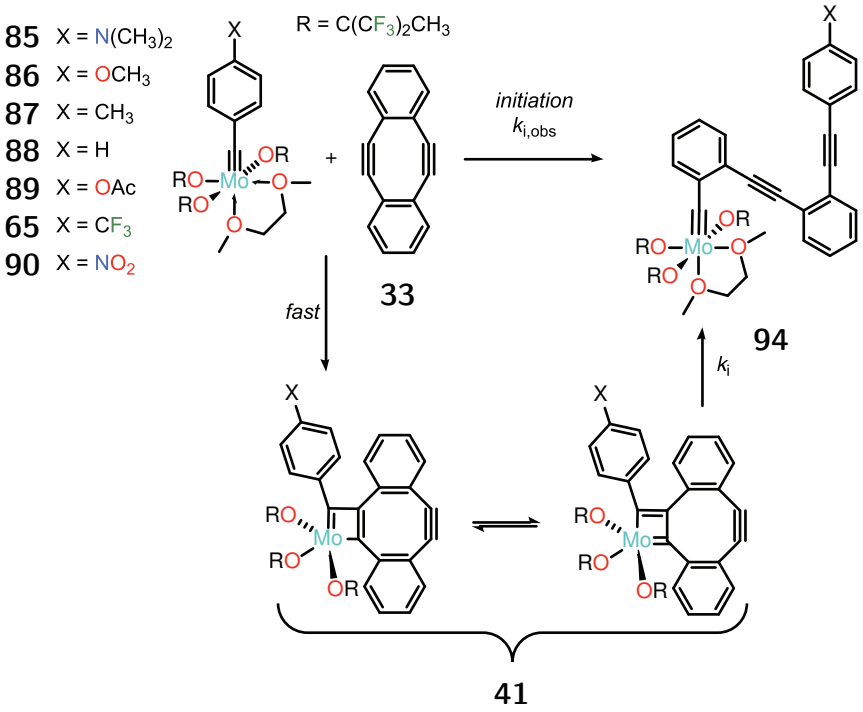

Scheme 3.6: ROAMP initiation step consisting of rapid coordination/cycloaddition of **33** followed by slow unimolecular cycloelimination, with the overall rate constant $k_{\mathrm{i,obs}}$ being approximately equal to k_{i}.

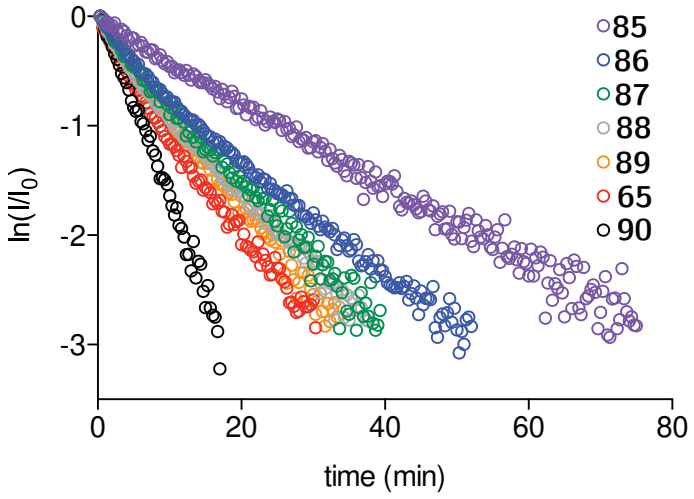

Figure 3.4: First-order kinetic plot of the rate-limiting ring-opening cycloelimination step of the initiation of ROAMP of **33** with Mo benzylidynes at 25 °C in C_6D_6.

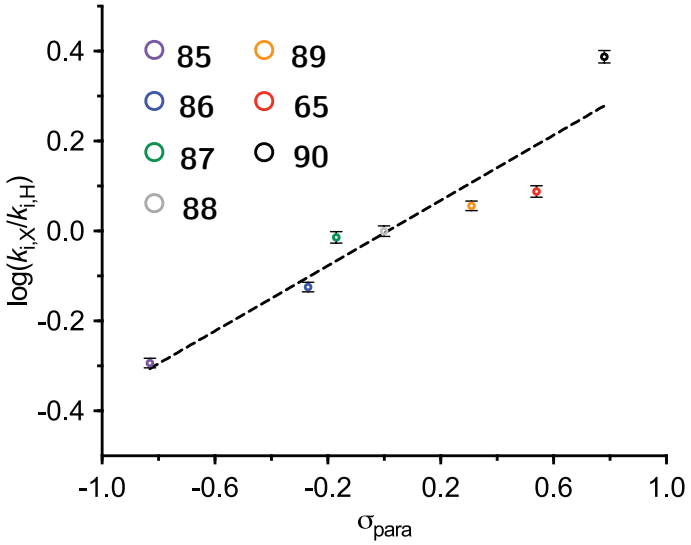

Figure 3.5: Hammett LFER analysis of the rate of ROAMP initiation (Scheme 3.6) as a function of benzylidyne substituent electronics. Line of best fit corresponds to a ρ of + 0.36(6).

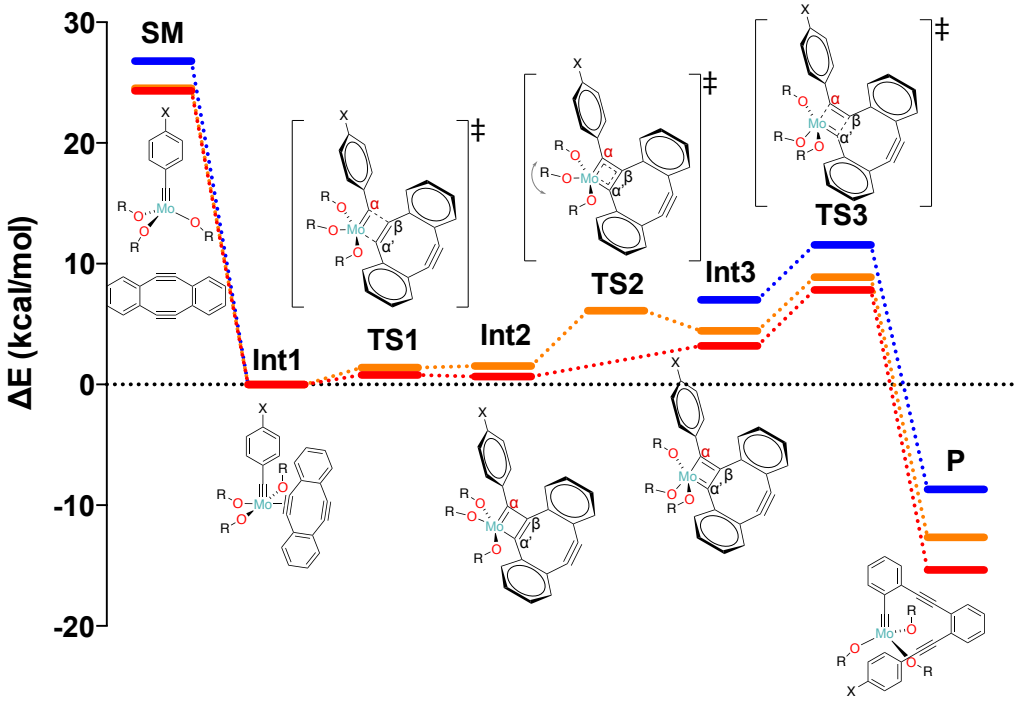

Figure 3.6: Calculated reaction coordinate diagram of the rate determining step in the ROAMP initiation reaction for three model complexes representing **88** (X = H, orange), **65** (X = CF_3, red), and **85** (X = $N(CH_3)_2$, blue). (DFT ωB97xD; CHNOF (6-31G+(d,p)); Mo (SDD ECP MWB28); ZPE corrected) R = $CCH_3(CF_3)_2$

results of density functional theory (DFT) calculations on three model complexes representative for the tetracoordinate Mo complexes resulting from the reversible dissociation of DME from the initiator (equilibria involving reversible association of DME were not included to reduce the number of potential intermediates and degrees of freedom). The coordination of **33** to the tetracoordinate complex **SM** is an exothermic process (–24 kcal mol^{-1}) and leads to intermediate **Int1**. A nearly barrierless cycloaddition step (**TS1**, for X = H) yields the initial metallacyclobutadiene intermediate **Int2** that is localized on a very flat potential energy surface. **Int2** undergoes a double bond isomerization and ligand sphere reorganization to give the secondary molybdacyclobutadiene **Int3**. While ^{19}F NMR spectroscopy suggests an equilibrium between interconverting metallacyclobutadienes, the barrier is only 1.5 kcal mol^{-1} by DFT gas phase calculations. The rate-determining step in the ROAMP initiation is associated with the cycloelimination leading from **Int3** through **TS3** to the product **P**. While theory underestimates the magnitude of the barriers, the relative trends **TS3**(X = $N(CH_3)_2$) > **TS3**(X = H) > **TS3**(X = CF_3) faithfully reproduce the experimental results.

Natural population analysis (NPA)[124] for X = H shows a buildup of negative charge at the benzylic α-position consistent with our Hammett LFER analysis. The charge decreases from +0.21 on the carbyne carbon atom in **Int1** to +0.14 in **TS1**, +0.07 in **Int2**, +0.11 in **TS2**, +0.03 in **Int3**, and finally –0.01 in the rate-limiting transition state **TS3**. As expected, electron donating substituents (X = $N(CH_3)_2$) lead to an increase of the activation barrier, while electron withdrawing groups (X = CF_3) stabilize the negative charge buildup in the transition state thereby lowering the energy of **TS3**.

3.6 Formulation and Application of ROAMP Initiator Design Rules

The observed rate acceleration attributed to the electronic stabilization of the cycloelimination transition state acts exclusively on the initiation step, k_i. The rate of propagation, k_p, is essentially unaffected by this substituent effect as the distance between the end group and the reaction center increases with each monomer in the growing polymer chain. Electron withdrawing substituents are thus uniquely suited to selectively increase k_i over k_p, a crucial requirement for the synthesis of living polymers with narrow molecular weight distributions.

This initiator effect is most apparent at high catalyst loadings (e.g. [**33**]/[Mo] = 10/1, Table 3.2). The molecular weight dispersity of the resulting polymers by SEC ranges from 2.1 for electron donating X = $N(CH_3)_2$ (**85**) to 1.3 for electron withdrawing substituents where X = OAc (**89**), CF_3 (**65**), NO_2 (**90**). Polymers resulting from ROAMP initiators **85** and **86** feature an electron-rich activated alkyne as an end group that promotes intra- and intermolecular chain-transfer reactions (depending on concentration). In fact, **85** is a far superior catalyst for the synthesis of cyclic PoPE (as compared to **15**), yielding > 60% macrocyclic products in less than 2 h. ROAMP initiators featuring electron-withdrawing groups instead deactivate the terminal alkyne preventing undesired chain-transfer processes

that contribute to a broadening of the dispersity.

Table 3.2: Molecular weight statistics for PoPEs prepared by ROAMP with various functionalized benzylidyne initiators.

X =	**[33]/[Mo]**	**M_n (SEC)**	**M_w (SEC)**	**Đ(M_w/M_n)**	**cyclic PoPE**
$N(CH_3)_2$	10/1	800	1700	2.1	60%
OCH_3	10/1	1800	3400	1.9	20%
CH_3	10/1	1900	3000	1.6	<1%
H	10/1	1800	2500	1.4	<1%
OAc	10/1	2500	3300	1.3	<1%
CF_3	10/1	2600	3400	1.3	<1%
NO_2	10/1	2600	3500	1.3	<1%

Besides the obvious mechanistic advantages provided by electron withdrawing substituents in a controlled living ROAMP ($k_i > k_p$), the versatile and mild carbyne transfer reaction with readily accessible (3,3,3-trifluoroprop-1-yn-1-yl)benzenes described above gives access to functional telechelic polymers. Electron-withdrawing substituents such as the OAc group in the acyloxybenzylidyne **84** provide a versatile functional handle that serves as an adaptable chemical linker that do not promote cyclic polymer formation. To demonstrate this concept, we synthesized several (3,3,3-trifluoroprop-1-yn-1-yl)benzenes bearing orthogonal polymerization initiators with electron-withdrawing ester linkages. The TBS-protected phenol derivative **74** is conveniently deprotected to the unstable free phenol **95**, which is immediately coupled with a functionalized carboxylic acid. The 2-bromoisobutyrate ester **96** could serve as an atom-transfer radical polymerization (ATRP) initiator, **97** bears a Hawker alkoxyamine for nitroxide-mediated polymerization (NMP), while **98** features a trithiocarbonate group that acts as a reversible addition-fragmentation chain-transfer (RAFT) agent (Scheme 3.7). While purification issues related to the equilibrating alkoxyamine diastereomers hampered the attempts to use **97**, benzylidyne transfer with **96** and **98** cleanly yields the functionalized Mo complexes **99** and **100**. ROAMP of **33** with functional initiators **99** or **100** followed by quenching with excess 3-hexyne yields initiator-functionalized PoPE **101** and **102**.

Attempts at chain extension of **101** under many metal-mediated ATRP conditions failed. Some reductive debromination of the initiator was observed that could be attributed to residual Mo species. Even after removing metal residues by column chromatography, both Cu[125] and Fe[126]-mediated ATRP systems gave uncontrolled radical polymerizations giving high molecular weight polymers with large dispersities (Đ = 7–14). Using unfunctionalized PoPE as an additive hindered ATRP using other initiators, suggesting that the alkynes of the polymer backbone were sequestering the metal centers that normally reversibly deactivate the active radical chains to provide polymerization control. This would make sense, since usually the role of ligands in ATRP is to promote the formation of the higher-valent metal halide deactivator (e.g. CuX_2); alkynes, being π-acceptor ligands could stabilize the low-valent "activator" state (e.g. CuX) and cause loss of polymerization control by preventing

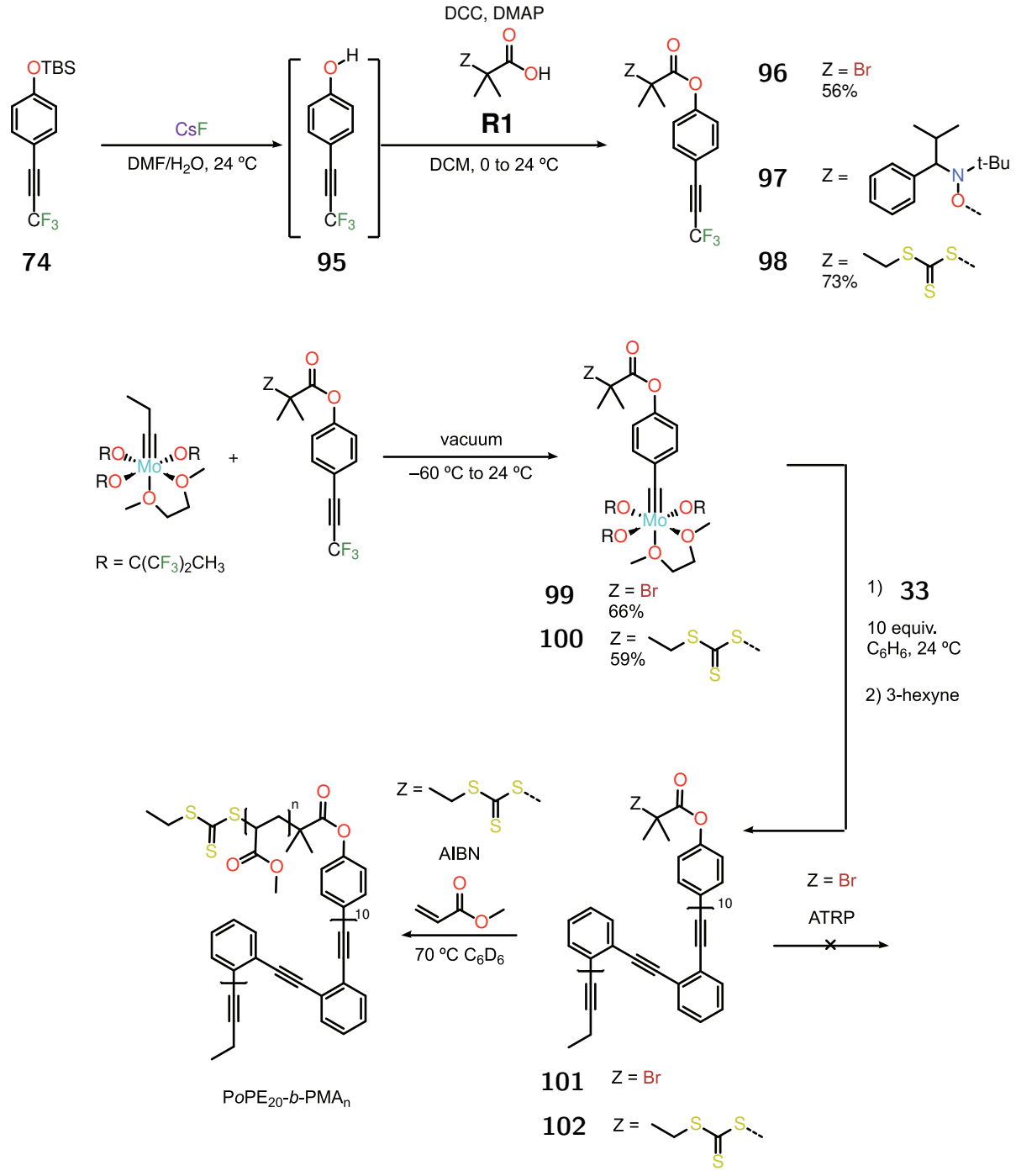

Scheme 3.7: Synthesis of bifunctional ROAMP initiators for chain extension by orthogonal radical polymerization.

radical chain deactivation. Even using Me_6TREN, one of the strongest Cu-binding ligands used in ATRP,[125] had essentially no effect.

In contrast to the failures of ATRP, using trithiocarbonate-bearing $PoPE_{20}$ **102** as a macroinitiator for metal-free RAFT polymerization works efficiently. Chain extension with methyl acrylate initiated by AIBN in benzene at 70 °C gives a *poly*(methyl acrylate) (PMA) block copolymer, PoPE-*block*-PMA. The amphiphilic block copolymer can be isolated from a small amounts of PMA homopolymer either by precipitation in ethanol, Soxhlet extraction with acetonitrile, or by preparative SEC depending on the weight of the PMA block. The molecular weight increases from 2.5 kDa for the PoPE macroinitiator, to 9.6 kDa (corresponding to $PoPE_{20}$-*block*-PMA_{90} by ^{1}H NMR analysis) without a significant broadening of the dispersity (Đ= 1.3). Block copolymers with molecular weights up to 36 kDa, $PoPE_{20}$-*block*-PMA_{380}, could be prepared with a slight broadening of the molecular weight distribution (Đ= 1.5).

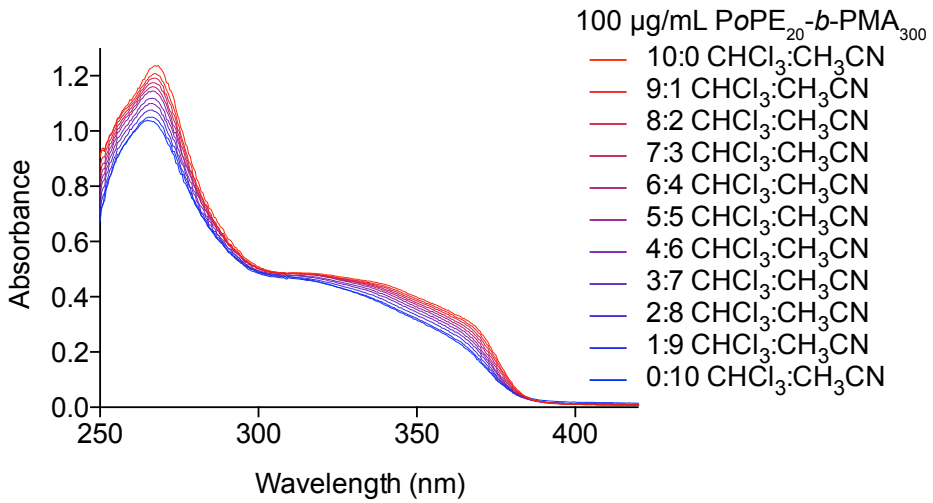

Figure 3.7: UV-Vis absorption spectrum of $PoPE_{20}$-*block*-PMA_{380} as a function of solvent polarity in $CHCl_3$/CH_3CN mixtures.

These amphiphilic block copolymers, unlike their PoPE homopolymers, are soluble in a wide range of polar and nonpolar solvents. This provided the opportunity to study their foldameric nature by examining their spectral properties as a function of solvent polarity. While PmPEs show a strong solvatochromic response due to folding in organic solvents,[83] when made soluble enough to test their response in water, only a weak hypochromic response is observed instead.[88] Similarly, the spectral features of $PoPE_{20}$-*block*-PMA_{380} vary hypochromically as the proportion of acetonitrile in chloroform increases (Figure 3.7); the absorption maximum decreases in intensity but barely shifts from 268.4 nm to 265.5 nm, while the shoulder at ∼330–370 nm decreases in instensity. This could either reflect the real minimal change in effective conjugation length and/or oscillator strength upon folding, or be a due to an already mostly-folded state even in the less-polar $CHCl_3$ solvent due to a locally polar solvent environment created by the polar PMA block. This is the first time that

the solvophobic folding of PoPEs has been studied in this way, but examining the role of the copolymer block would be necessary to disentangle these possible explanations for their spectral behavior.

3.7 Conclusion

Understanding electronic factors that control reactivity and selectivity in alkyne metathesis is a critical step in facilitating the design of successful ROAMP catalyst and monomer systems. This chapter described a regioselective carbyne transfer protocol using electronically-directed alkyne cross metathesis of (3,3,3-trifluoroprop-1-yn-1-yl)benzenes. This late-stage functionalization strategy provides easy access to a diverse range of functional Mo benzylidynes in a kinetically-controlled process that largely overrides the usual thermodynamic distribution of Mo products. It further enables the synthesis of ROAMP initiators bearing nucleophilic and electrophilic functional groups that are otherwise incompatible with traditional synthetic routes. Kinetic and Hammett LFER analysis reveals electron-deficient benzylidynes increase the rate of initiation k_{i} over the rate of propagation, k_{p}. The observed linear free energy relationship informs the rational design of functional ROAMP initiators, where electron-withdrawing groups not only lead to polymers with lower dispersity but also protect endgroup functionality from undesired cross metathesis. We demonstrate the power of this synthetic method and mechanistic insights in the facile synthesis of well-defined PoPE-containing block copolymers. Future studies designed to probe the effects of *substrate* electronics in ROAMP propagation rates would be a logical and valuable extension of this chapter, and would be critical to the successful preparation of block copolymers by ROAMP.

Chapter 4

Polymer-Templated Graphene Nanoribbons

In this chapter, graphene nanoribbons (GNRs) are introduced and motivations for their synthesis via alkyne-containing polymer templates are elaborated. The core concept of inverse-electron-demand Diels-Alder annulation of internal alkynes is applied to a retrosynthetic approach to chevron GNRs (cGNRs) based on 2,3,4,5-tetraarylcyclopentadienones and an alkyne-containing polymer precursor prepared by ROAMP.

4.1 Graphene Nanoribbons as a Target For ROAMP

Graphene nanoribbons (GNRs) straddle the border between linear, 1D ladder polymers and extended 2D graphene. While they share a host of the attractive physical and electronic properties of bulk 2D graphene, quantum confinement along one dimension opens a tunable bandgap that positions GNRs as privileged candidates for next-generation electronic devices. The extremely small (< 2 nm) lateral dimensions, the control of translational symmetry, and the chemical fidelity of edge structures required to manifest these quantum effects in a controlled and reproducible materials system defy traditional top-down synthetic approaches.[127] Bottom-up approaches instead give access to these narrow strips of graphene from molecular precursors via surface-mediated (Figure 4.1) or solution-phase polymerizations, allowing chemists to bring to bear the tools of organic and polymer chemistry to precisely engineer the location of every atom in each repeat unit at the sub-nanometer scale.[128] This strategy has enabled rapid advances in our understanding of the role of nanoribbon width,[129–131] dopant atom incorporation,[132–135] crystallographic symmetry,[136,137] and topological phenomena[138,139] in determining their electronic structure.

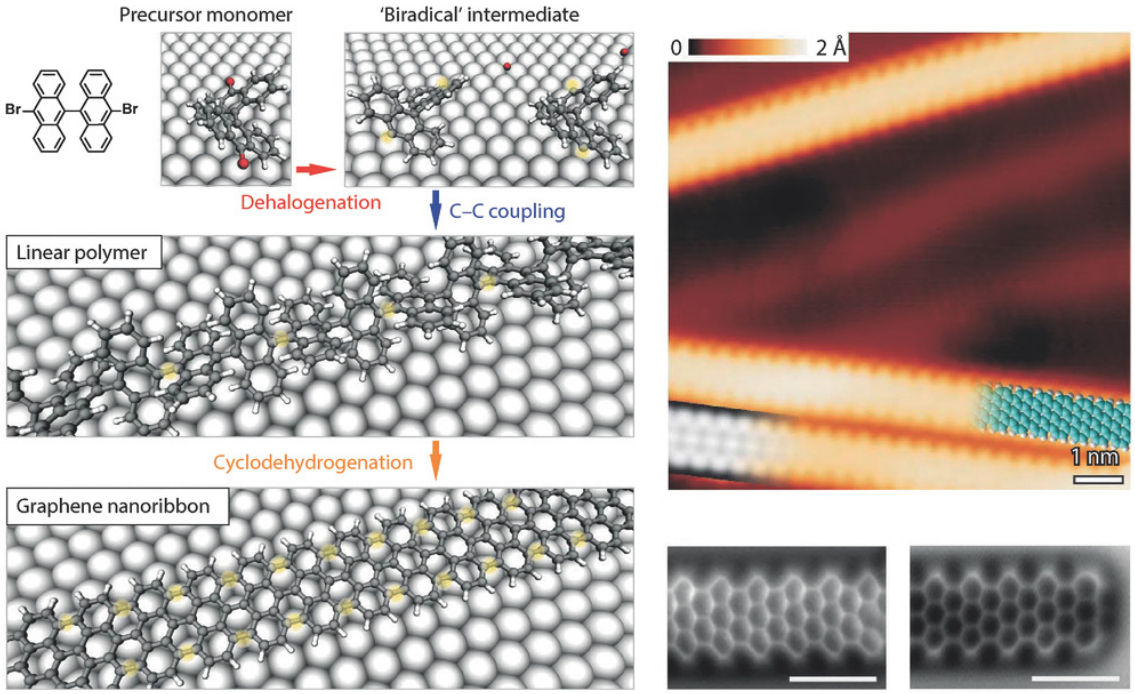

Figure 4.1: Surface-catalyzed step-growth polymerization/dehydrogenation approach to bottom-up synthesis of GNRs (left), and scanning-tunneling microscopy and non-contact atomic force microscopy images of the resulting GNRs (right). Reproduced from reference [140].

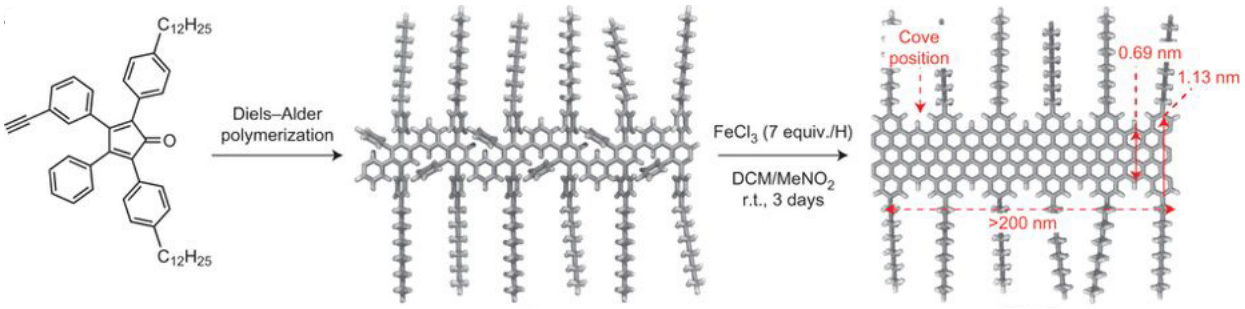

Figure 4.2: Solution-phase step-growth polymerization/Scholl oxidation approach to bottom-up synthesis of "cove" GNRs. Reproduced from reference [141].

However, the interface of two or more GNRs of dissimilar electronic band structures fused along a well-defined interface forms the basis of the most promising GNR device architectures.[142,143] While the synthesis of these heterojunctions can be facilitated by hierarchical growth strategies or by scanning probe tip manipulation, the former still yields a statistical distribution of junction interfaces within a single ribbon while the throughput of the latter is extremely limited.[144,145] These tools have proven adequate when small populations of single-junction GNRs are needed to study their electronic interfaces by single molecule spectroscopy, yet transistor device fabrication demands both high structural fidelity and throughput for realistic device yields. These problems are only magnified when multiple predetermined heterojunctions along a single GNR are desired.

The difficulty of assembling GNR heterojunctions is inherent to the techniques used to assemble polymeric GNR precursors, which to date have exclusively relied on step-growth polymerizations.[146] From a polymer perspective, a GNR heterojunction is analogous to the junction unit of a block copolymer; the logical solution to this statistical challenge is to prepare GNRs using a controlled, ideally living, (co)polymerization.[128] Living ring-opening metathesis polymerization (ROMP) has revolutionized the synthesis of precision polymeric materials and enabled ready access to polymers with control of sequence,[107,117] topology,[147] stereoregularity,[108] and self-assembly.[113,148] ROMP has become a valuable tool in polymer synthesis in large part due to its tolerance of complex, polyfunctional side chains. While the unsaturated polymer backbones prepared by ROMP are also primed for post-polymerization elaboration, this is a far less common strategy.[149–151] In the context of GNR synthesis, olefins are undoubtedly useful polyarylene building blocks, but alkynes are particularly valuable due to their redox equivalence to aromatic sp^2 carbons.[152–156] Ring-opening alkyne metathesis polymerization (ROAMP) therefore stands as a privileged technique to prepare alkyne-containing block copolymer precursors amenable to further elaboration of the carbon-carbon triple bonds into controlled GNR heterostructures.

4.2 Strained Cyclooctaphane Diynes for *Poly*(*m,m'*-biphenylene ethynylene)

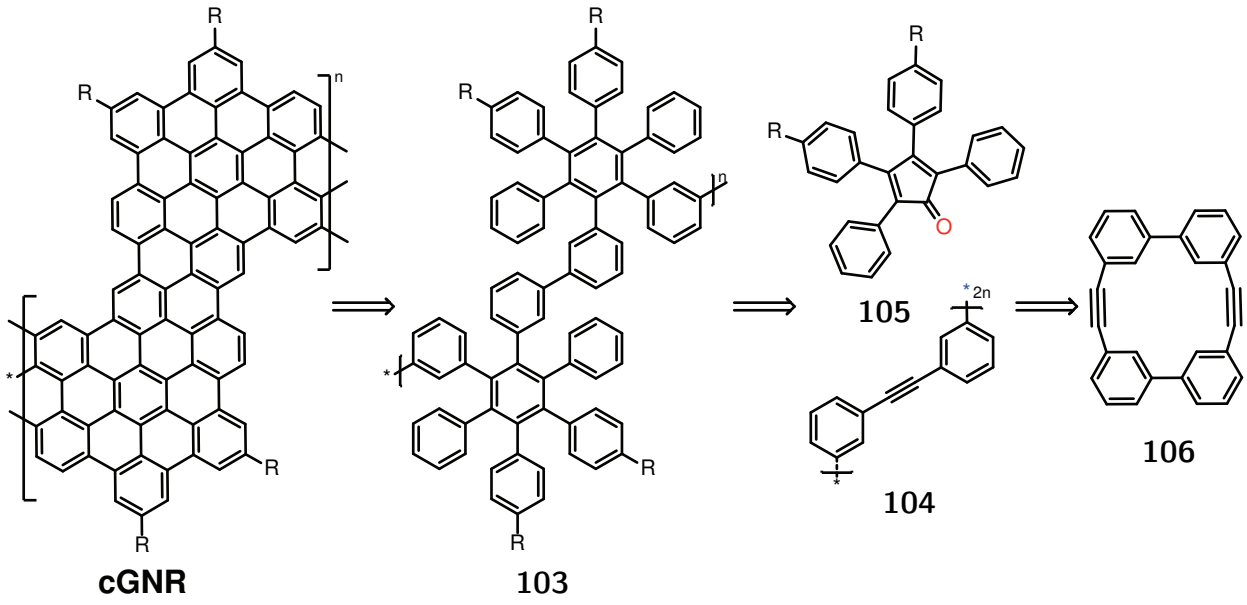

Scheme 4.1: Retrosynthetic analysis of cGNRs via inverse-electron demand Diels-Alder and ROAMP.

Leveraging the core concept of the inverse-electron-demand Diels-Alder, but turning instead to the 2,3,4,5-tetraarylcyclopentadienones, we can retrosynthetically decompose chevron GNRs (cGNRs) into a polyphenylene **103**, which can be accessed from alkyne-containing polymer, *poly*(*m,m'*-biphenylene ethynylene) (mmBPE) **104**, which in turn can be prepared by the ROAMP of cyclooctaphane diyne **106**.

Utsumi and coworkers, who did not report detailed procedures for its synthesis, first described diyne **106**.[157] Their first step, a low-yielding McMurry coupling, requires the tedious and low-yielding separation of the desired dimer from insoluble poly(*m,m'*-biphenylene vinylene) oligomers and was irreproducible in our hands. A less direct but more scalable route was sought, ultimately leading to the chromatography-free synthesis outlined in Scheme 4.2. We initially used a synthetic route analogous to the synthesis of **33** using a biaryl aldehyde precursor, but found the dimerization yields were low, the process scaled extremely poorly, and the chromatographic purification was onerous.

Suzuki coupling of sulfone **107** with boronic acid **108** afforded biaryl **109**, which was dimerized to bis(α-keto sulfone) **110** in a respectable 64% yield by reverse addition to base. After an initial dimerization, an electronically- and chelation-favored Z-enolate (Figure 4.3) places the remaining reaction sites in close proximity, enabling cyclization to proceed more rapidly than polymerization. The analogous aldehyde-containing biaryl gives only low yield

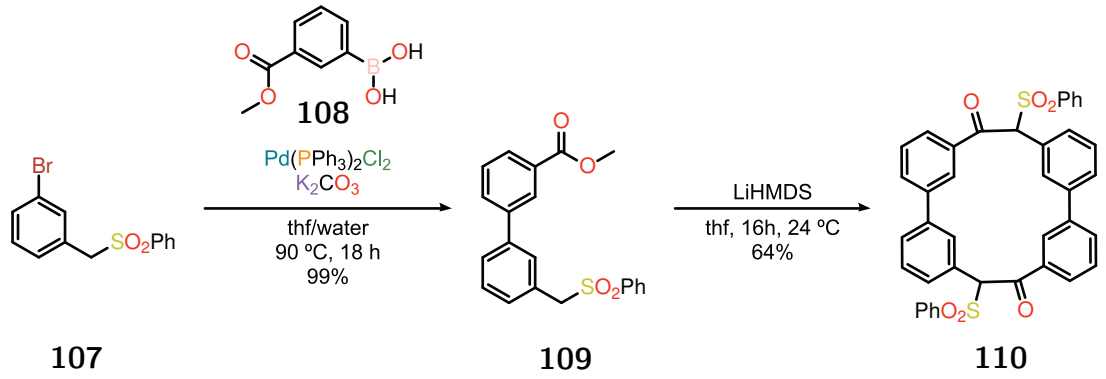

Scheme 4.2: Scalable, chromatography-free synthesis of the cyclooctaphane skeleton in **110**.

(<10%) of cyclic dimers under analogous conditions, presumably due to the free rotation of the intermediate open dimer. Upon workup, the resulting bis(α-keto sulfone) **110** is highly insoluble in nonpolar solvents and is easily separated from any oligomers by simply washing with chloroform.

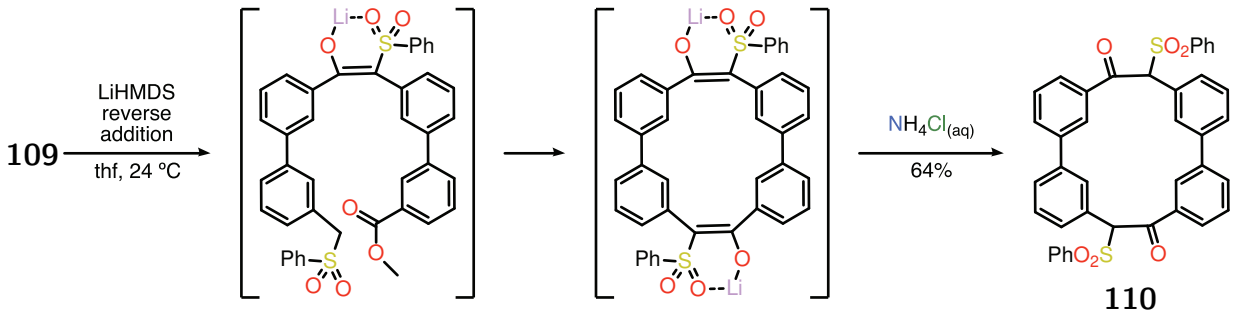

Scheme 4.3: High-yielding macrocyclization to give the 1,2,5,6(1,3)-tetrabenzenacyclooctaphane skeleton via electronically- and chelation-favored Z-enolate.

With the core framework of **106** assembled, the remaining steps require a reduction and elimination to the desired alkyne. The poor solubility of **110** in nonreducible, aprotic solvents severely hindered attempts at reduction with common hydride donors like $LiAlH_4$ or $NaBH_4$. Moreover, a ring-opening to give acyclic products was often observed upon reduction of the ketone, presumably via a retro-aldol-like elimination from the intermediate α-sulfonyl alcoholate. Ketone hydrosilylation chemistry was also investigated to avoid this potential side reaction, and while successful hydrosilylation of **110** with Et_3SiH and $(C_6F_5)_3B$ was observed once on an NMR scale, due to the extremely poor solubility of **110** in noncoordinating solvents it could not be replicated.

Turning instead to reductive cleavage of the sulfone, we found that under simple blue-light photoredox catalysis, **110** is cleanly desulfonylated to give diketone **111** in 94% yield using a

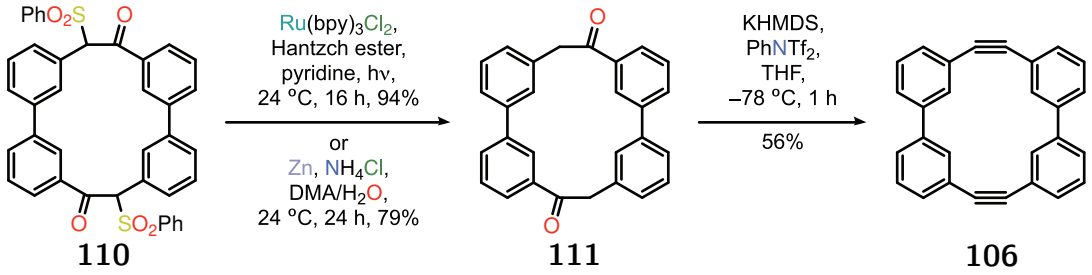

Scheme 4.4: Reductive desulfonylation and triflation/elimination to give **106**.

Hantzch ester as a H-atom donor. At larger scales, the same reduction can be performed with activated zinc dust, albeit at the cost of yield (79%) and purity, requiring a silica gel plug to remove ca. 5% each of mono-reduced product derived from **110** and an overreduced product derived from **111**. Under mild triflation conditions using N-phenyltriflimide and KHMDS, the desired bis(enol triflate) derived from **111** is readily eliminated by excess KHMDS in situ to **106**, even at −78 °C. We suspected that the ease of this elimination reflects the modest ring strain present in **106**, so a crystallographic study was undertaken.

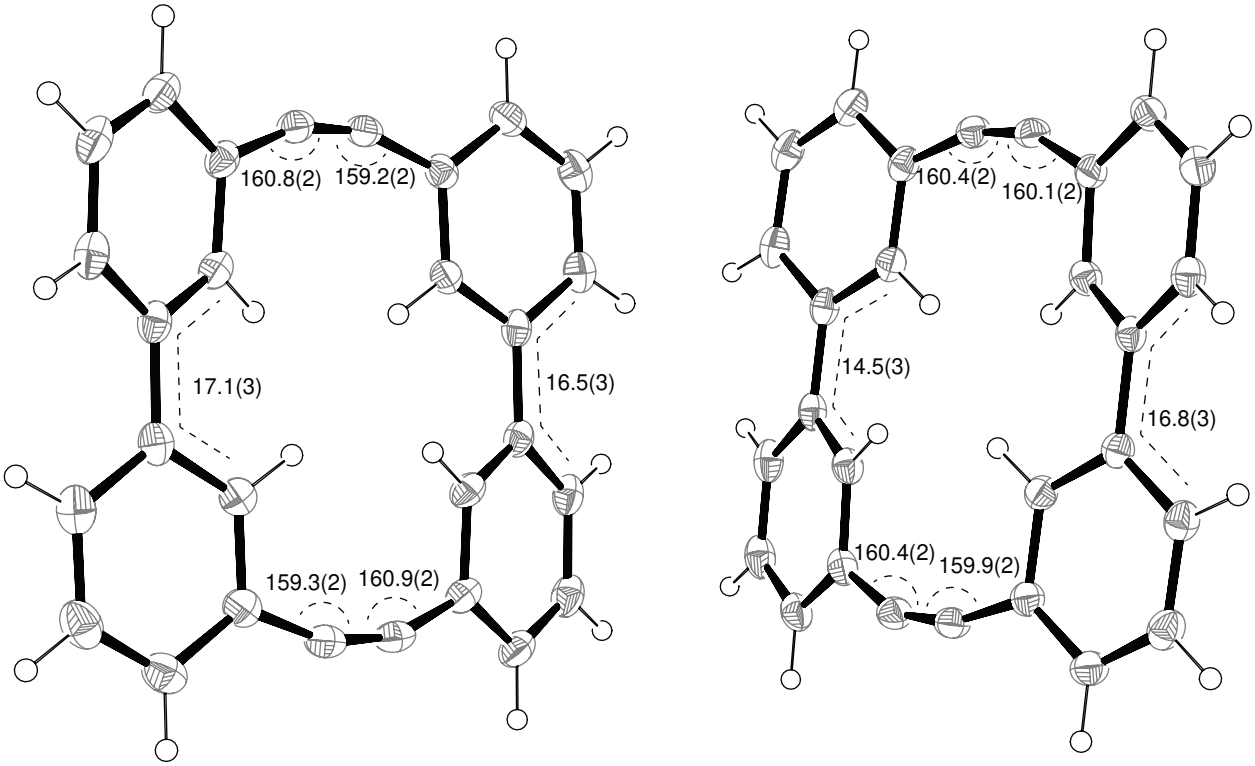

Figure 4.3: Single-crystal X-ray structure cyclooctaphane of diyne **106** depicting both molecules in the asymmetric unit. Thermal ellipsoids drawn at the 50% probability level, with hydrogens in calculated positions. Color code: C (gray), H (white).

Single crystals suitable for X-ray analysis were grown by slow cooling of a saturated benzene solution. While the resulting triclinic plates were uniformly 180° twins, they were of sufficient quality to satisfactorily solve both domains. The structure of the two molecules that make up the asymmetric unit are depicted in Figure 4.3. The C–C≡C bond angles of the strained alkynes average 160.1(6)°, making it the least angle-strained alkyne to be polymerized by ROAMP to date, and slightly more strained than Utsumi's methoxy derivative (160.7(3)°). The nearly planar macrocycle exhibits minimal torsion about the biaryl C-C bonds (average C–C–C–C dihedral 16.2(6)°), much smaller than the methoxy derivative crystallized by Utsumi (C–C–C–C dihedral 40.2(3)°).[157]

4.3 Catalyst Optimization for ROAMP of Low-Strain Monomers

The monomer **106** is only sparingly soluble in noncoordinating, aprotic solvents compatible with ROAMP catalysts. Solutions (>5 mM in **106**) concentrated enough for a reasonably efficient polymerization could only be prepared at elevated temperatures. Screening of polymerization conditions revealed that at T > 40 °C previously reported ROAMP catalysts were unable to discriminate between the mildly strained alkynes in **106** and the unstrained alkynes in the growing polymer backbone leading to stochastic chain-transfer and -termination processes by backbiting into the polymer chain. Efforts to increase the kinetic selectivity by lowering the reaction temperature or monomer concentration slowed the rate of polymerization to a crawl; at [**106**] = 2 mM (saturated in benzene at 24 °C), a 10% loading of Bellone's ROAMP catalyst [*p*-TolC≡Mo(ONO)(OR)]•KOR (R = $CCH_3(CF_3)_2$) **30** gave an initial TOF of < 2 d^{-1} at 24 °C (Scheme 4.5. After the prolonged reaction times required (>7 days for ca. 10 turnovers), the product distribution was dominated by short oligomers and cyclic polymers as shown by size exclusion chromatography (SEC, Figure 4.4).

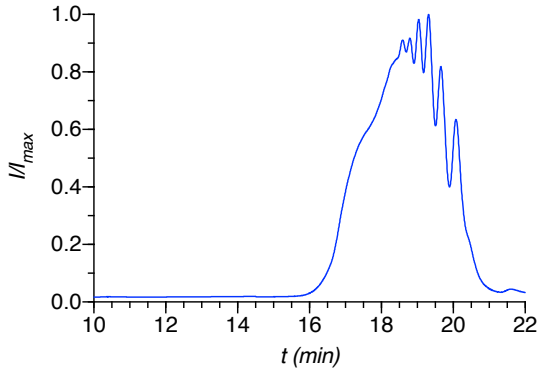

Figure 4.4: SEC trace of *poly*(*m,m'*-biphenylene ethynylene) from the polymerization of **106** with Bellone's catalyst **30** exhibiting low molecular weights and peaks due to cyclic oligomers.

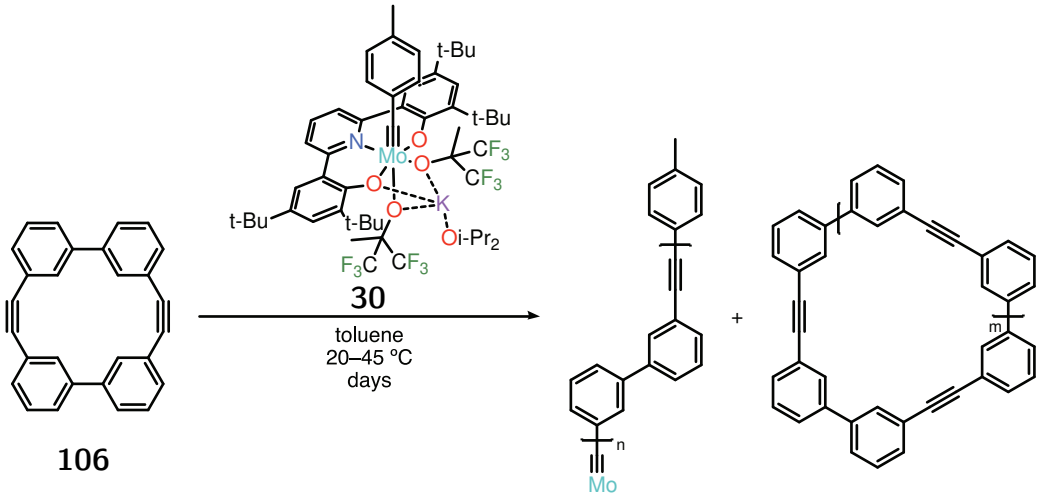

Scheme 4.5: Initial attempt at polymerization of **106** with Bellone's catalyst **30**.

Initially, we suspected that the reversibly-bound alkoxide in **30** was outcompeting the substrate **106**, whose NMR spectra were essentially unchanged by the addition of **106** until the initiation of ROAMP. We set out to prepare the neutral, pentacoordinate analogue, **112** (Scheme 4.6). Improving on the literature synthesis of the ONO pincer ligand **113**, room-temperature Suzuki coupling of 2,6-dibromopyridine with boronate **114** using the Organ group's PEPPSI catalyst[158] under strongly transmetallating conditions in lieu of a Negishi protocol requiring t-BuLi[159] gave **115** in 45% yield after aqueous workup and crystallization of the crude material from hexanes. Deprotection of the phenols in acidic methanol followed by recrystallization from methanol gave yellow blocks of **113•MeOH** which could be desolvated to give pure **113** in 86% yield. Metallation of the ligand with **44** with catalytic base gave the DME-bridged hemisolvate of the pincer complex **116** without the excess alkoxide equivalent. This complex did indeed polymerize **106** more rapidly than **30**, but it was no more selective. Heating to as little as 45 °C led to bimodal molecular weight distributions and the observation of cyclic polymer species due to nonselective metathesis.

A more selective catalyst that could not only differentiate between the mildly strained alkynes of **106** and the polymer backbone but also operate at a higher temperature was needed. While unpublished work by Dr. Hyangsoo Jeong in our group demonstrated that modification of the pincer ligand used in **30** and **116** led to almost universally poorer performance, that ONO pincer framework still left another site for potential modification: the supporting alkoxide. Addition of one equivalent of potassium tert-butoxide to complex **116** rapidly forms a green intermediate "ate" complex **118** by ^{1}H and ^{19}F NMR, which slowly eliminates the less basic ligand to precipitate the unfluorinated analog of **116** as the DME hemisolvate **119** (Scheme 4.7). This complex could be prepared by direct metallation of the pincer ligand **113** with the tert-butoxide complex **120** followed by desolvation in vacuo to remove a mixture of DME and tert-butanol occupying the 6th coordination site. X-ray qual-

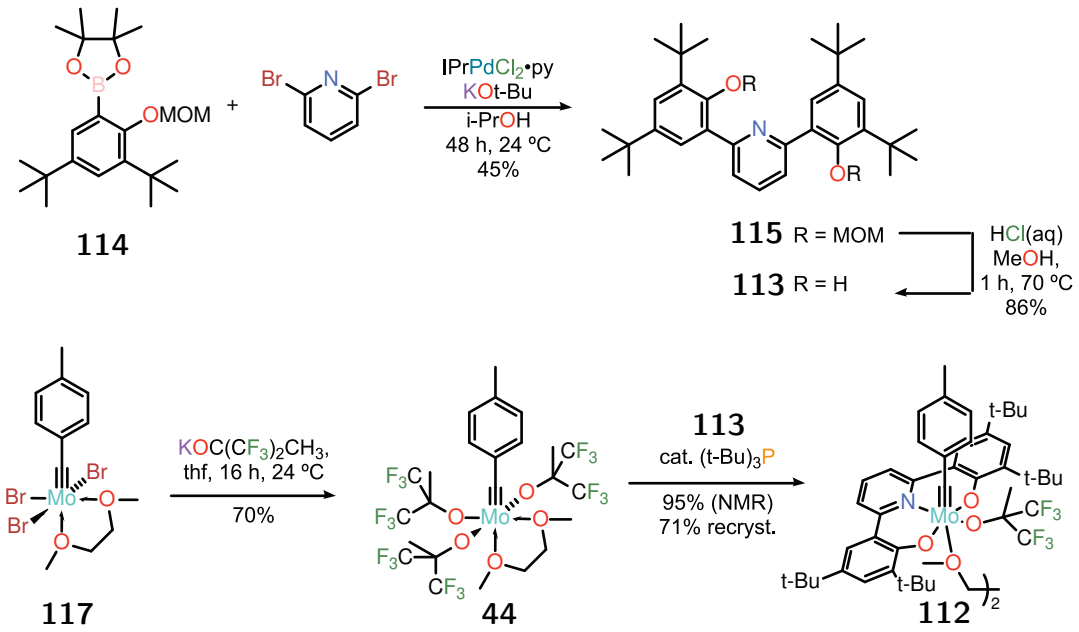

Scheme 4.6: Synthesis of neutral ONO pincer complex **112**.

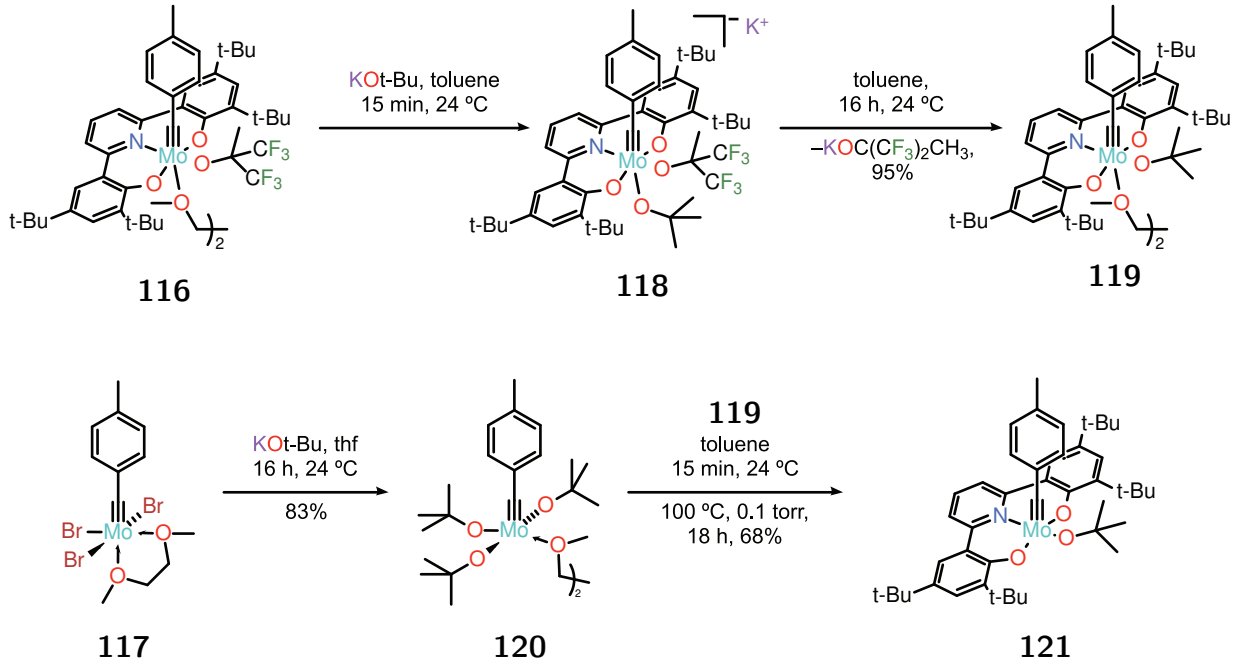

Scheme 4.7: Synthesis of neutral ONO pincer complex **121**.

ity crystals of the tert-butanol adduct of **121•t-BuOH** could be isolated from the reaction mixture by slow evaporation.

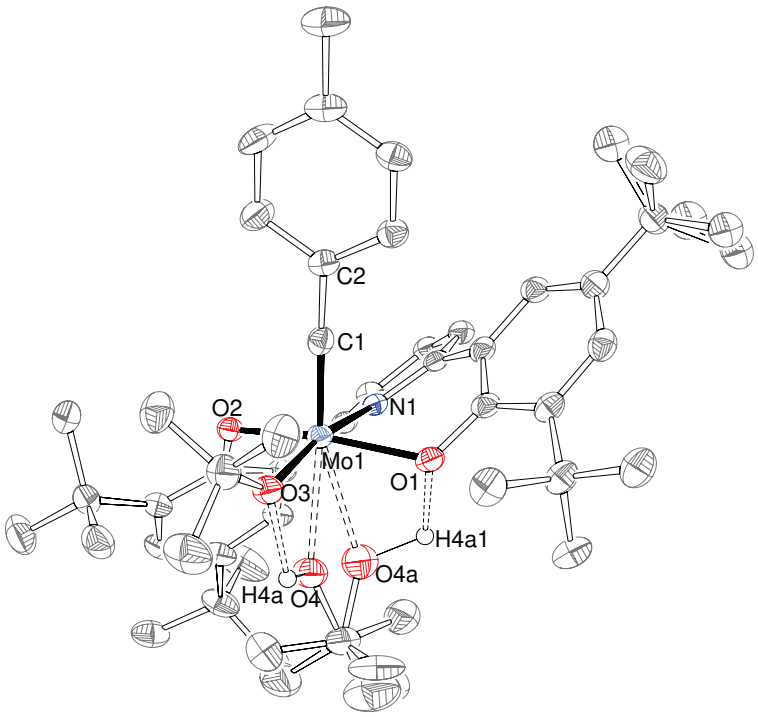

Figure 4.5: Single-crystal X-ray structure of ONO pincer complex **121•t-BuOH**. The tert-butanol coordinated in the axial position is disordered over two positions oriented toward two different hydrogen-bond acceptors, the alkoxide O (major) or phenoxide O (minor). Thermal ellipsoids drawn at the 50% probability level, with hydrogens attached to carbon omitted for clarity. Color code: C (gray), H (white), Mo (turquoise), O (red), N (blue).

The single crystal X-ray structure of **121•HOt-Bu** is depicted in Figure 4.5. The pseudo-octahedral coordination sphere is enforced by the *mer* coordination of the ONO pincer ligand in a twisted conformation analogous to that seen in **30**.[90] The expected Mo−C triple bond of 1.749(2) Å, Mo−$O_{phenoxide}$ bonds of 1.977(2) and 2.000(2) and Mo−Ot-Bu of 1.916(2) Å are relatively unremarkable, though uniformly shorter than the analogous distances in **30**. The axial position *trans* to the carbyne is occupied by a loosely-bound tert-butanol with a very long Mo-O distance of 2.452(3) or 2.497(8) Å, much longer than the axial alkoxide in **30** (2.248(2) Å). It is disordered over two possible hydrogen bonding positions, with the major occupancy corresponding to the shorter H-bonding (1.6(1) Å) distance to the more basic alkoxide oxygen and the minor to the weaker H-bond accepting phenolate (1.78(4) Å). The structural differences between **121•HOt-Bu** and **30** can be rationalized as the expected contraction of the bonds due to a more electrophilic Mo environment in **30** that is more than compensated for by the overall anionic charge. Together, this leads to slightly shorter

Mo-ligand bond lengths in **121•HOt-Bu** than **30** despite its reduced electrophilicity.

The more electron-rich pincer complex **121** with a tert-butoxide supporting ligand shows superior selectivity for even the subtly strained alkynes in **106** giving access to linear mmBPE **104** in high yield. While almost completely inactive below 60 °C, at 80 °C where **106** and the resulting polymers are reasonably soluble, complex **121** ring-opens **106** with a rate constant of approximately 2×10^2 $M^{-1}h^{-1}$. SEC analysis reveals that samples of **104** prepared with ROAMP catalyst **121** exhibit narrow molecular weight distributions (Đ= 1.2, Figure 4.9) and M_n that scale linearly with monomer loading and conversion, consistent with a living chain-growth polymerization mechanism.

MALDI-TOF mass spectrometry of **104** was initially very challenging to obtain, as addition of methanol or water failed to cleanly cleave the Mo pincer complex off the end of the polymer chain leading to inconsistent fragmentation patterns. Fortunately, the ONO pincer ligand could be removed by the addition of Bu_4NOH to the polymerization mixture. This had the added benefit of reducing the amount of *homolytic* Mo-C bond cleavage, giving protiodemetallated endgroups much more selectively (over radical reactions like chain doubling, oxidation, etc.) due to the propensity of alkyl molybdates (the initial product of hydrolytic removal of the ONO ligand) to undergo *heterolytic* Mo-C bond cleavage under basic conditions.[160]

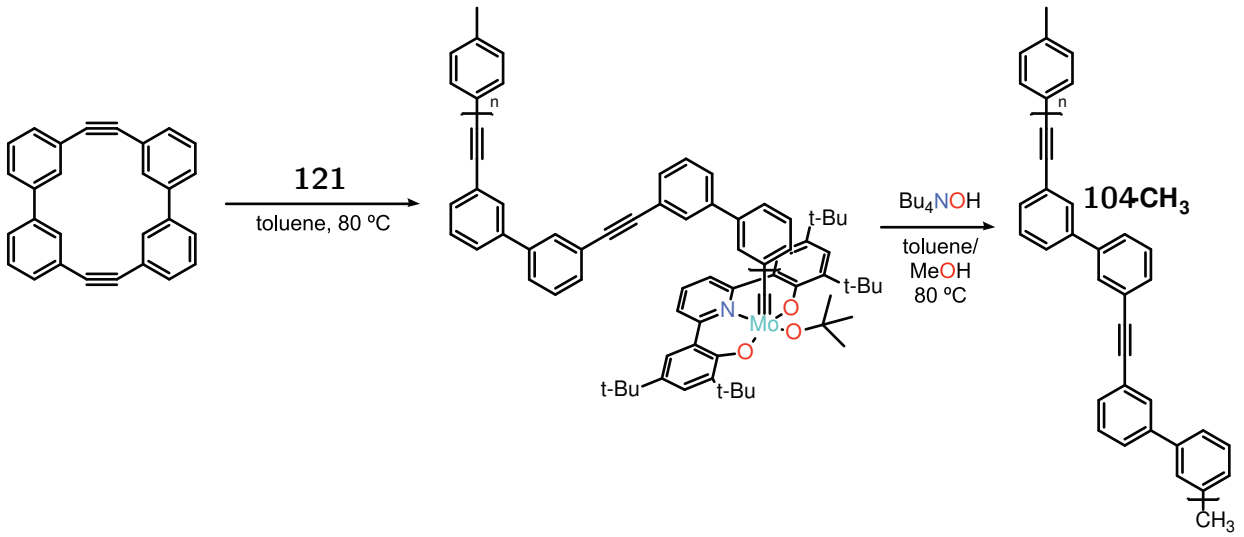

Scheme 4.8: ROAMP of **106** by electron-rich pincer **121** followed by base hydrolysis to give mmBPE **104-CH$_3$**.

After catalyst cleavage under these basic conditions (Scheme 4.8), Figure 4.6 shows a single family of peaks separated by integer repeat units of the monomer mass, ($\Delta m/z = 352$ u). This indicates that ROAMP catalyst **121** selectively reacts with strained alkynes in **106** over the unstrained triple bonds in the growing polymer backbone. This selectivity prevents undesired chain-transfer processes that would lead to cyclic polymers, fractional numbers

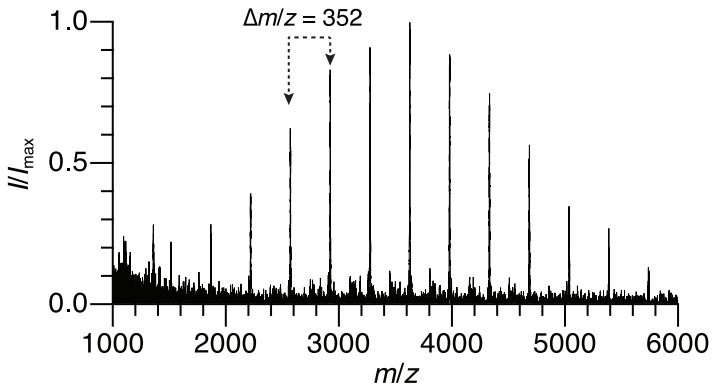

Figure 4.6: MALDI-TOF MS of *poly*(*m,m'*-biphenylene ethynylene) **104-CH$_3$** prepared by ROAMP of **106** with **121** followed by alkaline protiodemetallation.

of monomer units in the growing polymer chain (Δm/z = 176 u), and a broadening of the molecular weight distribution.

4.4 Functional Termination for Telechelic Polymer Templates

Based on the conceptual reverse of Chapter 3's electronically-directed cross metathesis for initiator functionalization, the metathesis with electron-rich alkynes developed by Dr. Hyangsoo Jeong,[161] we terminated these living polymers with selective chain-transfer reagents derived from ynamines or ynamides. Initial studies using ynamides such as **122** and **123** (Scheme 4.9) led to sluggish kinetics and incomplete reaction, even with large excesses and long reaction times (>48 h). Moreover, consistent with the findings described in Chapter 3, ynamides bearing electron-donating groups such as **122** introduced endgroups that were electronically activated towards metathesis by unterminated catalyst species. Combined with the slow rate of the cross metathesis reaction between the propagating species and ynamides, this led to undesired chain-doubling by cross metathesis between these endgroups and the still-active chain ends (Scheme 4.9).

While these ynamides were generally found to be superior to ynamines for inactivation of *tetracoordinate* ROAMP catalysts such as the benzylidynes in Chapter 3 due to the additional chelation by the amide oxygens in the molybdacyclobutadiene product, such a heptacoordinate product is not attainable with the bulky ONO pincer ligand surrounding the metal center in **121**.

To increase the rate of termination, we tried to minimize the steric bulk of the ynamine and maximize the polarity of the alkyne π bond in the form of N-(4-nitrophenylethynyl)dimethylamine **124**. Fortunately, the combination of factors gave acceptable reaction rates at temperatures where the metathesis activity of **121** was otherwise minimal (<60 °C). Complex **121** reacts irreversibly with two equivalents of **124** at 55 °C to give the expected cross

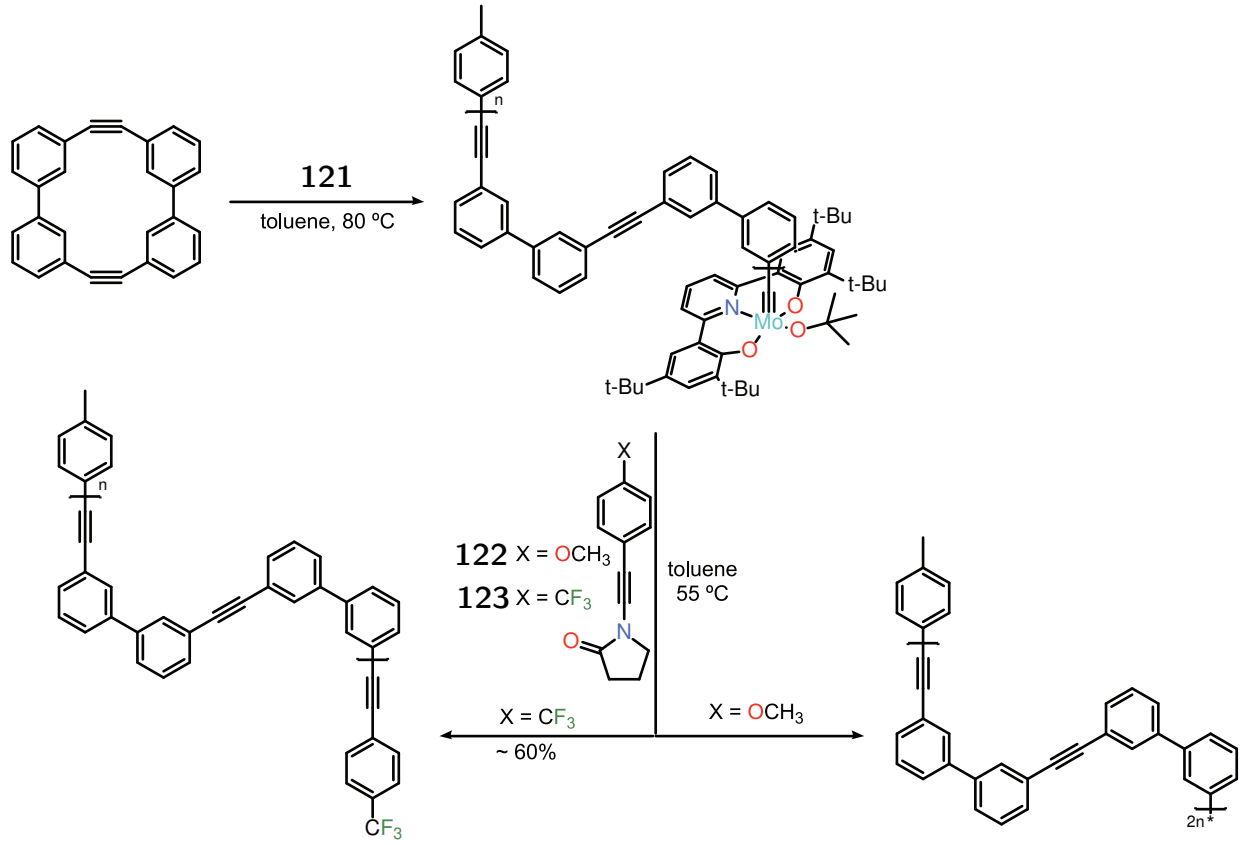

Scheme 4.9: Initial attempts to use electronically-directed cross metathesis to functionally terminate the propagating ROAMP species derived from **121**.

metathesis product and a paramagnetic, presumably Mo(IV) product. The paramagnetic NMR spectrum of the terminated species (Figure 4.7) exhibits eleven distinct paramagnetically shifted proton environments, which are *very approximately* integratable, consistent with a diaminomolybdacyclobutadiene complex such as **125**.[162]

Using this more active ynamine terminating reagent, the living polymer chain ends can be terminated with functional groups to give telechelic **104-NO$_2$**. NMR end-group analysis and MALDI-TOF MS (Figure 4.8) confirm the incorporation of a single nitrophenyl group per polymer chain.

4.5 Polyphenylenes by Lateral Extension of Alkyne Polymer Templates

With the M_n, Đ, and end groups of mmBPE **104** controlled by ROAMP, we turned to the lateral extension of the alkynes to yield the characteristic polyphenylene backbone of a cGNR. The inverse-electron demand Diels-Alder reaction between alkynes and 2,3,4,5-

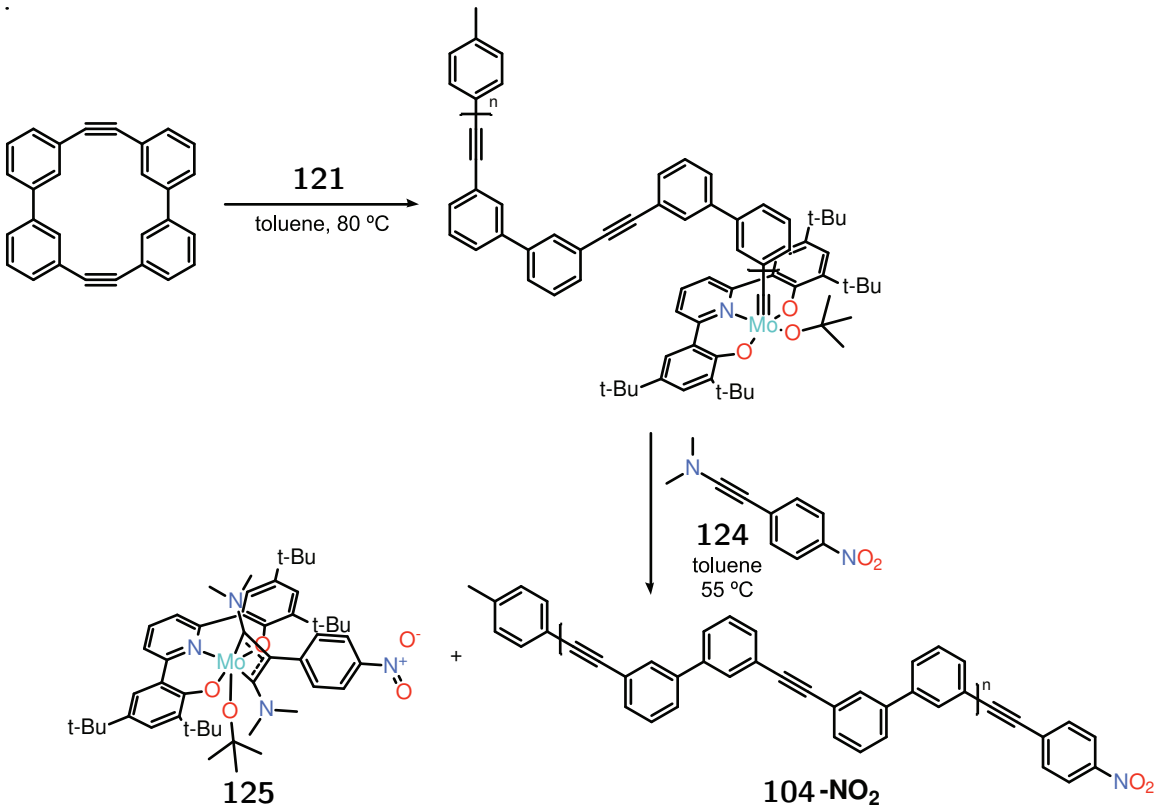

Scheme 4.10: Successful electronically-directed cross metathesis of **121** with **124** to give an inactive, paramagnetic molybdacyclobutadiene **125** and telechelic **104-NO_2**.

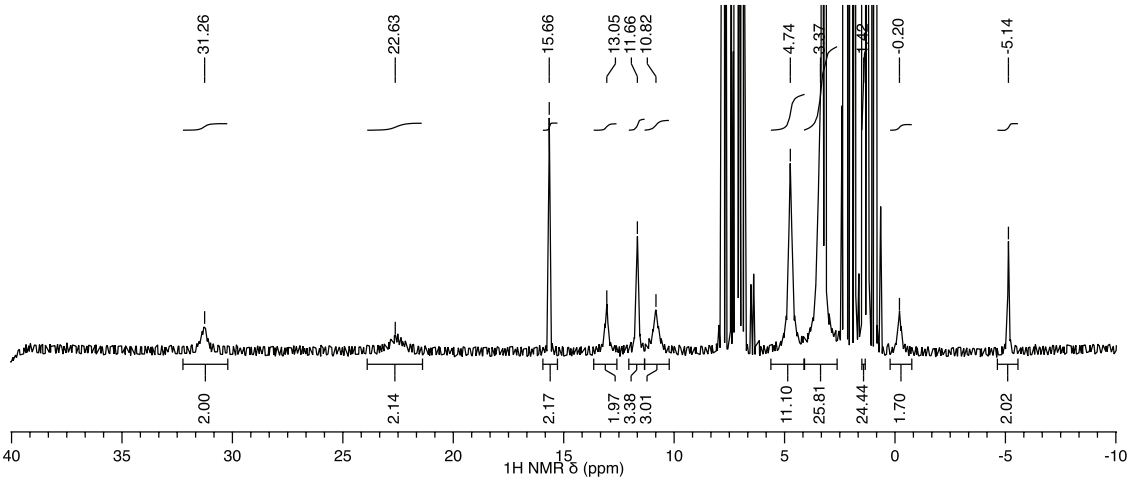

Figure 4.7: Paramagnetically shifted NMR spectrum of the putative Mo(IV) diaminometallacyclobutadiene **125** from metathesis of **121** with **124**.

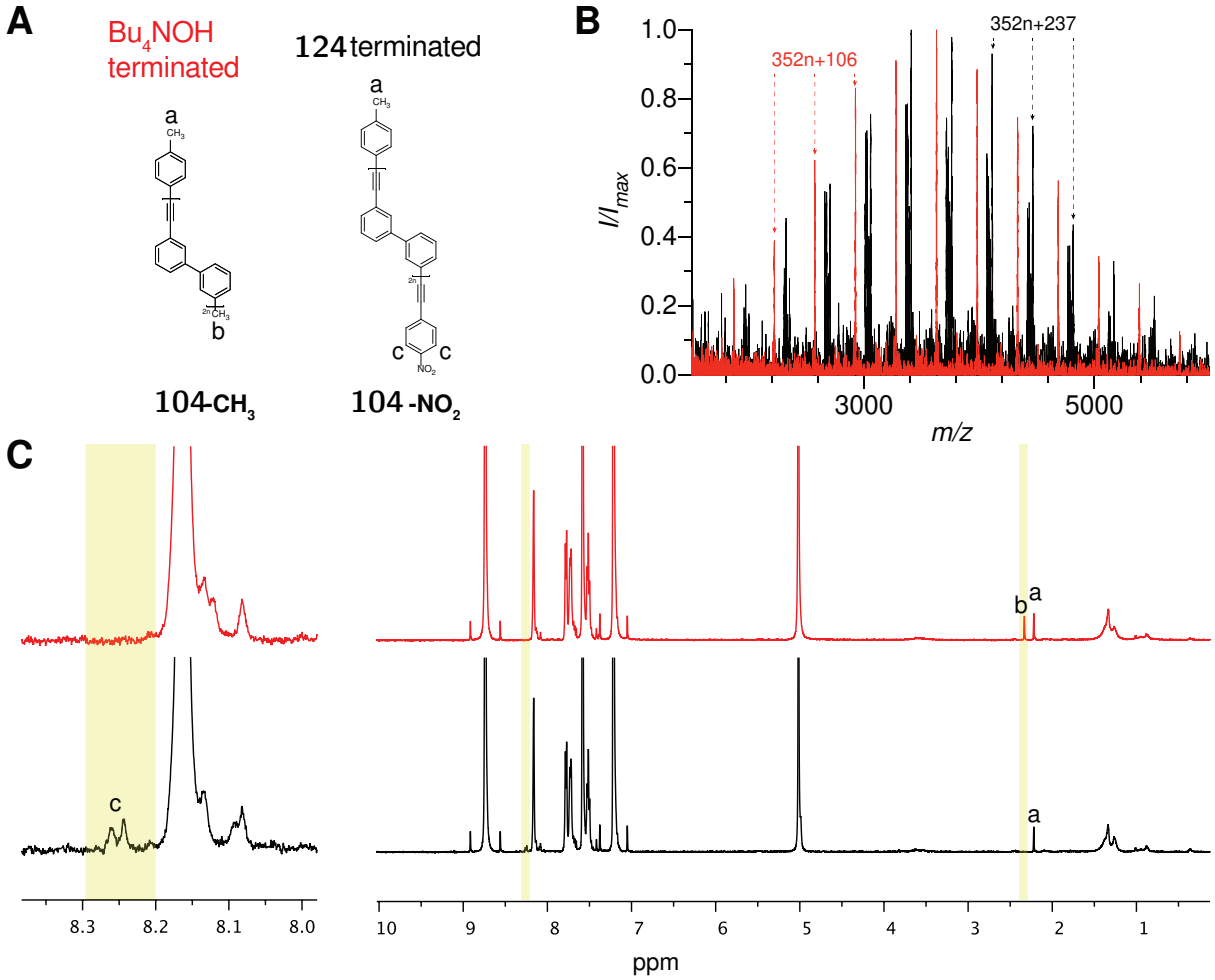

Figure 4.8: **A**. Structure of mmBPE **104-CH_3** after hydrolytic workup with Bu_4NOH or **104-NO_2** after functional termination by metathesis with ynamine **124**. **B**. MALDI-TOF MS of **104-CH_3** (red) or **104-NO_2** (black). The 4-nitrophenyl containing polymers show four families of ions with laser power-dependent abundance ($[M]^+$, $[M-O]^+$, $[M-2O+2H]^+$, $[M-NO2+H]^+$) due to the photoreduction of the nitro group in the presence of the dithranol matrix. **C**. ^1H NMR of mmBPE **104-CH_3** (red) or**104-NO_2** (black) showing the complete transformation of end groups.

tetraarylcyclopentadienones is a method commonly used in polyarylene synthesis that has been demonstrated to be extremely robust, chemoselective, and high yielding,[155] ideal criteria for a post-polymerization reaction. To screen annulation conditions, samples of mmBPE were also prepared by cross coupling polymerizations (Scheme 4.11). The achievable molecular weights were relatively low, and the polymers were predominantly cyclic by MADLI-TOF MS, highlighting a major downside to the cross-coupling approach.

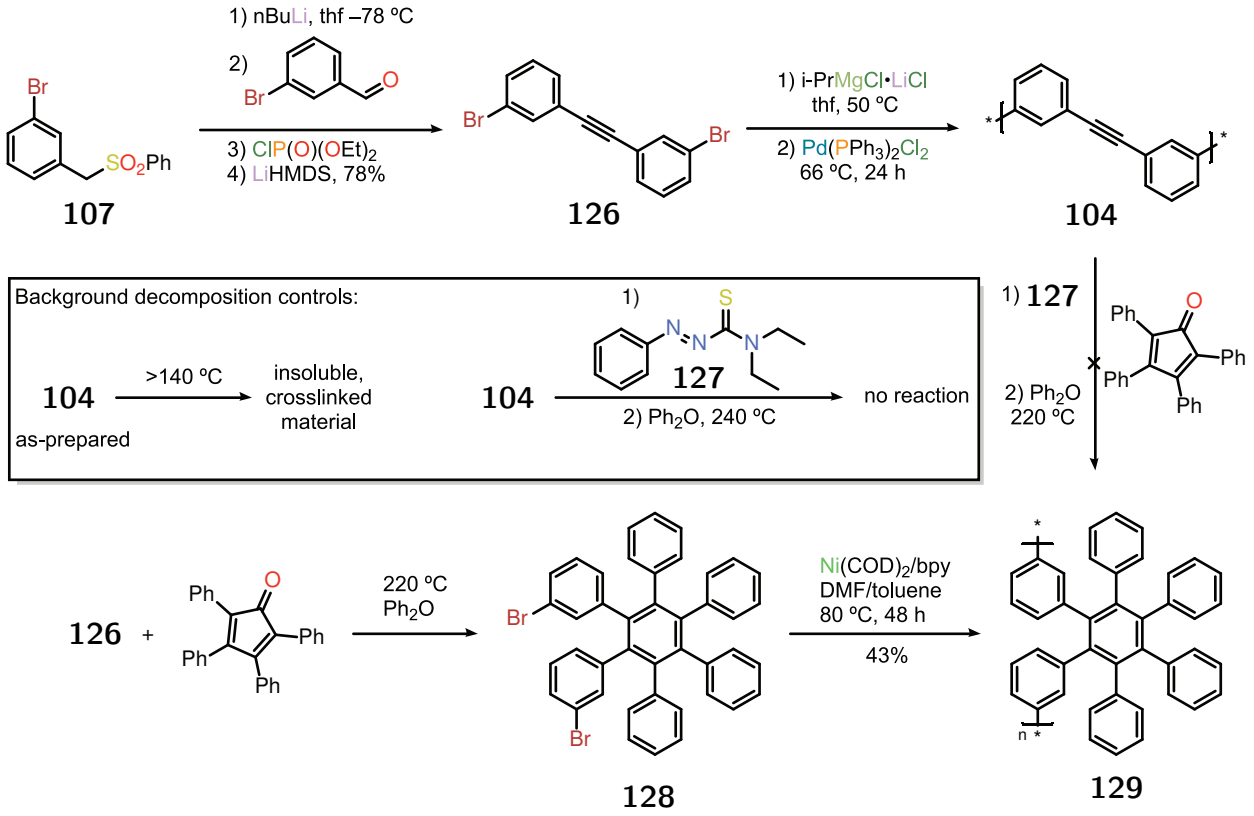

Scheme 4.11: Synthesis of bulk samples of mmBPE and insoluble polyphenylene **129** by cross-coupling.

Curiously, these materials were not thermally stable at temperatures where the Diels-Alder reaction would proceed; heating to >140 °C in dry xylenes or diphenyl ether in the absence of any Diels-Alder partner led to the precipitation of an insoluble powder. Presumably a crosslinked polymer, we suspected this was caused by residual catalyst residues present in the polymer that were crosslinking the alkynes by [2+2+2] chemistry. Indeed, using phenylazothioformamide derivative **127** to dissolve residual palladium that could be present as nanoparticles[163] followed by reprecipitation, the resulting mmBPE polymers were stable in solution and no longer self-crosslinked.

With the thermal stability of mmBPE established, lateral extension with unsubstituted 2,3,4,5-tetraphenylcyclopentadienone still leads to the precipitation of a surprisingly insolu-

ble polyphenylene from the reaction mixture, even at >220 °C! By mass balance, the reaction doesn't exceed ∼50% conversion before precipitation halts it completely. Independently synthesizing the same highly insoluble polyphenylene **129** by Yamamoto polymerization (Scheme 4.11) supported the precipitation-inhibition hypothesis. A solubilized version of the cyclopentadienone, **130**, was required to keep the annulated polymer soluble and enable complete conversion.

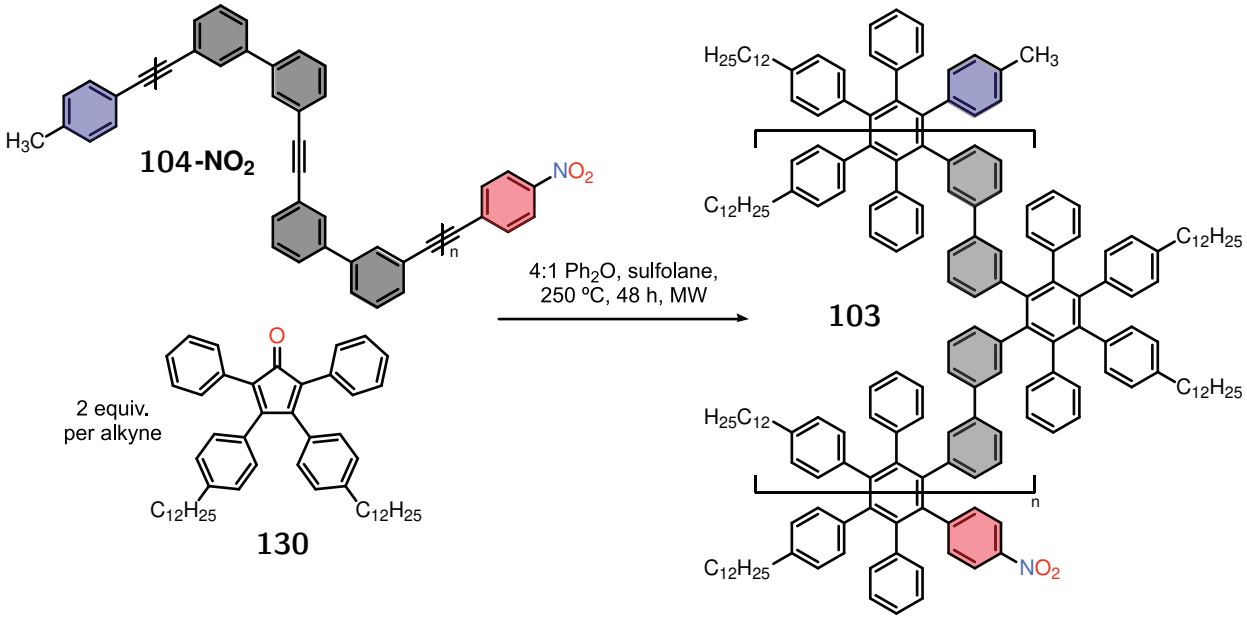

Scheme 4.12: Lateral extension of mmBPE **104-NO$_2$** to give **103** by exhaustive Diels-Alder annulation with **130**.

Diels-Alder reaction of mmBPE with cyclopentadienone **130** at 250 °C in a microwave reactor gave the desired solubilized polyphenylene **103** (Scheme 4.12). Now fully soluble in common organic solvents, SEC reveals an apparent increase in molecular weight along with a slight broadening of the molecular weight distribution as compared to the mmBPE precursor **104** (Figure 4.9). SEC traces of **103** prepared from mmBPE of >6 kDa exhibit a shoulder at higher molecular weights. Its relative area is not consistent from sample-to-sample, suggesting it might be an aggregation phenomenon and not due to a bimodal molecular weight distribution.

4.6 Trace Alkyne Detection in Polymer-to-Polymer Diels-Alder Annulations

Critical to any successful post-polymerization strategy is the quantification of the degree of functionalization. This is especially true for the synthesis of cGNRs from mmBPE, as any

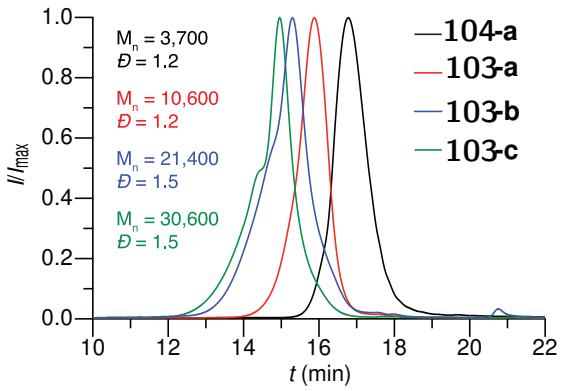

Figure 4.9: SEC traces of polyphenylene **103** prepared by Diels-Alder annulation of mmBPE **104-NO$_2$** with n = ∼10 (a), 20 (b), and 40 (c) with solubilized cyclopentadienone **130**.

structural defects induced by incomplete lateral extension will lead to defects in the resulting extended cGNR backbone. Initial attempts to monitor the reaction by ^{13}C NMR showed that unfunctionalized alkynes were difficult to detect in a reaction mixture of **104** with **130** after as little as 1 h at 250 °C largely due to the broadening of the resonances as the polymer backbone became more hindered. Even with isotopically labelled substrates the long T1 relaxation times of sp-hybridized carbon atoms make the detection of trace alkynes by ^{13}C NMR difficult.

To overcome this analytical challenge, we explored chemical methods to detect residual unreacted alkynes in samples of **103**. Oxidative cleavage of residual alkynes by e.g. ozonolysis or potassium permanganate proved unsuitable as they slowly degraded the aromatic backbone of **103** leading to false-positives even in polyphenylenes prepared by Yamamoto cross-coupling polymerizations. Instead, we turned to the highly active alkyne cross-metathesis catalysts utilized in Chapters 2 and 3 based on the [RC≡Mo(OC(CF$_3$)$_2$CH$_3$)$_3$] framework, capable of selectively depolymerizing residual alkynes along the backbone of **103** under mild conditions (Scheme 4.13).

Alkyne cross-metathesis of samples of **103-b** taken after 1 h, 2 h, and 4 h (SEC traces in Figure 4.10, right) in the presence of a ∼100-fold excess of 1,2-bis(4-trifluoromethylphenyl) acetylene **68** show a significant decrease in the M_n (Figure 4.10, left) indicative of residual unreacted alkynes in the polymer chain below the detection limit of routine ^{13}C NMR. A secondary advantage of our depolymerization strategy is that the alkyne metathesis catalyst **65** selectively transfers a 4-trifluoromethylphenyl group to each end of the two resulting polymer fragments that can readily be detected and quantified by ^{19}F NMR.

Figure 4.11 shows the ^{19}F NMR traces of depolymerized samples of **103-b** taken at varying reaction times. Integration of the CF$_3$ ^{19}F NMR signals against an internal standard of CF$_3$Si(CH$_3$)$_3$ reveal an average of >25, 19, and 2.5 unreacted alkynes per polymer chain after 1 h, 2 h, and 4 h, respectively. SEC traces of samples of **103-b** taken after 12 h (Figure

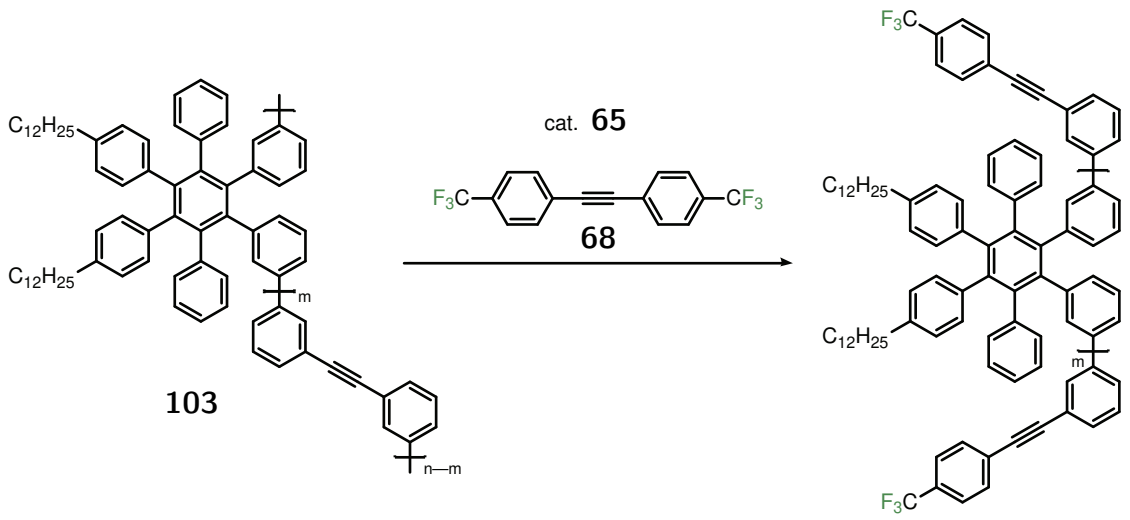

Scheme 4.13: Detection of trace residual alkynes by alkyne cross metathesis depolymerization.

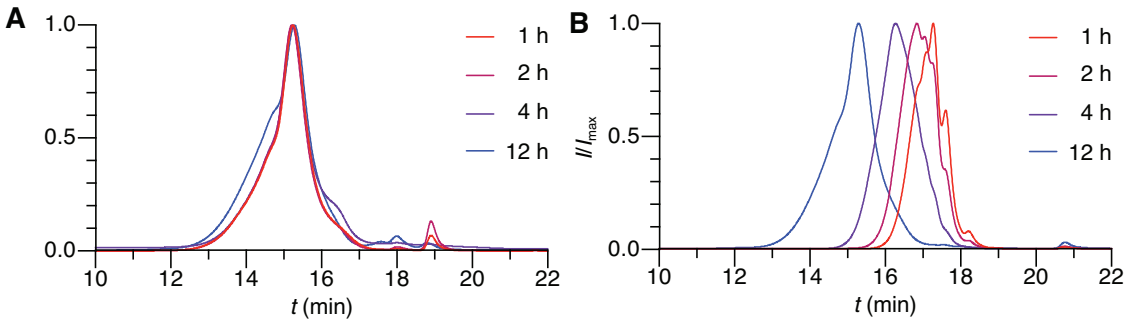

Figure 4.10: **A**. SEC of polyphenylene **103-b** taken at 1 h, 2 h, 4 h, and 12 h from the crude Diels-Alder reaction of mmBPE **104** with cyclopentadienone **130**. **B**. SEC after metathesis depolymerization to determine the extent of the Diels-Alder reaction to form polyphenylene **103-b**.

4.10, right) no longer show any decrease in the M_n when subjected to alkyne-cross metathesis depolymerization conditions (Figure 4.10, left). ^{19}F NMR spectra of the same samples also lack the signals that attributed to the incorporation of 4-trifluoromethylphenyl groups into the polymer chain ends as part of the alkyne-cross metathesis with **68**.

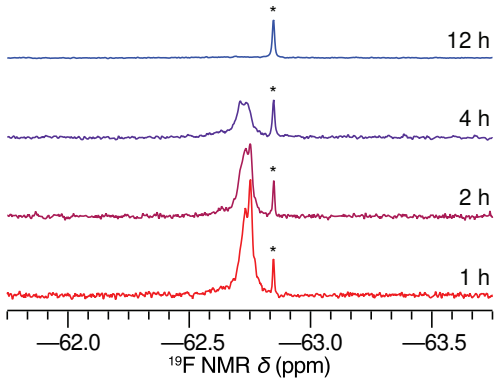

Figure 4.11: ^{19}F NMR of polyphenylene **103-b** samples subjected to depolymerization after varying Diels-Alder reaction durations (* denotes residual 1,2-bis(4-trifluoromethylphenyl)acetylene **68**)

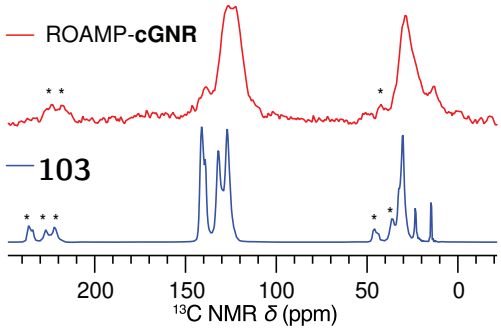

Figure 4.12: ^{1}H-^{13}C CP-MAS SSNMR spectra of polyphenylene **103** and ROAMP-cGNRs (*spinning side band) showing absence of alkyne signals in the 80-100 ppm region and the upfield shift of the fused GNR carbon core.

Lastly, we turned to solid state NMR spectroscopy as an independent method to confirm the exhaustive lateral extension of **104** with cyclopentadienone **130**. The spatial proximity of any residual alkyne carbon atom to the ortho hydrogen atoms of any adjacent aromatic ring (<2.7 Å) should enable their direct observation by cross-polarization solid-state NMR where signal recovery is limited by the much shorter hydrogen T1.[164] The ^{1}H−^{13}C CP-MAS SSNMR spectrum of **103** depicted in Figure 4.12 lacks the characteristic signatures (80−100 ppm) associated with alkynes. Microwave heating proved critical to the successful and exhaustive lateral extension of **104**. If the same reaction was performed in a thermal

heating bath, residual alkynes could still be detected by metathesis depolymerization even after >21 days. Efforts to drive the thermal reaction to completion at temperatures >265 °C led to decomposition of cyclopentadienone **130**.

4.7 Templated Polyphenylenes to GNRs

Oxidative cyclodehydrogenation of pristine samples of polyphenylene **103** under Scholl reaction conditions yielded ROAMP-cGNR as a black powder dispersible in nonpolar organic solvents. Solid-state ^{13}C NMR spectroscopy (Figure 4.12) further confirms the successful ring-fusion that yields the extended polycyclic aromatic backbone of cGNRs.[165] Characteristic resonances of quaternary carbons at 139 to 141 ppm are shifted to higher field following the lateral fusion of aromatic rings, leaving the downfield resonance for the alkylated GNR carbons visible at 139 ppm.

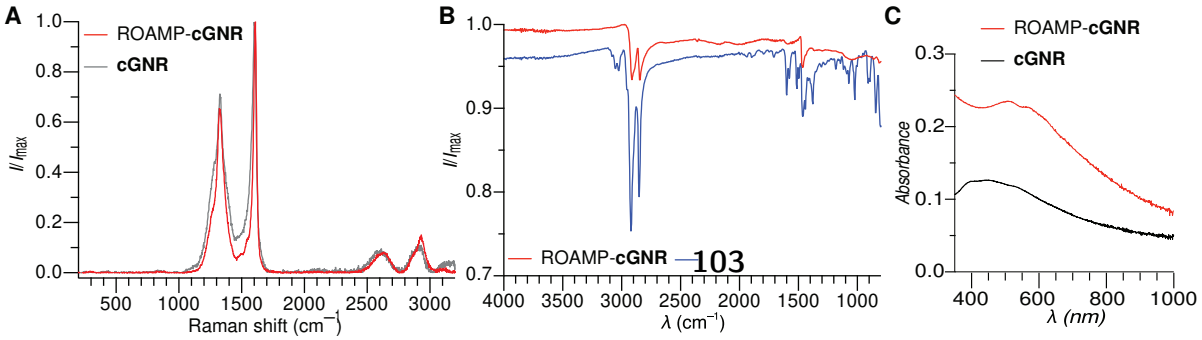

Figure 4.13: **A**. Raman spectra of ROAMP-cGNRs and an authentic sample of cGNRs prepared through Yamamoto step-growth polymerization (514 nm excitation). **B**. IR (ATR) of polyphenylene **103** and ROAMP-cGNRs. **C**. UV-Vis spectra of dispersions of ROAMP-cGNRs and cGNRs prepared through Yamamoto step-growth polymerization. Dispersions were prepared by sonicating 0.2 mg GNR in 2 mL NMP for 1 h and filtering through glass wool to remove large aggregates

A direct comparison of the Raman spectrum of ROAMP-cGNRs (Figure 4.13A) with an authentic sample of cGNRs prepared through Yamamoto step-growth polymerization shows the characteristic signatures of D (1330 cm^{-1}) and G (1610 cm^{-1}) peaks along with the expected 2D (2660 cm^{-1}), D+G (2935 cm^{-1}) overtones. IR spectra of ROAMP-cGNRs (Figure 4.13B) show a dramatic attenuation of the aromatic C−H stretching modes, centered around 3050 cm^{-1} in polyphenylene **103**, following the successful oxidative cyclodehydrogenation. UV-Vis spectra of ROAMP-cGNRs (Figure 4.13C) shows a broad visible absorption along with a shoulder centered at 550 nm characteristic for cGNRs.[165]

4.8 Heteroatom-doped Monomers for GNR Heterojunction Templates

The true power of a GNR template prepared by a living, chain-growth polymer would be not just to control lengths and endgroups but to access precise heterojunctions within a single GNR. To accomplish that, a second strained alkyne monomer compatible with the same post-polymerization modification step is required. Examining at the positions on the monomer **106** that are amenable to substitution, the only position where aryl-aryl bonds are not formed during cyclodehydrogenation is the *meta* position. From an electronic standpoint, substitutional doping to produce p- or n-type materials would be the most interesting, and replacing carbon with nitrogen at all four open positions would give a tetrapyridyl version of **106**, 1,2,5,6-(3,5)-tetrapyridinacyclooctaphane **131**.

Our approach to **131** followed the synthetic route initially outlined for the unsubstituted cyclooctaphane **106**, which is detailed in Scheme 4.14. The 3,3'-bipyridine motif is the least common bipyridine substitution and required a multistep synthesis of the Suzuki coupling partners. The boronate ester **133** can be prepared in two steps from commercial 3,5-dibromopyridine by magnesiation/formylation to give 5-bromonicotinaldehyde **132** in 76% yield followed by Miyaura borylation to the boronate **133** in 72% yield. The other coupling partner starts from nicotinic acid, which can be converted to the acid chloride hydrochloride, brominated in neat bromine, and then esterified with methanol to give methyl 5-bromonicotinate **134** in 60% yield over three steps. Reduction with sodium borohydride followed by continuous liquid-liquid extraction and distillation gives 5-bromopyridine-3-methanol **135** in 48% yield, which is converted to the hydrochloride to prevent polymerization during chlorination with thionyl chloride to give **136** quantitatively. Sulfonylation with sodium 4-toluenesulfinate gives **137** in 76% yield which undergoes efficient Suzuki coupling with **133** to give bipyridine **138** in 90% yield.

Dimerization of **138** by deprotonation of the sulfone with LiHMDS followed by addition to the aldehyde failed. NMR scale experiments with **140** revealed that nicotinaldehydes are quantitatively converted to their corresponding N-silyl imine with LiHMDS in THF. Exhaustive screening of other bases revealed that stronger bases like LDA or LiTMP led to decomposition, presumably by metallation of the pyridine ring. Na or Mg HMDS bases led to the same N-silyl imine formation while K bases led to decomposition. Weaker bases, such as Na, K, and Mg tert-butoxides led to aldehyde disproportionation through a Cannizarro-like reaction. Lithium alkoxides did so as well, but slowly enough that some dimerization could be observed.

Under those conditions, the initial dimeric lithium α-sulfonyl alcoholates slowly eliminated to give the bis(vinyl sulfone) **139**. The liberated LiOH slowly promotes a Cannizarro disproprotionation of the unreacted aldehydes, almost completely suppressing product formation at higher temperatures. Nevertheless, a pure sample of **139** could be isolated after prolonged reaction times at room temperature to test the subsequent step. Elimination of **139** with LiTMP on an NMR scale gave 1,2,5,6(3,5)-tetrapyridinacyclooctaphane-3,7-diyne

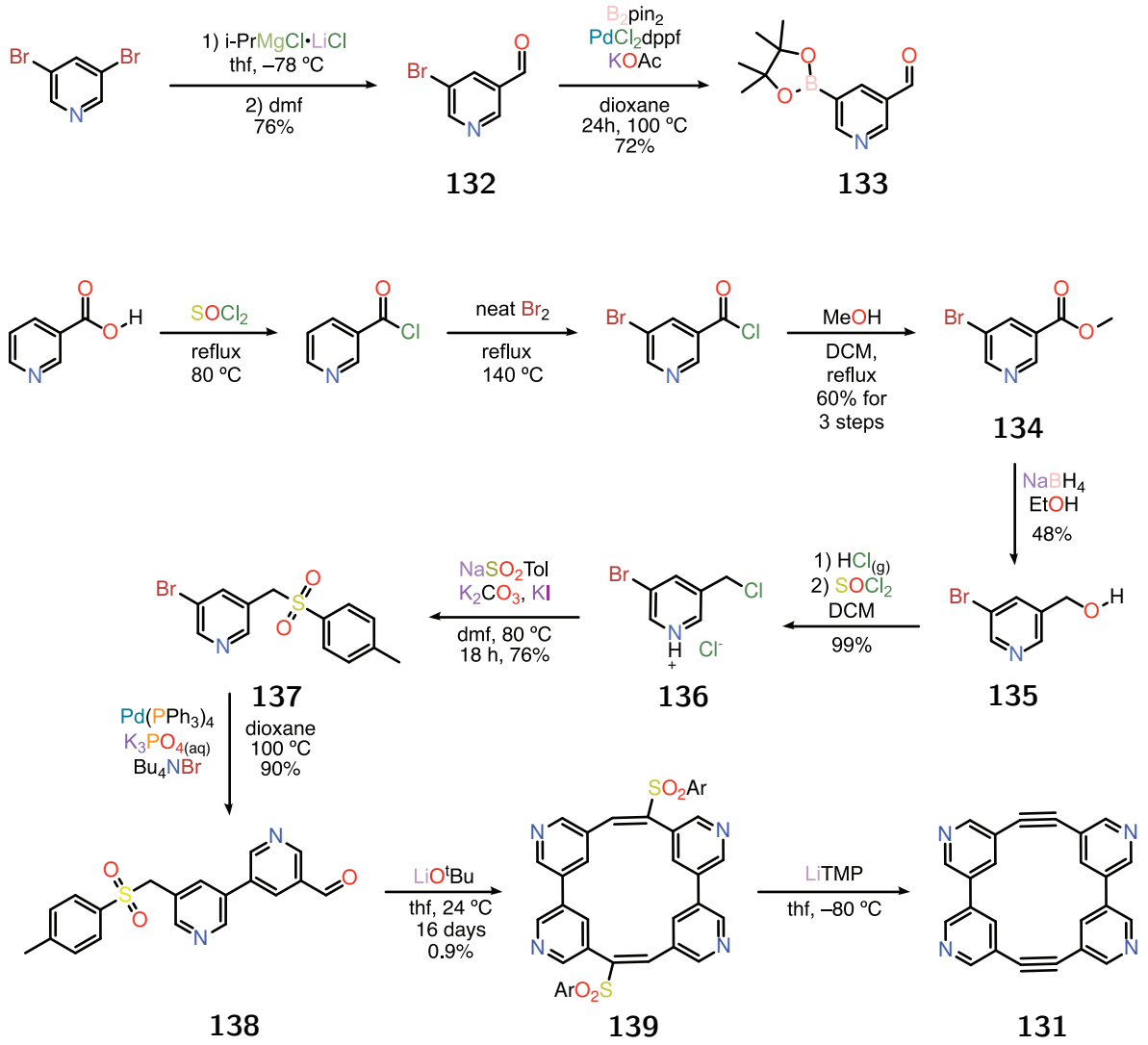

Scheme 4.14: Synthesis of N-doped tetrapyridinacyclooctaphane diyne **131**.

131, as evidenced by a new set of three downfield pyridine resonances corresponding to the symmetrized product. It appears stable to water and tolerates oxygen over at least 24 h, but decomposes on silica and alumina which has prevented isolation of the pure compound thus far.

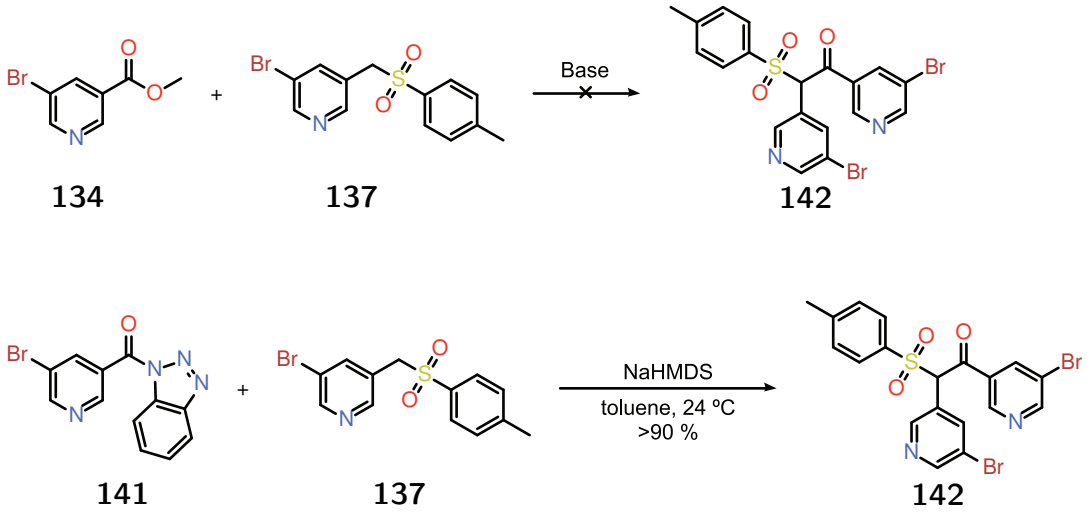

Scheme 4.15: Alternative coupling partners to form the tetrapyridinacyclooctaphane core of **131**.

The alternative coupling strategy used in the synthesis of **106** using an ester as an electrophile was not successful in the case of the pyridine analog. Attempts to couple **134** with **137** led to extremely sluggish reactions, forming a few % dimeric species over the course of several days. The α-sulfonyl anion of these pyridylmethyl sulfones were more stable than their benzyl analogues, requiring a more reactive electrophile for efficient coupling. Acylbenzotriazoles are known to efficiently acylate sulfonyl anions[166] and this case is no exception. The aroylbenzotriazole derivative **141** couples efficiently at room temperature with **137** in the presence of Li or NaHMDS to give the keto sulfone **143** in $>$ 90% (NMR) yield in under an hour at room temperature. Work towards the nitrogen-doped substrate **131** using these alternative coupling partners is ongoing.

4.9 Conclusion

While the alkyne-containing materials directly enabled by ROAMP are attractive synthetic targets on their own, the untapped potential of those same alkynes as synthetic handles for post-polymerization modification represents a unique opportunity to access other classes of π-conjugated materials via this controlled polymerization. This chapter described a retrosynthetic approach to graphene nanoribbons via the Diels-Alder annulation of *poly(m,m'*-biphenylene ethynylene) templates that can be disconnected into cyclic ROAMP monomers.

The combination of three developments enable the successful synthesis and annulation of living polymer templates to give telechelic GNRs: a scalable synthesis of the strained cyclooctaphanediyne monomer **106**, the development of a more highly selective ONO pincer ROAMP catalyst **121**, and the use of alkyne metathesis depolymerization to detect even trace unreacted alkynes. Initial work demonstrating the synthesis of telechelic cGNRs and a proof-of-principle synthesis of nitrogen-doped comonomer **131** represent work towards unlocking power of this living polymer template approach to sequence-controlled GNR materials.

Chapter 5

Summary and Outlook

This work catalogued the development of several alkyne metathesis strategies to enable the controlled synthesis of carbon-rich polymer materials. Setting the stage for the current state of the art, Chapter 1 detailed the historical development of homogenous alkyne metathesis catalysts, their synthesis, and the fundamental kinetic selectivity challenge of ROAMP. In Chapter 2, the first ROAMP synthesis of a fully-conjugated polymer, PoPE, was described and we elaborated a mechanistic understanding of this unique monomer-controlled metathesis polymerization with a metallacyclobutadiene resting state. We also examined the instability of these metallacyclobutadiene intermediates, formulating a structural hypothesis for the nature of the organomolybdenum species at inactivated polymer chain ends. Chapter 3 examined electronic effects in alkyne metathesis, leveraging electronically-directed alkyne cross metathesis to prepare a wide variety of Mo benzylidynes under kinetic control. These enabled the careful study of the impact of electronics on the rate of ROAMP initiation by LFER analysis, and facilitated the design of bifunctional initiators for orthogonal radical copolymerizations from PoPE macroinitiators. Finally, we extended the applications of ROAMP from alkyne-containing materials into GNRs in Chapter 4, demonstrating a versatile living polymer template strategy to prepare monodisperse, telechelic GNRs.

The future of ROAMP is a bright one. On the catalyst side, while the [ONO] pincer framework might seem to suffer from "Bercaw's law of initial optimization," we have barely begun to explore the huge potential chemical space encompassing possible ROAMP catalysts. Alternate pincer architectures that feature more or less rigid backbones, stronger or weaker donors, allosteric binding sites, or different overall charge states could enable new ways of tuning of catalyst performance. From a polymer perspective, we have only just begun to scratch the surface of potential materials that could benefit from preparation via a living ROAMP. While most of these would require a significant investment in the synthesis of new strained monomers, if our work on preparing GNRs from polymer templates is any indication, the advantages of a living ROAMP approach can be well worth the effort.

Appendix A

Experimental Details

A.1 Materials and General Methods

Unless otherwise stated, all manipulations of air and/or moisture sensitive compounds were carried out in oven-dried glassware, under an atmosphere of Ar or N_2. All solvents and reagents were purchased from Alfa Aesar, Spectrum Chemicals, Acros Organics, TCI America, Matrix Scientific, and Sigma-Aldrich and were used as received unless otherwise noted. Organic solvents were dried by passing through a column of alumina and were degassed by vigorous bubbling of N_2 or Ar through the solvent for 20 min. Diphenyl ether was purified by fractional crystallization from the melt. Sulfolane was stirred with powdered KOH (10 %w/v) for 24 h then fractionally distilled under reduced pressure (discarding the first and last 20%). Solid alkyne substrates were recrystallized under N_2 from anhydrous solvents prior to use. Liquid alkynes were dried over 4 Å molecular sieves. Inhibitor was removed from methyl acrylate by washing with aqueous KOH followed by passing through an alumina column. For air- and moisture-sensitive NMR, deuterated solvents were stirred 24 h over 10 %w/v drying agent (C_6D_6 and toluene-d_8, CaH_2; $CDCl_3$, P_2O_5) subjected to three freeze-pump-thaw cycles, and vacuum transferred onto activated molecular sieves.

Chromatography

Flash column chromatography was performed on SiliCycle silica gel (particle size 40−63 μm). Thin layer chromatography was performed using SiliCycle silica gel 60 ÅF-254 precoated plates (0.25 mm thick) or Analtech aluminum oxide F-254 pre-coated plates and visualized by UV absorption. Size-exclusion chromatography (SEC) was carried out in 0.75% ethanol-stabilized chloroform on a LC/MS Agilent 1260 Infinity set up with one guard and two Agilent Polypore 300 × 7.5 mm columns at 35 °C. All SEC analyses were performed on 0.2 mg/mL (or 50% of saturated, if soluble <0.2 mg/mL) solutions of polymer in $CHCl_3$. An injection volume of 25 μL and a flow rate of 1 mL/min were used. Calibration was based on narrow polydispersity polystyrene standards ranging from Mw = 100 to 4,068,981 Da.

NMR Spectroscopy

All ^{1}H, ^{13}C{^{1}H}, and ^{19}F NMR spectra were recorded on Bruker AV-700, AV-600, DRX-500, AV-500, and AVQ-400 spectrometers between 20 and 25 °C unless otherwise noted, and are referenced to (residual) solvent peaks ($CDCl_3$ ^{1}H NMR δ = 7.26 ppm, ^{13}C{^{1}H} NMR δ = 77.16 ppm; C_6D_6 ^{1}H NMR δ = 7.16 ppm, ^{13}C{^{1}H} NMR δ = 128.06 ppm; pyridine-d_5 ^{1}H NMR δ = 7.22 ppm, ^{13}C{^{1}H} NMR δ = 150.35 ppm) or hexafluorobenzene (^{19}F NMR δ = −162.90 ppm). Concentrations for kinetics measurements were determined by ^{1}H and ^{19}F NMR using the ERETIC method[167] against an external standard of 18.2 mM 1,3,5-tris(trifluoromethyl)benzene in C_6D_6.

Solid-state ^{1}H-^{13}C cross polarization (CP) spectra were collected on a Bruker AV-500 spectrometer equipped with a Bruker 4 mm ^{1}H/X probe, at 11 Tesla and a ^{13}C frequency of 125.7 MHz under 10 and 12 kHz magic-angle spinning (MAS) condition, using a contact time of 3 ms and a pulse delay of 5 s, and proton decoupling by two-pulse phase modulation (TPPM) at an angle of 15° and decoupling field strength of 60 kHz. The Hartmann-Hahn condition for CP experiments was calibrated on solid adamantane, which was also used as an external ^{13}C chemical shift reference (methine C δ = 29.46 ppm).

Other Spectroscopy Techniques

ATR-IR spectra were obtained on a Thermo Nicolet 6700 FTIR. Raman spectra were obtained on a Renishaw inVia Qontor Raman microscope using a 514 nm excitation. UV-Vis absorption spectra were acquired on a Varian Cary 50 spectrophotometer (Agilent, USA). Fluorescence emission spectra were acquired at an excitation wavelength of 300 nm on a Fluoromax-4 spectrofluorometer equipped with automatic polarizers, 1.0 nm slit widths for excitation/emission and a 0.5 s integration time. Quantum yields were calibrated to 1,4-bis(5-phenyloxazol-2-yl) benzene (POPOP) in cyclohexane (Φ_F = 0.97).[168]

Mass Spectrometry

High-resolution mass spectrometry (EI) was performed on an Autospec Premier (Waters) sector spectrometer in positive ionization mode. ESI mass spectrometry was performed on a Finnigan LTQFT (Thermo) spectrometer. MALDI mass spectrometry was performed on a Voyager-DE PRO (Applied Biosystems Voyager System 6322) in positive mode using a matrix of dithranol or 100:1 dithranol/$AgNO_3$.

X-ray Crystallography

X-ray crystallography of **106** was performed on a Rigaku XtaLab equipped with a MicroMax-007HF microfocus rotating anode source (Cu−Kα radiation), a Pilatus 200K detector, and an Oxford Cryostream at 100 K. Crystallographic data were solved with SHELXT, refined with SHELXL-2014, visualized with ORTEP, and finalized with Olex.

X-ray crystallography of Mo complexes was performed on a Bruker APEX II QUAZAR, using a Microfocus Sealed Source (Incoatec IμS; Mo−Kα radiation), Kappa Geometry with DX (Bruker-AXS build) goniostat, a Bruker APEX II detector, QUAZAR multilayer mirrors as the radiation monochromator, and Oxford Cryostream at 100 K. Crystallographic data were solved with SHELXT, refined with SHELXL-2014, visualized with ORTEP, and finalized with WinGX.

Computational details

Restricted density functional theory was performed at the ωB97xD[169] level of theory using the 6-31G basis with one diffuse and two (d,p) polarization functions for light atoms (CHNOF) and the Stuttgart-Dresden (SDD) basis on Mo using the MWB28 effective core potential as implemented in Gaussian 09 version D1.[170] Initial structures for intermediates and transition state searches were located by relaxed coordinate scans of C-C and Mo-C distances. All stationary points and transition states were verified by vibrational analysis, exhibiting only real or a single imaginary frequency along the reaction coordinate, respectively. Energies (in Hartrees) are for gas-phase reactions and include the contribution of vibrational zero-point energies. The derivative structures were located from the unsubstituted (X = H) case by substitution of the stationary point structure and reoptimization (Berny).

Previously Synthesized Compounds

The following compounds were prepared according to literature procedures:

$MoCl_4(NCCH_3)_2$ (**55**)[171]
$MesC{\equiv}Mo(OC(CF_3)_2CH_3)_3$ (**23**)[172]
^{13}C-labeled 5,6,11,12-tetradehydrobenzo[*a,e*][8]annulene (**33***)[173]
1,2-di-*o*-tolylethyne (**45**)[174]
2,2,2-trifluoro-1-(2,4,6-trimethoxyphenyl)ethan-1-one (**49**)[175]
tert-butyl(4-iodophenoxy)dimethylsilane[176]
$ZnCl_2{\bullet}$TMEDA[177]
2-(ethylthiocarbonothioylthio)-2-methylpropanoic acid[178]
4-iodo-N,N,3-trimethylaniline[179]
4-iodo-N,N-dimethylaniline[180]
2-(bromomethyl)benzonitrile (**34**)[96]
2-(bromomethyl)benzaldehyde (**37**)[97]
triphenyl(4-(trifluoromethyl)benzyl)phosphonium bromide[181]
1-methyl-4-(3,3,3-trifluoroprop-1-yn-1-yl)benzene (**75**)[182]
1-methoxy-4-(3,3,3-trifluoroprop-1-yn-1-yl)benzene (**80**)[183,184]
(3,3,3-trifluoroprop-1-yn-1-yl)benzene (**81**)[183]
1-nitro-4-(3,3,3-trifluoroprop-1-yn-1-yl)benzene (**82**)[183]
N-(tert-butyl)-2-methyl-1-phenylpropan-1-amine-N-oxyl[185]
Activated Zn dust[186]

1-bromo-3-((phenylsulfonyl)methyl)benzene (**107**)[187]
1,2-bis(4-trifluoromethylphenyl)acetylene[188]
pTolCMoBr$_3$•DME[90]
2-(3,5-di-t-Bu-2-(methoxymethoxy)phenyl)-4,4,5,5-tetramethyl-1,3,2-dioxaborolane[189]
IPrPdCl2•pyridine[158]
1-(2,2-dibromovinyl)-4-nitrobenzene[190]
N,N'-dimethylpiperazine-2,3-dione[191]
4-dodecylbromobenzene[192]
authentic samples of unsubstituted **cGNR**[165]

A.2 Synthetic Procedures

2-((phenylsulfonyl)methyl)benzaldehyde (36)

A 100 mL round-bottomed flask equipped with a reflux condenser was charged with **37** (4.47 g, 22.5 mmol) and sodium benzenesulfinate (4.43 g, 27.0 mmol) in DMF (25 mL). The mixture was heated to 80 °C for 16 h, then cooled to 24 °C and poured into ice-cold H_2O (75 mL). The slurry was stirred for 10 min and the brown solid filtered and washed with H_2O (100 mL) and dried. The brown solid was recrystallized from EtOAc/hexanes to give **36** (4.8 g, 18.5 mmol, 82%) as light brown crystals. ^{1}H NMR (500 MHz, $CDCl_3$) δ = 9.82 (s, 1H), 7.74 (dd, J = 6.8, 1.9 Hz, 1H), 7.68 (d, J = 7.5 Hz, 2H), 7.62 – 7.55 (m, 5H), 7.48 – 7.42 (m, 4H), 5.04 (s, 2H) ppm. Spectroscopic data are consistent with a previous report.[96]

(5E,11E)-5,11-bis(phenylsulfonyl)dibenzo[*a,e*][8]annulene (38)

Adapting the method of Orita, et. al.,[96] a 500 mL Schlenk flask was charged under N_2 with **36** (1.30 g, 5 mmol) and diethyl chlorophosphate (0.99 g, 5.8 mmol) in dry THF (250 mL). The reaction mixture was cooled to –78 °C (dry ice-acetone) and LiHMDS (1 M in THF, 10 mL, 10 mmol) was added dropwise. When the addition was complete, the wine-red reaction mixture was stirred overnight as the dry-ice bath was allowed to warm slowly to 24 °C. The reaction mixture was stirred at 24 °C until the color lightened to yellow-orange and then quenched with saturated aqueous NH_4Cl (300 mL). The mixture was extracted EtOAc (2 × 100 mL), washed with saturated aqueous NaCl (100 mL), dried over $MgSO_4$, and concentrated on a rotary evaporator. Column chromatography (SiO_2, 1:1 EtOAc:Hexanes) or Soxhlet extraction (heptanes, 84 h) gave **38** (0.98 g, 2.0 mmol, 81%) as a tan solid. ^{1}H NMR (600 MHz, $CDCl_3$) δ = 7.64 (t, J = 7.4 Hz, 2H), 7.52 – 7.44 (m, 6H), 7.41 (d, J = 8.2 Hz, 4H), 7.36 (s, 2H), 7.31 – 7.23 (m, 4H), 6.98 (d, J = 7.1 Hz, 2H) ppm. Spectroscopic data are consistent with a previous report.[96]

5,6,11,12-tetradehydrobenzo[*a,e*][8]annulene (33)

A 100 mL Schlenk flask was charged under N_2 at −78 °C with LDA (2 M in THF / heptanes / ethylbenzene, 6 mL, 12 mmol) in dry THF (50 mL). Under vigorous stirring, a solution of **144** (0.985 g, 2.04 mmol) in dry THF (10 mL) was added dropwise. The reaction mixture was stirred at –78 °C for 2 h, then quenched with saturated aqueous NH_4Cl and warmed to 24 °C. The mixture was partitioned between CH_2Cl_2 (300 mL) and H_2O (50 mL), and the organic layer washed with H_2O (100 mL), saturated aqueous NaCl (50 mL), dried over $MgSO_4$, and concentrated on a rotary evaporator below 30 °C. The brown residue was triturated at –40 °C with CH_2Cl_2/Hexanes (1:1) to give **33** (0.305 g, 1.5 mmol, 75%) as a bright yellow solid. ^{1}H NMR (600 MHz, $CDCl_3$) δ = 6.94 – 6.91 (m, 4H), 6.76 – 6.73 (m, 4 H) ppm; $^{13}C\{^1H\}$ NMR (126 MHz, $CDCl_3$) δ = 133.1, 129.3, 127.1, 109.6 ppm. Spectroscopic data are consistent with a previous report.[96]

N≡Mo(C(CF$_3$)$_2$CH$_3$)$_3$ (14)

Adapting the method of Gdula, et. al.,[60] a 250 mL Schlenk flask was charged under N_2 with $MoCl_4(NCCH_3)_2$ (**145**) (2.62 g, 8.19 mmol) and suspended in dry acetonitrile (120 mL). Solid NaN_3 (0.66 g, 10.02 mmol) was added to the brown suspension which slowly lightened to a red-orange solution. The mixture was stirred 16 h at 24 °C.The volatiles were removed *in vacuo* and the residue resuspended in toluene (120 mL). Solid $LiOC(CF_3)_2CH_3$ (4.39 g, 23.4 mmol) was added and the flask was sealed and stirred overnight. The orange-brown mixture was filtered through 2 cm plug of Celite with toluene (80 mL). The volatiles were removed from the yellow- orange filtrate *in vacuo* and the brown residue redissolved in minimal boiling toluene (60 mL) and crystallized at –35 °C to give **14** as a colorless crystalline solid (3.39 g, 67%). m.p. 110 °C (dec). ^{1}H NMR (400 MHz, C_6D_6) δ = 1.65 (s, 9H) ppm; $^{13}C\{^1H\}$ NMR (C_6D_6) δ = 122.7 (q, $^1J_{CF}$ = 287 Hz), 84.6 (m, $^2J_{CF}$ = 30 Hz), 15.4 ppm; ^{19}F NMR (376 MHz, C_6D_6) δ = –78.02 ppm. Spectroscopic data are consistent with a previous report.[60]

EtC≡Mo(OC(CF$_3$)$_2$CH$_3$)$_3$•DME (15)

A 150 mL thick-walled resealable bomb flask was charged under N_2 with **14** (1.99 g, 3.05 mmol) and 3-hexyne (3 g, 37 mmol) in dry toluene (100 mL). The flask was sealed and slowly heated to 85 °C over 30 min, then heated to 95 °C for 20 h until the reaction was complete by ^{19}F NMR (judged by taking an aliquot, adding excess DME, and diluting with dry C_6D_6). The mixture was cooled to 24 °C and 1,2-dimethoxyethane (0.5 mL) was added and stirred for 30 min. The volatiles were removed *in vacuo* and the dark brown residue extracted with diethyl ether (20 mL), filtered through a 5 cm pad of Celite, gently scraping the top of the Celite when it became clogged by polymeric material. The filtrate was concentrated to ca. 10 mL and cooled to –35 °C overnight gave **15** as red-orange blocks (900 mg). The mother liquor was evaporated and the residue recrystallized from minimal pentane (ca. 5 mL) at –35 °C to give second crop of (1.08 g). Total yield 1.98 g, 86%. Crystals for X-ray analysis were

grown from toluene. Spectroscopic data are consistent with a previous report.[60] ^{1}H NMR (600 MHz, C_6D_6) δ = 3.16 (s, 6H), 3.00 (s, 4H), 2.65 (q, J = 7.6 Hz, 2H), 1.71 (s, 9H), 0.59 (t, J = 7.6 Hz, 3H) ppm; ^{13}C{^{1}H} NMR (151 MHz. C_6D_6) δ = 309.8, 124.5 (q, $^{1}J_{CF}$ = 289 Hz), 83.3 (m, $^{2}J_{CF}$ = 29 Hz), 71.6, 63.8, 43.1, 18.9, 12.6 ppm; ^{19}F (376 MHz, C_6D_6) δ = –76.84 ppm; HRMS (EI) (m/z): $[EtC{\equiv}Mo(OC(CH_3)(CF_3)_2)_3]^+$ calcd. $[C_{15}H_{14}F_{18}MoO_3]$, 681.9710; found, 681.9720; Anal. calcd. for $[EtC{\equiv}Mo(OC(CH_3)(CF_3)_2)_3(DME)]$: C, 29.62; H, 3.14. Found: C, 29.35; H, 2.96; Crystal data: CCDC no., 1456633; formula, $C_{19}H_{24}F_{18}MoO_5$; fw, 770.32 g mol^{-1}; temp, 100(2) K; cryst. system, monoclinic; space group, P2(1)/n; color, orange; a, 11.4678(9) Å; b, 16.8911(14) Å; c, 13.8634(11) Å; α, 90.000°; β, 91.155(2)°; γ, 90.000°; V, 2684.8(4) Å3; Z, 4; R1, 0.0262; wR2, 0.0556; GOF, 1.197.

General procedure for ring-opening alkyne metathesis polymerization of 33

Preparation of linear poly-(o-phenylene ethynylene) A 5 mL vial was charged under N_2 with **33** (0.02 g, 0.10 mmol) in toluene (1.50 mL). **23** (3.8 mg, 5.0 μmol) in toluene (0.60 mL) was added at 24 °C and the mixture was stirred for 3 h. The reaction mixture was quenched with MeOH (10 mL). The solid precipitate was isolated by filtration and washed with MeOH (30 mL) to yield linear PoPE (0.02 g, 82%) as a brown solid. ^{1}H NMR (500 MHz, $CDCl_3$) δ = 7.56 – 7.45 (br, 56H), 7.20 – 7.09 (br, 56H), 6.81 (s, 2H), 2.46 (s, 6H), 2.24 (s, 3H) ppm; ^{13}C{^{1}H} NMR (126 MHz, $CDCl_3$) δ = 132.3, 128.1, 125.8, 92.6, 21.3 ppm.

Preparation of cyclic poly-(o-phenylene ethynylene) A 20 mL vial was charged under N_2 with **33** (0.06 g, 0.30 mmol) in toluene (1.50 mL). **15** (43.4 mg, 55.0 μmol) in toluene (0.50 mL) was added at 24 °C and the mixture was stirred for 24 h. The reaction mixture was quenched with MeOH (10 mL). The solid precipitate was isolated by filtration and washed with MeOH (30 mL). Soxhlet extraction (hexane) of the crude mixture yielded cyclic PoPE (0.01 g, 18%) as a brown solid. The polymer remaining in the extraction thimble (30 mg) was dissolved in chloroform (15 mL) and precipitated with pentane (60 mL). The filtrate was evaporated to yield additional pure cyclic PoPE (0.02 g, total yield 50%). ^{1}H NMR (600 MHz, $CDCl_3$) δ = 7.48 – 7.44 (m, 2H), 7.13 – 7.09 (m, 2H) ppm; ^{13}C{^{1}H} NMR (126 MHz, $CDCl_3$) δ = 132.2, 128.1, 125.7, 92.5 ppm.

1-(but-1-yn-1-yl)-2-methylbenzene (46)

A 50 mL Schlenk flask was charged with 1-butyne (4 mL, 50 mmol), 2-iodotoluene (1.5 mL, 11.8 mmol), triethylamine (3.1 mL, 22.5 mmol), $PdCl_2(PPh_3)_2$ (156 mg, 0.23 mmol), and CuI (73 mg, 0.38 mmol) in dry THF (30 mL) under N_2 at –78 °C. The reaction mixture was stirred at 22 °C for 24 h. The reaction mixture was poured into hexanes (50 mL) and filtered through celite. Distillation under reduced pressure yielded **46** (1.56 g, 10.8 mmol, 92%) as a yellow oil. b.p. 42–44 °C (1 torr); ^{1}H NMR (500 MHz, $CDCl_3$) δ = 7.37 (d, J = 7.5 Hz, 1H), 7.21–7.14 (m, 2H), 7.14–7.08 (m, 1H), 2.47 (q, J = 7.5 Hz, 2H), 2.43 (s, 3H), 1.27 (t, J = 7.5 Hz, 3H) ppm; ^{13}C{^{1}H} NMR (126 MHz, $CDCl_3$) δ = 140.0, 131.9, 129.4, 127.6, 125.5,

123.9, 95.8, 78.9, 20.8, 14.3, 13.4 ppm; HRMS (EI) m/z: $[C_{11}H_{12}]+$ calcd. $[C_{11}H_{12}]$ 144.0939; found 144.0939

1,1,1,3,3,3-hexafluoro-2-(pyridin-2-ylmethyl)propan-2-ol (47)

A 100 mL Schlenk flask was charged under N_2 with 2-picoline (0.49 mL, 5 mmol) in dry THF (30 mL) and cooled to −78 °C. A solution of nBuLi (2.2 M in cyclohexane, 2.3 mL, 5.1 mmol) was added dropwise over 1 min. The orange reaction mixture was stirred for 15 min and then hexafluoroacetone was bubbled through the reaction mixture until no further color change occurred. The dark purple-brown mixture was warmed to 24 °C and the volatiles were removed *in vacuo*. The residue was quenched with 25 mL saturated aqueous NH_4Cl and extracted with EtOAc (3 × 20 mL). The extracts were dried over Na_2SO_4 and concentrated on a rotary evaporator. Column chromatography (SiO_2, 1:1 EtOAc:Hexanes, then SiO_2, 1:9 to 1:4 EtOAc:Hexanes) followed by recrystallization from pentane (1 mL) at –78 °C gave **47** (160 mg, 0.62 mmol, 12 %) as a yellow oil that solidifies upon refrigeration. ^{1}H NMR (600 MHz, $CDCl_3$) δ = 9.25 (s, 1H), 8.50 – 8.46 (m, 1H), 7.76 (td, J = 7.7, 1.8 Hz, 1H), 7.31 (dd, J = 7.3, 5.3 Hz, 1H), 7.25 (d, J = 7.8 Hz, 1H), 3.32 (s, 2H) ppm; $^{13}C\{^1H\}$ NMR (151 MHz, $CDCl_3$) δ = 155.46, 147.8, 138.5, 124.5, 123.2 (q, $^1J_{CF}$ = 289 Hz), 123.0, 77.0 (hept, $^2J_{CF}$ = 29 Hz) ppm.

4,4,4-trifluoro-3-hydroxy-1-phenyl-3-(trifluoromethyl)butan-1-one (48)

A 30 mL thick-walled pressure tube was charged with acetophenone (5.02 g, 22.7 mmol) and hexafluoroacetone trihydrate (10 mL). The flask was sealed and heated to 145 °C for 48 h. The flask was cooled to 24 °C and vented. The reaction mixture was concentrated on a rotary evaporator and then fractionally distilled under reduced pressure. The first fraction containing acetophenone was discarded, and the fraction distilling at 55–57 °C and 0.1 torr was collected to give **48** (3.13 g, 10.9 mmol, 48%) as a viscous oil that solidifies on standing. ^{1}H NMR (600 MHz, $CDCl_3$) δ = 7.97 (dd, J = 8.4, 1.2 Hz, 2H), 7.70 (tt, J = 7.2, 1.2 Hz, 1H), 7.58 – 7.52 (m, 2H), 7.20 (s, 1H), 3.47 (s, 2H) ppm; $^{13}C\{^1H\}$ NMR (151 MHz, $CDCl_3$) δ = 199.7, 135.7, 135.4, 129.3, 128.7, 122.7 (q, $^1J_{CF}$ = 288 Hz), 76.6 (hept, $^2J_{CF}$ = 30 Hz), 32.3 ppm.

1,1,1,3,3,3-hexafluoro-2-(2,4,6-trimethoxyphenyl)propan-2-ol (50)

A 20 mL polyethylene vial was charged under N_2 with (**49**) (1.27 g, 4.81 mmol) and trifluoromethyltrimethylsilane (1.56 g, 11.0 mmol) in dry DME. Solid cesium fluoride (110 mg, 0.72 mmol) was added. The mixture was stirred at 24 °C for 72 h, then hydrolyzed by the addition of 1 M aqueous HCl (10 mL) and stirred overnight. The reaction mixture was diluted with EtOAc (10 mL), washed with saturated aqueous NaCl (2 × 10 mL), dried over Na_2SO_4 and concentrated on a rotary evaporator. Column chromatography (SiO_2, 1:10 to

1:3 EtOAc:Hexanes) gave **50** (0.14 g, 0.42 mmol, 8.3%) as a colorless solid as well as its trimethylsilyl ether (1.45 g). ^{1}H NMR (600 MHz, $CDCl_3$) δ = 7.89 (s, 1H), 6.22 (s, 2H), 3.94 (s, 3H), 3.83 (s, 3H), 3.79 (s, 3H) ppm; ^{13}C{^{1}H} NMR (151 MHz, $CDCl_3$) δ 162.4, 160.9, 160.4, 123.3 (q, $^1J_{CF}$ = 289 Hz), 101.0, 93.2, 93.0, 80.7 (hept, $^2J_{CF}$ = 31 Hz), 57.5, 56.0, 55.5 ppm.

[EtC≡Mo[ON](OC(CF$_3$)$_2$CH$_3$)$_2$]$_2$•DME (51)

A 4 mL vial was charged under N_2 with EtC≡Mo(OC(CF$_3$)$_2$CH$_3$)$_3$•DME (**15**) (41 mg, 0.054 mmol) in dry toluene (0.5 mL). **47** (13 mg, 0.050 mmol) was added and the reaction mixture was stirred at 24 °C for 1 h. The volatiles were removed *in vacuo* and the residue recrystallized from 10:1 pentane:toluene (2 mL) at –35 °C to give **51** (31 mg, 0.039 mmol, 78%) as red-orange crystals. The reaction appears quantitative by ^{1}H and ^{19}F NMR and recrystallization serves only to remove the slight excess of **15** that catalytically consumes the alkyne substrate in the next step. ^{1}H NMR (600 MHz, C_6D_6) δ = 8.39 (d, J = 5.6 Hz, 1H), 6.71 (t, J = 7.5 Hz, 1H), 6.41 (d, J = 7.6 Hz, 1H), 6.37 (t, J = 6.4 Hz, 1H), 3.35 (s, 2H), 3.15 (s, 3H), 2.83 – 2.51 (br, 2H), 1.75 (br, 6H), 0.46 (t, J = 7.5 Hz, 3H) ppm; ^{19}F NMR (565 MHz, C_6D_6) δ = –74.31 (br, 3F), –74.92 (br, 3F), –75.56 (br, 3F), –76.68 (br, 3F), –77.20 (br, 3F), –77.41 (br, 3F) ppm.

[EtC≡Mo[OO](OC(CF$_3$)$_2$CH$_3$)$_2$]$_2$•DME (52)

A 4 mL vial was charged under N_2 with EtC≡Mo(OC(CF$_3$)$_2$CH$_3$)$_3$•DME (**15**) (80 mg, 0.104 mmol) in dry toluene (0.5 mL). **48** (29 mg, 0.101 mmol) in toluene (0.25 mL) was added and stirred at 24 °C for 16 h. Pentane (0.5 mL) was added and the reaction cooled to –35 °C for 24 h. The crystals were filtered, washed with cold pentane, and dried *in vacuo* to give **52** (72.3 mg, 0.084 mmol, 84%) as an orange crystalline solid. The reaction appears quantitative by ^{1}H and ^{19}F NMR and recrystallization serves only to remove the slight excess of **15** that catalytically consumes the alkyne substrate in the next step. ^{1}H NMR (400 MHz, C_6D_6) δ = 7.66 (dd, J = 8.5, 1.2 Hz, 2H), 6.99 (tt, J = 7.4, 1.3 Hz, 1H), 6.86 (t, J = 7.8 Hz, 2H), 3.42 (s, 2H), 3.15 (s, 3H), 2.61 (q, J = 7.5 Hz, 2H), 1.78 (s, 6H), 0.50 (t, J = 7.5 Hz, 3H) ppm; ^{19}F NMR (376 MHz, C_6D_6) δ = –76.58 (br, 6F), –76.96 (br, 6F), –77.36 (q, J = 8.4 Hz, 6F) ppm.

[Et(–C$_6$H$_4$CCC$_6$H$_4$–)C$_3$Mo[OO](OC(CF$_3$)$_2$CH$_3$)$_2$]$_2$ (54)

A 4 mL vial was charged under N_2 with [EtC≡Mo[OO](OC(CF$_3$)$_2$CH$_3$)$_2$]$_2$•DME (**52**) (41 mg, 0.05 mmol) in dry toluene (0.5 mL). **33** (10 mg, 0.05 mmol) in dry toluene (0.5 mL) was added and stirred at 24 °C for 15 min. The volatiles were removed in *in vacuo* and the residue triturated with cold pentane. The pentane was removed *in vacuo* to give **54** (49 mg, 0.05 mmol, 99%) as a dark blue-black oil that eventually solidifies. ^{1}H NMR (400 MHz, C_6D_6) δ = 7.59 (dd, J = 8.4, 1.1 Hz, 2H), 7.34 (d, J = 8.2 Hz, 1H), 7.05 – 6.97 (m, 2H),

6.93 – 6.84 (m, 3H), 6.80 (td, J = 7.7, 1.4 Hz, 1H), 6.63 (td, J = 7.6, 1.2 Hz, 1H), 6.59 (d, J = 6.7 Hz, 1H), 6.46 (td, J = 7.7, 1.3 Hz, 1H), 3.47 (d, J = 16.6 Hz, 1H), 3.41 (q, J = 7.6 Hz, 2H), 2.16 (s, 3H), 1.82 (d, J = 16.7 Hz, 1H), 1.23 (s, 3H), 1.01 (t, J = 7.5 Hz, 3H) ppm; ^{19}F NMR (376 MHz, C_6D_6) δ = –75.22 (hept, J = 9.4 Hz, 3F), –75.82 (br, 3F), –77.08 (br, 3F), –77.24 (br, 3F), –77.55 – –77.87 (m, 6F) ppm.

$\mathbf{[Et(-C_6H_4CCC_6H_4-)C_3Mo[ON](OC(CF_3)_2CH_3)_2]_2}$ (53)

A 4 mL vial was charged under N_2 with [EtC≡Mo[ON](OC(CF$_3$)$_2$CH$_3$)$_2$]$_2$•DME (**51**) (16 mg, 0.02 mmol) in dry toluene (0.5 mL). **33** (4 mg, 0.02 mmol) in dry toluene (0.5 mL) was added and stirred at 24 °C for 15 min. The volatiles were removed in *in vacuo* and the residue triturated with cold pentane. The pentane was removed *in vacuo* to give **53** (19 mg, 0.02 mmol, 99%) as a dark blue-black oil that eventually solidifies. ^{1}H NMR (600 MHz, C_6D_6) δ = 8.48 (d, J = 5.3 Hz, 1H), 7.31 (d, J = 7.7 Hz, 1H), 7.03 (d, J = 7.4 Hz, 2H), 6.85 – 6.76 (m, 3H), 6.69 – 6.63 (m, 2H), 6.53 (t, J = 7.6 Hz, 1H), 6.07 (d, J = 7.6 Hz, 1H), 3.27 (dq, J = 14.6, 7.6 Hz, 1H), 2.96 (dq, J = 14.6, 7.6 Hz, 1H), 2.58 (d, J = 15.9 Hz, 1H), 2.40 (d, J = 15.9 Hz, 1H), 1.96 (s, 3H), 1.90 (s, 3H), 0.66 (t, J = 7.4 Hz, 3H) ppm; ^{19}F NMR (565 MHz, C_6D_6) δ = –73.43 (br, 3F), –74.64 (br, 3F), –75.03 (q, J = 10.4 Hz, 3F), –75.20 (br, 3F), –75.41 (q, J = 10.9 Hz, 3F), –77.20 (br, 3F) ppm.

1,1,1-trifluoro-3-(4-(trifluoromethyl)phenyl)-3-(triphenylphosphoranylidene)propan-2-one (78)

A 50 mL Schlenk flask was charged under N_2 with triphenyl(4-(trifluoromethyl)benzyl) phosphonium bromide (2.1 g, 4.2 mmol) in dry CH_2Cl_2 (10 mL). The reaction mixture was cooled to 0 °C and DABCO (1.0 g, 8.8 mmol) in cold CH_2Cl_2 (3 mL) was added dropwise. When the addition was complete, trifluoroacetic anhydride (0.6 mL, 4 mmol) was added over 90 min. The reaction was allowed to warm to 24 °C and stirred for 20 h. The reaction mixture was filtered and concentrated on a rotary evaporator. The residue was extracted with cold THF (20 mL) and concentrated on a rotary evaporator to an oil which was triturated with H_2O (20 mL) to give a colorless solid which was recrystallized from aqueous MeOH at 0 °C to give **78** (1.03 g, 2.05 mmol, 50%) as colorless blocks in two crops. ^{1}H NMR (600 MHz, $CDCl_3$) δ 7.57 – 7.49 (m, 9H), 7.42 (td, J = 7.8, 3.2 Hz, 6H), 7.23 (d, J = 8.2 Hz, 2H), 7.11 (d, J = 7.2 Hz, 2H) ppm. A useful ^{13}C{^{1}H} NMR could not be obtained due to extensive P-C and F-C coupling throughout the molecule.

1-(trifluoromethyl)-4-(3,3,3-trifluoroprop-1-yn-1-yl)benzene (64)

A 25 mL 2-neck round-bottomed flask equipped with a thermometer adapter and an outlet tube leading to a dry-ice/acetone cold-finger condenser with a vacuum adapter[193] was charged

with **78** (0.475 g, 0.92 mmol) and sodium carbonate (25 mg, 0.25 mmol). The apparatus was evacuated (2 torr) and the flask slowly heated to 200 °C. The product begins to distill out of the reaction mixture at 160 °C and is complete by 200 °C. The contents of the cold trap are thawed and decanted to give **64** (164 mg, 0.69 mmol, 75 %) as a colorless oil. ^{1}H NMR (600 MHz, $CDCl_3$) δ = 7.72 – 7.64 (m, 4H) ppm; $^{13}C\{^{1}H\}$ NMR (151 MHz, $CDCl_3$) δ = 132.74 (q, $^{4}J_{CF}$ = 1.6 Hz), 132.60 (q, $^{2}J_{CF}$ = 33.1 Hz), 125.58 (q, $^{3}J_{CF}$ = 3.8 Hz), 123.4 (q, $^{1}J_{CF}$ = 272.4 Hz), 122.2 (m, J_{CF} = 1.7 Hz), 114.5 (q, $^{1}J_{CF}$ = 258 Hz), 84.5 (q, $^{3}J_{CF}$ = 6.5 Hz), 77.4 (q, $^{2}J_{CF}$ = 53.0 Hz) ppm; ^{19}F NMR (565 MHz, C_6D_6) δ = -50.98 (s, 3F), –64.04 (s, 3F) ppm.

N,N-dimethyl-4-(3,3,3-trifluoroprop-1-yn-1-yl)aniline (73)

Adapting the method of Konno, et. al.,[184] a 100 mL Schlenk flask was charged under N_2 with LDA (2 M in THF, 2.5 mL, 5 mmol) in dry THF (30 mL) and cooled to –78 °C and 2-bromo-3,3,3-trifluoropropene (0.24 mL, 2.4 mmol) was added dropwise. The reaction mixture was stirred at –78 °C for 5 min, then $ZnCl_2$•TMEDA (658 mg, 2.6 mmol) was added in one portion and stirred for another 30 min at –78 °C and 1 h at 24 °C to generate $CF_3C{\equiv}CZnCl$•TMEDA (**83**). 4-iodo-N,N-dimethylaniline (300 mg, 1.2 mmol) was added, followed by $Pd(PPh_3)_4$ (139 mg, 0.12 mmol), and the reaction stirred at 24 °C for 48 h. The reaction was quenched with saturated aqueous NH_4Cl (50 mL) and extracted with Et_2O (3 × 20 mL). The combined organic phases were washed with saturated aqueous NaCl, dried over $MgSO_4$, and concentrated on a rotary evaporator. The residue was filtered through a thin silica plug with 1:1 EtOAc:hexanes and sublimed at 80 °C/0.1 torr to give **73** (204 mg, 0.96 mmol, 80%) as a colorless solid. ^{1}H NMR (600 MHz, $CDCl_3$) δ = 7.40 (d, J = 8.9 Hz, 2H), 6.62 (d, J = 8.9 Hz, 2H), 3.02 (s, 6H) ppm; $^{13}C\{^{1}H\}$ NMR (151 MHz, $CDCl_3$) δ = 151.7, 133.9, 115.6 (q, $^{1}J_{CF}$ = 256 Hz), 111.6, 104.4, 89.1 (q, $^{3}J_{CF}$ = 6.4 Hz), 74.4 (q, $^{2}J_{CF}$ = 52 Hz), 40.1 ppm; ^{19}F NMR (376 MHz, $CDCl_3$) δ = –49.90 ppm; HRMS (ESI-TOF) m/z: $[C_{11}H_{10}F_3N{+}H]^+$ calcd. 214.0838; found 214.0836. Spectroscopic data are consistent with a previous report.[123]

tert-butyldimethyl(4-(3,3,3-trifluoroprop-1-yn-1-yl)phenoxy)silane (74)

Adapting the method of Konno, et. al.,[184] a 100 mL Schlenk flask was charged under N_2 with LDA (2 M in THF, 2.5 mL, 5 mmol) in dry THF (10 mL) and cooled to –78 °C and 2-bromo-3,3,3-trifluoropropene (0.75 mL, 7.5 mmol) was added dropwise. The reaction mixture was stirred at –78 °C for 5 min, then $ZnCl_2$•TMEDA (2.1 g, 8.25 mmol) was added in one portion and stirred for another 30 min at –78 °C and 1 h at 24 °C to generate $CF_3C{\equiv}CZnCl$•TMEDA (**83**). The reaction mixture was transferred by cannula to a 100 mL sealable Schlenk flask charged with tert-butyl(4-iodophenoxy)dimethylsilane, (1.67 g, 5 mmol) and $Pd(PPh_3)_4$ (115 mg, 0.1 mmol) in THF (10 mL). The flask was sealed and heated at 70 °C for 18 h. The reaction was cooled to 24 °C, quenched with saturated

aqueous NH_4Cl (100 mL), and extracted with EtOAc (2 × 20 mL). The combined organic phases were washed with saturated aqueous NaCl, dried over $MgSO_4$, and concentrated on a rotary evaporator. Column chromatography (SiO_2, pentanes) yields **74** (795 mg, 2.65 mmol, 53%) as a colorless oil. ^{1}H NMR (600 MHz, $CDCl_3$) δ = 7.44 (d, J = 8.6 Hz, 2H), 6.84 (d, J = 8.6 Hz, 2H), 0.98 (s, 9H), 0.22 (s, 6H) ppm; $^{13}C\{^1H\}$ NMR (151 MHz, $CDCl_3$) δ = 158.3, 134.3, 120.7, 115.2 (q, $^1J_{CF}$ = 256 Hz), 111.2, 87.2 (q, $^3J_{CF}$ = 6.5 Hz), 75.1 (q, $^2J_{CF}$ = 52.2 Hz), 25.7, 18.4, –4.3 ppm; ^{19}F NMR (376 MHz, $CDCl_3$) δ = –50.60 ppm; HRMS (ESI-TOF) m/z: $[C_{15}H_{19}F_3OSi]^+$ calcd. 300.1157; found 300.1153.

4-(3,3,3-trifluoroprop-1-yn-1-yl)phenyl acetate (84)

Adapting the method of Konno, et. al.,[184] a 100 mL Schlenk flask was charged under N_2 with LDA (2 M in THF, 5.5 mL, 11 mmol) in dry THF (30 mL) and cooled to –78 °C and 2-bromo-3,3,3-trifluoropropene (0.50 mL, 5 mmol) was added dropwise. The reaction mixture was stirred at –78 °C for 5 min, then $ZnCl_2$•TMEDA (1.52 g, 6 mmol) was added in one portion and stirred for another 30 min at –78 °C and 1 h at 24 °C to generate $CF_3C{\equiv}CZnCl$•TMEDA (**83**). 4-iodophenyl acetate (873 mg, 3.3 mmol) was added, followed by $Pd(PPh_3)_4$ (192 mg, 0.16 mmol), and the reaction stirred at 24 °C for 48 h. The reaction was quenched with saturated aqueous NH_4Cl (100 mL) and extracted with EtOAc (3 × 40 mL). The combined organic phases were washed with saturated aqueous NaCl, dried over $MgSO_4$, and concentrated on a rotary evaporator. The residue was filtered through a thin silica plug with 1:4 EtOAc:hexanes and distilled bulb-to-bulb at 50 °C/0.1 torr to give **84** (125 mg, 0.54 mmol, 16%) as a pale yellow, low-melting solid. ^{1}H NMR (500 MHz, $CDCl_3$) δ = 7.58 (d, J = 8.6 Hz, 2H), 7.15 (d, J = 8.6 Hz, 2H), 2.32 (s, 3H) ppm; $^{13}C\{^1H\}$ NMR (126 MHz, $CDCl_3$) δ = 169.0, 152.6, 133.9 (q, $^5J_{CF}$ = 1.4 Hz), 122.3, 116.1 (q, $^4J_{CF}$ = 1.8 Hz), 114.9 (q, $^1J_{CF}$ = 257 Hz), 85.8 (q, $^3J_{CF}$ = 6.4 Hz), 75.91 (q, $^2J_{CF}$ = 53 Hz) ppm; ^{19}F NMR (470 MHz, $CDCl_3$) δ = –50.60 ppm; HRMS (ESI-TOF) m/z: $[C_{11}H_7F_3O_2]^+$ calcd. 228.0398; found 228.0399.

(4-((CH$_3$)$_2$N)(C$_6$H$_4$)C≡Mo(OC(CH$_3$)(CF$_3$)$_2$)$_3$•(DME) (85)

A 10 mL flask was charged under N_2 with **15** (77 mg, 0.1 mmol) in toluene (2 mL). **73** (21 mg, 0.1 mmol) was added at 24 °C to the reaction mixture. The flask was immediately placed under dynamic vacuum (0.1 torr) and the reaction mixture stirred for 1 h at 24 °C. The solvent was removed *in vacuo* at 24 °C and the residue was recrystallized from pentane/toluene (3:1, 1.5 mL) at –30 °C to yield **85** (41 mg, 0.048 mmol, 48%) as a dark crystalline solid. ^{1}H NMR (600 MHz, C_6D_6) δ = 7.12 (d, J = 9.0 Hz, 2H), 6.15 (d, J = 9.0 Hz, 2H), 3.32 (s, 6H), 3.10 (s, 4H), 2.37 (s, 6H), 1.96 (s, 9H) ppm; $^{13}C\{^1H\}$ NMR (151 MHz. C_6D_6) δ = 297.7, 150.2, 134.5, 132.1, 124.9 (q, $^1J_{CF}$ = 289 Hz), 110.8, 84.1 (m, $^2J_{CF}$ = 29 Hz), 71.6, 63.7, 39.3, 19.3 ppm; ^{19}F NMR (376 MHz, C_6D_6) δ = –76.71 ppm; HRMS (EI) m/z: $[4\text{-}((CH_3)_2N)(C_6H_4)C{\equiv}Mo(OC(CH_3)(CF_3)_2)_3]^+$ calcd $[C_{21}H_{19}F_{18}MoNO_3]$ 773.0132; found 773.0132; Anal. calcd for [4-((CH$_3$)$_2$N)(C$_6$H$_4$)C≡Mo(OC(CH$_3$)(CF$_3$)$_2$)$_3$(DME)]: C, 34.86;

H, 3.39; N, 1.63. Found: C, 35.23; H, 3.41; N, 1.63. Dark green plates suitable for X-ray diffraction were grown from saturated pentane/Et_2O (1:1) solution at –35 °C. **85** crystallizes in the monoclinic space group P 21/n, a = 14.3977(5) Å, b = 14.4686(6) Å, c = 15.8068(7) Å, β = 100.490(2)°, Z = 4, GOF on F^2 = 1.051, R indices (all data) R1 = 0.0426, wR2 = 0.1021.

4-$(CH_3O)(C_6H_4)C{\equiv}Mo(OC(CH_3)(CF_3)_2)_3$(DME)] (86)

A 10 mL flask was charged under N_2 with **15** (77 mg, 0.1 mmol) in toluene (2 mL). The solution was cooled to 0 °C and **80** (22 mg, 0.11 mmol) was added to the reaction mixture. The flask was immediately placed under dynamic vacuum (0.1 torr) and removed from the cooling bath to warm to 24 °C. The solvent was removed *in vacuo* at 24 °C and the residue was recrystallized from pentane/toluene (4:1, 1 mL) at –30 °C to yield **86** (56 mg, 0.066 mmol, 66%) as a red crystalline solid. ^{1}H NMR (600 MHz, C_6D_6) δ = 7.07 (d, J = 8.8 Hz, 2H), 6.48 (d, J = 8.8 Hz, 2H), 3.28 (s, 6H), 3.17 (s, 3H), 3.08 (s, 4H), 1.87 (s, 9H) ppm; ^{13}C{^{1}H} NMR (151 MHz. C_6D_6) δ = 295.3, 160.5, 137.9, 132.3, 124.8 (q, $^1J_{CF}$ = 290 Hz), 113.7, 84.1 (m, $^2J_{CF}$ = 29 Hz), 63.8, 54.9, 19.2 ppm; ^{19}F NMR (470 MHz, C_6D_6) δ = –76.68 ppm; HRMS (EI) m/z: [4-$(CH_3O)(C_6H_4)C{\equiv}Mo(OC(CH_3)(CF_3)_2)_3]^+$ calcd [$C_{20}H_{16}F_{18}MoO_4$] 759.9815; found 759.9830; Anal. calcd for [4-$((CH_3O)(C_6H_4)C{\equiv}Mo(OC(CH_3)(CF_3)_2)_3$(DME)]: C, 33.98; H, 3.09. Found: C, 34.27; H, 3.04.

4-$CH_3(C_6H_4)C{\equiv}Mo(OC(CH_3)(CF_3)_2)_3$(DME) (87)

A 10 mL flask was charged under N_2 with **15** (77 mg, 0.1 mmol) in toluene (2 mL). The solution was cooled to –20 °C and **75** (22 mg, 0.11 mmol) was added to the reaction mixture. The flask was immediately placed under dynamic vacuum (0.1 torr) and removed from the cooling bath to warm to 24 °C. The solvent was removed *in vacuo* at 24 °C and the residue was recrystallized from pentane/Et_2O (4:1, 1 mL) at –30 °C to yield **87** (69 mg, 0.083 mmol, 83%) as an orange crystalline solid. ^{1}H NMR (500 MHz, C_6D_6) δ = 7.05 (d, J = 8.0 Hz, 2H), 6.76 (d, J = 8.0 Hz, 2H), 3.29 (s, 6H), 3.06 (s, 4H), 2.03 (s, 3H), 1.84 (s, 9H) ppm; ^{19}F NMR (376 MHz, C_6D_6) δ = –76.85 ppm; HRMS (EI) m/z: [4-$CH_3(C_6H_4)C{\equiv}Mo(OC(CH_3)(CF_3)_2)_3]^+$ calcd [$C_{20}H_{16}F_{18}MoO_3$] 743.9866; found 743.9854. Spectroscopic data are consistent with previous reports.[90]

PhC≡Mo$(OC(CH_3)(CF_3)_2)_3$(DME) (88)

A 10 mL flask was charged under N_2 with **15** (77 mg, 0.1 mmol) in toluene (2 mL). The solution was cooled to –20 °C and **81** (34 mg, 0.2 mmol, 2 equiv due to its high volatility) was added to the reaction mixture. The flask was immediately placed under dynamic vacuum (0.1 torr) and removed from the cooling bath to warm to 24 °C. The solvent was removed *in vacuo* at 24 °C and the residue was recrystallized from pentane/Et_2O (1:1, 2 mL) at –30 °C to yield **88** (65 mg, 0.079 mmol, 79%) as a red-orange crystalline solid. ^{1}H NMR (400 MHz,

C_6D_6) δ = 7.11 (d, J = 7.4 Hz, 2H), 6.96 (t, J = 7.9 Hz, 2H), 6.75 (t, J = 7.5 Hz, 1H), 3.25 (s, 6H), 3.03 (s, 4H), 1.81 (s, 9H) ppm; ^{19}F NMR (376 MHz, C_6D_6) δ = –76.67 ppm; HRMS (EI) m/z: $[(C_6H_5)C{\equiv}Mo(OC(CH_3)(CF_3)_2)_3]^+$ calcd $[C_{19}H_{14}F_{18}MoO_3]$ 729.9710; found 729.9722. Spectroscopic data are consistent with previous reports.[29]

4-(AcO)(C_6H_4)C≡Mo(OC(CH_3)(CF_3)$_2$)$_3$(DME) (89)

A 10 mL flask was charged under N_2 with **15** (77 mg, 0.1 mmol) in toluene (2 mL). The solution was cooled to –60 °C and **84** (23 mg, 0.1 mmol) was added to the reaction mixture. The flask was immediately placed under dynamic vacuum (0.1 torr) and removed from the cooling bath to warm to 24 °C. The solvent was removed *in vacuo* at 24 °C and the residue was recrystallized from pentane/Et_2O (4:1, 1.5 mL) at –30 °C to yield **89** (67 mg, 0.077 mmol, 77%) as a dark red crystalline solid. ^{1}H NMR (400 MHz, C_6D_6) δ = 7.12 (d, J = 8.7 Hz, 2H), 6.92 (d, J = 8.7 Hz, 2H), 3.24 (s, 6H), 3.06 (s, 4H), 1.79 (s, 9H), 1.70 (s, 3H) ppm; ^{13}C{^{1}H} NMR (126 MHz. C_6D_6) δ = 293.17, 168.3, 151.7, 141.1, 124.7 (q, $^1J_{CF}$ = 290 Hz), 121.6, 84.0 (m, $^2J_{CF}$ = 29 Hz), 71.6, 63.6, 20.4, 19.0 ppm; ^{19}F NMR (376 MHz, C_6D_6) δ = –76.70 ppm; HRMS (EI) m/z: [4-AcO(C_6H_4)C≡Mo(OC(CH_3)(CF_3)$_2$)$_3$]$^+$ calcd $[C_{21}H_{16}F_{18}MoO_5]$ 787.9764; found 787.9765; Anal. calcd for [4-AcO(C_6H_4)C≡Mo(OC(CH_3)(CF_3)$_2$)$_3$(DME)]: C, 34.26; H, 2.99. Found: C, 34.59; H, 3.34.

4-CF_3(C_6H_4)C≡Mo(OC(CH_3)(CF_3)$_2$)$_3$(DME) (65)

A 20 mL flask was charged under N_2 with **15** (231 mg, 0.3 mmol) in toluene (6 mL). The solution was cooled to –60 °C and **64** (87 mg, 0.36 mmol, 1.2 equiv) was added to the reaction mixture. The flask was immediately placed under dynamic vacuum (0.1 torr) and removed from the cooling bath to warm to 24 °C. The solvent was removed *in vacuo* at 24 °C and the residue was recrystallized from toluene (3 mL) at –25 °C and washed with cold pentane/Et_2O (1:1, 1 mL) to yield **65** (196 mg, 0.22 mmol, 74%) as an orange crystalline solid. ^{1}H NMR (600 MHz, C_6D_6) δ = 7.12 (d, J = 8.2 Hz, 2H), 6.95 (d, J = 8.2 Hz, 2H), 3.22 (s, 6H), 3.03 (s, 4H), 1.73 (s, 9H) ppm; ^{13}C{^{1}H} NMR (126 MHz. $CDCl_3$) δ = 291.8, 145.3, 130.7 (q, $^2J_{CF}$ = 33 Hz), 130.3, 125.5 (q, $^3J_{CF}$ = 3.7 Hz), 123.9 (q, $^1J_{CF}$ = 289 Hz), 123.4 (q, $^1J_{CF}$ = 272 Hz), 83.7 (m, $^2J_{CF}$ = 29 Hz), 72.0, 64.0, 19.0 ppm; ^{19}F NMR (564 MHz, C_6D_6) δ = –62.71 (s, 3F), –76.63 (s, 18 F) ppm; HRMS (EI) m/z: [4-CF_3(C_6H_4)C≡Mo(OC(CH_3)(CF_3)$_2$)$_3$]$^+$ calcd $[C_{20}H_{13}F_{21}MoO_3]$ 797.9583; found 797.9583; Anal. calcd for [4-CF_3(C_6H_4)C≡Mo(OC(CH_3)(CF_3)$_2$)$_3$(DME)]: C, 32.52; H, 2.62. Found: C, 32.39; H, 2.73.

4-O_2N(C_6H_4)C≡Mo(OC(CH_3)(CF_3)$_2$)$_3$(DME) (90)

A 10 mL flask was charged under N_2 with **15** (154 mg, 0.2 mmol) in toluene (4 mL). The solution was cooled to –60 °C and **82** (44 mg, 0.2 mmol) was added to the reaction mixture. The flask was immediately placed under dynamic vacuum (0.1 torr) and removed from the

cooling bath to warm to 24 °C. The solvent was removed *in vacuo* at 24 °C and the residue was recrystallized from pentane/Et_2O (1:1, 1 mL) at –30 °C to yield **90** (77 mg, 0.89 mmol, 45%) as a dark red crystalline solid. ^{1}H NMR (500 MHz, C_6D_6) δ = 7.58 (d, J = 8.9 Hz, 2H), 6.79 (d, J = 8.9 Hz, 2H), 3.21 (s, 6H), 3.02 (s, 4H), 1.71 (s, 9H) ppm; ^{13}C{^{1}H} NMR (126 MHz. C_6D_6) δ = 290.5, 147.1, 146.3, 130.4, 124.6 (q, $^1J_{CF}$ = 290 Hz), 123.7, 84.0 (m, $^2J_{CF}$ = 29 Hz), 71.7, 64.4, 18.9 ppm; ^{19}F NMR (376 MHz, C_6D_6) δ = –76.69 ppm; HRMS (EI) m/z: [4-$O_2N(C_6H_4)C{\equiv}Mo(OC(CH_3)(CF_3)_2)_3]^+$ calcd [$C_{19}H_{13}F_{18}MoNO_5$] 774.9560; found 774.9560; Anal. calcd for [4-$O_2N(C_6H_4)C{\equiv}Mo(OC(CH_3)(CF_3)_2)_3$(DME)]: C, 32.00; H, 2.69; N, 1.62. Found: C, 32.25; H, 2.60; N, 1.55. Orange prisms (yellow in transmission) suitable for X-ray diffraction were grown from saturated pentane/toluene (1:1) solution at –35 °C. The compound crystallizes in the monoclinic space group $P2_1$, a = 9.4048(5) Å, b = 9.2801(5) Å, c = 17.2135(9) Å, β = 98.630(3)°, Z = 2, GOF on F^2 = 0.994, R indices (all data) R1 = 0.0544, wR2 = 0.0820.

N,N,3-trimethyl-4-(3,3,3-trifluoroprop-1-yn-1-yl)aniline (91)

A 25 mL sealable Schlenk tube was charged under N_2 with 4-iodo-N,N,3-trimethylaniline (783 mg, 3 mmol) and $Pd(PPh_3)_4$ (170 mg, 0.15 mmol) in dry THF (3.5 mL). A solution of $CF_3C{\equiv}CZnCl{\bullet}$TMEDA (**83**) prepared by the method of Konno, et. al.[184] (0.28 M in THF/cyclohexane, 16 mL, 4.5 mmol) was added and the flask sealed and heated to 66 °C for 16 h. The reaction was cooled to 24 °C and quenched with saturated aqueous NH_4Cl (20 mL) and diluted with EtOAc (200 mL). The organic layer was separated, washed with H_2O (50 mL) and saturated aqueous NaCl (50 mL) and concentrated on a rotary evaporator to a dark oil. The oil was filtered through a plug of basic alumina with EtOAc (50 mL), concentrated on a rotary evaporator, and distilled under reduced pressure (50 °C, 10 torr) to give **91** (230 mg, 1.0 mmol, 34%) as a yellow oil that solidified on standing. ^{1}H NMR (500 MHz, $CDCl_3$) δ = 7.36 (d, J = 8.2 Hz, 1H), 6.53 – 6.45 (m, 2H), 3.01 (s, 6H), 2.41 (s, 3H) ppm; ^{13}C{^{1}H} NMR (126 MHz, $CDCl_3$) δ = 151.7, 143.1, 134.2 (q, $^4J_{CF}$ = 1.6 Hz), 115.7 (q, $^1J_{CF}$ = 255.6 Hz), 112.6, 109.4, 104.7, 88.4 (q, $^3J_{CF}$ = 6.4 Hz), 77.8 (q, $^2J_{CF}$ = 51.6 Hz), 40.1, 21.0 ppm; ^{19}F NMR (376 MHz, $CDCl_3$) δ = –49.65 ppm.

4-(3,3,3-trifluoroprop-1-yn-1-yl)phenyl 2-bromo-2-methylpropanoate (96)

A 10 mL Schlenk tube was charged under N_2 with **74** (147 mg, 0.49 mmol) in dry THF (5 mL). The reaction mixture was cooled to 0 °C and TBAF (1M in THF, 0.52 mL, 0.52 mmol) was added. The yellow mixture was stirred for 30 min before adding excess 2-bromoisobutyryl bromide (0.12 mL). The clear mixture was warmed to 24 °C and stirred for 16 h before quenching with saturated aqueous $NaHCO_3$ (5 mL) and EtOAc (10 mL). The organic layer was separated, washed with H_2O (10 mL), and saturated aqueous NaCl (10 mL), dried over Na_2SO_4 and concentrated on a rotary evaporator to a yellow oil. Column chromatography (SiO_2 1:9 to 1:4 CH_2Cl_2:pentane) gave **96** (91 mg, 0.27 mmol, 56%) as a colorless crystalline

solid. ^{1}H NMR (600 MHz, $CDCl_3$) δ = 7.61 (d, J = 8.6 Hz, 2H), 7.20 (d, J = 8.7 Hz, 2H), 2.07 (s, 6H) ppm; ^{13}C{^{1}H} NMR (151 MHz, $CDCl_3$) δ = 169.9, 152.7, 134.1 (q, $^{5}J_{CF}$ = 1.5 Hz), 121.9, 116.6 (q, $^{4}J_{CF}$ = 1.8 Hz), 114.9 (q, $^{1}J_{CF}$ = 257.0 Hz), 85.7 (q, $^{3}J_{CF}$ = 5.8 Hz), 76.2 (q, $^{2}J_{CF}$ = 52.6 Hz), 55.1, 30.7 ppm; ^{19}F NMR (376 MHz, $CDCl_3$) δ –51.11 ppm.

4-(3,3,3-trifluoroprop-1-yn-1-yl)phenyl 2-(((ethylthio)carbonothioyl)thio)-2-methylpropanoate (98)

A 25 mL Schlenk flask was charged under N_2 with **74** (300 mg, 1 mmol) in degassed DMF (15 mL). A degassed saturated aqueous solution of CsF (1 mL) was added and stirred for 1 h at 24 °C. The reaction mixture was poured into H_2O (25 mL), extracted with Et_2O (3 × 10 mL), washed with saturated aqueous NaCl, dried over $MgSO_4$, and concentrated on a rotary evaporator at 24 °C. The intermediate free phenol is unstable even at 0 °C, and was immediately reconstituted in dry, degassed CH_2Cl_2 (10 mL) and transferred to a 25 mL flask charged with 4-dimethylaminopyridine (6 mg, 0.05 equiv.) and 2-(((ethylthio)carbonothioyl)thio)-2-methylpropanoic acid (224 mg, 1 mmol, 1 equiv.) under N_2. The mixture was cooled to 0 °C and dicyclohexylcarbodiimide (241 mg, 1.17 mmol) in dry CH_2Cl_2 (2 mL) was added dropwise. The reaction mixture was warmed to 24 °C and stirred for 4 h. The reaction mixture was filtered through a plug of silica gel with CH_2Cl_2 and the filtrate concentrated on a rotary evaporator to give **98** (287 mg, 0.73 mmol, 73%) as a viscous yellow oil. ^{1}H NMR (600 MHz, C_6D_6) δ = 6.95 – 6.92 (m, 2H), 6.90 – 6.86 (m, 2H), 2.87 (q, J = 7.4 Hz, 2H), 1.57 (s, 6H), 0.86 (t, J = 7.4 Hz, 3H) ppm; ^{13}C{^{1}H} NMR (151 MHz, C_6D_6) δ = 221.9, 170.7, 153. 5, 134.0, 122.2, 115. 8 (q, $^{4}J_{CF}$ = 1.7 Hz), 115.7 (q, $^{1}J_{CF}$ = 257 Hz), 86.8 (q, $^{3}J_{CF}$ = 6.4 Hz), 76.0 (q, $^{2}J_{CF}$ = 52 Hz), 55.9, 31.4, 25.1, 12.7 ppm; ^{19}F NMR (376 MHz, C_6D_6) δ = –51.04 ppm.

2-((tert-butyl(2-methyl-1-phenylpropyl)amino)oxy)-2-methylpropanoic acid (146)

A 25 mL Schlenk flask was charged under N_2 with Cu powder (0.51 g, 7.8 mmol), PMDETA (1.31 g, 7.5 mmol), and CuBr (1.1 g, 7.5 mmol) in degassed MeOH (10 mL). 2-bromoisobutyric acid (1.4 g, 7.8 mmol) and N-(tert-butyl)-2-methyl-1-phenylpropan-1-amine-N-oxyl (1.5 g, 6.8 mmol) in degassed MeOH (5 mL) were added dropwise over 10 min. The reaction mixture was stirred for 4 h at 24 °C and then filtered. The filtrate was concentrated on a rotary evaporator to a green oil which was partitioned between 50 % saturated aqueous $NaHSO_4$ and CH_2Cl_2 (50 mL). The organic layer was separated and the aqueous layer extracted with CH_2Cl_2 (2 × 50 mL). The organic extracts were dried over Na_2SO_4 and concentrated on a rotary evaporator to a colorless oil which crystallized on standing at –40 °C. The crystals were washed with cold hexanes and dried *in vacuo* to give **97** (1.4 g, 4.6 mmol, 70 %) as colorless crystals containing a 3:7 mixture of diastereomers. ^{1}H NMR (600 MHz, $CDCl_3$) δ = 7.38 – 7.35 (m, 2H), 7.35 – 7.31 (m, 1H), 7.30 – 7.26 (m, 2H), 3.98 (d, J = 9.9 Hz, 1H,

minor), 3.80 (d, J = 10.0 Hz, 1H, major), 2.48 (ddt, J = 13.0, 9.9, 6.5 Hz, 1H, minor), 2.26 (ddt, J = 13.0, 10.1, 6.5 Hz, 1H, major), 1.80 (s, 3H, major), 1.79 (s, 3H, minor), 1.60 (s, 3H, major), 1.57 (s, 3H, minor), 1.27 (d, J = 6.4 Hz, 3H, minor), 1.26 (d, J = 6.3 Hz, 3H, major), 1.11 (s, 9H, major), 1.08 (s, 9H, minor), 0.62 (d, J = 6.6 Hz, 3H, minor), 0.47 (d, J = 6.7 Hz, 3H, major) ppm; $^{13}C\{^{1}H\}$ NMR (151 MHz, $CDCl_3$, both diastereomers) δ = 176.3, 139.4, 138.7, 131.6, 129.6, 128.5, 128.0, 127.8, 127.7, 75.7, 73.5, 65.0, 64.3, 31.4, 31.1, 28.9, 28.9, 27.8, 26.7, 26.4, 25.7, 23.5, 22.7, 22.5, 21.7 ppm;

4-(O(C=O)C(CH$_3$)$_2$Br)(C$_6$H$_4$)C≡Mo(OC(CH$_3$)(CF$_3$)$_2$)$_3$(DME) (99)

A 10 mL flask was charged under N_2 with **15** (39 mg, 0.05 mmol) in toluene (2 mL). The solution was cooled to –60 °C and **96** (16.7 mg, 0.05 mmol) was added to the reaction mixture. The flask was immediately placed under dynamic vacuum (0.1 torr) and removed from the cooling bath to warm to 24 °C. The solvent was removed *in vacuo* at 24 °C and the residue was extracted with pentane and evaporated to yield **99** (29 mg, 0.029 mmol, 58%) as a red-brown oil. ^{1}H NMR (400 MHz, C_6D_6) δ = 7.06 – 7.03 (m, 2H), 6.88 – 6.80 (m, 2H), 3.23 (s, 6H), 3.03 (s, 4H), 1.77 (s, 9H), 1.73 (s, 6H) ppm; ^{19}F NMR (376 MHz, C_6D_6) δ = –76.70 ppm;

4-(O(C=O)C(CH$_3$)$_2$S(C=S)SCH$_2$CH$_3$)(C$_6$H$_4$)C≡Mo(OC(CH$_3$)(CF$_3$)$_2$)$_3$(DME) (100)

A 10 mL flask was charged under N_2 with **15** (154 mg, 0.2 mmol) in toluene (4 mL). The solution was cooled to –60 °C and **98** (78 mg, 0.2 mmol) was added to the reaction mixture. The flask was immediately placed under dynamic vacuum (0.1 torr) and removed from the cooling bath to warm to 24 °C. The solvent was removed *in vacuo* at 24 °C. The solid residue was dissolved in minimum pentane and precipitated with perfluoromethylcyclohexane (10 mL) at 24 °C to yield **100** (122 mg, 0.12 mmol, 59%) as an orange powder. ^{1}H NMR (600 MHz, C_6D_6) δ = 7.05 (a q, J = 8.9 Hz, 2H), 3.23 (s, 6H), 3.05 (s, 4H), 2.87 (q, J = 7.4 Hz, 2H), 1.76 (s, 9H), 1.60 (s, 6H), 0.84 (t, J = 7.4 Hz, 3H) ppm; $^{13}C\{^{1}H\}$ NMR (151 MHz. C_6D_6) δ = 293.7, 222.4, 171.3, 152.4, 141.6, 131.9, 125.0 (q, $^{1}J_{CF}$ = 289 Hz), 122.0, 84.4 (m, $^{2}J_{CF}$ = 29 Hz), 71.9, 64.2, 56.2, 31.8, 25.5, 19.4, 13.0; ^{19}F NMR (376 MHz, C_6D_6) δ = –76.70 ppm; HRMS (ESI-TOF) m/z: [4-(EtSCS$_2$C(CH$_3$)$_2$CO$_2$)(C$_6$H$_4$)C≡Mo(OC(CH$_3$)(CF$_3$)$_2$)$_3$+AcO]$^-$ calcd [$C_{28}H_{27}F_{18}MoO_7S_3$] 1010.9686; found 1010.9653.

Preparation of PoPE-*block*-PMA

A J. Young tube was charged with trithiocarbonate-functionalized PoPE **102** (9 mg, 4 μmol), methyl acrylate (35 mg, 0.4 mmol) and AIBN (0.2 mg, 1.2 μmol) in C_6D_6 (0.5 mL). The reaction mixture was degassed and heated to 70 °C for 16 h. The reaction mixture was

cooled to –40 °C and diluted with EtOH (15 mL). The precipitate was washed with EtOH (5 mL), dried under vacuum, disolved in MeCN (4 mL), filtered (0.2 μm nylon membrane), and evaporated to yield PoPE-*block*-PMA (16 mg, 42%) as a brown solid. ^{1}H NMR (600 MHz, $CDCl_3$) δ = 7.50 (br, 40H), 7.15 (br, 40H), 3.66 (s, 270H), 3.37 (q, J = 7.4 Hz, 2H), 2.58 (br, 1 H), 2.33 (br, 90H), 1.93 (br, 30H), 1.69 (br, 90H), 1.60 – 1.41 (m, 60H), 1.40 – 1.19 (m, 119H) ppm; ^{13}C{^{1}H} NMR (151 MHz, $CDCl_3$) δ = 175.0, 132.2, 128.1, 125.7, 92.6, 51.8, 41.6 – 41.3 (m), 36.3 – 34.1(m) ppm; ^{13}C{^{1}H} NMR (151 MHz, $CDCl_3$) δ = 175.0, 132.2, 128.1, 125.7, 92.6, 51.8, 41.6 – 41.3 (m), 36.3 – 34.1(m) ppm.

2,6-bis(3,5-di-tert-butyl-2-(methoxymethoxy)phenyl)pyridine "MOM$_2$[ONO]" (115)

In a N_2-filled glovebox a 20 mL vial was charged with KOtBu (1.16g, 10.4 mmol, 2.6 equiv.) and IPrPdCl_2•pyridine (51 mg, 0.08 mmol, 0.02 equiv.) and capped with a septum. The vial was removed from the glovebox and 8 mL degassed 2-propanol was added. This yellow precatalyst solution darkened to deep red over 2 min. A separate 100 mL Schlenk flask was charged with 2,6-dibromopyridine (948 mg, 4 mmol, 1 equiv.) and 2-(3,5-di-tert-butyl-2-(methoxymethoxy)phenyl)-4,4,5,5-tetramethyl-1,3,2-dioxaborolane (3.74 g, 9.6 mmol, 2.4 equiv.) suspended in 30 mL degassed 2-propanol. The red catalyst solution was added by syringe with vigorous stirring, accompanied by the formation of a copious precipitate. The slurry was stirred at 24 °C for 48 h and then quenched by pouring into H_2O (100 mL). The mixture was extracted with 1:1 EtOAc:hexanes (2 × 40 mL), the organic extracts dried over Na_2SO_4 and concentrated on a rotary evaporator to a tan solid. Recrystallization from hexane (20 mL) at 0 °C gave MOM$_2$[ONO] **115** (1.08 g, 1.8 mmol, 45%) as a colorless solid. ^{1}H NMR (600 MHz, $CDCl_3$) δ = 7.77 – 7.73 (m, 1H), 7.71 – 7.68 (m, 2H), 7.60 (d, J = 2.5 Hz, 2H), 7.44 (d, J = 2.5 Hz, 2H), 4.63 (s, 4H), 3.40 (s, 6H), 1.50 (s, 18H), 1.36 (s, 18H) ppm; ^{13}C{^{1}H} NMR (151 MHz, $CDCl_3$) δ = 158.3, 151.4, 146.0, 142.4, 136.1, 134.1, 126.7, 125.1, 123.1, 99.6, 57.5, 35.6, 34.7, 31.6, 31.0 ppm. Spectroscopic data are consistent with a previous report.[159]

6,6'-(pyridine-2,6-diyl)bis(2,4-di-tert-butylphenol) "H$_2$[ONO]" (113)

A 200 mL round-bottom flask with reflux condenser was charged with MOM$_2$[ONO] (**115**) (1.08 g, 1.8 mmol) suspended in MeOH (75 mL). Concentrated HCl (25 mL) was added and the mixture stirred at 70 °C for 1 h. The reaction was cooled to 0 °C and filtered to give a light yellow solid. Recrystallization from MeOH at –40 °C gave as bright yellow crystals of H$_2$[ONO]•MeOH which were dried for 16 h at 80 °C and 0.1 torr to give H$_2$[ONO] (756 mg, 1.55 mmol, 86%) as a pale yellow powder. ^{1}H NMR (600 MHz, $CDCl_3$) δ = 10.59 (s, 2H), 8.01 (t, J = 8.0 Hz, 1H), 7.67 (d, J = 8.0 Hz, 2H), 7.51 (d, J = 2.3 Hz, 2H), 7.46 (d, J = 2.3 Hz, 2H), 1.49 (s, 18H), 1.39 (s, 18H) ppm; ^{13}C{^{1}H} NMR (151 MHz, $CDCl_3$) δ 157.5, 153.3, 141.5, 139.9, 137.4, 126.4, 122.9, 121.2, 120.4, 35.5, 34.5, 31.8, 29.7 ppm. Spectroscopic data are consistent with a previous report.[159]

[*p*TolC≡Mo[ONO]OC(CF$_3$)$_2$CH$_3$]$_2$•DME (112)

A 4 mL vial was charged under N_2 with TolC≡Mo(OC(CF$_3$)$_2$CH$_3$)$_3$•DME (**44**) (215 mg, 0.26 mmol) and tri-tert-butylphosphine (2.5 mg, 0.012 mmol) in dry toluene (1 mL). H_2[ONO] (**113**) (118 mg, 0.24 mmol) in dry toluene (1 mL) was added and stirred at 24 °C for 16 h and the reaction cooled to –35 °C for 24 h. The resulting crystals were filtered, washed with cold pentane, and dried *in vacuo* to give **112** (166 mg, 0.18 mmol, 71%) as a red-orange microcrystalline solid that crystallizes with 1 equiv. toluene per Mo. ^{1}H NMR (400 MHz, C_6D_6) δ = 7.74 (d, J = 2.4 Hz, 2H), 7.32 (d, J = 2.4 Hz, 2H), 7.17 (d, J = 7.9 Hz, 2H), 6.88 (t, J = 7.9 Hz, 1H), 6.53 (d, J = 7.9 Hz, 2H), 6.40 (d, J = 7.9 Hz, 2H), 3.23 (s, 2H), 2.99 (s, 3H), 2.07 (s, 3H), 1.82 (s, 3H), 1.75 (s, 18H), 1.40 (s, 18H) ppm; ^{19}F NMR (376 MHz, C_6D_6) δ = –75.63 ppm.

[*p*TolC≡Mo[ONO]OC(CH$_3$)$_3$]$_2$•DME (121•0.5DME)

A J. Young tube was charged with **112** (18 mg, 0.02 mmol) suspended in dry C_6D_6 (0.5 mL). KOt-Bu (0.05 M in C_6D_6, 40 μL, 0.02 mmol) was added and the orange suspension turned green and became homogeneous. ^{1}H and ^{19}F NMR suggest a 1:1 adduct is formed initially, presumably the mixed alkoxide "-ate" complex. The mixture was allowed to stand at 24 °C for 24 h and a yellow-orange powder slowly precipitated. This was filtered, washed with cold pentane and dried briefly *in vacuo* to give **121•0.5DME** (11 mg, 0.12 mmol, 60%) as a yellow-orange microcrystalline solid that crystallizes with 1 equiv. of toluene per Mo. It liberates bound DME and (more slowly) toluene *in vacuo*. ^{1}H NMR (600 MHz, C_6D_6) δ = 7.74 (d, J = 2.5 Hz, 2H), 7.29 (d, J = 2.5 Hz, 2H), 7.23 (d, J = 7.8 Hz, 2H), 6.97 (t, J = 7.9 Hz, 1H), 6.51 (d, J = 7.9 Hz, 2H), 6.38 (d, J = 8.2 Hz, 2H), 3.32 (s, 2H), 3.10 (s, 3H), 1.82 – 1.79 (m, 27H), 1.39 (s, 18H) ppm.

methyl 3'-((phenylsulfonyl)methyl)-[1,1'-biphenyl]-3-carboxylate (109)

A 500 mL Schlenk flask equipped with a reflux condenser and stir bar was charged with 1-bromo-3-((phenylsulfonyl)methyl)benzene (4.81 g, 15.5 mmol), (3-(methoxycarbonyl)phenyl) boronic acid (3.46 g, 19.2 mmol, 1.25 equiv.), (PPh_3)$_2$$PdCl_2$ (0.56 g, 0.8 mmol, 0.05 equiv.), and K_2CO_3 (14.7 g, 107 mmol, 6.7 equiv.). Degassed 1:1 v/v H_2O:THF (200 mL) was added and the reaction mixture stirred for 16 h under N_2 at 90 °C. The reaction mixture was cooled to 24 °C and quenched with saturated aqueous NH_4Cl (50 mL), extracted with EtOAc (2 × 25 mL), washed with H_2O (50 mL) and saturated aqueous NaCl (50 mL), dried over $MgSO_4$ and concentrated on a rotary evaporator. The dark brown solid was taken up in hot EtOAc (50 mL), filtered through celite to remove insoluble material, and evaporated. The residue was recrystallized from minimal EtOAc/hexane (1:1) and washed with hexane to give **109** (6.0 g, 15.5 mmol, 99%) as light brown needles. ^{1}H NMR (500 MHz, $CDCl_3$) δ = 8.05 (s, 1H), 8.01 (d, J = 7.8 Hz, 1H), 7.69 – 7.66 (m, 2H), 7.66 – 7.59 (m, 2H), 7.56 (d, J = 7.8

Hz, 1H), 7.48 (t, J = 7.7 Hz, 3H), 7.37 (t, J = 7.7 Hz, 1H), 7.21 (s, 1H), 7.16 (d, J = 7.6 Hz, 1H), 4.38 (s, 2H), 3.96 (s, 3H) ppm; $^{13}C\{^1H\}$ NMR (126 MHz, $CDCl_3$) δ 167.0, 140.61, 140.59, 137.8, 134.0, 131.6, 130.8, 130.3, 129.7, 129.3, 129.1, 129.0, 129.0, 128.9, 128.8, 128.2, 127.7, 63.0, 52.4 ppm; HRMS (ESI-TOF) m/z: $[C_{21}H_{18}O_4S+Na]^+$ calcd. 389.0818; found 389.0814.

4,8-bis(phenylsulfonyl)-1,2,5,6(1,3)-tetrabenzenacyclooctaphane-3,7-dione (110)

An oven-dried 1 L Schlenk flask was charged under N_2 with **109** (1.46 g, 4 mmol) in dry THF (450 mL). This mixture was added dropwise by cannula over 8 h to a second 1 L oven-dried Schlenk flask charged under N_2 with LiHMDS (1 M in THF, 17.6 mL, 17.6 mmol, 4.4 equiv.) in dry THF (50 mL). When the addition was complete, the reaction mixture was quenched with saturated aqueous NH_4Cl (50 mL) and H_2O (50 mL), extracted with EtOAc (2 × 50 mL), washed with saturated aqueous NaCl (50 mL), dried over $MgSO_4$ and concentrated on a rotary evaporator to a beige solid. The solid was triturated with MeOH (20 mL), then $CHCl_3$ (25 mL) and dried *in vacuo* to give **110** (860 mg, 1.28 mmol, 64%) as a colorless solid. ^1H NMR (600 MHz, pyridine-d_5) δ = 8.82 (s, 2H), 8.72 (s, 2H), 8.09 (d, J = 8.0 Hz, 2H), 7.88 (d, J = 7.3 Hz, 4H), 7.86 (d, J = 7.8 Hz, 2H), 7.81 (d, J = 7.7 Hz, 2H), 7.49 – 7.40 (m, 6H), 7.35 – 7.28 (m, 6H), 7.08 (s, 2H) ppm; $^{13}C\{^1H\}$ NMR (151 MHz, pyridine-d_5) δ = 190.1, 141.7, 140.4, 139.5, 137.0, 134.7, 132.1, 132.0, 131.9, 131.0, 130.8, 130.6, 130.5, 129.6, 129.4, 129.2, 128.2, 78.1 ppm; HRMS (ESI-TOF) m/z: $[C_{40}H_{28}O_6S_2+H]^+$ calcd. 667.1255; found 667.1265. The same reaction run at 400% scale (6.2 g **109**, 16 mmol) in the same volume of solvent gave **110** (2.15 g, 3.2 mmol) in 41% yield.

1,2,5,6(1,3)-tetrabenzenacyclooctaphane-3,7-dione (111)

Photoredox reduction: A 25 mL soda-lime glass vial with a septum cap was charged with **110** (400 mg, 0.6 mmol), $Ru(bpy)_3Cl_2$ (13 mg, 0.02 mmol, 3.3 mol%), diethyl-2,6-dimethyl-1,4-dihydropyridine-3,5-dicarboxylate (334 mg, 1.32 mmol, 2.2 equiv.) in pyridine (20 mL). The reaction mixture was degassed by sparging with N_2 for 20 min and then irradiated by blue LED light (Westinghouse 0315100 15W PAR38 Outdoor LED flood light) for 16 h. When TLC (1:2:1 EtOAc:Hex:CH_2Cl_2, Rf: **110** = 0.40, **111** = 0.76) indicated reaction was complete, the dark red-orange reaction mixture was poured into H_2O (200 mL) and filtered through a pad of Celite (2 cm × 5 cm dia). The filter cake was washed with H_2O until the filtrate was colorless (ca. 100 mL), then with MeOH until the filtrate was colorless (ca. 50 mL). The product was eluted from the filter cake with CH_2Cl_2 (300 mL), and concentrated on a rotary evaporator to give **111** (220 mg, 0.57 mmol, 94%) as a pale orange solid. ^1H NMR (600 MHz, $CDCl_3$) δ = 8.57 (s, 2H), 8.01 (s, 2H), 7.99 (d, J = 7.9 Hz, 2H), 7.78 (d, J = 7.5 Hz, 2H), 7.53 (t, J = 7.7 Hz, 2H), 7.43 – 7.32 (m, 7H), 4.39 (s, 4H) ppm; $^{13}C\{^1H\}$ NMR (151 MHz, $CDCl_3$) δ = 196.7, 141.0, 140.5, 137.5, 136.3, 130.68 , 129.9, 129.7, 129.2, 128.1, 127.5, 126.0, 49.3 ppm; HRMS (EI) m/z: $[C_{28}H_{20}O_2]^+$ calcd. 388.1463; found 338.1463.

Zinc Reduction: A 500 mL Schlenk flask was charged under N_2 with **110** (2.0 g, 3 mmol) and saturated aqueous NH_4Cl (20 mL) suspended in 4:1 DMAc:H_2O (250 mL). The reaction mixture was degassed by vigorous sparging with N_2 for 20 min and then activated Zn dust (19.5 g, 300 mmol, 100 equiv.) was added and the reaction stirred for 24 h at 24 °C. The reaction mixture was filtered and the filter cake washed with DMAc (25 mL). The filtrate was diluted with H_2O (800 mL), stirred for 5 min, and filtered. The solid was washed with H_2O (250 mL), 0.2 M HCl (100 mL), H_2O (250 mL), and dried under suction. The colorless solid was extracted with warm $CHCl_3$ (200 mL), filtered to remove any remaining Zn salts, and evaporated to give **111** (856 mg, 2.2 mmol, 79%) as a colorless solid of ∼90% purity by ^1H NMR, sufficiently pure for the next step. Analytically pure **111** (522 mg, 1.35 mmol, ∼60% recovery) can be obtained after filtering through a plug of SiO_2 with $CHCl_3$.

1,2,5,6(1,3)-tetrabenzenacyclooctaphane-3,7-diyne (106)

A 500 mL oven-dried Schlenk flask under N_2 was charged with **111** (754mg, 1.94 mmol) and N-phenyltriflimide (2.1 g, 6 mmol, 3 equiv.) in dry THF (150 mL). The reaction mixture was cooled to –78 °C and solid KHMDS (2.4 g, 12 mmol, 6 equiv.) was added in one portion. The reaction was stirred at –78 °C for 2 h and then warmed to 24 °C and quenched with H_2O (40 mL). The organic layer was separated and concentrated on a rotary evaporator. The wet residue was triturated with MeOH (20 mL) to give a colorless solid, which was extracted with hot pyridine (30 mL) and filtered. Recrystallization from pyridine at 0 °C gave **106** (380 mg, 1.08 mmol, 56%) as a colorless crystalline solid. The material is analytically pure, but its subsequent polymerization is more reproducible after a second recrystallization from anhydrous THF under N_2. ^1H NMR (600 MHz, $CDCl_3$) δ = 8.52 (t, J = 1.7 Hz, 4H), 7.73 – 7.71 (dm, J = 7.7 Hz, 4H), 7.46 (t, J = 7.7 Hz, 4H), 7.31 – 7.29 (dm, J = 7.7 Hz, 4H) ppm; HRMS (EI) m/z: $[C_{28}H_{16}]^+$ calcd. 352.1252; found 352.1257. Spectroscopic data are consistent with a previous report.[157] Colorless plates, uniformly 180° twins but suitable for X-ray diffraction, were grown by slow cooling of a saturated benzene solution from 80 to 22 °C. **106** crystallizes in the triclinic spacegroup P-1, a = 5.5153(2) Å, b = 15.9898(7) Å, c = 20.1319(5) Å, α = 97.836(3)°, β = 86.477(3)°, γ = 89.047(4)°, Z = 2, GOF on F^2 = 1.076, R indices (all data) R1 = 0.0645, wR2 = 0.1496. Solid **106** should be stored under N_2 but can be handled in air; signs of decomposition (yellow color, reduced solubility) develop over the course of several weeks when stored at ambient conditions.

*p*TolCMo(OC(CH$_3$)$_3$)$_3$•(DME)$_{0.5}$ (120)

In an N_2-filled glovebox a 20 mL vial was charged with KOt-Bu (336 mg, 3 mmol, 3 equiv.) in dry THF. Solid *p*TolCMoBr$_3$•DME (529 mg, 1 mmol) was added slowly with stirring over 10 min. The brown slurry was stirred 16 h at 24 °C and the volatiles removed *in vacuo*. The brown residue was extracted with pentane (2 × 5 mL), filtered through celite, and evaporated to a brown oil which crystallized on standing at –30 °C giving *p*TolCMo(OC(CH$_3$)$_3$)$_3$ (370 mg, 83%) as brown solid containing a variable amount of 1,2-dimethoxyethane (typically

ca. 0.25 equiv.) but of sufficient purity for subsequent steps. If required, stoichiometric material can be obtained as follows: the crude solid is dissolved in pentane (1 mL) and 1,2-dimethoxyethane (100 μL), concentrated to a brown oil *in vacuo* at 24 °C until crystallization begins. The oil is cooled to –30 °C for 72 h, after which the mother liquor is carefully decanted by syringe from the light brown crystals, which are quickly washed with –30 °C pentane (2 × 1 mL) and dried briefly *in vacuo* to give pTolCMo(OC(CH$_3$)$_3$)$_3$•(DME)$_{0.5}$ (**120**) (276 mg, 0.59 mmol, 70% recovery) as light brown crystals. ^{1}H NMR (500 MHz, CDCl$_3$) δ = 7.23 (d, J = 8.0 Hz, 2H), 7.07 (d, J = 8.0 Hz, 2H), 3.55 (s, 2H), 3.40 (s, 3H), 2.35 (s, 3H), 1.44 (s, 27H) ppm; ^{13}C{^{1}H} NMR NMR (126 MHz, CDCl$_3$) δ = 276.7, 144.0, 136.6, 129.5, 128.6, 80.0, 72.0, 59.2, 32.8, 21.4 ppm; Anal. for [pTolCMo(OC(CH$_3$)$_3$)$_3$•(DME)$_{0.5}$] calcd. C 57.01, H 8.48; found C 56.92, H 8.22.

*p*TolCMo[ONO]OC(CH$_3$)$_3$ (121)

In an N$_2$-filled glovebox a 20 mL vial was charged with pTolCMo(OC(CH$_3$)$_3$)$_3$•(DME)$_{0.5}$ (**120**) (254 mg, 0.55 mmol) in dry toluene (4 mL) and H$_2$[ONO] (**113**) (244 mg, 0.5 mmol) in dry toluene (2 mL) was added dropwise over 1 min. After stirring for 15 min at 24 °C the volatiles were removed *in vacuo*. The brown residue was suspended in pentane (3 mL) and filtered. The yellow solid was washed with pentane (2 × 1 mL) and dried at for 18 h at 100 °C and 0.1 torr to give **121** (256 mg, 0.34 mmol, 68%) as a yellow powder. ^{1}H NMR (500 MHz, C$_6$D$_6$) δ = 7.74 (d, J = 2.4 Hz, 2H), 7.29 (d, J = 2.4 Hz, 2H), 7.23 (d, J = 7.9 Hz, 2H), 6.97 (t, J = 7.9 Hz, 1H), 6.51 (d, J = 8.0 Hz, 2H), 6.37 (d, J = 8.1 Hz, 2H), 1.85 – 1.76 (m, 30H), 1.39 (s, 18H) ppm; ^{13}C{^{1}H} NMR (126 MHz, CDCl$_3$) δ = 305.4, 163.0, 157.4, 142.2, 141.1, 137.9, 137.5, 137.1, 129.5, 127.8, 126.4, 125.7, 124.6, 123.0, 83.3, 35.8, 34.5, 33.0, 31.9, 30.7, 21.4 ppm; Anal. for [pTolCMo[ONO](OC(CH$_3$)$_3$)] calcd. C 71.31, H 7.85, N 1.85; found C 71.21, H 7.57, N 2.04. Orange blocks of **121•t-BuOH** suitable for X-ray analysis were grown at 24 °C by slow evaporation of a pentane solution of the crude mixture of DME and t-BuOH solvates prior to desolvation. **121•t-BuOH** crystallizes in the monoclinic spacegroup P21/c, a = 15.9057(6) Å, b = 15.2617(5) Å, c = 19.1797(7) Å, β = 93.394(2)°, Z = 4, GOF on F^2 = 1.077, R indices (all data) R1 = 0.0450, wR2 = 0.0966.

N,N-dimethyl-2-(4-nitrophenyl)ethyn-1-amine (124)

A 100 mL Schlenk tube was charged under N$_2$ with 1-(2,2-dibromovinyl)-4-nitrobenzene (0.92 g, 3 mmol) in dry Et$_2$O (25 mL) at 0 °C. Dimethylamine (1.7 mL, 24 mmol, 8 equiv.) was condensed into a graduated Schlenk tube held at 0 °C, diluted with dry Et$_2$O (10 mL) and transferred by cannula into the flask containing 1-(2,2-dibromovinyl)-4-nitrobenzene. Solid KOt-Bu (336 mg, 3 mmol, 1 equiv.) was added in one portion triggering the formation of a copious precipitate. The reaction was warmed to 24 °C and stirred for 3 h. The solids were filtered off under N$_2$ and the volatiles removed *in vacuo*. The residue was extracted with toluene (10 mL) and filtered. The toluene filtrate was layered with pentane (10 mL) and cooled to –30 °C to yield **124** (0.48 g, 84%) as orange crystals. ^{1}H NMR (500 MHz, CDCl$_3$)

δ = 8.07 (dm, J = 9.0 Hz, 2H), 7.23 (dm, J = 9.0 Hz, 2H), 2.92 (s, 6H) ppm; 13C1H NMR (151 MHz, $CDCl_3$) δ = 144.2, 133.9, 128.3, 123.9, 106.4, 64.5, 43.5 ppm. Spectroscopic data are consistent with a previous report.[194]

Ring-opening alkyne metathesis polymerization of 106

In an N_2-filled glovebox a resealable Schlenk tube was charged with solid **106**, **147**, and Ph_3CH (internal standard). Freshly dried toluene (0.3 mL per mg **106**) was added and the flask was sealed, removed from the glovebox, and connected to a Schlenk line. The flask was immersed in a preheated 80 °C oil bath and stirred vigorously until all of **106** had dissolved (typically 2–3 min) at which point a 0.1 mL aliquot was taken, diluted with 0.5 mL dry C_6D_6 and analyzed by NMR to verify the initial ratio of **106**:**121**:Ph_3CH (by integration of the internal proton of **106** at 8.15 ppm, the upfield t-Bu groups at 1.38 ppm for **121** and 1.32 ppm for the initiated catalyst species, and the methine of Ph_3CH at 5.41 ppm). When >90% conversion of **106** was reached (NMR) the reaction temperature was lowered to 55 °C and ynamine **124** (100 equiv. to **121**) in minimal dry toluene was added. The reaction was stirred at 55 °C for 24 h and then the catalyst was hydrolyzed by the addition of 1 M Bu_4NOH solution in MeOH (100 equiv. to **121**) and stirred for 90 min at 80 °C. The reaction mixture was poured into 5 volumes of EtOH, filtered, washed with EtOH and hexane and dried *in vacuo* to give *poly(m,m'*-biphenylene ethynylene) (**104**) in > 90% yield. Raman (powder, λ = 514 nm) 1009, 1138, 1279, 1299, 1314, 1586, 1605, 2220 (ν C≡C) cm^{-1}; ^1H NMR (500 MHz, pyridine-d_5) δ = 8.25 (d, J = 8.5 Hz, 2H), 8.16 (s, 40H), 7.77 (d, J = 7.1 Hz, 41H), 7.72 (d, 6.5 Hz, 44H), 7.51 (t, J = 6.9 Hz, 44H), 2.22 (s, 3H); $^{13}C\{^1H\}$ NMR (126 MHz, pyridine-d_5) δ = 141.2, 131.7, 131.2, 130.2, 128.2, 124.7, 90.9 ppm.

4,4'-didodecylbenzil (148)

Adapting the method of Mueller-Westerhoff and Zhou,[191] a 200 mL Schlenk tube was charged under N_2 with 4-dodecylbromobenzene (4.68 g, 14.4 mmol) in dry THF (100 mL). The reaction mixture was cooled to –64 °C ($CHCl_3$/dry ice) and nBuLi (6 mL, 2.2 M in cyclohexane, 13.2 mmol) was added dropwise. The reaction mixture was stirred at –64 °C for 1 h. In a separate 500 mL Schlenk round bottom flask under N_2, a suspension of 1,4-dimethylpiperazine-2,3-dione (DMPD) (852 mg, 6 mmol) in dry THF (100 mL) was cooled to 0 °C. The solution of 4-dodecylphenyllithium was transferred by cannula into the cold suspension of DMPD over 1 min. The reaction mixture was stirred at 0 °C for 1.5 h, then decanted by cannula into rapidly stirring 1 M HCl (100 mL). The organic phase was separated and the aqueous layer extracted with hexanes (2 × 50 mL). The combined organic phases were washed with 1 M HCl (50 mL), H_2O (50 mL), saturated aqueous NaCl (50 mL), dried over $MgSO_4$, and concentrated on a rotary evaporator to an orange oil. Recrystallization from absolute ethanol (40 mL) gave **148** (2.06 g, 3.8 mmol, 63%) as pale yellow needles. ^1H NMR (500 MHz, $CDCl_3$) δ = 7.88 (d, J = 7.9 Hz, 4H), 7.30 (d, J = 7.9 Hz, 4H), 2.67 (t, J = 7.6 Hz, 4H), 1.70 – 1.56 (m, 4H), 1.36 – 1.20 (m, 36H), 0.88 (t, J = 6.7 Hz, 6H) ppm; $^{13}C\{^1H\}$ NMR

(126 MHz, $CDCl_3$) δ = 194.7, 151.2, 131.0, 130.2, 129.2, 36.4, 32.1, 31.2, 29.8, 29.8, 29.7, 29.6, 29.5, 29.4, 22.8, 14.3 ppm. Spectroscopic data are consistent with a previous report.[192]

3,4-bis(4-dodecylphenyl)-2,5-diphenylcyclopentadienone (130)

A 100 mL Schlenk flask equipped with a reflux condenser and magnetic stir bar was charged under N_2 with **148** (1.5 g, 2.7 mmol) and 1,3-diphenylacetone (572 mg, 2.7 mmol, 1 equiv.) in dry dioxane (20 mL). The reaction mixture was heated to vigorous reflux in a 110 °C bath and Bu_4NOH (1 M in MeOH, 2.7 mL, 1 equiv.) was added. The flask headspace was purged with N_2 for 3 min to remove the MeOH as it boiled off and then stirred at reflux at 110 °C for 30 min. The hot reaction mixture was poured into H_2O (50 mL) and extracted with CH_2Cl_2 (3 × 20 mL). The organic extracts were dried over Na_2SO_4, concentrated on a rotary evaporator, and dried in high vacuum to a gummy solid. Column chromatography (SiO_2, 3:7 CH_2Cl_2:hexanes) gave **130** (1.19 g, 1.65 mmol, 62%) as a purple solid. ^{1}H NMR (500 MHz, $CDCl_3$) δ = 7.26 – 7.17 (m, 10H), 6.97 (d, J = 8.1 Hz, 4H), 6.81 (d, J = 8.1 Hz, 4H), 2.56 (t, J = 7.5 Hz, 4H), 1.64 – 1.53 (m, 4H), 1.27 (br s, 36H), 0.89 (t, J = 6.9 Hz, 6H). ppm; $^{13}C\{^1H\}$ NMR (126 MHz, $CDCl_3$) δ = 200.6, 154.8, 143.6, 131.2, 130.4, 130.3, 129.5, 128.1, 128.0, 127.4, 125.0, 35.9, 32.1, 31.2, 29.9, 29.8, 29.8, 29.7, 29.5, 29.3, 22.9, 14.3 ppm. Spectroscopic data are consistent with a previous report.[195]

This reaction is highly irreproducible; yield varies from 14-62%, with a ∼40% average. Often a second column (SiO_2, slow gradient elution with 0:1 to 1:1 CH_2Cl_2:hexanes) is required. Occasionally a dodecylated impurity that cannot be separated chromatographically is present, but it does not appear to interfere with the subsequent use of **130**.

Post-polymerization Diels-Alder annulation of *poly*(*m,m'*-biphenylene ethynylene) to 103

A 0.5 mL microwave vial with a stir bar was charged under N_2 with *poly*(*m,m'*-biphenylene ethynylene) (**104**) (12 mg) and cyclopentadienone **130** (99 mg, 0.14 mmol, 2 equiv. per alkyne) in dry 4:1 w/w Ph_2O:sulfolane (0.45 g). The vial was capped and heated to 250 °C in a microwave reactor for 12 h. The vial was brought back into the glove box, uncapped to vent the internal CO pressure, and re-capped. To ensure complete conversion, heating was continued for 36 h at 250 °C in a microwave reactor. After cooling to 24 °C, the reaction mixture was diluted with toluene (1 mL), poured into EtOH (20 mL), and filtered. The solid was redissolved in hexane (1 mL) and precipitated with acetone (15 mL) to remove unreacted **130** and its decomposition products. The resulting gummy latex was centrifuged and the supernatant decanted. The pellet was re-dissolved in hexane (1 mL) and precipitated in EtOH (20 mL), filtered, washed with EtOH (20 mL), and dried *in vacuo* at 100 °C to constant weight to give polyphenylene **103** (49 mg, 83%) as a colorless solid. ^{1}H NMR (500 MHz, $CDCl_3$) δ =7.23 – 6.06 (m, 26H), 2.33 (s, 4H), 1.39 (s, 4H), 1.25 (s, 32H), 1.11 (s, 4H), 0.87 (s, 6H) ppm; $^{13}C\{^1H\}$ NMR (126 MHz, $CDCl_3$, 50 mM $Cr(acac)_3$) δ = 140.1 (br), 138.2 (br), 131.4 (br), 126.7 (br), 35.5, 32.1, 31.4, 29.9, 29.5, 29.1, 22.9, 14.3 ppm; ^{13}C SSNMR

(^{1}H-^{13}C CP, 126 MHz, 12 kHz MAS) δ = 141.2, 139.2, 131.9, 126.9, 36.1, 32.7, 30.4, 23.4, 14.7 ppm.

ROAMP-cGNR

A 600 mL Schlenk flask was charged under N_2 with polyphenylene **103** (62 mg) in dry CH_2Cl_2 (350 mL). The reaction mixture was vigorously sparged with N_2 for 15 min. $FeCl_3$ (1.27 g, 7.8 mmol, 7 equiv. per H) dissolved in dry CH_3NO_2 (10 mL) was added and the reaction mixture was stirred at 24 °C for 84 h, continuously sparging with CH_2Cl_2-saturated N_2. When HCl evolution had ceased, the reaction was quenched by the addition of MeOH (200 mL) and filtered. The solid was washed with MeOH (200 mL), 0.5 M HCl in 50% aqueous MeOH (100 mL), 1 M HCl (100 mL), deionized H_2O (200 mL), acetone (200 mL), EtOAc (200 mL), and hexane (100 mL). The solid was re-suspended by a 15-min sonication in toluene (100 mL), filtered, washed with toluene (100 mL) and CH_2Cl_2 (200 mL). The solid was re-suspended by a 15-min sonication in EtOH (100 mL), filtered, washed with EtOH (100 mL) and MeOH (200 mL) and dried *in vacuo* at 100 °C to constant weight to give **ROAMP-cGNR** (61 mg, 99%) as a black solid. ^{13}C SSNMR (^{1}H-^{13}C CP, 126 MHz, 12 kHz MAS, 50%wt in KBr) δ = 138.6, 126.8, 122.5, 28.8, 13.2 ppm; Raman (powder, λ = 514 nm) 1325 (D), 1610 (G), 2637 (2D), 2933 (D+G) cm^{-1}.

Methyl 5-bromonicotinate (134)

Adapting the method of Thompson and Gaudino,[196] a 100 mL round bottom flask with a reflux condenser topped with a drying tube was charged with nicotinic acid (10 g, 80 mmol) suspended in thionyl chloride (25 mL). The reaction mixture was heated to reflux in a 95 °C oil bath until all of the solids dissolved (∼2 h). The reaction mixture was cooled to 24 °C and the condenser replaced with a distillation head. The excess thionyl chloride was distilled off at atmospheric pressure in a 110 °C bath. To the residue, which solidified on cooling, was added bromine (13.4 g, 84 mmol, 1.05 equiv). The distillation head was replaced with a reflux condenser topped with a drying tube and the reaction mixture heated to reflux in a 150 °C bath for 12 h. The residue, which solidified on cooling to 24 °C, was suspended in dry CH_2Cl_2 (40 mL). The reaction mixture was brought to reflux for 10 min and then removed from the heat as MeOH (10 mL) was added dropwise through the condenser at a rate sufficient to maintain a gentle reflux (approx. 20 min for addition). After the exotherm subsides, an additional 10 mL MeOH was added and the reaction mixture refluxed for 2 h at (∼55 °C bath temperature). After cooling to 24 °C, the reaction mixture was poured into 100 mL saturated aqueous K_2CO_3. The organic layer was separated and the aqueous phase extracted with CH_2Cl_2 (4 × 30 mL). The organic phases were combined, washed with saturated aqueous Na_2SO_3 (2 × 30 mL), H_2O (30 mL), dried over Na_2SO_4, and concentrated on a rotary evaporator to a yellow solid. The solid was recrystallized from hot 2:3 H_2O/MeOH to give pure **134** (10.4 g, 48 mmol, 60%) as pale pink needles. ^{1}H NMR (400 MHz, $CDCl_3$) δ = 9.09 (d, J = 1.6 Hz, 1H), 8.81 (d, J = 2.2 Hz, 1H), 8.42 (t, J = 1.9 Hz, 1H), 3.95 (s, 2H)

ppm; $^{13}C\{^1H\}$ NMR (101 MHz, $CDCl_3$) δ = 164.6, 159.6, 154.6, 148.9, 139.8, 127.5, 52.9. Spectroscopic data are consistent with a previous report.[196]

(5-bromopyridin-3-yl)methanol (135)

Adapting the method of Hemel, et. al.,[197] a 500 mL two-neck round bottom flask equipped with a thermometer was charged with **134** (20.68 g, 96 mmol) suspended in absolute ethanol (200 mL). The reaction mixture was cooled in an ice bath and $NaBH_4$ (8.3 g, 220 mmol, 2.3 equiv.) was added slowly over 15 min, maintaining an internal temperature below 10 °C. The flask was equipped with a reflux condenser and the reaction mixture was stirred for 1 h and then removed from the ice bath. Upon warming the reaction mixture begins liberating hydrogen gas and the internal temperature rises to ∼50 °C over 2 h. After the initial exotherm subsided, the reaction mixture was heated to reflux in a 95 °C bath for 15 h. The reaction mixture was concentrated on a rotary evaporator to ∼100 mL, diluted with acetone (100 mL), and refluxed 1 h in a 65 °C bath. The reaction mixture was again concentrated to 100 mL and diluted with saturated aqueous K_2CO_3 (100 mL). The mixture was brought to reflux in 110 °C bath for 30 min, at which point all of the solids had dissolved. The reaction mixture was again concentrated to 100 mL on a rotary evaporator to remove liberated EtOH, and the aqueous concentrate was subjected to continuous liquid-liquid extraction with CH_2Cl_2 (300 mL) for 18 h. The CH_2Cl_2 extract was dried over Na_2SO_4, filtered through a pad of Celite, and concentrated to an orange oil, which was distilled under reduced pressure (140 mtorr, 140 °C bath temperature) and after a yellow forerun distilling at 70-100 °C, **135** (8.56 g, 46 mmol, 48%) was collected as a colorless oil (b.p. 102-107 °C, 140 mtorr) which crystallized on standing. ^1H NMR (400 MHz, $CDCl_3$) δ = 8.56 (d, J = 2.1 Hz, 1H), 8.46 (d, J = 1.5 Hz, 1H), 7.89 (t, J = 2.0 Hz, 1H), 4.72 (s, 2H). Spectroscopic data are consistent with a previous report.[197]

3-bromo-5-(chloromethyl)pyridinium chloride (136)

Adapting the method of Hemel, et. al.,[197] a 100 mL two-neck round bottom flask an outlet bubbler and a septum was charged with **135** (8.5 g, 45 mmol) in CH_2Cl_2 (40 mL). $HCl_{(g)}$ was bubbled through the reaction mixture until saturated, forming a copious precipitate. DMF (0.1 mL) was added, followed by dropwise addition of thionyl chloride (6.5 mL, 90 mmol, 2 equiv.). The reaction mixture was stirred at 24 °C for 18 h and then poured into cyclohexane (100 mL). The precipitate was filtered, washed with cyclohexane, and dried *in vacuo* to give pure **136** (10.9 g, 45 mmol, 99%) as a tan solid in quantitative yield. ^1H NMR (600 MHz, DMSO-d_6) δ = 8.74 (d, J = 2.2 Hz, 1H), 8.69 (d, J = 1.8 Hz, 1H), 8.26 (t, J = 2.0 Hz, 1H), 7.56 (s, 1H), 4.83 (s, 2H) ppm; $^{13}C\{^1H\}$ NMR (151 MHz, DMSO-d_6) δ = 149.4, 147.6, 139.9, 136.1, 120.2, 42.0 ppm.

3-bromo-5-(tosylmethyl)pyridine (137)

A 500 mL round bottom flask equipped with a reflux condenser was charged with **136** (5.82 g, 24 mmol), sodium 4-methylbenzenesulfinate (5.2 g, 29 mmol, 1.2 equiv.), anhydrous K_2CO_3 (5.35 g, 39 mmol, 1.6 equiv.), and KI (200 mg, 1.2 mmol, 0.05 equiv.) in DMF (200 mL). The reaction mixture was heated at 85 °C for 18 h, cooled to 24 °C and poured into ice-cold H_2O (600 mL). The precipitated solids were filtered, washed with H_2O (200 mL), and dried *in vacuo* to give **137** (6.44 g, 20 mmol, 83%) as a colorless solid. ^{1}H NMR (500 MHz, $CDCl_3$) δ = 8.62 (d, J = 1.9 Hz, 1H), 8.08 (d, J = 1.4 Hz, 1H), 7.73 (t, J = 2.0 Hz, 1H), 7.54 (d, J = 8.3 Hz, 2H), 7.30 (d, J = 8.0 Hz, 2H), 4.24 (s, 2H), 2.44 (s, 3H) ppm; ^{13}C{^{1}H} NMR (126 MHz, $CDCl_3$) δ = 151.2, 149.3, 145.7, 140.8, 134.3, 130.1, 128.7, 126.4, 120.7, 59.5, 21.8 ppm.

5-bromonicotinaldehyde (132)

A 100 mL Schlenk tube was charged under N_2 with 3,5-dibromopyridine (7.7 g, 32.5 mmol) in anhydrous THF (25 mL). The reaction mixture was cooled to –78 °C and a solution of i-PrMgCl•LiCl (32.5 mmol, 1.3 M in THF, 25 mL) was added dropwise. The reaction mixture was stirred at –78 °C for 2 h, then anhydrous DMF (5 mL, 65 mmol, 2 equiv.) was added and the reaction mixture stirred for 16 h at 24 °C. The reaction was quenched by pouring into saturated aqueous NH_4Cl (100 mL), the organic phase was separated and the aqueous layer extracted with Et_2O (6 × 20 mL). The combined organic phases were washed with saturated aqueous NaCl (30 mL), dried over $MgSO_4$, and concentrated on a rotary evaporator. The residue was recrystallized from hot hexanes to give **132** (3.65 g, 20 mmol, 60%) as a beige crystalline solid of sufficient purity (>90%) for subsequent steps. Analytically pure material can be obtained by sublimation or column chromatography, albeit with significant losses during the latter procedure. ^{1}H NMR (600 MHz, $CDCl_3$) δ = 10.06 (s, 1H), 8.97 (d, J = 1.7 Hz, 1H), 8.89 (d, J = 2.3 Hz, 1H), 8.29 (t, J = 2.0 Hz, 1H); ^{13}C{^{1}H} NMR (151 MHz, $CDCl_3$) δ = 189.3, 155.9, 150.0, 138.1, 132.6, 121.8. Spectroscopic data are consistent with a previous report.[198]

5-(4,4,5,5-tetramethyl-1,3,2-dioxaborolan-2-yl)nicotinaldehyde (133)

A 50 mL Schlenk tube equipped with a reflux condenser was charged under N_2 with **132** (554 mg, 3 mmol), B_2pin_2 (761 mg, 3 mmol, 1 equiv.), anhydrous KOAc (980 mg, 10 mmol, 3.3 equiv.), dppfPdCl_2 (110 mg, 0.15 mmol, 5 mol%) in anhydrous dioxane (35 mL). The reaction mixture was degassed by vigorous sparging with N_2 for 20 min, then heated 110 °C for 24 h. The reaction mixture was cooled to 24 °C, poured into 100 mL wet Et_2O, filtered through Celite, and concentrated on a rotary evaporator to a dark oil. This residue was extracted with pentane (100 mL), filtered, and evaporated to give a tan solid which was triturated with cold (0 °C) Et_2O (10 mL) and filtered to give **133** (250 mg) as a colorless

solid. The Et_2O filtrate was cooled to –40 °C to give a second crop (total yield, 505 mg, 2.2 mmol, 72%) of **133**. ^{1}H NMR (600 MHz, $CDCl_3$) δ = 10.12 (s, 1H), 9.16 – 9.13 (m, 2H), 8.54 (t, J = 1.9 Hz, 1H), 1.37 (s, 12H) ppm; $^{13}C\{^1H\}$ NMR (151 MHz, $CDCl_3$) δ = 191.1, 160.1, 153.5, 143.1, 130.9, 84.9, 25.0 ppm, C bonded to B not observed.

5'-(tosylmethyl)-[3,3'-bipyridine]-5-carbaldehyde (138)

A 250 mL Schlenk flask equipped with a reflux condenser was charged under N_2 with **137** (978 mg, 3 mmol), **133** (769 mg, 3.3 mmol), tetrabutylammonium bromide (48 mg, 0.15 mmol), and solid K_3PO_4 (1.4 g, 6.6 mmol) in H_2O (4 mL) and dioxane (40 mL). The reaction mixture was subjected to three freeze-pump-thaw cycles and then $Pd(PPh_3)_4$ (173 mg, 0.15 mmol) was added and the reaction mixture heated to 120 °C for 2.5 h. The reaction mixture was cooled to 24 °C and dried over Na_2SO_4, and concentrated on a rotary evaporator and dried *in vacuo* to give a brown oil. Trituration with Et_2O (10 mL) gives **138** (949 mg, 2.7 mmol, 90%) as a brown solid. ^{1}H NMR (600 MHz, $CDCl_3$) δ = 10.21 (s, 1H), 9.12 (s, 1H), 9.00 (s, 1H), 8.85 (s, 1H), 8.32 (s, 1H), 8.27 (t, J = 2.1 Hz, 1H), 7.79 (s, 1H), 7.58 (d, J = 8.2 Hz, 2H), 7.32 (d, J = 8.1 Hz, 2H), 4.38 (s, 2H), 2.45 (s, 3H) ppm; $^{13}C\{^1H\}$ NMR (151 MHz, $CDCl_3$) δ = 190.3, 153.1, 151.9, 151.5, 148.3, 145.8, 136.9, 134.6, 133.9, 133.5, 132.3, 131.6, 130.1, 128.7, 125.4, 60.0, 21.8 ppm.

(3E,7E)-3,7-ditosyl-1,2,5,6(3,5)-tetrapyridinacyclooctaphane-3,7-diene (139)

A 250 mL Erlenmeyer flask was charged under Ar with **138** (353 mg, 1.0 mmol) suspended in THF (200 mL). LiOtBu (410 mg, 5.1 mmol) was added and the yellow mixture darkens slightly. The reaction flask was sealed with a septum and stirred at 24 ° for 16 d. The reaction was quenched with saturated aqueous NH_4Cl and the organic layer separated and concentrated on a rotary evaporator. Prep TLC (Al_2O_3, 1:30 EtOH:$CHCl_3$, isolating the second, nonfluorescent band) gave **139** (3.0 mg, 0.0045 mmol, 0.9%) as a colorless solid. ^{1}H NMR (700 MHz, $CDCl_3$) δ = 8.82 (d, J = 8.8 Hz, 4H), 8.58 (d, J = 2.2 Hz, 2H), 8.25 (s, 2H), 8.04 (d, J = 1.8 Hz, 2H), 7.71 (t, J = 2.1 Hz, 2H), 7.58 (d, J = 8.0 Hz, 4H), 7.48 (t, J = 1.8 Hz, 2H), 7.32 (d, J = 8.1 Hz, 4H), 2.43 (s, 6H) ppm; LRMS (MALDI-TOF) m/z: $[C_{38}H_{28}N_4O_4S_2+Na]^+$ calcd. 691.1; found 691.4.

1,2,5,6(3,5)-tetrapyridinacyclooctaphane-3,7-diyne (131)

A screw-cap NMR tube with a septum cap was charged under N_2 with **139** (1.9 mg, 0.0028 mmol) in THF-d_8 (0.7 mL). The reaction mixture was cooled to –80 °C in an NMR spectrometer, then ejected and a solution of LiTMP (0.05 M in THF-d_8, 0.12 mL, 0.0056 mmol, 2 equiv.) was added and the tube shaken and returned to the spectrometer. A new, symmetrized species consistent with **131** had formed by ^{1}H NMR. Two further additions of LiTMP (0.1 mL, 0.1 mL) gave no noticeable increase in conversion of **139** but solids began

to precipitate from the NMR tube preventing further analysis. The mixture was quenched with pivalic acid (0.05 M in THF-d_8, 0.2 mL) and warmed to 24 °C, poured into H_2O (2 mL), and extracted with C_6D_6 (1 mL). ^{1}H NMR indicated that **131** was still present in roughly the same proportion to the starting material **139** as before workup. The solvent was removed *in vacuo* and reconstituted in $CDCl_3$, in which **131** also appears stable over 24 h. Attempts to purify the sample by prep TLC on alumina did not yield any recoverable amount of **131**. ^{1}H NMR (500 MHz, C_6D_6) δ = 8.71 (d, J = 2.3 Hz, 4H), 8.49 (d, J = 2.0 Hz, 4H), 7.47 (t, J = 2.2 Hz, 4H) ppm.

Appendix B

X-ray Structure Determination & Refinement

Table B.1: Crystal data and structure refinement for **15**.

Identification code	CCDC 1456633	
Empirical formula	$C_{19}H_{24}F_{18}MoO_5$	
Formula weight	770.32	
Temperature	100(2) K	
Wavelength	0.71073 Å	
Crystal system	Monoclinic	
Space group	P2(1)/n	
Unit cell dimensions	a = 11.4678(9) Å	$\alpha = 90.000°$
	b = 16.8911(14) Å	$\beta = 91.155(2)°$
	c = 13.8634(11) Å	$\gamma = 90.000°$
Volume	2684.8(4) $Å^3$	
Z	4	
Density (calculated)	1.906 Mg/m^3	
Absorption coefficient	0.644 mm^{-1}	
F(000)	1528	
Crystal size	0.160 x 0.160 x 0.080 mm^3	
Theta range for data collection	1.901 to 25.387°	
Index ranges	$-13 \leq h \leq 13$, $-20 \leq k \leq 20$, $-16 \leq l \leq 16$	
Reflections collected	72070	
Independent reflections	4933 [R(int) = 0.0277]	
Completeness to theta = 25.00°	100.0%	
Absorption correction	Semi-empirical from equivalents	
Max. and min. transmission	0.9561 and 0.8355	
Refinement method	Full-matrix least-squares on F^2	
Data / restraints / parameters	4933 / 0 / 393	
Goodness-of-fit on F^2	1.179	
Final R indices [$I>2\sigma(I)$]	R1 = 0.0262, wR2 = 0.0556	
R indices (all data)	R1 = 0.0316, wR2 = 0.0601	
Largest diff. peak and hole	0.386 and –0.476 $e^-Å^{-3}$	

Table B.2: Atomic coordinates ($\times 10^4$) and equivalent isotropic displacement parameters (Å^2 $\times 10^3$) for **15**. U(eq) is defined as one third of the trace of the orthogonalized U^{ij} tensor.

Atom	x	y	z	U(eq)
C(1)	6515(2)	2284(1)	2591(2)	20(1)
C(2)	6652(2)	2091(2)	3632(2)	29(1)
C(3)	7690(4)	1615(2)	3900(2)	68(1)
C(4)	8786(2)	3316(1)	1395(2)	19(1)
C(5)	9647(2)	2618(2)	1312(2)	25(1)
C(6)	9164(2)	3999(2)	733(2)	25(1)
C(7)	8788(2)	3598(2)	2442(2)	25(1)
C(8)	5016(2)	4132(1)	1988(2)	19(1)
C(9)	3755(2)	4326(1)	1663(2)	23(1)
C(10)	5071(2)	3992(1)	3083(2)	22(1)
C(11)	5786(2)	4840(1)	1747(2)	23(1)
C(12)	4088(2)	1362(1)	1503(2)	16(1)
C(13)	4603(2)	543(1)	1735(2)	19(1)
C(14)	3104(2)	1283(1)	734(2)	22(1)
C(15)	3588(2)	1716(1)	2417(2)	23(1)
C(16)	7714(2)	822(1)	1146(2)	23(1)
C(17)	6912(2)	1389(1)	-309(2)	21(1)
C(18)	6902(2)	2174(1)	-814(2)	21(1)
C(19)	6026(2)	3443(1)	-766(2)	22(1)
F(1)	9648(1)	2290(1)	435(1)	31(1)
F(2)	9380(1)	2043(1)	1934(1)	31(1)
F(3)	10749(1)	2833(1)	1525(1)	39(1)
F(4)	9217(1)	3783(1)	-194(1)	32(1)
F(5)	8392(1)	4591(1)	773(1)	33(1)
F(6)	10204(1)	4301(1)	984(1)	38(1)
F(7)	3694(1)	4420(1)	706(1)	31(1)
F(8)	3001(1)	3759(1)	1890(1)	37(1)
F(9)	3366(1)	5003(1)	2044(1)	32(1)
F(10)	4517(1)	3339(1)	3356(1)	28(1)
F(11)	4609(1)	4599(1)	3578(1)	33(1)
F(12)	6182(1)	3930(1)	3398(1)	28(1)
F(13)	2637(1)	1989(1)	548(1)	31(1)
F(14)	3474(1)	996(1)	-104(1)	29(1)
F(15)	2234(1)	811(1)	1016(1)	41(1)
F(16)	3814(1)	37(1)	2086(1)	29(1)
F(17)	5068(1)	191(1)	966(1)	25(1)

F(18)	5461(1)	603(1)	2403(1)	26(1)
O(1)	4926(1)	1829(1)	1072(1)	16(1)
O(2)	5339(1)	3470(1)	1467(1)	18(1)
O(3)	7701(1)	3078(1)	1035(1)	17(1)
O(4)	7213(1)	1518(1)	702(1)	18(1)
O(5)	6041(1)	2659(1)	-370(1)	17(1)
Mo(1)	6262(1)	2515(1)	1385(1)	13(1)

Table B.4: Bond lengths [Å] and angles [°] for **15**.

C(1)-C(2)	1.485(3)
C(1)-Mo(1)	1.736(2)
C(2)-C(3)	1.477(4)
C(2)-H(14A)	0.9900
C(2)-H(14B)	0.9900
C(3)-H(15A)	0.9800
C(3)-H(15B)	0.9800
C(3)-H(15C)	0.9800
C(4)-O(3)	1.390(3)
C(4)-C(7)	1.528(3)
C(4)-C(6)	1.542(3)
C(4)-C(5)	1.543(3)
C(5)-F(1)	1.336(3)
C(5)-F(2)	1.339(3)
C(5)-F(3)	1.343(3)
C(6)-F(6)	1.337(3)
C(6)-F(5)	1.338(3)
C(6)-F(4)	1.339(3)
C(7)-H(5A)	0.9800
C(7)-H(5B)	0.9800
C(7)-H(5C)	0.9800
C(8)-O(2)	1.387(3)
C(8)-C(11)	1.526(3)
C(8)-C(10)	1.536(3)
C(8)-C(9)	1.541(3)
C(9)-F(8)	1.333(3)
C(9)-F(7)	1.336(3)
C(9)-F(9)	1.341(3)
C(10)-F(10)	1.332(3)
C(10)-F(12)	1.344(3)
C(10)-F(11)	1.348(3)
C(11)-H(9A)	0.9800
C(11)-H(9B)	0.9800
C(11)-H(9C)	0.9800
C(12)-O(1)	1.388(3)
C(12)-C(15)	1.524(3)
C(12)-C(13)	1.536(3)
C(12)-C(14)	1.543(3)

C(13)-F(17)	1.340(3)
C(13)-F(18)	1.342(3)
C(13)-F(16)	1.342(3)
C(14)-F(13)	1.331(3)
C(14)-F(14)	1.337(3)
C(14)-F(15)	1.341(3)
C(15)-H(13A)	0.9800
C(15)-H(13B)	0.9800
C(15)-H(13C)	0.9800
C(16)-O(4)	1.442(3)
C(16)-H(16A)	0.9800
C(16)-H(16B)	0.9800
C(16)-H(16C)	0.9800
C(17)-O(4)	1.453(3)
C(17)-C(18)	1.499(3)
C(17)-H(17A)	0.9900
C(17)-H(17B)	0.9900
C(18)-O(5)	1.431(3)
C(18)-H(18A)	0.9900
C(18)-H(18B)	0.9900
C(19)-O(5)	1.434(3)
C(19)-H(19A)	0.9800
C(19)-H(19B)	0.9800
C(19)-H(19C)	0.9800
O(1)-Mo(1)	1.9632(15)
O(2)-Mo(1)	1.9326(15)
O(3)-Mo(1)	1.9740(15)
O(4)-Mo(1)	2.2283(15)
O(5)-Mo(1)	2.4526(15)

C(2)-C(1)-Mo(1)	176.44(19)
C(3)-C(2)-C(1)	115.7(2)
C(3)-C(2)-H(14A)	108.4
C(1)-C(2)-H(14A)	108.4
C(3)-C(2)-H(14B)	108.4
C(1)-C(2)-H(14B)	108.4
H(14A)-C(2)-H(14B)	107.4
C(2)-C(3)-H(15A)	109.5
C(2)-C(3)-H(15B)	109.5
H(15A)-C(3)-H(15B)	109.5
C(2)-C(3)-H(15C)	109.5

H(15A)-C(3)-H(15C)	109.5
H(15B)-C(3)-H(15C)	109.5
O(3)-C(4)-C(7)	114.59(18)
O(3)-C(4)-C(6)	105.25(18)
C(7)-C(4)-C(6)	109.64(19)
O(3)-C(4)-C(5)	108.76(18)
C(7)-C(4)-C(5)	108.70(19)
C(6)-C(4)-C(5)	109.82(19)
F(1)-C(5)-F(2)	106.92(19)
F(1)-C(5)-F(3)	107.08(19)
F(2)-C(5)-F(3)	106.3(2)
F(1)-C(5)-C(4)	113.4(2)
F(2)-C(5)-C(4)	110.54(19)
F(3)-C(5)-C(4)	112.22(19)
F(6)-C(6)-F(5)	106.92(19)
F(6)-C(6)-F(4)	107.26(19)
F(5)-C(6)-F(4)	106.6(2)
F(6)-C(6)-C(4)	113.1(2)
F(5)-C(6)-C(4)	109.93(19)
F(4)-C(6)-C(4)	112.73(19)
C(4)-C(7)-H(5A)	109.5
C(4)-C(7)-H(5B)	109.5
H(5A)-C(7)-H(5B)	109.5
C(4)-C(7)-H(5C)	109.5
H(5A)-C(7)-H(5C)	109.5
H(5B)-C(7)-H(5C)	109.5
O(2)-C(8)-C(11)	110.83(18)
O(2)-C(8)-C(10)	112.57(18)
C(11)-C(8)-C(10)	108.95(19)
O(2)-C(8)-C(9)	106.15(18)
C(11)-C(8)-C(9)	108.26(19)
C(10)-C(8)-C(9)	109.96(19)
F(8)-C(9)-F(7)	107.40(19)
F(8)-C(9)-F(9)	107.28(19)
F(7)-C(9)-F(9)	106.16(19)
F(8)-C(9)-C(8)	112.84(19)
F(7)-C(9)-C(8)	110.25(19)
F(9)-C(9)-C(8)	112.54(19)
F(10)-C(10)-F(12)	107.27(19)
F(10)-C(10)-F(11)	106.92(18)
F(12)-C(10)-F(11)	105.90(18)

F(10)-C(10)-C(8)	113.46(19)
F(12)-C(10)-C(8)	110.70(18)
F(11)-C(10)-C(8)	112.17(19)
C(8)-C(11)-H(9A)	109.5
C(8)-C(11)-H(9B)	109.5
H(9A)-C(11)-H(9B)	109.5
C(8)-C(11)-H(9C)	109.5
H(9A)-C(11)-H(9C)	109.5
H(9B)-C(11)-H(9C)	109.5
O(1)-C(12)-C(15)	114.22(18)
O(1)-C(12)-C(13)	109.62(17)
C(15)-C(12)-C(13)	109.23(18)
O(1)-C(12)-C(14)	104.74(17)
C(15)-C(12)-C(14)	109.02(18)
C(13)-C(12)-C(14)	109.88(18)
F(17)-C(13)-F(18)	106.59(18)
F(17)-C(13)-F(16)	106.71(18)
F(18)-C(13)-F(16)	106.72(18)
F(17)-C(13)-C(12)	112.95(18)
F(18)-C(13)-C(12)	110.51(18)
F(16)-C(13)-C(12)	112.95(18)
F(13)-C(14)-F(14)	106.85(19)
F(13)-C(14)-F(15)	106.92(19)
F(14)-C(14)-F(15)	106.81(19)
F(13)-C(14)-C(12)	110.06(19)
F(14)-C(14)-C(12)	113.00(18)
F(15)-C(14)-C(12)	112.84(19)
C(12)-C(15)-H(13A)	109.5
C(12)-C(15)-H(13B)	109.5
H(13A)-C(15)-H(13B)	109.5
C(12)-C(15)-H(13C)	109.5
H(13A)-C(15)-H(13C)	109.5
H(13B)-C(15)-H(13C)	109.5
O(4)-C(16)-H(16A)	109.5
O(4)-C(16)-H(16B)	109.5
H(16A)-C(16)-H(16B)	109.5
O(4)-C(16)-H(16C)	109.5
H(16A)-C(16)-H(16C)	109.5
H(16B)-C(16)-H(16C)	109.5
O(4)-C(17)-C(18)	108.47(18)
O(4)-C(17)-H(17A)	110.0

C(18)-C(17)-H(17A)	110.0
O(4)-C(17)-H(17B)	110.0
C(18)-C(17)-H(17B)	110.0
H(17A)-C(17)-H(17B)	108.4
O(5)-C(18)-C(17)	107.67(18)
O(5)-C(18)-H(18A)	110.2
C(17)-C(18)-H(18A)	110.2
O(5)-C(18)-H(18B)	110.2
C(17)-C(18)-H(18B)	110.2
H(18A)-C(18)-H(18B)	108.5
O(5)-C(19)-H(19A)	109.5
O(5)-C(19)-H(19B)	109.5
H(19A)-C(19)-H(19B)	109.5
O(5)-C(19)-H(19C)	109.5
H(19A)-C(19)-H(19C)	109.5
H(19B)-C(19)-H(19C)	109.5
C(12)-O(1)-Mo(1)	141.64(13)
C(8)-O(2)-Mo(1)	148.94(14)
C(4)-O(3)-Mo(1)	142.88(14)
C(16)-O(4)-C(17)	111.96(16)
C(16)-O(4)-Mo(1)	129.02(13)
C(17)-O(4)-Mo(1)	114.49(12)
C(18)-O(5)-C(19)	111.49(16)
C(18)-O(5)-Mo(1)	108.20(12)
C(19)-O(5)-Mo(1)	118.12(12)
C(1)-Mo(1)-O(2)	102.25(9)
C(1)-Mo(1)-O(1)	101.24(9)
O(2)-Mo(1)-O(1)	94.60(6)
C(1)-Mo(1)-O(3)	102.76(9)
O(2)-Mo(1)-O(3)	94.27(6)
O(1)-Mo(1)-O(3)	151.98(6)
C(1)-Mo(1)-O(4)	99.52(8)
O(2)-Mo(1)-O(4)	158.23(6)
O(1)-Mo(1)-O(4)	81.15(6)
O(3)-Mo(1)-O(4)	80.80(6)
C(1)-Mo(1)-O(5)	171.68(8)
O(2)-Mo(1)-O(5)	86.02(6)
O(1)-Mo(1)-O(5)	76.96(5)
O(3)-Mo(1)-O(5)	77.20(6)
O(4)-Mo(1)-O(5)	72.21(5)

Table B.6: Anisotropic displacement parameters (Å^2 $\times 10^3$) for **15**. The anisotropic displacement factor exponent takes the form: $-2p^2[h^2a^{*2}U^{11} + ... + 2hka^*b^*U^{12}]$

Atom	U11	U22	U33	U23	U13	U12
C(1)	21(1)	14(1)	25(1)	-3(1)	0(1)	-1(1)
C(2)	32(1)	34(2)	19(1)	3(1)	-3(1)	-1(1)
C(3)	95(3)	80(3)	28(2)	11(2)	4(2)	62(2)
C(4)	14(1)	19(1)	24(1)	-4(1)	0(1)	-2(1)
C(5)	18(1)	27(1)	30(1)	-7(1)	-2(1)	-2(1)
C(6)	20(1)	25(1)	31(1)	-5(1)	2(1)	-8(1)
C(7)	23(1)	27(1)	26(1)	-7(1)	-4(1)	-1(1)
C(8)	19(1)	13(1)	24(1)	-4(1)	2(1)	1(1)
C(9)	21(1)	16(1)	33(1)	-5(1)	2(1)	0(1)
C(10)	25(1)	18(1)	25(1)	-6(1)	5(1)	1(1)
C(11)	22(1)	15(1)	31(1)	-1(1)	2(1)	-2(1)
C(12)	17(1)	12(1)	19(1)	1(1)	3(1)	-3(1)
C(13)	21(1)	15(1)	22(1)	1(1)	1(1)	-1(1)
C(14)	18(1)	20(1)	26(1)	3(1)	1(1)	-3(1)
C(15)	27(1)	19(1)	25(1)	-2(1)	8(1)	-2(1)
C(16)	25(1)	15(1)	29(1)	1(1)	-3(1)	6(1)
C(17)	25(1)	19(1)	19(1)	-5(1)	2(1)	2(1)
C(18)	22(1)	22(1)	18(1)	-2(1)	4(1)	2(1)
C(19)	26(1)	19(1)	20(1)	7(1)	0(1)	1(1)
F(1)	28(1)	31(1)	33(1)	-12(1)	4(1)	3(1)
F(2)	31(1)	26(1)	36(1)	1(1)	-7(1)	7(1)
F(3)	16(1)	40(1)	60(1)	-16(1)	-7(1)	1(1)
F(4)	36(1)	32(1)	27(1)	-2(1)	7(1)	-9(1)
F(5)	33(1)	20(1)	46(1)	3(1)	8(1)	-2(1)
F(6)	27(1)	37(1)	49(1)	-4(1)	1(1)	-18(1)
F(7)	32(1)	31(1)	31(1)	-4(1)	-7(1)	8(1)
F(8)	21(1)	28(1)	63(1)	6(1)	-1(1)	-6(1)
F(9)	30(1)	24(1)	42(1)	-8(1)	3(1)	10(1)
F(10)	34(1)	23(1)	28(1)	0(1)	9(1)	-5(1)
F(11)	43(1)	26(1)	29(1)	-11(1)	9(1)	6(1)
F(12)	30(1)	30(1)	25(1)	-4(1)	-4(1)	-1(1)
F(13)	30(1)	30(1)	33(1)	6(1)	-3(1)	12(1)
F(14)	32(1)	31(1)	24(1)	-7(1)	-8(1)	1(1)
F(15)	25(1)	52(1)	45(1)	18(1)	-8(1)	-19(1)
F(16)	30(1)	17(1)	39(1)	10(1)	4(1)	-5(1)
F(17)	28(1)	18(1)	29(1)	-4(1)	2(1)	5(1)
F(18)	29(1)	23(1)	26(1)	4(1)	-7(1)	2(1)

O(1)	18(1)	14(1)	17(1)	0(1)	1(1)	-3(1)
O(2)	20(1)	13(1)	20(1)	-4(1)	2(1)	1(1)
O(3)	16(1)	16(1)	20(1)	-1(1)	-1(1)	-4(1)
O(4)	22(1)	12(1)	20(1)	-1(1)	-1(1)	4(1)
O(5)	17(1)	17(1)	16(1)	1(1)	2(1)	0(1)
Mo(1)	14(1)	10(1)	14(1)	-1(1)	1(1)	-1(1)

Table B.8: Crystal data and structure refinement for **52**.

Identification code	**52**	
Empirical formula	$C_{24}H_{23}F_{18}MoO_5$	
Formula weight	829.36	
Temperature	100(2) K	
Wavelength	0.71073 Å	
Crystal system	Triclinic	
Space group	P -1	
Unit cell dimensions	a = 10.5563(5) Å	$\alpha = 69.169(2)^\circ$
	b = 11.8181(6) Å	$\beta = 87.724(2)^\circ$
	c = 12.8237(6) Å	$\gamma = 78.651(2)^\circ$
Volume	1465.21(12) $Å^3$	
Z	2	
Density (calculated)	1.880 Mg/m^3	
Absorption coefficient	0.598 mm^{-1}	
F(000)	822	
Crystal size	0.200 x 0.200 x 0.080 mm^3	
Theta range for data collection	1.700 to 25.463°	
Index ranges	-12≤h≤12, -14≤k≤14, -15≤l≤15	
Reflections collected	30322	
Independent reflections	5413 [R(int) = 0.0383]	
Completeness to theta = 25.000°	100.0 %	
Absorption correction	None	
Refinement method	Full-matrix least-squares on F^2	
Data / restraints / parameters	5413 / 0 / 457	
Goodness-of-fit on F^2	1.073	
Final R indices [I>2σ(I)]	R1 = 0.0242, wR2 = 0.0583	
R indices (all data)	R1 = 0.0260, wR2 = 0.0594	
Extinction coefficient	n/a	
Largest diff. peak and hole	0.584 and -0.403 $e^-Å^{-3}$	

Table B.9: Atomic coordinates ($\times 10^4$) and equivalent isotropic displacement parameters (Å$^2 \times 10^3$) for **52**. U(eq) is defined as one third of the trace of the orthogonalized U^{ij} tensor.

Atom	x	y	z	U(eq)
C(1)	7749(2)	2966(2)	3875(2)	17(1)
C(2)	8429(2)	2466(2)	4981(2)	23(1)
C(3)	8195(2)	3347(2)	5628(2)	32(1)
C(4)	8544(2)	5583(2)	1887(2)	16(1)
C(5)	9959(2)	5129(2)	2341(2)	23(1)
C(6)	8484(2)	6671(2)	763(2)	20(1)
C(7)	7710(2)	6048(2)	2731(2)	18(1)
C(8)	6294(2)	6199(2)	2471(2)	16(1)
C(9)	5384(2)	7387(2)	2192(2)	17(1)
C(10)	4069(2)	7406(2)	2103(2)	21(1)
C(11)	3190(2)	8517(2)	1755(2)	28(1)
C(12)	3625(2)	9617(2)	1488(2)	30(1)
C(13)	4926(2)	9609(2)	1573(2)	30(1)
C(14)	5806(2)	8505(2)	1927(2)	24(1)
C(15)	4564(2)	2609(2)	3830(2)	16(1)
C(16)	3792(2)	3701(2)	4118(2)	21(1)
C(17)	3630(2)	1987(2)	3428(2)	21(1)
C(18)	5314(2)	1675(2)	4878(2)	23(1)
C(19)	8798(2)	1120(2)	2325(2)	17(1)
C(20)	8394(2)	59(2)	3303(2)	21(1)
C(21)	8937(2)	761(2)	1277(2)	20(1)
C(22)	10077(2)	1375(2)	2605(2)	22(1)
O(1)	8108(1)	4665(1)	1678(1)	15(1)
O(2)	5893(1)	5277(1)	2491(1)	15(1)
O(3)	5309(1)	3064(1)	2914(1)	14(1)
O(4)	7802(1)	2148(1)	2054(1)	14(1)
O(5)	6048(1)	4094(1)	688(1)	16(1)
F(1)	10041(1)	4236(1)	3344(1)	34(1)
F(2)	10464(1)	6029(1)	2455(1)	42(1)
F(3)	10718(1)	4669(1)	1687(1)	34(1)
F(4)	7271(1)	7040(1)	337(1)	26(1)
F(5)	8821(1)	7660(1)	868(1)	28(1)
F(6)	9229(1)	6367(1)	6(1)	28(1)
F(7)	4581(1)	4241(1)	4487(1)	27(1)
F(8)	2955(1)	3345(1)	4932(1)	32(1)
F(9)	3110(1)	4572(1)	3245(1)	25(1)

F(10)	2799(1)	1520(1)	4205(1)	34(1)
F(11)	4305(1)	1037(1)	3175(1)	28(1)
F(12)	2934(1)	2737(1)	2517(1)	27(1)
F(13)	8562(1)	193(1)	4280(1)	27(1)
F(14)	9094(1)	-1047(1)	3379(1)	31(1)
F(15)	7158(1)	2(1)	3222(1)	26(1)
F(16)	9986(1)	-113(1)	1338(1)	37(1)
F(17)	9044(1)	1733(1)	373(1)	26(1)
F(18)	7920(1)	332(1)	1086(1)	25(1)
Mo(1)	7011(1)	3467(1)	2554(1)	12(1)
C(23)	4873(4)	3851(4)	442(3)	15(1)
C(24)	6913(4)	4323(4)	-271(3)	20(1)
C(23A)	6213(4)	5057(4)	-287(3)	17(1)
C(24A)	5562(4)	3100(4)	470(3)	21(1)

Table B.11: Bond lengths [Å] and angles [°] for **52**.

C(1)-C(2)	1.481(3)
C(1)-Mo(1)	1.7427(19)
C(2)-C(3)	1.526(3)
C(2)-H(2A)	0.9900
C(2)-H(2B)	0.9900
C(3)-H(3A)	0.9800
C(3)-H(3B)	0.9800
C(3)-H(3C)	0.9800
C(4)-O(1)	1.369(2)
C(4)-C(5)	1.546(3)
C(4)-C(6)	1.547(3)
C(4)-C(7)	1.551(3)
C(5)-F(3)	1.319(2)
C(5)-F(2)	1.333(2)
C(5)-F(1)	1.335(2)
C(6)-F(6)	1.329(2)
C(6)-F(5)	1.338(2)
C(6)-F(4)	1.340(2)
C(7)-C(8)	1.506(3)
C(7)-H(7A)	0.9900
C(7)-H(7B)	0.9900
C(8)-O(2)	1.237(2)
C(8)-C(9)	1.470(3)
C(9)-C(10)	1.393(3)
C(9)-C(14)	1.401(3)
C(10)-C(11)	1.386(3)
C(10)-H(10)	0.9500
C(11)-C(12)	1.386(3)
C(11)-H(11)	0.9500
C(12)-C(13)	1.381(3)
C(12)-H(12)	0.9500
C(13)-C(14)	1.381(3)
C(13)-H(13)	0.9500
C(14)-H(14)	0.9500
C(15)-O(3)	1.390(2)
C(15)-C(18)	1.528(3)
C(15)-C(16)	1.538(3)
C(15)-C(17)	1.541(3)

C(16)-F(7)	1.334(2)
C(16)-F(9)	1.336(2)
C(16)-F(8)	1.345(2)
C(17)-F(12)	1.329(2)
C(17)-F(10)	1.340(2)
C(17)-F(11)	1.341(2)
C(18)-H(18A)	0.9800
C(18)-H(18B)	0.9800
C(18)-H(18C)	0.9800
C(19)-O(4)	1.389(2)
C(19)-C(22)	1.523(3)
C(19)-C(21)	1.540(3)
C(19)-C(20)	1.542(3)
C(20)-F(15)	1.329(2)
C(20)-F(13)	1.339(2)
C(20)-F(14)	1.342(2)
C(21)-F(17)	1.330(2)
C(21)-F(18)	1.339(2)
C(21)-F(16)	1.342(2)
C(22)-H(22A)	0.9800
C(22)-H(22B)	0.9800
C(22)-H(22C)	0.9800
O(1)-Mo(1)	2.0037(13)
O(2)-Mo(1)	2.2052(12)
O(3)-Mo(1)	1.9457(12)
O(4)-Mo(1)	1.9225(12)
O(5)-C(23A)	1.392(4)
O(5)-C(23)	1.398(4)
O(5)-C(24)	1.481(4)
O(5)-C(24A)	1.484(4)
O(5)-Mo(1)	2.4386(12)
C(23)-C(23A)#1	1.507(6)
C(23)-H(23A)	0.9900
C(23)-H(23B)	0.9900
C(24)-H(24A)	0.9800
C(24)-H(24B)	0.9800
C(24)-H(24C)	0.9800
C(23A)-C(23)#1	1.507(6)
C(23A)-H(23C)	0.9900
C(23A)-H(23D)	0.9900
C(24A)-H(24D)	0.9800

C(24A)-H(24E)	0.9800
C(24A)-H(24F)	0.9800
C(2)-C(1)-Mo(1)	175.99(16)
C(1)-C(2)-C(3)	114.01(17)
C(1)-C(2)-H(2A)	108.8
C(3)-C(2)-H(2A)	108.8
C(1)-C(2)-H(2B)	108.8
C(3)-C(2)-H(2B)	108.8
H(2A)-C(2)-H(2B)	107.6
C(2)-C(3)-H(3A)	109.5
C(2)-C(3)-H(3B)	109.5
H(3A)-C(3)-H(3B)	109.5
C(2)-C(3)-H(3C)	109.5
H(3A)-C(3)-H(3C)	109.5
H(3B)-C(3)-H(3C)	109.5
O(1)-C(4)-C(5)	110.21(15)
O(1)-C(4)-C(6)	107.06(15)
C(5)-C(4)-C(6)	109.17(16)
O(1)-C(4)-C(7)	112.84(15)
C(5)-C(4)-C(7)	108.85(15)
C(6)-C(4)-C(7)	108.64(15)
F(3)-C(5)-F(2)	107.26(17)
F(3)-C(5)-F(1)	106.79(17)
F(2)-C(5)-F(1)	107.03(17)
F(3)-C(5)-C(4)	112.25(16)
F(2)-C(5)-C(4)	112.21(17)
F(1)-C(5)-C(4)	110.99(16)
F(6)-C(6)-F(5)	107.83(15)
F(6)-C(6)-F(4)	107.13(16)
F(5)-C(6)-F(4)	106.35(16)
F(6)-C(6)-C(4)	112.60(16)
F(5)-C(6)-C(4)	112.84(16)
F(4)-C(6)-C(4)	109.75(15)
C(8)-C(7)-C(4)	110.32(15)
C(8)-C(7)-H(7A)	109.6
C(4)-C(7)-H(7A)	109.6
C(8)-C(7)-H(7B)	109.6
C(4)-C(7)-H(7B)	109.6
H(7A)-C(7)-H(7B)	108.1
O(2)-C(8)-C(9)	119.17(17)

O(2)-C(8)-C(7)	117.90(16)
C(9)-C(8)-C(7)	122.94(17)
C(10)-C(9)-C(14)	119.12(18)
C(10)-C(9)-C(8)	118.72(18)
C(14)-C(9)-C(8)	121.97(17)
C(11)-C(10)-C(9)	120.4(2)
C(11)-C(10)-H(10)	119.8
C(9)-C(10)-H(10)	119.8
C(12)-C(11)-C(10)	119.8(2)
C(12)-C(11)-H(11)	120.1
C(10)-C(11)-H(11)	120.1
C(13)-C(12)-C(11)	120.3(2)
C(13)-C(12)-H(12)	119.8
C(11)-C(12)-H(12)	119.8
C(12)-C(13)-C(14)	120.3(2)
C(12)-C(13)-H(13)	119.9
C(14)-C(13)-H(13)	119.9
C(13)-C(14)-C(9)	120.11(19)
C(13)-C(14)-H(14)	119.9
C(9)-C(14)-H(14)	119.9
O(3)-C(15)-C(18)	115.51(15)
O(3)-C(15)-C(16)	108.71(15)
C(18)-C(15)-C(16)	108.77(16)
O(3)-C(15)-C(17)	104.70(15)
C(18)-C(15)-C(17)	109.34(16)
C(16)-C(15)-C(17)	109.67(16)
F(7)-C(16)-F(9)	107.16(16)
F(7)-C(16)-F(8)	106.42(16)
F(9)-C(16)-F(8)	107.01(15)
F(7)-C(16)-C(15)	110.74(16)
F(9)-C(16)-C(15)	112.94(16)
F(8)-C(16)-C(15)	112.22(16)
F(12)-C(17)-F(10)	107.19(16)
F(12)-C(17)-F(11)	106.71(16)
F(10)-C(17)-F(11)	106.33(16)
F(12)-C(17)-C(15)	113.44(16)
F(10)-C(17)-C(15)	113.12(16)
F(11)-C(17)-C(15)	109.61(16)
C(15)-C(18)-H(18A)	109.5
C(15)-C(18)-H(18B)	109.5
H(18A)-C(18)-H(18B)	109.5

C(15)-C(18)-H(18C)	109.5
H(18A)-C(18)-H(18C)	109.5
H(18B)-C(18)-H(18C)	109.5
O(4)-C(19)-C(22)	113.19(16)
O(4)-C(19)-C(21)	105.01(15)
C(22)-C(19)-C(21)	109.58(16)
O(4)-C(19)-C(20)	109.15(15)
C(22)-C(19)-C(20)	110.59(16)
C(21)-C(19)-C(20)	109.14(16)
F(15)-C(20)-F(13)	106.91(16)
F(15)-C(20)-F(14)	107.04(16)
F(13)-C(20)-F(14)	106.65(15)
F(15)-C(20)-C(19)	112.70(15)
F(13)-C(20)-C(19)	111.00(17)
F(14)-C(20)-C(19)	112.18(16)
F(17)-C(21)-F(18)	106.84(16)
F(17)-C(21)-F(16)	106.89(16)
F(18)-C(21)-F(16)	106.65(16)
F(17)-C(21)-C(19)	110.71(16)
F(18)-C(21)-C(19)	112.75(16)
F(16)-C(21)-C(19)	112.63(16)
C(19)-C(22)-H(22A)	109.5
C(19)-C(22)-H(22B)	109.5
H(22A)-C(22)-H(22B)	109.5
C(19)-C(22)-H(22C)	109.5
H(22A)-C(22)-H(22C)	109.5
H(22B)-C(22)-H(22C)	109.5
C(4)-O(1)-Mo(1)	132.00(11)
C(8)-O(2)-Mo(1)	128.73(12)
C(15)-O(3)-Mo(1)	140.59(11)
C(19)-O(4)-Mo(1)	141.74(12)
C(23A)-O(5)-C(23)	101.2(2)
C(23A)-O(5)-C(24)	41.4(2)
C(23)-O(5)-C(24)	112.6(2)
C(23A)-O(5)-C(24A)	112.8(2)
C(23)-O(5)-C(24A)	41.4(2)
C(24)-O(5)-C(24A)	94.7(2)
C(23A)-O(5)-Mo(1)	130.19(18)
C(23)-O(5)-Mo(1)	125.35(17)
C(24)-O(5)-Mo(1)	118.14(17)
C(24A)-O(5)-Mo(1)	113.92(17)

C(1)-Mo(1)-O(4)	100.64(7)
C(1)-Mo(1)-O(3)	101.73(7)
O(4)-Mo(1)-O(3)	100.24(5)
C(1)-Mo(1)-O(1)	100.34(7)
O(4)-Mo(1)-O(1)	96.10(5)
O(3)-Mo(1)-O(1)	149.48(5)
C(1)-Mo(1)-O(2)	99.48(7)
O(4)-Mo(1)-O(2)	159.44(5)
O(3)-Mo(1)-O(2)	79.68(5)
O(1)-Mo(1)-O(2)	76.10(5)
C(1)-Mo(1)-O(5)	177.40(7)
O(4)-Mo(1)-O(5)	76.79(5)
O(3)-Mo(1)-O(5)	79.26(5)
O(1)-Mo(1)-O(5)	79.64(5)
O(2)-Mo(1)-O(5)	83.05(4)
O(5)-C(23)-C(23A)#1	111.3(3)
O(5)-C(23)-H(23A)	109.4
C(23A)#1-C(23)-H(23A)	109.4
O(5)-C(23)-H(23B)	109.4
C(23A)#1-C(23)-H(23B)	109.4
H(23A)-C(23)-H(23B)	108.0
O(5)-C(24)-H(24A)	109.5
O(5)-C(24)-H(24B)	109.5
H(24A)-C(24)-H(24B)	109.5
O(5)-C(24)-H(24C)	109.5
H(24A)-C(24)-H(24C)	109.5
H(24B)-C(24)-H(24C)	109.5
O(5)-C(23A)-C(23)#1	109.7(3)
O(5)-C(23A)-H(23C)	109.7
C(23)#1-C(23A)-H(23C)	109.7
O(5)-C(23A)-H(23D)	109.7
C(23)#1-C(23A)-H(23D)	109.7
H(23C)-C(23A)-H(23D)	108.2
O(5)-C(24A)-H(24D)	109.5
O(5)-C(24A)-H(24E)	109.5
H(24D)-C(24A)-H(24E)	109.5
O(5)-C(24A)-H(24F)	109.5
H(24D)-C(24A)-H(24F)	109.5
H(24E)-C(24A)-H(24F)	109.5

Symmetry transformations used to generate equivalent atoms: #1 -x+1,-y+1,-z

Table B.13: Anisotropic displacement parameters ($Å^2 \times 10^3$)for **52**. The anisotropic displacement factor exponent takes the form: $-2p^2[h^2a^{*2}U^{11} + ... + 2hka^*b^*U^{12}]$

Atom	U11	U22	U33	U23	U13	U12
C(1)	16(1)	15(1)	20(1)	-8(1)	2(1)	-1(1)
C(2)	25(1)	25(1)	19(1)	-8(1)	-6(1)	2(1)
C(3)	44(1)	33(1)	20(1)	-12(1)	-8(1)	-2(1)
C(4)	14(1)	18(1)	21(1)	-10(1)	1(1)	-4(1)
C(5)	18(1)	28(1)	29(1)	-16(1)	0(1)	-6(1)
C(6)	17(1)	21(1)	28(1)	-12(1)	6(1)	-9(1)
C(7)	18(1)	18(1)	20(1)	-9(1)	0(1)	-4(1)
C(8)	17(1)	18(1)	12(1)	-7(1)	3(1)	-4(1)
C(9)	21(1)	17(1)	14(1)	-8(1)	3(1)	-3(1)
C(10)	22(1)	17(1)	24(1)	-9(1)	3(1)	-3(1)
C(11)	23(1)	24(1)	34(1)	-11(1)	0(1)	3(1)
C(12)	35(1)	17(1)	32(1)	-7(1)	2(1)	7(1)
C(13)	40(1)	14(1)	37(1)	-11(1)	9(1)	-7(1)
C(14)	22(1)	22(1)	32(1)	-15(1)	5(1)	-6(1)
C(15)	17(1)	15(1)	16(1)	-4(1)	3(1)	-4(1)
C(16)	21(1)	21(1)	19(1)	-7(1)	6(1)	-5(1)
C(17)	22(1)	20(1)	20(1)	-5(1)	6(1)	-9(1)
C(18)	24(1)	20(1)	18(1)	0(1)	3(1)	-2(1)
C(19)	13(1)	13(1)	22(1)	-6(1)	-1(1)	2(1)
C(20)	21(1)	14(1)	23(1)	-4(1)	-3(1)	0(1)
C(21)	16(1)	19(1)	26(1)	-10(1)	0(1)	-1(1)
C(22)	16(1)	22(1)	28(1)	-10(1)	-2(1)	-2(1)
O(1)	15(1)	15(1)	18(1)	-9(1)	1(1)	-5(1)
O(2)	14(1)	14(1)	17(1)	-6(1)	2(1)	-3(1)
O(3)	14(1)	13(1)	13(1)	-3(1)	1(1)	-2(1)
O(4)	13(1)	12(1)	16(1)	-4(1)	-1(1)	1(1)
O(5)	17(1)	18(1)	13(1)	-5(1)	-2(1)	-3(1)
F(1)	19(1)	45(1)	31(1)	-7(1)	-7(1)	1(1)
F(2)	25(1)	38(1)	75(1)	-32(1)	-16(1)	-8(1)
F(3)	16(1)	52(1)	40(1)	-28(1)	2(1)	1(1)
F(4)	23(1)	26(1)	25(1)	0(1)	-2(1)	-8(1)
F(5)	32(1)	23(1)	37(1)	-14(1)	9(1)	-16(1)
F(6)	35(1)	28(1)	25(1)	-12(1)	14(1)	-11(1)
F(7)	32(1)	27(1)	28(1)	-16(1)	2(1)	-7(1)
F(8)	34(1)	31(1)	30(1)	-12(1)	21(1)	-8(1)
F(9)	23(1)	17(1)	29(1)	-6(1)	0(1)	3(1)
F(10)	34(1)	40(1)	33(1)	-11(1)	14(1)	-24(1)

F(11)	35(1)	20(1)	35(1)	-14(1)	3(1)	-7(1)
F(12)	24(1)	26(1)	28(1)	-5(1)	-7(1)	-7(1)
F(13)	37(1)	23(1)	17(1)	-3(1)	-2(1)	-6(1)
F(14)	37(1)	14(1)	35(1)	-5(1)	-7(1)	5(1)
F(15)	22(1)	23(1)	28(1)	-1(1)	0(1)	-9(1)
F(16)	29(1)	40(1)	44(1)	-27(1)	-2(1)	14(1)
F(17)	30(1)	30(1)	21(1)	-11(1)	9(1)	-12(1)
F(18)	29(1)	25(1)	28(1)	-14(1)	1(1)	-11(1)
Mo(1)	12(1)	12(1)	12(1)	-4(1)	-1(1)	-1(1)
C(23)	18(2)	15(2)	14(2)	-4(2)	-1(2)	-7(2)
C(24)	17(2)	28(3)	17(2)	-10(2)	3(2)	-6(2)
C(23A)	15(2)	21(2)	13(2)	-4(2)	-1(2)	-6(2)
C(24A)	25(2)	19(3)	23(2)	-11(2)	-3(2)	-6(2)

Table B.15: Hydrogen coordinates ($\times 10^4$) and isotropic displacement parameters ($Å^2 \times 10^3$) for **52**.

Atom	x	y	z	U(eq)
H(2A)	9369	2260	4875	28
H(2B)	8147	1691	5434	28
H(3A)	8588	4065	5242	48
H(3B)	8584	2921	6382	48
H(3C)	7263	3621	5676	48
H(7A)	7930	5450	3498	21
H(7B)	7899	6850	2693	21
H(10)	3772	6652	2282	25
H(11)	2293	8526	1699	33
H(12)	3024	10380	1245	36
H(13)	5218	10366	1386	36
H(14)	6700	8504	1992	28
H(18A)	5887	1024	4685	34
H(18B)	4705	1309	5432	34
H(18C)	5829	2093	5187	34
H(22A)	10356	2001	1952	33
H(22B)	10732	613	2814	33
H(22C)	9966	1676	3230	33
H(23A)	4673	3125	1057	18
H(23B)	4948	3653	-248	18
H(24A)	7155	3574	-456	30
H(24B)	7693	4548	-76	30
H(24C)	6463	4999	-917	30
H(23C)	6220	4786	-935	20
H(23D)	7051	5296	-242	20
H(24D)	4803	3463	-40	31
H(24E)	5322	2520	1175	31
H(24F)	6240	2661	131	31

Table B.17: Crystal data and structure refinement for **54**

Identification code	**54**	
Empirical formula	$C_{38}\,H_{26}\,F_{18}\,Mo\,O_4$	
Formula weight	984.53	
Temperature	100(2) K	
Wavelength	0.71073 Å	
Crystal system	Monoclinic	
Space group	P 21/c	
Unit cell dimensions	a = 18.4440(12) Å	$\alpha = 90°$
	b = 30.019(2) Å	$\beta = 97.050(3)°$
	c = 13.6296(9) Å	$\gamma = 90°$
Volume	7489.3(9) $Å^3$	
Z	8	
Density (calculated)	1.746 Mg/m^3	
Absorption coefficient	0.482 mm^{-1}	
F(000)	3920	
Crystal size	0.350 x 0.180 x 0.050 mm^3	
Theta range for data collection	1.112 to 25.348°	
Index ranges	-22≤h≤21, -35≤k≤36, -16≤l≤16	
Reflections collected	341893	
Independent reflections	13717 [R(int) = 0.0927]	
Completeness to theta = 25.000°	100.00%	
Absorption correction	None	
Refinement method	Full-matrix least-squares on F^2	
Data / restraints / parameters	13717 / 0 / 1260	
Goodness-of-fit on F^2	1.139	
Final R indices [I>2σ(I)]	R1 = 0.0619, wR2 = 0.1433	
R indices (all data)	R1 = 0.0842, wR2 = 0.1570	
Extinction coefficient	n/a	
Largest diff. peak and hole	1.399 and -0.722 $e^-Å^{-3}$	

Table B.18: Atomic coordinates ($\times 10^4$) and equivalent isotropic displacement parameters ($\text{Å}^2 \times 10^3$) for **54**. U(eq) is defined as one third of the trace of the orthogonalized U^{ij} tensor.

Atom	x	y	z	U(eq)
C(1)	4233(3)	4371(2)	7655(4)	20(1)
C(2)	3646(3)	4670(2)	7177(4)	24(1)
C(3)	3945(4)	5088(2)	6745(5)	39(2)
C(4)	4912(3)	4367(2)	8308(4)	21(1)
C(5)	5486(3)	4658(2)	8783(4)	24(1)
C(6)	5783(3)	4990(2)	8240(4)	26(1)
C(7)	6381(3)	5237(2)	8665(5)	33(1)
C(8)	6671(3)	5160(2)	9636(5)	39(2)
C(9)	6370(3)	4844(2)	10192(5)	34(1)
C(10)	5778(3)	4591(2)	9783(4)	29(1)
C(11)	5392(3)	4270(2)	10305(4)	29(1)
C(12)	4898(3)	4024(2)	10450(4)	30(1)
C(13)	4211(3)	3817(2)	10205(4)	28(1)
C(14)	3784(4)	3609(2)	10870(4)	35(2)
C(15)	3096(4)	3461(2)	10540(5)	38(2)
C(16)	2809(3)	3515(2)	9569(5)	38(2)
C(17)	3218(3)	3712(2)	8896(4)	30(1)
C(18)	3917(3)	3862(2)	9202(4)	24(1)
C(19)	4354(3)	4052(2)	8469(4)	22(1)
C(20)	6486(3)	3916(2)	6881(4)	22(1)
C(21)	6731(3)	3471(2)	6458(4)	26(1)
C(22)	6855(3)	4307(2)	6401(4)	27(1)
C(23)	6713(3)	3928(2)	8012(4)	22(1)
C(24)	6305(3)	3588(2)	8560(4)	21(1)
C(25)	6711(3)	3290(2)	9287(4)	20(1)
C(26)	7431(3)	3163(2)	9208(4)	26(1)
C(27)	7771(3)	2853(2)	9847(4)	26(1)
C(28)	7412(3)	2680(2)	10599(4)	27(1)
C(29)	6712(3)	2814(2)	10703(4)	27(1)
C(30)	6353(3)	3114(2)	10052(4)	24(1)
C(31)	4354(3)	2832(2)	7553(4)	24(1)
C(32)	3606(3)	2663(2)	7050(5)	31(1)
C(33)	4970(3)	2518(2)	7293(4)	28(1)
C(34)	4356(3)	2826(2)	8675(4)	28(1)
C(35)	4212(3)	3858(2)	4987(4)	27(1)
C(36)	3393(4)	3819(3)	4645(5)	47(2)

C(37)	4559(3)	4203(2)	4341(4)	33(1)
C(38)	4577(4)	3410(2)	4862(4)	35(1)
C(39)	9189(3)	3087(2)	1917(4)	22(1)
C(40)	9288(3)	2599(2)	1775(4)	23(1)
C(41)	9023(3)	2324(2)	2596(4)	26(1)
C(42)	8659(3)	3409(2)	2174(4)	22(1)
C(43)	7917(3)	3433(2)	2462(4)	23(1)
C(44)	7689(3)	3139(2)	3155(4)	24(1)
C(45)	7002(3)	3163(2)	3446(4)	27(1)
C(46)	6512(3)	3490(2)	3059(4)	33(1)
C(47)	6718(3)	3787(2)	2370(4)	31(1)
C(48)	7416(3)	3760(2)	2056(4)	25(1)
C(49)	7655(3)	4020(2)	1286(4)	29(1)
C(50)	8023(3)	4115(2)	648(4)	29(1)
C(51)	8594(3)	4038(2)	45(4)	27(1)
C(52)	8654(3)	4241(2)	-863(4)	34(1)
C(53)	9186(4)	4101(2)	-1428(4)	39(2)
C(54)	9646(4)	3760(2)	-1105(4)	35(2)
C(55)	9609(3)	3556(2)	-198(4)	28(1)
C(56)	9094(3)	3696(2)	402(4)	24(1)
C(57)	9088(3)	3509(2)	1395(4)	23(1)
C(58)	9264(3)	3888(2)	4782(4)	29(1)
C(59)	9795(4)	4236(2)	5268(4)	37(2)
C(60)	9062(5)	3564(3)	5575(6)	43(2)
C(69)	10808(3)	4274(2)	1906(5)	31(1)
C(70)	11109(4)	4592(2)	2742(5)	40(2)
C(71)	11455(5)	4124(3)	1357(5)	46(2)
C(73)	11013(3)	2944(2)	3692(4)	27(1)
C(74)	11577(3)	2781(2)	3031(5)	43(2)
C(75)	10843(3)	2555(2)	4380(4)	33(1)
C(76)	11330(4)	3334(2)	4338(5)	45(2)
O(1)	5736(2)	3948(1)	6624(3)	22(1)
O(2)	5633(2)	3563(1)	8410(2)	19(1)
O(3)	4457(2)	3248(1)	7126(2)	21(1)
O(4)	4261(2)	4028(1)	5944(3)	22(1)
O(5)	9624(2)	3633(1)	4145(3)	25(1)
O(6)	9238(2)	4237(1)	2689(3)	26(1)
O(7)	10573(2)	3886(1)	2333(3)	27(1)
O(8)	10370(2)	3023(1)	3077(3)	23(1)
F(1)	6464(2)	3126(1)	6922(3)	37(1)
F(2)	7455(2)	3421(1)	6610(3)	41(1)

F(3)	6524(2)	3420(1)	5510(2)	46(1)
F(4)	6561(2)	4688(1)	6619(3)	52(1)
F(5)	7564(2)	4330(1)	6712(3)	36(1)
F(6)	6792(2)	4274(1)	5423(3)	50(1)
F(7)	3412(2)	2280(1)	7434(3)	39(1)
F(8)	3088(2)	2963(1)	7170(3)	39(1)
F(9)	3605(2)	2601(1)	6081(3)	39(1)
F(10)	5084(2)	2551(1)	6341(2)	37(1)
F(11)	5600(2)	2611(1)	7836(3)	33(1)
F(12)	4822(2)	2090(1)	7452(3)	35(1)
F(13)	3085(2)	3551(2)	5259(3)	75(2)
F(14)	3045(2)	4211(2)	4634(3)	70(1)
F(15)	3245(2)	3645(2)	3738(3)	64(1)
F(16)	4322(3)	4611(1)	4442(3)	56(1)
F(17)	4439(2)	4106(1)	3378(2)	51(1)
F(18)	5277(2)	4208(1)	4575(3)	51(1)
F(23)	8734(2)	3775(2)	6263(3)	68(1)
F(27)	11506(2)	4919(1)	2429(3)	50(1)
F(31)	11334(2)	2465(2)	2414(3)	60(1)
F(32)	11781(2)	3121(2)	2490(4)	74(2)
F(33)	12185(2)	2628(2)	3566(3)	59(1)
F(34)	11408(2)	2453(1)	5052(3)	47(1)
F(35)	10286(2)	2664(1)	4864(3)	48(1)
F(36)	10652(2)	2183(1)	3885(3)	42(1)
Mo(1)	4839(1)	3846(1)	7206(1)	17(1)
Mo(2)	9764(1)	3566(1)	2778(1)	18(1)
C(61)	8629(6)	4151(4)	4178(8)	28(2)
C(62)	8846(4)	4406(3)	3309(6)	28(2)
C(63)	8591(6)	4872(4)	3138(9)	24(2)
C(64)	8369(4)	5140(3)	3889(7)	33(2)
C(65)	8214(5)	5581(3)	3720(9)	39(2)
C(66)	8249(8)	5766(6)	2786(13)	43(5)
C(67)	8449(5)	5501(3)	2038(8)	42(2)
C(68)	8613(6)	5059(3)	2189(9)	35(2)
C(72)	10300(5)	4490(3)	1075(6)	26(2)
F(19)	10113(4)	4483(2)	4609(4)	39(1)
F(20)	10369(6)	4037(3)	5805(7)	58(3)
F(21)	9495(9)	4502(5)	5856(10)	67(4)
F(22)	9710(8)	3354(8)	6059(16)	51(4)
F(24)	8703(6)	3217(4)	5210(10)	65(4)
F(25)	10504(4)	4820(2)	2933(5)	40(2)

F(26)	11407(5)	4416(3)	3481(7)	37(2)
F(28)	12061(8)	3979(5)	2057(8)	40(3)
F(29)	11313(5)	3745(3)	795(7)	36(2)
F(30)	11750(3)	4413(2)	811(4)	41(1)
C(61A)	8452(13)	4028(8)	4545(16)	27(5)
C(62A)	9456(8)	4581(5)	2147(11)	18(4)
C(63A)	9082(14)	5015(6)	2217(14)	26(4)
C(64A)	8644(13)	5061(8)	2930(20)	26(6)
C(65A)	8291(10)	5476(8)	3057(19)	33(5)
C(66A)	8390(20)	5816(17)	2420(40)	43(5)
C(67A)	8773(12)	5752(8)	1628(16)	42(5)
C(68A)	9146(11)	5353(7)	1530(15)	35(5)
C(72A)	10123(11)	4556(7)	1532(15)	26(2)
F(19A)	9617(8)	4597(4)	4651(8)	35(3)
F(20A)	10456(13)	4138(8)	5388(14)	53(6)
F(21A)	9630(20)	4398(11)	6160(20)	45(6)
F(22A)	9474(16)	3388(17)	5950(40)	41(7)
F(24A)	8420(10)	3328(8)	5103(17)	26(4)
F(25A)	10684(6)	4702(4)	3500(11)	35(3)
F(26A)	11709(9)	4365(8)	3441(19)	33(5)
F(28A)	11961(16)	4068(10)	1711(18)	34(5)
F(29A)	11055(12)	3893(8)	649(18)	55(6)
F(30A)	11419(8)	4563(5)	722(11)	41(1)

Table B.20: Bond lengths [Å] and angles [°] for **54**.

C(1)-C(4)	1.445(7)
C(1)-C(19)	1.463(7)
C(1)-C(2)	1.493(7)
C(1)-Mo(1)	2.067(5)
C(2)-C(3)	1.518(8)
C(2)-H(2A)	0.99
C(2)-H(2B)	0.99
C(3)-H(3A)	0.98
C(3)-H(3B)	0.98
C(3)-H(3C)	0.98
C(4)-C(19)	1.435(7)
C(4)-C(5)	1.462(8)
C(4)-Mo(1)	2.159(5)
C(5)-C(6)	1.393(8)
C(5)-C(10)	1.418(8)
C(6)-C(7)	1.393(8)
C(6)-H(6)	0.95
C(7)-C(8)	1.385(9)
C(7)-H(7)	0.95
C(8)-C(9)	1.375(9)
C(8)-H(8)	0.95
C(9)-C(10)	1.389(8)
C(9)-H(9)	0.95
C(10)-C(11)	1.436(9)
C(11)-C(12)	1.208(8)
C(12)-C(13)	1.413(9)
C(13)-C(18)	1.414(8)
C(13)-C(14)	1.416(8)
C(14)-C(15)	1.367(9)
C(14)-H(14)	0.95
C(15)-C(16)	1.373(9)
C(15)-H(15)	0.95
C(16)-C(17)	1.392(8)
C(16)-H(16)	0.95
C(17)-C(18)	1.381(8)
C(17)-H(17)	0.95
C(18)-C(19)	1.472(7)
C(19)-Mo(1)	2.127(5)

C(20)-O(1)	1.388(6)
C(20)-C(22)	1.544(7)
C(20)-C(21)	1.544(7)
C(20)-C(23)	1.546(7)
C(21)-F(3)	1.312(7)
C(21)-F(2)	1.334(6)
C(21)-F(1)	1.336(6)
C(22)-F(4)	1.314(6)
C(22)-F(5)	1.327(6)
C(22)-F(6)	1.327(7)
C(23)-C(24)	1.518(7)
C(23)-H(23A)	0.99
C(23)-H(23B)	0.99
C(24)-O(2)	1.233(6)
C(24)-C(25)	1.471(7)
C(25)-C(26)	1.397(7)
C(25)-C(30)	1.404(7)
C(26)-C(27)	1.373(8)
C(26)-H(26)	0.95
C(27)-C(28)	1.389(8)
C(27)-H(27)	0.95
C(28)-C(29)	1.376(8)
C(28)-H(28)	0.95
C(29)-C(30)	1.376(8)
C(29)-H(29)	0.95
C(30)-H(30)	0.95
C(31)-O(3)	1.399(6)
C(31)-C(34)	1.530(8)
C(31)-C(33)	1.551(7)
C(31)-C(32)	1.549(8)
C(32)-F(7)	1.329(7)
C(32)-F(9)	1.334(7)
C(32)-F(8)	1.338(7)
C(33)-F(11)	1.327(7)
C(33)-F(12)	1.337(6)
C(33)-F(10)	1.343(6)
C(34)-H(34A)	0.98
C(34)-H(34B)	0.98
C(34)-H(34C)	0.98
C(35)-O(4)	1.393(6)
C(35)-C(38)	1.524(8)
C(35)-C(36)	1.530(9)

C(35)-C(37)	1.547(8)
C(36)-F(13)	1.337(8)
C(36)-F(15)	1.339(8)
C(36)-F(14)	1.338(9)
C(37)-F(16)	1.313(7)
C(37)-F(18)	1.324(7)
C(37)-F(17)	1.337(6)
C(38)-H(38A)	0.98
C(38)-H(38B)	0.98
C(38)-H(38C)	0.98
C(39)-C(42)	1.447(7)
C(39)-C(57)	1.452(7)
C(39)-C(40)	1.492(7)
C(39)-Mo(2)	2.063(5)
C(40)-C(41)	1.520(7)
C(40)-H(40A)	0.99
C(40)-H(40B)	0.99
C(41)-H(41A)	0.98
C(41)-H(41B)	0.98
C(41)-H(41C)	0.98
C(42)-C(57)	1.431(7)
C(42)-C(43)	1.471(7)
C(42)-Mo(2)	2.154(5)
C(43)-C(44)	1.396(8)
C(43)-C(48)	1.412(7)
C(44)-C(45)	1.376(7)
C(44)-H(44)	0.95
C(45)-C(46)	1.392(8)
C(45)-H(45)	0.95
C(46)-C(47)	1.382(9)
C(46)-H(46)	0.95
C(47)-C(48)	1.407(8)
C(47)-H(47)	0.95
C(48)-C(49)	1.421(8)
C(49)-C(50)	1.201(8)
C(50)-C(51)	1.431(8)
C(51)-C(52)	1.397(8)
C(51)-C(56)	1.426(8)
C(52)-C(53)	1.384(9)
C(52)-H(52)	0.95
C(53)-C(54)	1.367(9)
C(53)-H(53)	0.95

C(54)-C(55)	1.389(8)
C(54)-H(54)	0.95
C(55)-C(56)	1.392(8)
C(55)-H(55)	0.95
C(56)-C(57)	1.467(7)
C(57)-Mo(2)	2.136(5)
C(58)-O(5)	1.385(6)
C(58)-C(59)	1.526(8)
C(58)-C(60)	1.534(9)
C(58)-C(61A)	1.55(2)
C(58)-C(61)	1.561(12)
C(59)-F(20A)	1.25(2)
C(59)-F(21)	1.303(16)
C(59)-F(20)	1.350(13)
C(59)-F(19)	1.354(8)
C(59)-F(21A)	1.37(4)
C(59)-F(19A)	1.387(13)
C(60)-F(22A)	1.01(3)
C(60)-F(24)	1.301(14)
C(60)-F(23)	1.336(7)
C(60)-F(22)	1.438(15)
C(60)-F(24A)	1.46(3)
C(69)-O(7)	1.396(6)
C(69)-C(72)	1.523(10)
C(69)-C(70)	1.536(9)
C(69)-C(72A)	1.55(2)
C(69)-C(71)	1.552(10)
C(70)-F(26)	1.209(12)
C(70)-F(27)	1.326(7)
C(70)-F(25)	1.360(9)
C(70)-F(25A)	1.410(13)
C(70)-F(26A)	1.53(2)
C(71)-F(28A)	1.01(3)
C(71)-F(30)	1.304(8)
C(71)-F(29A)	1.34(3)
C(71)-F(29)	1.378(12)
C(71)-F(28)	1.443(13)
C(71)-F(30A)	1.573(16)
C(73)-O(8)	1.386(7)
C(73)-C(76)	1.536(8)
C(73)-C(74)	1.537(8)
C(73)-C(75)	1.552(8)

C(74)-F(31)	1.312(9)
C(74)-F(32)	1.337(7)
C(74)-F(33)	1.341(7)
C(75)-F(35)	1.329(7)
C(75)-F(36)	1.331(7)
C(75)-F(34)	1.336(7)
C(76)-H(76A)	0.98
C(76)-H(76B)	0.98
C(76)-H(76C)	0.98
O(1)-Mo(1)	1.946(3)
O(2)-Mo(1)	2.230(3)
O(3)-Mo(1)	1.928(3)
O(4)-Mo(1)	1.984(3)
O(5)-Mo(2)	1.923(3)
O(6)-C(62)	1.283(8)
O(6)-C(62A)	1.358(17)
O(6)-Mo(2)	2.232(4)
O(7)-Mo(2)	1.935(4)
O(8)-Mo(2)	1.990(3)
C(61)-C(62)	1.506(13)
C(61)-H(61A)	0.99
C(61)-H(61B)	0.99
C(62)-C(63)	1.485(14)
C(63)-C(64)	1.403(14)
C(63)-C(68)	1.416(15)
C(64)-C(65)	1.367(13)
C(64)-H(64)	0.95
C(65)-C(66)	1.40(2)
C(65)-H(65)	0.95
C(66)-C(67)	1.38(2)
C(66)-H(66)	0.95
C(67)-C(68)	1.370(14)
C(67)-H(67)	0.95
C(68)-H(68)	0.95
C(72)-H(72A)	0.98
C(72)-H(72B)	0.98
C(72)-H(72C)	0.98
C(61A)-H(61C)	0.98
C(61A)-H(61D)	0.98
C(61A)-H(61E)	0.98
C(62A)-C(63A)	1.48(3)
C(62A)-C(72A)	1.57(3)

C(63A)-C(64A)	1.35(4)
C(63A)-C(68A)	1.40(3)
C(64A)-C(65A)	1.42(4)
C(64A)-H(64A)	0.95
C(65A)-C(66A)	1.37(5)
C(65A)-H(65A)	0.95
C(66A)-C(67A)	1.38(5)
C(66A)-H(66A)	0.95
C(67A)-C(68A)	1.39(3)
C(67A)-H(67A)	0.95
C(68A)-H(68A)	0.95
C(72A)-H(72D)	0.99
C(72A)-H(72E)	0.99

C(4)-C(1)-C(19)	59.1(4)
C(4)-C(1)-C(2)	143.3(5)
C(19)-C(1)-C(2)	139.4(4)
C(4)-C(1)-Mo(1)	73.5(3)
C(19)-C(1)-Mo(1)	71.8(3)
C(2)-C(1)-Mo(1)	135.9(4)
C(1)-C(2)-C(3)	112.7(5)
C(1)-C(2)-H(2A)	109
C(3)-C(2)-H(2A)	109
C(1)-C(2)-H(2B)	109
C(3)-C(2)-H(2B)	109
H(2A)-C(2)-H(2B)	107.8
C(2)-C(3)-H(3A)	109.5
C(2)-C(3)-H(3B)	109.5
H(3A)-C(3)-H(3B)	109.5
C(2)-C(3)-H(3C)	109.5
H(3A)-C(3)-H(3C)	109.5
H(3B)-C(3)-H(3C)	109.5
C(19)-C(4)-C(1)	61.1(4)
C(19)-C(4)-C(5)	145.2(5)
C(1)-C(4)-C(5)	142.4(5)
C(19)-C(4)-Mo(1)	69.2(3)
C(1)-C(4)-Mo(1)	66.6(3)
C(5)-C(4)-Mo(1)	136.2(4)
C(6)-C(5)-C(10)	119.0(5)
C(6)-C(5)-C(4)	120.2(5)
C(10)-C(5)-C(4)	120.6(5)
C(5)-C(6)-C(7)	120.1(6)

C(5)-C(6)-H(6)	119.9
C(7)-C(6)-H(6)	119.9
C(8)-C(7)-C(6)	120.2(6)
C(8)-C(7)-H(7)	119.9
C(6)-C(7)-H(7)	119.9
C(9)-C(8)-C(7)	120.4(6)
C(9)-C(8)-H(8)	119.8
C(7)-C(8)-H(8)	119.8
C(8)-C(9)-C(10)	120.5(6)
C(8)-C(9)-H(9)	119.8
C(10)-C(9)-H(9)	119.8
C(9)-C(10)-C(5)	119.7(6)
C(9)-C(10)-C(11)	125.4(5)
C(5)-C(10)-C(11)	114.8(5)
C(12)-C(11)-C(10)	156.9(6)
C(11)-C(12)-C(13)	154.5(6)
C(18)-C(13)-C(12)	114.3(5)
C(18)-C(13)-C(14)	118.9(6)
C(12)-C(13)-C(14)	126.6(5)
C(15)-C(14)-C(13)	120.0(6)
C(15)-C(14)-H(14)	120
C(13)-C(14)-H(14)	120
C(14)-C(15)-C(16)	120.8(6)
C(14)-C(15)-H(15)	119.6
C(16)-C(15)-H(15)	119.6
C(15)-C(16)-C(17)	120.6(6)
C(15)-C(16)-H(16)	119.7
C(17)-C(16)-H(16)	119.7
C(18)-C(17)-C(16)	120.1(6)
C(18)-C(17)-H(17)	119.9
C(16)-C(17)-H(17)	119.9
C(17)-C(18)-C(13)	119.6(5)
C(17)-C(18)-C(19)	119.2(5)
C(13)-C(18)-C(19)	121.1(5)
C(4)-C(19)-C(1)	59.8(4)
C(4)-C(19)-C(18)	145.2(5)
C(1)-C(19)-C(18)	136.3(5)
C(4)-C(19)-Mo(1)	71.7(3)
C(1)-C(19)-Mo(1)	67.4(3)
C(18)-C(19)-Mo(1)	139.2(4)
O(1)-C(20)-C(22)	108.4(4)
O(1)-C(20)-C(21)	107.1(4)

C(22)-C(20)-C(21)	109.7(4)
O(1)-C(20)-C(23)	112.9(4)
C(22)-C(20)-C(23)	109.0(4)
C(21)-C(20)-C(23)	109.7(4)
F(3)-C(21)-F(2)	107.8(4)
F(3)-C(21)-F(1)	107.2(5)
F(2)-C(21)-F(1)	105.1(5)
F(3)-C(21)-C(20)	113.9(5)
F(2)-C(21)-C(20)	111.8(4)
F(1)-C(21)-C(20)	110.5(4)
F(4)-C(22)-F(5)	107.5(5)
F(4)-C(22)-F(6)	107.8(5)
F(5)-C(22)-F(6)	106.6(4)
F(4)-C(22)-C(20)	110.6(4)
F(5)-C(22)-C(20)	111.7(4)
F(6)-C(22)-C(20)	112.3(5)
C(24)-C(23)-C(20)	112.6(4)
C(24)-C(23)-H(23A)	109.1
C(20)-C(23)-H(23A)	109.1
C(24)-C(23)-H(23B)	109.1
C(20)-C(23)-H(23B)	109.1
H(23A)-C(23)-H(23B)	107.8
O(2)-C(24)-C(25)	119.5(5)
O(2)-C(24)-C(23)	120.5(5)
C(25)-C(24)-C(23)	119.9(5)
C(26)-C(25)-C(30)	119.5(5)
C(26)-C(25)-C(24)	121.6(5)
C(30)-C(25)-C(24)	118.8(5)
C(27)-C(26)-C(25)	120.0(5)
C(27)-C(26)-H(26)	120
C(25)-C(26)-H(26)	120
C(26)-C(27)-C(28)	120.1(5)
C(26)-C(27)-H(27)	120
C(28)-C(27)-H(27)	120
C(29)-C(28)-C(27)	120.3(5)
C(29)-C(28)-H(28)	119.9
C(27)-C(28)-H(28)	119.9
C(28)-C(29)-C(30)	120.5(5)
C(28)-C(29)-H(29)	119.7
C(30)-C(29)-H(29)	119.7
C(29)-C(30)-C(25)	119.5(5)
C(29)-C(30)-H(30)	120.2

C(25)-C(30)-H(30)	120.2
O(3)-C(31)-C(34)	116.3(4)
O(3)-C(31)-C(33)	107.8(4)
C(34)-C(31)-C(33)	108.0(4)
O(3)-C(31)-C(32)	105.5(4)
C(34)-C(31)-C(32)	109.4(4)
C(33)-C(31)-C(32)	109.7(4)
F(7)-C(32)-F(9)	107.5(5)
F(7)-C(32)-F(8)	107.6(4)
F(9)-C(32)-F(8)	107.5(5)
F(7)-C(32)-C(31)	112.2(5)
F(9)-C(32)-C(31)	112.1(4)
F(8)-C(32)-C(31)	109.7(5)
F(11)-C(33)-F(12)	107.0(4)
F(11)-C(33)-F(10)	107.1(4)
F(12)-C(33)-F(10)	106.7(4)
F(11)-C(33)-C(31)	111.1(5)
F(12)-C(33)-C(31)	112.1(4)
F(10)-C(33)-C(31)	112.4(4)
C(31)-C(34)-H(34A)	109.5
C(31)-C(34)-H(34B)	109.5
H(34A)-C(34)-H(34B)	109.5
C(31)-C(34)-H(34C)	109.5
H(34A)-C(34)-H(34C)	109.5
H(34B)-C(34)-H(34C)	109.5
O(4)-C(35)-C(38)	116.6(5)
O(4)-C(35)-C(36)	105.2(5)
C(38)-C(35)-C(36)	109.3(5)
O(4)-C(35)-C(37)	107.8(4)
C(38)-C(35)-C(37)	108.0(5)
C(36)-C(35)-C(37)	109.9(5)
F(13)-C(36)-F(15)	106.7(6)
F(13)-C(36)-F(14)	107.2(6)
F(15)-C(36)-F(14)	106.9(6)
F(13)-C(36)-C(35)	109.6(5)
F(15)-C(36)-C(35)	113.1(6)
F(14)-C(36)-C(35)	112.9(6)
F(16)-C(37)-F(18)	107.6(5)
F(16)-C(37)-F(17)	106.9(5)
F(18)-C(37)-F(17)	106.2(5)
F(16)-C(37)-C(35)	113.4(5)
F(18)-C(37)-C(35)	110.0(5)

F(17)-C(37)-C(35)	112.4(5)
C(35)-C(38)-H(38A)	109.5
C(35)-C(38)-H(38B)	109.5
H(38A)-C(38)-H(38B)	109.5
C(35)-C(38)-H(38C)	109.5
H(38A)-C(38)-H(38C)	109.5
H(38B)-C(38)-H(38C)	109.5
C(42)-C(39)-C(57)	59.2(4)
C(42)-C(39)-C(40)	141.5(5)
C(57)-C(39)-C(40)	143.4(5)
C(42)-C(39)-Mo(2)	73.3(3)
C(57)-C(39)-Mo(2)	72.5(3)
C(40)-C(39)-Mo(2)	134.0(4)
C(39)-C(40)-C(41)	112.6(4)
C(39)-C(40)-H(40A)	109.1
C(41)-C(40)-H(40A)	109.1
C(39)-C(40)-H(40B)	109.1
C(41)-C(40)-H(40B)	109.1
H(40A)-C(40)-H(40B)	107.8
C(40)-C(41)-H(41A)	109.5
C(40)-C(41)-H(41B)	109.5
H(41A)-C(41)-H(41B)	109.5
C(40)-C(41)-H(41C)	109.5
H(41A)-C(41)-H(41C)	109.5
H(41B)-C(41)-H(41C)	109.5
C(57)-C(42)-C(39)	60.6(4)
C(57)-C(42)-C(43)	143.5(5)
C(39)-C(42)-C(43)	141.0(5)
C(57)-C(42)-Mo(2)	69.8(3)
C(39)-C(42)-Mo(2)	66.6(3)
C(43)-C(42)-Mo(2)	139.0(4)
C(44)-C(43)-C(48)	117.8(5)
C(44)-C(43)-C(42)	121.1(5)
C(48)-C(43)-C(42)	121.1(5)
C(45)-C(44)-C(43)	121.8(5)
C(45)-C(44)-H(44)	119.1
C(43)-C(44)-H(44)	119.1
C(44)-C(45)-C(46)	120.4(5)
C(44)-C(45)-H(45)	119.8
C(46)-C(45)-H(45)	119.8
C(47)-C(46)-C(45)	119.4(5)
C(47)-C(46)-H(46)	120.3

C(45)-C(46)-H(46)	120.3
C(46)-C(47)-C(48)	120.6(5)
C(46)-C(47)-H(47)	119.7
C(48)-C(47)-H(47)	119.7
C(47)-C(48)-C(43)	120.0(5)
C(47)-C(48)-C(49)	124.9(5)
C(43)-C(48)-C(49)	114.9(5)
C(50)-C(49)-C(48)	156.9(6)
C(49)-C(50)-C(51)	153.9(6)
C(52)-C(51)-C(56)	119.8(5)
C(52)-C(51)-C(50)	125.7(5)
C(56)-C(51)-C(50)	114.3(5)
C(53)-C(52)-C(51)	120.0(6)
C(53)-C(52)-H(52)	120
C(51)-C(52)-H(52)	120
C(54)-C(53)-C(52)	120.1(5)
C(54)-C(53)-H(53)	119.9
C(52)-C(53)-H(53)	119.9
C(53)-C(54)-C(55)	121.4(6)
C(53)-C(54)-H(54)	119.3
C(55)-C(54)-H(54)	119.3
C(54)-C(55)-C(56)	120.1(5)
C(54)-C(55)-H(55)	119.9
C(56)-C(55)-H(55)	119.9
C(55)-C(56)-C(51)	118.5(5)
C(55)-C(56)-C(57)	120.7(5)
C(51)-C(56)-C(57)	120.8(5)
C(42)-C(57)-C(39)	60.3(4)
C(42)-C(57)-C(56)	146.4(5)
C(39)-C(57)-C(56)	140.4(5)
C(42)-C(57)-Mo(2)	71.2(3)
C(39)-C(57)-Mo(2)	67.1(3)
C(56)-C(57)-Mo(2)	135.5(4)
O(5)-C(58)-C(59)	108.6(5)
O(5)-C(58)-C(60)	105.5(5)
C(59)-C(58)-C(60)	109.0(5)
O(5)-C(58)-C(61A)	123.0(9)
C(59)-C(58)-C(61A)	117.1(9)
C(60)-C(58)-C(61A)	90.5(10)
O(5)-C(58)-C(61)	109.6(5)
C(59)-C(58)-C(61)	106.4(6)
C(60)-C(58)-C(61)	117.5(6)

F(21)-C(59)-F(20)	107.6(8)
F(21)-C(59)-F(19)	108.8(9)
F(20)-C(59)-F(19)	103.1(7)
F(20A)-C(59)-F(21A)	106.5(17)
F(20A)-C(59)-F(19A)	114.8(12)
F(21A)-C(59)-F(19A)	101.3(12)
F(20A)-C(59)-C(58)	117.5(11)
F(21)-C(59)-C(58)	112.9(9)
F(20)-C(59)-C(58)	110.7(6)
F(19)-C(59)-C(58)	113.2(5)
F(21A)-C(59)-C(58)	115.4(18)
F(19A)-C(59)-C(58)	100.4(7)
F(22A)-C(60)-F(23)	106(3)
F(24)-C(60)-F(23)	113.3(7)
F(24)-C(60)-F(22)	100.3(12)
F(23)-C(60)-F(22)	108.0(11)
F(22A)-C(60)-F(24A)	119(3)
F(23)-C(60)-F(24A)	97.3(10)
F(22A)-C(60)-C(58)	117(2)
F(24)-C(60)-C(58)	113.2(8)
F(23)-C(60)-C(58)	111.3(6)
F(22)-C(60)-C(58)	110.0(11)
F(24A)-C(60)-C(58)	104.5(11)
O(7)-C(69)-C(72)	118.1(5)
O(7)-C(69)-C(70)	108.2(5)
C(72)-C(69)-C(70)	114.9(6)
O(7)-C(69)-C(72A)	108.1(8)
C(70)-C(69)-C(72A)	96.4(9)
O(7)-C(69)-C(71)	104.7(5)
C(72)-C(69)-C(71)	101.8(6)
C(70)-C(69)-C(71)	108.0(5)
C(72A)-C(69)-C(71)	130.0(9)
F(26)-C(70)-F(27)	112.3(7)
F(26)-C(70)-F(25)	111.2(7)
F(27)-C(70)-F(25)	100.8(5)
F(27)-C(70)-F(25A)	116.1(7)
F(27)-C(70)-F(26A)	98.3(10)
F(25A)-C(70)-F(26A)	94.2(11)
F(26)-C(70)-C(69)	115.6(7)
F(27)-C(70)-C(69)	112.6(5)
F(25)-C(70)-C(69)	103.0(6)
F(25A)-C(70)-C(69)	120.4(7)

F(26A)-C(70)-C(69)	110.7(11)
F(28A)-C(71)-F(29A)	131(2)
F(30)-C(71)-F(29)	107.2(7)
F(30)-C(71)-F(28)	103.6(8)
F(29)-C(71)-F(28)	101.4(10)
F(28A)-C(71)-C(69)	122.6(16)
F(30)-C(71)-C(69)	118.7(7)
F(29A)-C(71)-C(69)	96.3(10)
F(29)-C(71)-C(69)	113.8(7)
F(28)-C(71)-C(69)	110.4(8)
F(28A)-C(71)-F(30A)	112.2(19)
F(29A)-C(71)-F(30A)	93.1(13)
C(69)-C(71)-F(30A)	92.2(7)
O(8)-C(73)-C(76)	116.9(5)
O(8)-C(73)-C(74)	106.9(5)
C(76)-C(73)-C(74)	109.9(5)
O(8)-C(73)-C(75)	105.9(4)
C(76)-C(73)-C(75)	108.5(5)
C(74)-C(73)-C(75)	108.5(5)
F(31)-C(74)-F(32)	107.2(6)
F(31)-C(74)-F(33)	107.3(6)
F(32)-C(74)-F(33)	106.7(5)
F(31)-C(74)-C(73)	113.7(5)
F(32)-C(74)-C(73)	109.8(5)
F(33)-C(74)-C(73)	111.8(5)
F(35)-C(75)-F(36)	106.5(5)
F(35)-C(75)-F(34)	107.6(5)
F(36)-C(75)-F(34)	107.0(5)
F(35)-C(75)-C(73)	109.9(5)
F(36)-C(75)-C(73)	112.7(5)
F(34)-C(75)-C(73)	112.8(5)
C(73)-C(76)-H(76A)	109.5
C(73)-C(76)-H(76B)	109.5
H(76A)-C(76)-H(76B)	109.5
C(73)-C(76)-H(76C)	109.5
H(76A)-C(76)-H(76C)	109.5
H(76B)-C(76)-H(76C)	109.5
C(20)-O(1)-Mo(1)	139.2(3)
C(24)-O(2)-Mo(1)	130.9(3)
C(31)-O(3)-Mo(1)	151.0(3)
C(35)-O(4)-Mo(1)	132.7(3)
C(58)-O(5)-Mo(2)	142.8(3)

C(62)-O(6)-Mo(2)	126.7(4)
C(62A)-O(6)-Mo(2)	124.1(7)
C(69)-O(7)-Mo(2)	146.7(3)
C(73)-O(8)-Mo(2)	133.0(3)
O(3)-Mo(1)-O(1)	116.47(15)
O(3)-Mo(1)-O(4)	93.06(15)
O(1)-Mo(1)-O(4)	89.80(14)
O(3)-Mo(1)-C(1)	121.35(17)
O(1)-Mo(1)-C(1)	121.28(17)
O(4)-Mo(1)-C(1)	78.19(18)
O(3)-Mo(1)-C(19)	97.41(17)
O(1)-Mo(1)-C(19)	138.44(18)
O(4)-Mo(1)-C(19)	112.83(17)
C(1)-Mo(1)-C(19)	40.8(2)
O(3)-Mo(1)-C(4)	134.80(17)
O(1)-Mo(1)-C(4)	100.75(17)
O(4)-Mo(1)-C(4)	112.69(17)
C(1)-Mo(1)-C(4)	39.9(2)
C(19)-Mo(1)-C(4)	39.10(19)
O(3)-Mo(1)-O(2)	83.60(14)
O(1)-Mo(1)-O(2)	81.04(13)
O(4)-Mo(1)-O(2)	167.53(13)
C(1)-Mo(1)-O(2)	113.80(17)
C(19)-Mo(1)-O(2)	79.56(16)
C(4)-Mo(1)-O(2)	77.57(16)
O(5)-Mo(2)-O(7)	116.90(16)
O(5)-Mo(2)-O(8)	91.54(15)
O(7)-Mo(2)-O(8)	91.98(15)
O(5)-Mo(2)-C(39)	120.27(18)
O(7)-Mo(2)-C(39)	121.94(18)
O(8)-Mo(2)-C(39)	77.48(18)
O(5)-Mo(2)-C(57)	136.92(18)
O(7)-Mo(2)-C(57)	98.77(18)
O(8)-Mo(2)-C(57)	111.58(18)
C(39)-Mo(2)-C(57)	40.4(2)
O(5)-Mo(2)-C(42)	99.21(18)
O(7)-Mo(2)-C(42)	135.98(18)
O(8)-Mo(2)-C(42)	112.38(17)
C(39)-Mo(2)-C(42)	40.1(2)
C(57)-Mo(2)-C(42)	38.98(19)
O(5)-Mo(2)-O(6)	81.31(15)
O(7)-Mo(2)-O(6)	83.19(15)

O(8)-Mo(2)-O(6)	168.34(14)
C(39)-Mo(2)-O(6)	114.07(18)
C(57)-Mo(2)-O(6)	79.72(17)
C(42)-Mo(2)-O(6)	78.04(16)
C(62)-C(61)-C(58)	114.6(7)
C(62)-C(61)-H(61A)	108.6
C(58)-C(61)-H(61A)	108.6
C(62)-C(61)-H(61B)	108.6
C(58)-C(61)-H(61B)	108.6
H(61A)-C(61)-H(61B)	107.6
O(6)-C(62)-C(63)	117.6(8)
O(6)-C(62)-C(61)	122.9(7)
C(63)-C(62)-C(61)	119.5(8)
C(64)-C(63)-C(68)	118.9(10)
C(64)-C(63)-C(62)	122.8(10)
C(68)-C(63)-C(62)	118.2(9)
C(65)-C(64)-C(63)	120.4(10)
C(65)-C(64)-H(64)	119.8
C(63)-C(64)-H(64)	119.8
C(64)-C(65)-C(66)	120.4(12)
C(64)-C(65)-H(65)	119.8
C(66)-C(65)-H(65)	119.8
C(67)-C(66)-C(65)	119.5(15)
C(67)-C(66)-H(66)	120.2
C(65)-C(66)-H(66)	120.2
C(68)-C(67)-C(66)	121.4(12)
C(68)-C(67)-H(67)	119.3
C(66)-C(67)-H(67)	119.3
C(67)-C(68)-C(63)	119.4(11)
C(67)-C(68)-H(68)	120.3
C(63)-C(68)-H(68)	120.3
C(69)-C(72)-H(72A)	109.5
C(69)-C(72)-H(72B)	109.5
H(72A)-C(72)-H(72B)	109.5
C(69)-C(72)-H(72C)	109.5
H(72A)-C(72)-H(72C)	109.5
H(72B)-C(72)-H(72C)	109.5
C(58)-C(61A)-H(61C)	109.5
C(58)-C(61A)-H(61D)	109.5
H(61C)-C(61A)-H(61D)	109.5
C(58)-C(61A)-H(61E)	109.5
H(61C)-C(61A)-H(61E)	109.5

H(61D)-C(61A)-H(61E)	109.5
O(6)-C(62A)-C(63A)	117.6(13)
O(6)-C(62A)-C(72A)	123.8(13)
C(63A)-C(62A)-C(72A)	118.4(15)
C(64A)-C(63A)-C(68A)	121(2)
C(64A)-C(63A)-C(62A)	117.5(17)
C(68A)-C(63A)-C(62A)	121.3(18)
C(63A)-C(64A)-C(65A)	120(2)
C(63A)-C(64A)-H(64A)	120
C(65A)-C(64A)-H(64A)	120
C(66A)-C(65A)-C(64A)	119(3)
C(66A)-C(65A)-H(65A)	120.7
C(64A)-C(65A)-H(65A)	120.7
C(65A)-C(66A)-C(67A)	121(4)
C(65A)-C(66A)-H(66A)	119.5
C(67A)-C(66A)-H(66A)	119.5
C(66A)-C(67A)-C(68A)	120(3)
C(66A)-C(67A)-H(67A)	120
C(68A)-C(67A)-H(67A)	120
C(63A)-C(68A)-C(67A)	118.5(18)
C(63A)-C(68A)-H(68A)	120.7
C(67A)-C(68A)-H(68A)	120.7
C(69)-C(72A)-C(62A)	120.5(14)
C(69)-C(72A)-H(72D)	107.2
C(62A)-C(72A)-H(72D)	107.2
C(69)-C(72A)-H(72E)	107.2
C(62A)-C(72A)-H(72E)	107.2
H(72D)-C(72A)-H(72E)	106.8

Table B.22: Anisotropic displacement parameters ($Å^2 \times 10^3$) for **54**. The anisotropic displacement factor exponent takes the form: $-2p^2[h^2a^{*2}U^{11} + ... + 2hka^*b^*U^{12}]$

Atom	U11	U22	U33	U23	U13	U12
C(1)	20(3)	22(3)	21(3)	-4(2)	11(2)	-1(2)
C(2)	20(3)	31(3)	21(3)	0(2)	2(2)	6(2)
C(3)	43(4)	29(3)	46(4)	9(3)	9(3)	9(3)
C(4)	23(3)	21(3)	20(3)	1(2)	8(2)	4(2)
C(5)	18(3)	25(3)	29(3)	-5(2)	2(2)	5(2)
C(6)	16(3)	23(3)	39(3)	-1(2)	4(2)	4(2)
C(7)	23(3)	23(3)	53(4)	-9(3)	7(3)	1(2)
C(8)	25(3)	36(4)	55(4)	-20(3)	-4(3)	2(3)
C(9)	34(3)	34(3)	33(3)	-13(3)	-1(3)	8(3)
C(10)	30(3)	30(3)	25(3)	-6(2)	-2(2)	14(3)
C(11)	35(3)	31(3)	19(3)	-5(2)	0(2)	14(3)
C(12)	37(4)	38(3)	16(3)	-2(2)	3(2)	17(3)
C(13)	36(3)	25(3)	24(3)	2(2)	10(2)	12(2)
C(14)	48(4)	33(3)	26(3)	8(3)	13(3)	19(3)
C(15)	42(4)	34(3)	43(4)	14(3)	25(3)	12(3)
C(16)	34(4)	34(3)	49(4)	10(3)	21(3)	7(3)
C(17)	28(3)	32(3)	32(3)	1(2)	14(3)	6(2)
C(18)	26(3)	24(3)	24(3)	1(2)	11(2)	13(2)
C(19)	17(3)	23(3)	26(3)	1(2)	5(2)	3(2)
C(20)	15(3)	29(3)	24(3)	4(2)	7(2)	1(2)
C(21)	20(3)	31(3)	31(3)	-4(2)	11(2)	-3(2)
C(22)	23(3)	27(3)	31(3)	3(2)	8(2)	4(2)
C(23)	23(3)	20(3)	25(3)	2(2)	4(2)	0(2)
C(24)	26(3)	20(3)	17(3)	-5(2)	7(2)	1(2)
C(25)	18(3)	23(3)	17(3)	-3(2)	-2(2)	0(2)
C(26)	26(3)	27(3)	24(3)	-2(2)	4(2)	-3(2)
C(27)	25(3)	26(3)	27(3)	-4(2)	0(2)	0(2)
C(28)	28(3)	27(3)	25(3)	4(2)	-5(2)	-4(2)
C(29)	27(3)	29(3)	27(3)	3(2)	6(2)	-3(2)
C(30)	21(3)	30(3)	21(3)	-2(2)	0(2)	-1(2)
C(31)	24(3)	23(3)	27(3)	0(2)	8(2)	1(2)
C(32)	25(3)	32(3)	41(4)	1(3)	16(3)	-4(3)
C(33)	26(3)	24(3)	34(3)	3(2)	12(3)	1(2)
C(34)	30(3)	23(3)	32(3)	4(2)	9(3)	1(2)
C(35)	31(3)	31(3)	18(3)	-3(2)	3(2)	0(2)
C(36)	40(4)	67(5)	33(4)	-2(3)	-5(3)	-2(4)
C(37)	43(4)	37(4)	19(3)	1(2)	0(3)	0(3)

C(38)	53(4)	31(3)	23(3)	-6(2)	9(3)	2(3)
C(39)	25(3)	26(3)	16(3)	0(2)	2(2)	-1(2)
C(40)	27(3)	22(3)	21(3)	0(2)	3(2)	2(2)
C(41)	36(3)	20(3)	23(3)	1(2)	5(2)	3(2)
C(42)	27(3)	17(3)	21(3)	0(2)	5(2)	1(2)
C(43)	19(3)	28(3)	22(3)	-6(2)	-1(2)	0(2)
C(44)	18(3)	27(3)	28(3)	-2(2)	0(2)	1(2)
C(45)	21(3)	35(3)	26(3)	-3(2)	3(2)	-2(2)
C(46)	17(3)	48(4)	32(3)	-8(3)	2(2)	1(3)
C(47)	22(3)	32(3)	39(4)	-5(3)	1(3)	4(2)
C(48)	20(3)	23(3)	30(3)	-3(2)	-3(2)	1(2)
C(49)	24(3)	23(3)	37(3)	1(3)	-7(3)	6(2)
C(50)	28(3)	23(3)	34(3)	8(2)	-5(3)	2(2)
C(51)	32(3)	18(3)	28(3)	1(2)	-6(2)	-6(2)
C(52)	42(4)	27(3)	29(3)	6(3)	-7(3)	-5(3)
C(53)	68(5)	30(3)	20(3)	1(3)	7(3)	-12(3)
C(54)	58(4)	32(3)	17(3)	-5(2)	11(3)	-3(3)
C(55)	43(4)	21(3)	21(3)	-2(2)	6(2)	0(2)
C(56)	26(3)	22(3)	22(3)	-2(2)	0(2)	-6(2)
C(57)	26(3)	20(3)	23(3)	-2(2)	5(2)	-2(2)
C(58)	35(3)	28(3)	24(3)	-5(2)	4(2)	5(3)
C(59)	50(5)	35(4)	26(3)	-7(3)	7(3)	-13(3)
C(60)	54(5)	41(4)	38(4)	-19(3)	28(4)	-16(4)
C(69)	25(3)	26(3)	42(4)	4(3)	10(3)	-6(2)
C(70)	52(4)	28(3)	44(4)	0(3)	21(3)	-8(3)
C(71)	56(5)	55(5)	31(4)	-4(3)	19(4)	-31(4)
C(73)	22(3)	27(3)	33(3)	4(2)	7(2)	1(2)
C(74)	26(3)	58(4)	49(4)	18(4)	18(3)	12(3)
C(75)	27(3)	45(4)	26(3)	6(3)	6(3)	4(3)
C(76)	30(4)	43(4)	56(4)	2(3)	-16(3)	1(3)
O(1)	17(2)	31(2)	19(2)	3(2)	6(2)	-1(2)
O(2)	16(2)	22(2)	19(2)	1(1)	8(1)	7(1)
O(3)	23(2)	19(2)	20(2)	1(1)	5(2)	-3(2)
O(4)	23(2)	27(2)	19(2)	1(2)	4(2)	2(2)
O(5)	29(2)	29(2)	17(2)	-2(2)	7(2)	-3(2)
O(6)	31(2)	20(2)	28(2)	-5(2)	2(2)	4(2)
O(7)	27(2)	27(2)	29(2)	2(2)	13(2)	1(2)
O(8)	22(2)	25(2)	24(2)	3(2)	6(2)	5(2)
F(1)	45(2)	28(2)	43(2)	-9(2)	26(2)	-10(2)
F(2)	25(2)	34(2)	66(3)	-8(2)	14(2)	3(2)
F(3)	61(3)	57(2)	24(2)	-11(2)	12(2)	15(2)

F(4)	54(2)	27(2)	82(3)	18(2)	42(2)	12(2)
F(5)	21(2)	35(2)	51(2)	9(2)	6(2)	-7(1)
F(6)	55(2)	68(3)	28(2)	13(2)	9(2)	-23(2)
F(7)	35(2)	33(2)	51(2)	-2(2)	17(2)	-9(2)
F(8)	26(2)	38(2)	54(2)	-2(2)	10(2)	-1(2)
F(9)	35(2)	46(2)	37(2)	-8(2)	6(2)	-16(2)
F(10)	41(2)	40(2)	34(2)	2(2)	21(2)	6(2)
F(11)	23(2)	31(2)	47(2)	2(2)	7(2)	1(1)
F(12)	37(2)	21(2)	49(2)	1(2)	16(2)	1(1)
F(13)	45(3)	128(4)	51(3)	8(3)	-4(2)	-47(3)
F(14)	37(2)	111(4)	56(3)	-9(3)	-16(2)	30(2)
F(15)	56(3)	98(3)	34(2)	-17(2)	-15(2)	-15(2)
F(16)	99(3)	36(2)	37(2)	10(2)	19(2)	10(2)
F(17)	80(3)	54(2)	18(2)	2(2)	8(2)	-6(2)
F(18)	40(2)	74(3)	40(2)	21(2)	6(2)	-14(2)
F(23)	52(3)	110(4)	50(3)	-46(2)	38(2)	-31(2)
F(27)	55(2)	41(2)	51(2)	14(2)	-6(2)	-26(2)
F(31)	59(3)	81(3)	43(2)	-2(2)	23(2)	32(2)
F(32)	49(3)	94(4)	85(3)	59(3)	42(2)	24(2)
F(33)	27(2)	92(3)	60(3)	29(2)	15(2)	25(2)
F(34)	39(2)	62(3)	37(2)	21(2)	-4(2)	9(2)
F(35)	43(2)	69(3)	36(2)	17(2)	23(2)	16(2)
F(36)	47(2)	29(2)	51(2)	10(2)	6(2)	0(2)
Mo(1)	16(1)	20(1)	16(1)	0(1)	5(1)	1(1)
Mo(2)	19(1)	20(1)	18(1)	1(1)	6(1)	1(1)
C(61)	33(6)	29(6)	24(6)	-5(4)	13(4)	6(4)
C(62)	29(5)	26(4)	29(5)	-7(3)	9(4)	-1(4)
C(63)	23(5)	17(6)	33(6)	1(5)	9(4)	2(5)
C(64)	21(4)	39(5)	39(5)	-14(4)	3(4)	3(4)
C(65)	26(5)	30(5)	59(7)	-15(5)	1(5)	4(4)
C(66)	13(8)	21(6)	92(17)	-7(9)	-8(6)	2(5)
C(67)	40(6)	33(6)	47(6)	4(5)	-13(5)	2(5)
C(68)	28(6)	38(6)	36(7)	-6(5)	-3(5)	2(5)
C(72)	32(5)	24(4)	20(5)	-4(4)	-2(4)	-3(3)
F(19)	38(4)	47(3)	31(3)	0(2)	5(3)	-17(3)
F(20)	65(6)	56(5)	47(6)	2(4)	-23(5)	-21(4)
F(21)	74(9)	64(9)	68(9)	-48(7)	28(7)	-13(6)
F(22)	78(12)	45(5)	32(5)	15(4)	20(8)	31(9)
F(24)	82(9)	66(8)	57(7)	-24(5)	42(7)	-48(6)
F(25)	61(4)	30(3)	30(3)	-7(3)	12(3)	2(3)
F(26)	52(6)	34(4)	25(3)	1(3)	3(5)	-7(5)

F(28)	23(5)	59(6)	40(7)	5(5)	4(5)	2(4)
F(29)	35(5)	42(5)	34(4)	-8(3)	21(4)	0(3)
F(30)	32(4)	57(4)	39(3)	19(3)	18(3)	-1(3)
C(61A)	33(13)	34(13)	12(11)	-5(9)	-9(9)	-1(10)
C(62A)	9(8)	28(9)	14(8)	-9(7)	-5(6)	4(7)
C(63A)	39(13)	14(9)	24(10)	7(7)	5(10)	-7(9)
C(64A)	24(11)	15(14)	36(17)	16(12)	-4(10)	-5(10)
C(65A)	17(10)	31(14)	50(16)	0(12)	0(9)	0(9)
C(66A)	13(8)	21(6)	92(17)	-7(9)	-8(6)	2(5)
C(67A)	39(12)	47(14)	36(12)	11(10)	-7(10)	14(11)
C(68A)	37(11)	39(11)	36(11)	6(9)	27(9)	4(9)
C(72A)	32(5)	24(4)	20(5)	-4(4)	-2(4)	-3(3)
F(19A)	43(8)	27(6)	37(7)	1(5)	5(6)	-15(6)
F(20A)	52(10)	71(14)	39(12)	-17(10)	15(10)	-33(9)
F(21A)	58(12)	38(11)	34(12)	-8(8)	-14(9)	1(8)
F(22A)	25(13)	60(18)	43(15)	24(11)	24(12)	18(12)
F(24A)	25(9)	37(9)	16(6)	-1(6)	2(7)	-8(6)
F(25A)	27(7)	42(8)	37(8)	-13(6)	12(6)	-4(5)
F(26A)	19(9)	35(8)	45(9)	2(6)	-2(8)	10(8)
F(28A)	13(10)	48(13)	41(15)	-6(11)	6(12)	4(8)
F(29A)	51(14)	76(17)	45(12)	-27(11)	31(11)	-7(9)
F(30A)	32(4)	57(4)	39(3)	19(3)	18(3)	-1(3)

Table B.24: Hydrogen coordinates ($\times 10^4$) and isotropic displacement parameters ($Å^2 \times 10^3$) for **54**.

Atom	x	y	z	U(eq)
H(2A)	3322	4757	7673	29
H(2B)	3347	4504	6644	29
H(3A)	4229	5258	7272	59
H(3B)	3540	5271	6437	59
H(3C)	4261	5004	6246	59
H(6)	5577	5049	7579	31
H(7)	6590	5458	8287	39
H(8)	7081	5328	9919	47
H(9)	6568	4797	10862	41
H(14)	3975	3573	11544	42
H(15)	2814	3319	10987	45
H(16)	2325	3416	9356	45
H(17)	3017	3744	8224	35
H(23A)	7244	3870	8151	27
H(23B)	6618	4230	8261	27
H(26)	7685	3292	8712	31
H(27)	8253	2758	9775	31
H(28)	7651	2467	11044	33
H(29)	6475	2698	11229	33
H(30)	5867	3201	10120	29
H(34A)	4772	3000	8987	42
H(34B)	4399	2518	8914	42
H(34C)	3900	2956	8845	42
H(38A)	5088	3424	5158	53
H(38B)	4556	3340	4156	53
H(38C)	4322	3178	5191	53
H(40A)	9812	2536	1748	28
H(40B)	9016	2509	1134	28
H(41A)	9262	2427	3237	39
H(41B)	9144	2009	2506	39
H(41C)	8493	2356	2574	39
H(44)	8017	2916	3433	29
H(45)	6860	2956	3913	33
H(46)	6039	3508	3266	39
H(47)	6387	4011	2107	37
H(52)	8330	4475	-1094	40
H(53)	9232	4243	-2041	47

H(54)	9998	3661	-1509	42
H(55)	9936	3321	13	34
H(76A)	11428	3585	3914	67
H(76B)	11785	3240	4729	67
H(76C)	10978	3425	4782	67
H(61A)	8237	3939	3936	34
H(61B)	8424	4363	4627	34
H(64)	8325	5015	4519	40
H(65)	8082	5763	4240	47
H(66)	8136	6071	2668	52
H(67)	8474	5628	1404	50
H(68)	8740	4880	1661	42
H(72A)	10277	4304	481	39
H(72B)	10486	4786	934	39
H(72C)	9810	4518	1276	39
H(61C)	8379	4177	3900	40
H(61D)	8324	4233	5056	40
H(61E)	8140	3764	4529	40
H(64A)	8571	4817	3355	31
H(65A)	7991	5515	3570	39
H(66A)	8198	6102	2535	52
H(67A)	8781	5979	1145	50
H(68A)	9436	5313	1008	42
H(72D)	9934	4443	866	31
H(72E)	10291	4865	1445	31

Table B.26: Crystal data and structure refinement for **85**

Identification code	CCDC 1535050	
Empirical formula	$C_{25}\,H_{29}\,F_{18}\,Mo\,N\,O_5$	
Formula weight	861.43	
Temperature	100(2) K	
Wavelength	0.71073 Å	
Crystal system	Monoclinic	
Space group	P 21/n	
Unit cell dimensions	a = 14.3977(5) Å	$\alpha = 90°$
	b = 14.4686(6) Å	$\beta = 100.490(2)°$
	c = 15.8068(7) Å	$\gamma = 90°$
Volume	3237.8(2) $Å^3$	
Z	4	
Density (calculated)	1.767 Mg/m^3	
Absorption coefficient	0.545 mm^{-1}	
F(000)	1720	
Crystal size	0.300 x 0.150 x 0.100 mm^3	
Theta range for data collection	1.761 to 25.375°	
Index ranges	$-17 \leq h \leq 16$, $-17 \leq k \leq 17$, $-19 \leq l \leq 19$	
Reflections collected	84947	
Independent reflections	5937 [R(int) = 0.0432]	
Completeness to theta = 25.000°	100.0 %	
Absorption correction	Semi-empirical from equivalents	
Max. and min. transmission	0.745 and 0.694	
Refinement method	Full-matrix least-squares on F^2	
Data / restraints / parameters	5937 / 0 / 451	
Goodness-of-fit on F^2	1.051	
Final R indices [$I>2\sigma(I)$]	R1 = 0.0396, wR2 = 0.0997	
R indices (all data)	R1 = 0.0426, wR2 = 0.1021	
Extinction coefficient	n/a	
Largest diff. peak and hole	1.837 and -0.606 $e^-Å^{-3}$	

Table B.27: Atomic coordinates ($\times 10^4$) and equivalent isotropic displacement parameters ($\text{Å}^2 \times 10^3$) for **85**. U(eq) is defined as one third of the trace of the orthogonalized U^{ij} tensor.

Atom	x	y	z	U(eq)
Mo(1)	3122(1)	8282(1)	4386(1)	12(1)
F(13)	953(1)	8181(1)	2680(1)	25(1)
F(14)	1425(1)	9522(1)	2355(1)	23(1)
F(15)	-17(1)	9327(2)	2496(1)	29(1)
F(18)	1204(1)	10517(1)	4790(1)	27(1)
F(17)	1369(2)	10894(1)	3512(1)	30(1)
F(16)	3(1)	10519(1)	3768(1)	32(1)
O(1)	4390(1)	7798(1)	4344(1)	16(1)
F(3)	5968(2)	5983(1)	5193(1)	34(1)
O(3)	2098(1)	9196(1)	4068(1)	15(1)
F(4)	6254(1)	6552(1)	3675(1)	32(1)
O(4)	3038(2)	8362(1)	2968(1)	16(1)
O(2)	3389(2)	8674(2)	5571(1)	18(1)
O(5)	3932(2)	9672(1)	4084(1)	19(1)
F(11)	4745(1)	8202(2)	6869(1)	37(1)
F(1)	4724(2)	6417(2)	5635(1)	41(1)
F(2)	5858(2)	7362(2)	5644(2)	46(1)
F(6)	5286(2)	7507(2)	2966(1)	45(1)
F(9)	4046(2)	9910(2)	6890(2)	50(1)
F(5)	6218(2)	7950(2)	4108(2)	49(1)
F(10)	3804(2)	8037(2)	7769(1)	55(1)
F(8)	2594(2)	10128(2)	6232(2)	55(1)
F(12)	3700(2)	7100(2)	6685(2)	53(1)
F(7)	2867(2)	9602(2)	7512(2)	60(1)
N(1)	709(2)	3766(2)	4433(2)	26(1)
C(00Q)	871(2)	9087(2)	2824(2)	20(1)
C(6)	1958(2)	4834(2)	5031(2)	23(1)
C(5)	1097(2)	4631(2)	4472(2)	19(1)
C(7)	2387(2)	5683(2)	5016(2)	23(1)
C(18)	1131(2)	9291(2)	3795(2)	16(1)
C(4)	678(2)	5354(2)	3935(2)	20(1)
C(10)	4904(2)	6994(2)	4282(2)	17(1)
C(3)	1118(2)	6198(2)	3918(2)	17(1)
C(00Y)	3602(2)	9075(2)	2665(2)	21(1)
C(1)	2478(2)	7252(2)	4421(2)	17(1)
C(010)	3609(2)	9924(2)	3208(2)	22(1)

C(2)	1992(2)	6385(2)	4449(2)	18(1)
C(12)	5374(2)	6693(2)	5193(2)	22(1)
C(11)	4342(2)	6178(2)	3843(2)	24(1)
C(19)	525(2)	8680(2)	4264(2)	22(1)
C(20)	924(2)	10309(2)	3961(2)	22(1)
C(016)	2842(2)	7627(2)	2348(2)	23(1)
C(14)	3122(2)	8572(3)	6369(2)	27(1)
C(018)	3944(2)	10463(2)	4641(2)	25(1)
C(13)	5677(2)	7254(2)	3761(2)	25(1)
C(8)	-247(3)	3610(2)	3975(2)	30(1)
C(9)	1148(3)	3048(2)	5015(3)	36(1)
C(15)	2118(3)	8222(3)	6324(3)	46(1)
C(17)	3843(3)	7979(3)	6931(2)	36(1)
C(16)	3160(3)	9577(3)	6750(2)	39(1)

Table B.29: Bond lengths [Å] and angles [°] for **85**.

Mo(1)-C(1)	1.761(3)
Mo(1)-O(2)	1.928(2)
Mo(1)-O(1)	1.968(2)
Mo(1)-O(3)	1.975(2)
Mo(1)-O(4)	2.226(2)
Mo(1)-O(5)	2.415(2)
F(13)-C(00Q)	1.339(4)
F(14)-C(00Q)	1.340(4)
F(15)-C(00Q)	1.336(4)
F(18)-C(20)	1.332(4)
F(17)-C(20)	1.341(4)
F(16)-C(20)	1.340(4)
O(1)-C(10)	1.391(4)
F(3)-C(12)	1.337(4)
O(3)-C(18)	1.387(4)
F(4)-C(13)	1.334(4)
O(4)-C(016)	1.438(4)
O(4)-C(00Y)	1.447(4)
O(2)-C(14)	1.392(4)
O(5)-C(010)	1.427(4)
O(5)-C(018)	1.442(4)
F(11)-C(17)	1.359(5)
F(1)-C(12)	1.327(4)
F(2)-C(12)	1.324(4)
F(6)-C(13)	1.332(4)
F(9)-C(16)	1.344(5)
F(5)-C(13)	1.329(4)
F(10)-C(17)	1.338(4)
F(8)-C(16)	1.314(5)
F(12)-C(17)	1.335(5)
F(7)-C(16)	1.346(4)
N(1)-C(5)	1.369(4)
N(1)-C(8)	1.452(5)
N(1)-C(9)	1.453(5)
C(00Q)-C(18)	1.541(4)
C(6)-C(7)	1.376(4)
C(6)-C(5)	1.415(5)
C(6)-H(6)	0.9500

C(5)-C(4)	1.412(4)
C(7)-C(2)	1.405(4)
C(7)-H(7)	0.9500
C(18)-C(19)	1.525(4)
C(18)-C(20)	1.536(4)
C(4)-C(3)	1.378(4)
C(4)-H(4)	0.9500
C(10)-C(11)	1.525(4)
C(10)-C(12)	1.538(4)
C(10)-C(13)	1.547(4)
C(3)-C(2)	1.405(4)
C(3)-H(3)	0.9500
C(00Y)-C(010)	1.498(4)
C(00Y)-H(00A)	0.9900
C(00Y)-H(00B)	0.9900
C(1)-C(2)	1.441(4)
C(010)-H(01A)	0.9900
C(010)-H(01B)	0.9900
C(11)-H(11A)	0.9800
C(11)-H(11B)	0.9800
C(11)-H(11C)	0.9800
C(19)-H(19A)	0.9800
C(19)-H(19B)	0.9800
C(19)-H(19C)	0.9800
C(016)-H(01C)	0.9800
C(016)-H(01D)	0.9800
C(016)-H(01E)	0.9800
C(14)-C(17)	1.506(5)
C(14)-C(15)	1.521(5)
C(14)-C(16)	1.571(5)
C(018)-H(01F)	0.9800
C(018)-H(01G)	0.9800
C(018)-H(01H)	0.9800
C(8)-H(8A)	0.9800
C(8)-H(8B)	0.9800
C(8)-H(8C)	0.9800
C(9)-H(9A)	0.9800
C(9)-H(9B)	0.9800
C(9)-H(9C)	0.9800
C(15)-H(15A)	0.9800
C(15)-H(15B)	0.9800

C(15)-H(15C)	0.9800
C(1)-Mo(1)-O(2)	103.40(12)
C(1)-Mo(1)-O(1)	101.32(11)
O(2)-Mo(1)-O(1)	96.62(9)
C(1)-Mo(1)-O(3)	101.68(11)
O(2)-Mo(1)-O(3)	93.30(9)
O(1)-Mo(1)-O(3)	152.04(8)
C(1)-Mo(1)-O(4)	98.23(11)
O(2)-Mo(1)-O(4)	158.11(8)
O(1)-Mo(1)-O(4)	82.24(8)
O(3)-Mo(1)-O(4)	78.93(8)
C(1)-Mo(1)-O(5)	170.57(11)
O(2)-Mo(1)-O(5)	85.90(8)
O(1)-Mo(1)-O(5)	78.77(8)
O(3)-Mo(1)-O(5)	75.94(8)
O(4)-Mo(1)-O(5)	72.39(7)
C(10)-O(1)-Mo(1)	143.94(18)
C(18)-O(3)-Mo(1)	143.59(18)
C(016)-O(4)-C(00Y)	110.8(2)
C(016)-O(4)-Mo(1)	127.95(18)
C(00Y)-O(4)-Mo(1)	116.06(17)
C(14)-O(2)-Mo(1)	144.1(2)
C(010)-O(5)-C(018)	110.8(2)
C(010)-O(5)-Mo(1)	108.73(17)
C(018)-O(5)-Mo(1)	119.57(18)
C(5)-N(1)-C(8)	120.5(3)
C(5)-N(1)-C(9)	119.9(3)
C(8)-N(1)-C(9)	118.0(3)
F(15)-C(00Q)-F(14)	106.7(2)
F(15)-C(00Q)-F(13)	107.2(3)
F(14)-C(00Q)-F(13)	106.6(2)
F(15)-C(00Q)-C(18)	112.3(3)
F(14)-C(00Q)-C(18)	113.6(3)
F(13)-C(00Q)-C(18)	110.1(2)
C(7)-C(6)-C(5)	121.2(3)
C(7)-C(6)-H(6)	119.4
C(5)-C(6)-H(6)	119.4
N(1)-C(5)-C(4)	121.6(3)
N(1)-C(5)-C(6)	121.5(3)
C(4)-C(5)-C(6)	116.9(3)

C(6)-C(7)-C(2)	121.7(3)
C(6)-C(7)-H(7)	119.1
C(2)-C(7)-H(7)	119.1
O(3)-C(18)-C(19)	115.0(2)
O(3)-C(18)-C(20)	104.9(2)
C(19)-C(18)-C(20)	109.0(2)
O(3)-C(18)-C(00Q)	109.8(2)
C(19)-C(18)-C(00Q)	108.5(3)
C(20)-C(18)-C(00Q)	109.5(2)
C(3)-C(4)-C(5)	121.3(3)
C(3)-C(4)-H(4)	119.3
C(5)-C(4)-H(4)	119.3
O(1)-C(10)-C(11)	115.8(2)
O(1)-C(10)-C(12)	108.7(2)
C(11)-C(10)-C(12)	108.2(3)
O(1)-C(10)-C(13)	106.2(2)
C(11)-C(10)-C(13)	108.6(3)
C(12)-C(10)-C(13)	109.3(3)
C(4)-C(3)-C(2)	121.6(3)
C(4)-C(3)-H(3)	119.2
C(2)-C(3)-H(3)	119.2
O(4)-C(00Y)-C(010)	109.9(2)
O(4)-C(00Y)-H(00A)	109.7
C(010)-C(00Y)-H(00A)	109.7
O(4)-C(00Y)-H(00B)	109.7
C(010)-C(00Y)-H(00B)	109.7
H(00A)-C(00Y)-H(00B)	108.2
C(2)-C(1)-Mo(1)	177.3(2)
O(5)-C(010)-C(00Y)	108.3(2)
O(5)-C(010)-H(01A)	110.0
C(00Y)-C(010)-H(01A)	110.0
O(5)-C(010)-H(01B)	110.0
C(00Y)-C(010)-H(01B)	110.0
H(01A)-C(010)-H(01B)	108.4
C(7)-C(2)-C(3)	117.1(3)
C(7)-C(2)-C(1)	120.5(3)
C(3)-C(2)-C(1)	122.4(3)
F(2)-C(12)-F(1)	106.8(3)
F(2)-C(12)-F(3)	106.7(3)
F(1)-C(12)-F(3)	106.3(3)
F(2)-C(12)-C(10)	113.3(3)

F(1)-C(12)-C(10)	110.2(3)
F(3)-C(12)-C(10)	113.0(3)
C(10)-C(11)-H(11A)	109.5
C(10)-C(11)-H(11B)	109.5
H(11A)-C(11)-H(11B)	109.5
C(10)-C(11)-H(11C)	109.5
H(11A)-C(11)-H(11C)	109.5
H(11B)-C(11)-H(11C)	109.5
C(18)-C(19)-H(19A)	109.5
C(18)-C(19)-H(19B)	109.5
H(19A)-C(19)-H(19B)	109.5
C(18)-C(19)-H(19C)	109.5
H(19A)-C(19)-H(19C)	109.5
H(19B)-C(19)-H(19C)	109.5
F(18)-C(20)-F(16)	106.4(3)
F(18)-C(20)-F(17)	106.8(3)
F(16)-C(20)-F(17)	106.5(3)
F(18)-C(20)-C(18)	110.6(2)
F(16)-C(20)-C(18)	113.2(3)
F(17)-C(20)-C(18)	112.9(3)
O(4)-C(016)-H(01C)	109.5
O(4)-C(016)-H(01D)	109.5
H(01C)-C(016)-H(01D)	109.5
O(4)-C(016)-H(01E)	109.5
H(01C)-C(016)-H(01E)	109.5
H(01D)-C(016)-H(01E)	109.5
O(2)-C(14)-C(17)	108.7(3)
O(2)-C(14)-C(15)	114.2(3)
C(17)-C(14)-C(15)	112.6(3)
O(2)-C(14)-C(16)	104.7(3)
C(17)-C(14)-C(16)	109.2(3)
C(15)-C(14)-C(16)	107.0(3)
O(5)-C(018)-H(01F)	109.5
O(5)-C(018)-H(01G)	109.5
H(01F)-C(018)-H(01G)	109.5
O(5)-C(018)-H(01H)	109.5
H(01F)-C(018)-H(01H)	109.5
H(01G)-C(018)-H(01H)	109.5
F(5)-C(13)-F(6)	107.2(3)
F(5)-C(13)-F(4)	106.9(3)
F(6)-C(13)-F(4)	106.1(3)

F(5)-C(13)-C(10)	112.9(3)
F(6)-C(13)-C(10)	110.3(3)
F(4)-C(13)-C(10)	113.1(3)
N(1)-C(8)-H(8A)	109.5
N(1)-C(8)-H(8B)	109.5
H(8A)-C(8)-H(8B)	109.5
N(1)-C(8)-H(8C)	109.5
H(8A)-C(8)-H(8C)	109.5
H(8B)-C(8)-H(8C)	109.5
N(1)-C(9)-H(9A)	109.5
N(1)-C(9)-H(9B)	109.5
H(9A)-C(9)-H(9B)	109.5
N(1)-C(9)-H(9C)	109.5
H(9A)-C(9)-H(9C)	109.5
H(9B)-C(9)-H(9C)	109.5
C(14)-C(15)-H(15A)	109.5
C(14)-C(15)-H(15B)	109.5
H(15A)-C(15)-H(15B)	109.5
C(14)-C(15)-H(15C)	109.5
H(15A)-C(15)-H(15C)	109.5
H(15B)-C(15)-H(15C)	109.5
F(12)-C(17)-F(10)	108.5(3)
F(12)-C(17)-F(11)	107.7(3)
F(10)-C(17)-F(11)	105.6(3)
F(12)-C(17)-C(14)	108.6(3)
F(10)-C(17)-C(14)	113.5(3)
F(11)-C(17)-C(14)	112.8(3)
F(8)-C(16)-F(9)	110.3(4)
F(8)-C(16)-F(7)	106.3(3)
F(9)-C(16)-F(7)	106.6(3)
F(8)-C(16)-C(14)	110.3(3)
F(9)-C(16)-C(14)	111.1(3)
F(7)-C(16)-C(14)	111.9(3)

Table B.31: Anisotropic displacement parameters ($Å^2 \times 10^3$)for **85**. The anisotropic displacement factor exponent takes the form: $-2p^2[h^2a^{*2}U^{11} + ... + 2hka^*b^*U^{12}]$

Atom	U11	U22	U33	U23	U13	U12
Mo(1)	13(1)	13(1)	11(1)	0(1)	2(1)	0(1)
F(13)	30(1)	22(1)	22(1)	-5(1)	1(1)	-3(1)
F(14)	27(1)	27(1)	15(1)	5(1)	4(1)	2(1)
F(15)	20(1)	42(1)	23(1)	0(1)	-5(1)	5(1)
F(18)	31(1)	26(1)	23(1)	-7(1)	3(1)	7(1)
F(17)	41(1)	16(1)	36(1)	5(1)	12(1)	2(1)
F(16)	25(1)	33(1)	37(1)	-2(1)	0(1)	15(1)
O(1)	15(1)	14(1)	18(1)	-1(1)	4(1)	1(1)
F(3)	36(1)	31(1)	33(1)	8(1)	5(1)	19(1)
O(3)	15(1)	16(1)	14(1)	1(1)	3(1)	0(1)
F(4)	29(1)	33(1)	37(1)	1(1)	17(1)	12(1)
O(4)	21(1)	16(1)	12(1)	-1(1)	5(1)	-2(1)
O(2)	18(1)	25(1)	12(1)	-2(1)	2(1)	0(1)
O(5)	20(1)	14(1)	22(1)	-2(1)	3(1)	-2(1)
F(11)	23(1)	46(1)	37(1)	7(1)	-7(1)	5(1)
F(1)	33(1)	66(2)	26(1)	19(1)	11(1)	11(1)
F(2)	57(2)	30(1)	39(1)	-2(1)	-28(1)	0(1)
F(6)	43(1)	61(2)	35(1)	24(1)	22(1)	23(1)
F(9)	51(2)	60(2)	36(1)	-20(1)	4(1)	-20(1)
F(5)	40(1)	38(1)	78(2)	-20(1)	38(1)	-18(1)
F(10)	74(2)	77(2)	14(1)	10(1)	8(1)	30(2)
F(8)	65(2)	62(2)	35(1)	-8(1)	1(1)	37(1)
F(12)	82(2)	31(1)	46(1)	5(1)	13(1)	4(1)
F(7)	86(2)	66(2)	31(1)	-10(1)	22(1)	17(2)
N(1)	31(2)	16(1)	32(2)	2(1)	11(1)	-6(1)
C(00Q)	19(2)	21(2)	20(2)	2(1)	2(1)	0(1)
C(6)	20(2)	20(2)	29(2)	8(1)	7(1)	1(1)
C(5)	22(2)	18(2)	22(2)	-2(1)	13(1)	-2(1)
C(7)	17(2)	22(2)	29(2)	5(1)	3(1)	-1(1)
C(18)	15(1)	19(2)	15(1)	2(1)	2(1)	3(1)
C(4)	20(2)	21(2)	19(2)	-4(1)	6(1)	-3(1)
C(10)	16(2)	15(1)	20(2)	0(1)	4(1)	2(1)
C(3)	20(2)	16(1)	16(1)	0(1)	4(1)	2(1)
C(00Y)	23(2)	22(2)	20(2)	4(1)	10(1)	-2(1)
C(1)	17(2)	19(2)	15(1)	3(1)	2(1)	4(1)
C(010)	24(2)	18(2)	24(2)	5(1)	7(1)	-3(1)
C(2)	18(2)	16(1)	20(2)	1(1)	7(1)	-1(1)

C(12)	21(2)	20(2)	25(2)	0(1)	2(1)	3(1)
C(11)	24(2)	17(2)	28(2)	-4(1)	1(1)	1(1)
C(19)	18(2)	25(2)	23(2)	3(1)	4(1)	1(1)
C(20)	22(2)	21(2)	22(2)	2(1)	4(1)	5(1)
C(016)	31(2)	22(2)	16(2)	-7(1)	3(1)	2(1)
C(14)	24(2)	44(2)	12(2)	-2(1)	4(1)	-6(2)
C(018)	24(2)	18(2)	33(2)	-9(1)	2(1)	-2(1)
C(13)	25(2)	22(2)	32(2)	-1(1)	11(1)	4(1)
C(8)	34(2)	24(2)	35(2)	-7(2)	15(2)	-14(2)
C(9)	51(2)	19(2)	42(2)	7(2)	15(2)	-5(2)
C(15)	50(3)	66(3)	26(2)	-6(2)	16(2)	-20(2)
C(17)	45(2)	40(2)	22(2)	1(2)	6(2)	4(2)
C(16)	52(3)	40(2)	25(2)	-3(2)	8(2)	9(2)

Table B.33: Crystal data and structure refinement for **90**.

Identification code	CCDC 1535051	
Empirical formula	$C_{23}\,H_{23}\,F_{18}\,Mo\,N\,O_7$	
Formula weight	863.36	
Temperature	100(2) K	
Wavelength	0.71073 Å	
Crystal system	Monoclinic	
Space group	P 21	
Unit cell dimensions	a = 9.4048(5) Å	$\alpha = 90°$
	b = 9.2801(5) Å	$\beta = 98.630(3)°$
	c = 17.2135(9) Å	$\gamma = 90°$
Volume	1485.34(14) $Å^3$	
Z	2	
Density (calculated)	1.930 Mg/m^3	
Absorption coefficient	0.600 mm^{-1}	
F(000)	856	
Crystal size	0.300 x 0.100 x 0.050 mm^3	
Theta range for data collection	1.196 to 25.437°	
Index ranges	$-11 \leq h \leq 11$, $-11 \leq k \leq 11$, $-18 \leq l \leq 20$	
Reflections collected	12658	
Independent reflections	5057 [R(int) = 0.0429]	
Completeness to theta = 25.000°	100.0 %	
Absorption correction	Semi-empirical from equivalents	
Max. and min. transmission	0.7452 and 0.6463	
Refinement method	Full-matrix least-squares on F^2	
Data / restraints / parameters	5057 / 1 / 451	
Goodness-of-fit on F^2	0.994	
Final R indices [$I>2\sigma(I)$]	R1 = 0.0400, wR2 = 0.0768	
R indices (all data)	R1 = 0.0544, wR2 = 0.0820	
Absolute structure parameter	-0.04(2)	
Extinction coefficient	n/a	
Largest diff. peak and hole	0.830 and -0.376 $e^-Å^{-3}$	

Table B.34: Atomic coordinates ($\times 10^4$) and equivalent isotropic displacement parameters ($\text{Å}^2 \times 10^3$) for **90**. U(eq) is defined as one third of the trace of the orthogonalized U^{ij} tensor.

Atom	x	y	z	U(eq)
Mo(1)	6236(1)	3805(1)	7644(1)	17(1)
F(6)	1831(5)	2994(5)	6168(3)	29(1)
F(2)	4122(5)	2110(4)	5533(2)	29(1)
F(1)	3703(4)	3910(6)	4740(2)	27(1)
F(5)	1885(4)	5082(4)	6698(2)	27(1)
F(4)	1564(4)	4874(5)	5436(2)	29(1)
F(12)	4040(4)	4931(5)	9746(2)	31(1)
F(10)	4896(5)	7037(5)	10039(2)	33(1)
F(9)	2635(4)	5874(5)	8364(3)	34(1)
F(13)	9424(5)	5111(5)	8912(3)	40(1)
F(3)	5791(4)	3661(6)	5434(2)	26(1)
F(8)	3378(5)	7994(5)	8730(2)	36(1)
F(11)	6323(5)	5240(5)	9989(2)	38(1)
F(7)	3798(5)	7129(4)	7630(2)	33(1)
O(2)	5342(5)	4799(5)	8423(3)	19(1)
F(14)	10228(4)	3815(7)	8029(2)	36(1)
F(15)	11229(4)	3680(7)	9232(2)	45(1)
F(18)	8592(5)	104(5)	8902(3)	45(1)
O(1)	4527(4)	3861(6)	6840(2)	17(1)
F(16)	10720(5)	886(5)	9329(3)	40(1)
F(17)	9904(5)	934(5)	8100(3)	45(1)
O(5)	4873(5)	1718(5)	7930(3)	20(1)
O(4)	6758(5)	2028(5)	6860(3)	24(1)
O(6)	11295(5)	8441(5)	5214(3)	32(2)
O(3)	7614(5)	2745(5)	8394(3)	22(1)
O(7)	11470(7)	9895(7)	6216(4)	56(2)
C(11)	4325(8)	6012(8)	5992(5)	26(2)
C(4)	9193(8)	6896(8)	5778(4)	24(2)
C(5)	10018(7)	7898(8)	6229(4)	22(2)
C(14)	5100(8)	5829(8)	9643(4)	24(2)
C(18)	9952(7)	3810(12)	8768(4)	29(2)
C(16)	8907(8)	2646(9)	8917(5)	26(2)
C(12)	5168(8)	6141(8)	8767(4)	21(2)
C(3)	8306(7)	6003(8)	6126(4)	21(2)
C(7)	9084(8)	7141(7)	7377(4)	23(2)
C(2)	8233(7)	6114(7)	6932(4)	19(2)

C(15)	6380(8)	7214(8)	8706(5)	32(2)
C(10)	2283(8)	4353(9)	6106(5)	25(2)
C(6)	9967(8)	8043(8)	7020(4)	26(2)
C(9)	4375(7)	3531(8)	5460(4)	25(2)
C(21)	6299(8)	614(7)	7091(4)	26(2)
C(1)	7316(8)	5115(7)	7287(4)	19(2)
C(8)	3931(8)	4445(7)	6129(4)	20(2)
C(13)	3727(8)	6778(8)	8382(4)	26(2)
C(22)	4824(8)	709(8)	7296(4)	27(2)
C(17)	9532(8)	1139(8)	8804(4)	27(2)
C(20)	8054(8)	1942(8)	6482(5)	28(2)
C(23)	3455(8)	1907(9)	8144(5)	33(2)
C(19)	8605(8)	2755(9)	9767(4)	34(2)
N(1)	10996(6)	8798(9)	5858(3)	28(1)

Table B.36: Bond lengths [Å] and angles [°] for **90**.

Mo(1)-C(1)	1.754(7)
Mo(1)-O(2)	1.922(4)
Mo(1)-O(3)	1.952(5)
Mo(1)-O(1)	1.958(4)
Mo(1)-O(4)	2.232(5)
Mo(1)-O(5)	2.414(4)
F(6)-C(10)	1.340(8)
F(2)-C(9)	1.349(8)
F(1)-C(9)	1.350(8)
F(5)-C(10)	1.323(8)
F(4)-C(10)	1.336(9)
F(12)-C(14)	1.331(9)
F(10)-C(14)	1.341(7)
F(9)-C(13)	1.323(8)
F(13)-C(18)	1.343(11)
F(3)-C(9)	1.344(7)
F(8)-C(13)	1.341(8)
F(11)-C(14)	1.331(8)
F(7)-C(13)	1.347(8)
O(2)-C(12)	1.400(8)
F(14)-C(18)	1.335(7)
F(15)-C(18)	1.344(7)
F(18)-C(17)	1.334(8)
O(1)-C(8)	1.378(8)
F(16)-C(17)	1.348(8)
F(17)-C(17)	1.325(8)
O(5)-C(22)	1.433(8)
O(5)-C(23)	1.447(8)
O(4)-C(21)	1.455(8)
O(4)-C(20)	1.467(8)
O(6)-N(1)	1.229(7)
O(3)-C(16)	1.403(9)
O(7)-N(1)	1.238(9)
C(11)-C(8)	1.527(10)
C(11)-H(11A)	0.9800
C(11)-H(11B)	0.9800
C(11)-H(11C)	0.9800
C(4)-C(5)	1.375(10)

C(4)-C(3)	1.375(10)
C(4)-H(4)	0.9500
C(5)-C(6)	1.377(10)
C(5)-N(1)	1.458(9)
C(14)-C(12)	1.545(10)
C(18)-C(16)	1.508(12)
C(16)-C(19)	1.535(11)
C(16)-C(17)	1.541(11)
C(12)-C(15)	1.529(10)
C(12)-C(13)	1.534(10)
C(3)-C(2)	1.402(10)
C(3)-H(3)	0.9500
C(7)-C(6)	1.385(10)
C(7)-C(2)	1.398(10)
C(7)-H(7)	0.9500
C(2)-C(1)	1.460(9)
C(15)-H(15A)	0.9800
C(15)-H(15B)	0.9800
C(15)-H(15C)	0.9800
C(10)-C(8)	1.548(10)
C(6)-H(6)	0.9500
C(9)-C(8)	1.538(10)
C(21)-C(22)	1.485(10)
C(21)-H(21A)	0.9900
C(21)-H(21B)	0.9900
C(22)-H(22A)	0.9900
C(22)-H(22B)	0.9900
C(20)-H(20A)	0.9800
C(20)-H(20B)	0.9800
C(20)-H(20C)	0.9800
C(23)-H(23A)	0.9800
C(23)-H(23B)	0.9800
C(23)-H(23C)	0.9800
C(19)-H(19A)	0.9800
C(19)-H(19B)	0.9800
C(19)-H(19C)	0.9800

C(1)-Mo(1)-O(2)	104.4(3)
C(1)-Mo(1)-O(3)	102.6(3)
O(2)-Mo(1)-O(3)	95.60(19)
C(1)-Mo(1)-O(1)	101.0(3)

O(2)-Mo(1)-O(1)	94.69(19)
O(3)-Mo(1)-O(1)	150.9(2)
C(1)-Mo(1)-O(4)	96.2(2)
O(2)-Mo(1)-O(4)	159.32(18)
O(3)-Mo(1)-O(4)	80.95(19)
O(1)-Mo(1)-O(4)	79.9(2)
C(1)-Mo(1)-O(5)	168.8(2)
O(2)-Mo(1)-O(5)	86.65(17)
O(3)-Mo(1)-O(5)	77.35(17)
O(1)-Mo(1)-O(5)	76.18(19)
O(4)-Mo(1)-O(5)	72.68(16)
C(12)-O(2)-Mo(1)	144.5(4)
C(8)-O(1)-Mo(1)	145.0(4)
C(22)-O(5)-C(23)	110.3(5)
C(22)-O(5)-Mo(1)	109.1(4)
C(23)-O(5)-Mo(1)	119.5(4)
C(21)-O(4)-C(20)	111.9(5)
C(21)-O(4)-Mo(1)	113.5(4)
C(20)-O(4)-Mo(1)	125.5(4)
C(16)-O(3)-Mo(1)	151.9(5)
C(8)-C(11)-H(11A)	109.5
C(8)-C(11)-H(11B)	109.5
H(11A)-C(11)-H(11B)	109.5
C(8)-C(11)-H(11C)	109.5
H(11A)-C(11)-H(11C)	109.5
H(11B)-C(11)-H(11C)	109.5
C(5)-C(4)-C(3)	119.3(7)
C(5)-C(4)-H(4)	120.4
C(3)-C(4)-H(4)	120.4
C(4)-C(5)-C(6)	121.6(6)
C(4)-C(5)-N(1)	118.7(6)
C(6)-C(5)-N(1)	119.7(7)
F(11)-C(14)-F(12)	107.3(6)
F(11)-C(14)-F(10)	107.1(6)
F(12)-C(14)-F(10)	106.8(6)
F(11)-C(14)-C(12)	110.7(6)
F(12)-C(14)-C(12)	112.9(6)
F(10)-C(14)-C(12)	111.7(6)
F(14)-C(18)-F(13)	107.7(7)
F(14)-C(18)-F(15)	106.4(5)
F(13)-C(18)-F(15)	107.1(7)

F(14)-C(18)-C(16)	112.9(7)
F(13)-C(18)-C(16)	110.1(6)
F(15)-C(18)-C(16)	112.4(7)
O(3)-C(16)-C(18)	111.6(6)
O(3)-C(16)-C(19)	110.0(6)
C(18)-C(16)-C(19)	109.5(7)
O(3)-C(16)-C(17)	106.8(7)
C(18)-C(16)-C(17)	111.0(7)
C(19)-C(16)-C(17)	108.0(6)
O(2)-C(12)-C(15)	114.5(6)
O(2)-C(12)-C(13)	108.1(6)
C(15)-C(12)-C(13)	109.8(6)
O(2)-C(12)-C(14)	105.7(5)
C(15)-C(12)-C(14)	109.3(6)
C(13)-C(12)-C(14)	109.3(6)
C(4)-C(3)-C(2)	120.7(7)
C(4)-C(3)-H(3)	119.7
C(2)-C(3)-H(3)	119.7
C(6)-C(7)-C(2)	120.1(7)
C(6)-C(7)-H(7)	120.0
C(2)-C(7)-H(7)	120.0
C(7)-C(2)-C(3)	118.8(6)
C(7)-C(2)-C(1)	122.0(6)
C(3)-C(2)-C(1)	119.1(6)
C(12)-C(15)-H(15A)	109.5
C(12)-C(15)-H(15B)	109.5
H(15A)-C(15)-H(15B)	109.5
C(12)-C(15)-H(15C)	109.5
H(15A)-C(15)-H(15C)	109.5
H(15B)-C(15)-H(15C)	109.5
F(5)-C(10)-F(4)	108.4(6)
F(5)-C(10)-F(6)	106.9(6)
F(4)-C(10)-F(6)	106.5(7)
F(5)-C(10)-C(8)	110.5(6)
F(4)-C(10)-C(8)	112.1(6)
F(6)-C(10)-C(8)	112.2(6)
C(5)-C(6)-C(7)	119.5(7)
C(5)-C(6)-H(6)	120.3
C(7)-C(6)-H(6)	120.3
F(3)-C(9)-F(2)	106.3(6)
F(3)-C(9)-F(1)	106.0(5)

F(2)-C(9)-F(1)	106.0(6)
F(3)-C(9)-C(8)	110.9(6)
F(2)-C(9)-C(8)	113.4(6)
F(1)-C(9)-C(8)	113.6(6)
O(4)-C(21)-C(22)	109.7(6)
O(4)-C(21)-H(21A)	109.7
C(22)-C(21)-H(21A)	109.7
O(4)-C(21)-H(21B)	109.7
C(22)-C(21)-H(21B)	109.7
H(21A)-C(21)-H(21B)	108.2
C(2)-C(1)-Mo(1)	174.8(6)
O(1)-C(8)-C(11)	115.8(6)
O(1)-C(8)-C(9)	109.2(6)
C(11)-C(8)-C(9)	108.1(6)
O(1)-C(8)-C(10)	105.8(6)
C(11)-C(8)-C(10)	108.3(6)
C(9)-C(8)-C(10)	109.5(6)
F(9)-C(13)-F(8)	107.6(6)
F(9)-C(13)-F(7)	106.3(6)
F(8)-C(13)-F(7)	106.0(6)
F(9)-C(13)-C(12)	113.5(6)
F(8)-C(13)-C(12)	113.0(6)
F(7)-C(13)-C(12)	109.9(6)
O(5)-C(22)-C(21)	107.1(6)
O(5)-C(22)-H(22A)	110.3
C(21)-C(22)-H(22A)	110.3
O(5)-C(22)-H(22B)	110.3
C(21)-C(22)-H(22B)	110.3
H(22A)-C(22)-H(22B)	108.5
F(17)-C(17)-F(18)	106.4(6)
F(17)-C(17)-F(16)	106.4(6)
F(18)-C(17)-F(16)	106.8(6)
F(17)-C(17)-C(16)	113.8(6)
F(18)-C(17)-C(16)	111.4(6)
F(16)-C(17)-C(16)	111.6(6)
O(4)-C(20)-H(20A)	109.5
O(4)-C(20)-H(20B)	109.5
H(20A)-C(20)-H(20B)	109.5
O(4)-C(20)-H(20C)	109.5
H(20A)-C(20)-H(20C)	109.5
H(20B)-C(20)-H(20C)	109.5

O(5)-C(23)-H(23A)	109.5
O(5)-C(23)-H(23B)	109.5
H(23A)-C(23)-H(23B)	109.5
O(5)-C(23)-H(23C)	109.5
H(23A)-C(23)-H(23C)	109.5
H(23B)-C(23)-H(23C)	109.5
C(16)-C(19)-H(19A)	109.5
C(16)-C(19)-H(19B)	109.5
H(19A)-C(19)-H(19B)	109.5
C(16)-C(19)-H(19C)	109.5
H(19A)-C(19)-H(19C)	109.5
H(19B)-C(19)-H(19C)	109.5
O(6)-N(1)-O(7)	123.8(6)
O(6)-N(1)-C(5)	119.0(7)
O(7)-N(1)-C(5)	117.2(6)

Table B.38: Anisotropic displacement parameters ($Å^2 \times 10^3$)for **90**. The anisotropic displacement factor exponent takes the form: $-2p^2[h^2a^{*2}U^{11} + ... + 2hka^*b^*U^{12}]$

Atom	U11	U22	U33	U23	U13	U12
Mo(1)	15(1)	14(1)	22(1)	-1(1)	4(1)	-1(1)
F(6)	23(3)	24(3)	41(3)	-2(2)	4(2)	-5(2)
F(2)	30(3)	22(3)	37(3)	-5(2)	10(2)	-6(2)
F(1)	28(2)	31(2)	21(2)	0(2)	0(2)	4(3)
F(5)	22(2)	31(3)	29(3)	-6(2)	4(2)	5(2)
F(4)	25(2)	33(2)	26(3)	6(2)	-1(2)	6(2)
F(12)	36(3)	24(2)	34(3)	1(2)	12(2)	-4(2)
F(10)	43(3)	24(3)	32(3)	-11(2)	9(2)	3(2)
F(9)	23(2)	34(3)	45(3)	10(2)	3(2)	-1(2)
F(13)	44(3)	22(3)	48(3)	-1(2)	-7(2)	-5(2)
F(3)	22(2)	30(2)	28(2)	-3(2)	9(2)	1(2)
F(8)	43(3)	26(3)	37(3)	-5(2)	4(2)	13(2)
F(11)	31(3)	46(3)	34(3)	-2(2)	-3(2)	17(2)
F(7)	48(3)	25(2)	26(2)	4(2)	4(2)	2(2)
O(2)	21(3)	12(2)	25(3)	-5(2)	7(2)	0(2)
F(14)	29(2)	44(2)	37(2)	11(3)	13(2)	-6(3)
F(15)	27(2)	49(3)	54(3)	17(3)	-8(2)	-8(3)
F(18)	37(3)	22(3)	73(4)	12(2)	-4(3)	-1(2)
O(1)	20(2)	16(2)	17(2)	5(3)	3(2)	-2(3)
F(16)	30(3)	31(3)	58(3)	1(2)	-4(2)	12(2)
F(17)	54(3)	41(3)	42(3)	-11(2)	10(2)	18(3)
O(5)	20(3)	16(3)	23(3)	0(2)	4(2)	-2(2)
O(4)	29(3)	17(3)	28(3)	0(2)	11(2)	2(2)
O(6)	27(3)	37(4)	36(3)	6(2)	14(2)	1(2)
O(3)	18(3)	19(3)	28(3)	2(2)	2(2)	1(2)
O(7)	70(5)	38(4)	66(4)	-11(3)	29(4)	-34(4)
C(11)	24(4)	18(4)	39(5)	5(3)	12(4)	1(3)
C(4)	22(4)	22(4)	30(4)	1(3)	6(3)	2(3)
C(5)	17(4)	18(4)	33(5)	4(3)	10(3)	3(3)
C(14)	23(4)	16(4)	32(5)	-7(4)	3(4)	5(4)
C(18)	21(4)	30(4)	33(4)	7(5)	-3(3)	-1(5)
C(16)	21(4)	17(4)	38(5)	6(3)	1(4)	1(3)
C(12)	22(4)	19(4)	25(4)	-3(3)	8(3)	-3(3)
C(3)	12(4)	19(4)	32(5)	2(3)	4(3)	3(3)
C(7)	24(4)	18(4)	26(4)	1(3)	1(4)	-1(3)
C(2)	14(4)	15(4)	29(4)	3(3)	10(3)	6(3)
C(15)	34(5)	18(4)	47(5)	-16(4)	20(4)	-10(4)

C(10)	26(5)	24(4)	24(5)	0(3)	-3(4)	-4(4)
C(6)	26(4)	14(4)	37(5)	-5(3)	4(4)	-1(3)
C(9)	15(3)	29(6)	29(4)	1(3)	2(3)	-2(3)
C(21)	37(5)	16(4)	27(4)	-2(3)	6(4)	-2(4)
C(1)	18(4)	14(4)	27(4)	-5(3)	8(3)	0(3)
C(8)	20(4)	20(4)	20(4)	2(3)	0(3)	5(3)
C(13)	33(5)	19(4)	27(4)	-3(3)	14(4)	-2(4)
C(22)	36(5)	16(4)	30(4)	1(3)	5(4)	-8(4)
C(17)	22(4)	26(5)	32(5)	4(3)	3(4)	-1(4)
C(20)	23(5)	28(5)	36(5)	0(4)	15(4)	2(4)
C(23)	24(5)	38(5)	37(5)	10(4)	6(4)	-3(4)
C(19)	20(4)	46(5)	33(5)	12(4)	-4(4)	1(4)
N(1)	22(3)	23(3)	40(4)	5(4)	8(3)	-2(4)

Table B.40: Crystal data and structure refinement for **106**

Identification code	CCDC 1873210	
Empirical formula	$C_{56}H_{32}$	
Formula weight	704.81	
Temperature	100(2) K	
Wavelength	1.54184 Å	
Crystal system	Triclinic	
Space group	P -1	
Unit cell dimensions	a = 5.5153(2) Å	$\alpha = 87.836(3)^\circ$
	b = 15.9898(7) Å	$\beta = 86.477(3)^\circ$
	c = 20.1319(5) Å	$\gamma = 89.047(4)^\circ$
Volume	1770.60(11) $Å^3$	
Z	2	
Density (calculated)	1.322 Mg/m^3	
Absorption coefficient	0.571 mm^{-1}	
F(000)	736	
Crystal size	0.220 x 0.070 x 0.060 mm^3	
Theta range for data collection	3.471 to 77.363°	
Index ranges	$-6\leq h\leq 6$, $-20\leq k\leq 20$, $-25\leq l\leq 25$	
Reflections collected	10787	
Independent reflections	10787 [R(int) = 0.0694]	
Completeness to theta = 67.684°	97.7 %	
Absorption correction	Semi-empirical from equivalents	
Max. and min. transmission	1.00000 and 0.95946	
Refinement method	Full-matrix least-squares on F^2	
Data / restraints / parameters	10787 / 0 / 506	
Goodness-of-fit on F^2	1.076	
Final R indices [$I>2\sigma(I)$]	R1 = 0.0496, wR2 = 0.1378	
R indices (all data)	R1 = 0.0645, wR2 = 0.1496	
Extinction coefficient	n/a	
Largest diff. peak and hole	0.175 and –0.212 $e^- Å^{-3}$	

Table B.41: Atomic coordinates ($\times 10^4$) and equivalent isotropic displacement parameters (Å^2 $\times 10^3$) for **106**. U(eq) is defined as one third of the trace of the orthogonalized U^{ij} tensor.

Atom	x	y	z	U(eq)
C(23)	4300(3)	10529(1)	1843(1)	25(1)
C(16)	2443(3)	9837(1)	4179(1)	27(1)
C(21)	5022(3)	10608(1)	2537(1)	25(1)
C(26)	2668(4)	10354(1)	554(1)	31(1)
C(43)	6911(3)	3885(1)	3818(1)	29(1)
C(13)	-1134(3)	8790(1)	4362(1)	29(1)
C(44)	5260(3)	4362(1)	3963(1)	30(1)
C(17)	4096(3)	10297(1)	3727(1)	26(1)
C(9)	-3792(3)	8132(1)	3605(1)	28(1)
C(3)	-3549(3)	8350(1)	1719(1)	29(1)
C(55)	992(3)	5229(1)	1203(1)	29(1)
C(41)	8651(3)	3413(1)	3417(1)	28(1)
C(22)	3524(3)	10275(1)	3063(1)	26(1)
C(45)	3247(3)	4940(1)	3894(1)	27(1)
C(8)	-2988(3)	8373(1)	2382(1)	28(1)
C(12)	-2182(4)	8317(1)	4900(1)	34(1)
C(14)	-1992(3)	8700(1)	3732(1)	28(1)
C(20)	7142(3)	11001(1)	2705(1)	28(1)
C(56)	1488(3)	5235(1)	1873(1)	28(1)
C(30)	4351(4)	4260(1)	661(1)	31(1)
C(25)	4473(4)	10913(1)	668(1)	33(1)
C(50)	2438(3)	4996(1)	3250(1)	27(1)
C(15)	836(3)	9367(1)	4370(1)	28(1)
C(19)	7679(3)	11054(1)	3365(1)	30(1)
C(7)	-4495(3)	8048(1)	2910(1)	28(1)
C(52)	-2198(3)	5977(1)	2139(1)	32(1)
C(24)	5271(4)	11010(1)	1298(1)	30(1)
C(29)	2715(3)	4745(1)	806(1)	30(1)
C(27)	1668(3)	9866(1)	1086(1)	28(1)
C(42)	8138(3)	3391(1)	2749(1)	28(1)
C(28)	2537(3)	9952(1)	1717(1)	27(1)
C(4)	-5657(4)	7953(1)	1564(1)	34(1)
C(18)	6192(3)	10707(1)	3885(1)	29(1)
C(36)	7202(3)	3636(1)	1371(1)	29(1)
C(10)	-4805(4)	7665(1)	4155(1)	33(1)
C(51)	-67(3)	5591(1)	2356(1)	28(1)

C(40)	10782(3)	3026(1)	3623(1)	32(1)
C(49)	592(3)	5548(1)	3063(1)	28(1)
C(53)	-2666(4)	6001(1)	1471(1)	36(1)
C(1)	-274(3)	9275(1)	1076(1)	29(1)
C(31)	6350(4)	3683(1)	733(1)	30(1)
C(2)	-1868(3)	8802(1)	1266(1)	30(1)
C(54)	-1109(4)	5631(1)	995(1)	34(1)
C(48)	-525(4)	6032(1)	3564(1)	32(1)
C(37)	9704(3)	3038(1)	2264(1)	28(1)
C(11)	-4014(4)	7766(1)	4786(1)	37(1)
C(38)	11847(3)	2660(1)	2482(1)	32(1)
C(39)	12339(4)	2649(1)	3151(1)	35(1)
C(46)	2111(4)	5434(1)	4381(1)	34(1)
C(6)	-6626(4)	7659(1)	2739(1)	34(1)
C(47)	229(4)	5972(1)	4205(1)	36(1)
C(5)	-7161(4)	7605(1)	2081(1)	36(1)
C(35)	9022(3)	3076(1)	1559(1)	29(1)
C(32)	7443(4)	3172(1)	247(1)	37(1)
C(34)	10077(4)	2570(1)	1062(1)	36(1)
C(33)	9310(4)	2627(1)	418(1)	40(1)

Table B.43: Bond lengths [Å] and angles [°] for **106**.

C(23)-C(28)	1.392(2)
C(23)-C(24)	1.399(2)
C(23)-C(21)	1.486(2)
C(16)-C(15)	1.206(3)
C(16)-C(17)	1.440(3)
C(21)-C(22)	1.398(3)
C(21)-C(20)	1.402(2)
C(26)-C(25)	1.384(3)
C(26)-C(27)	1.393(3)
C(26)-H(26)	0.9500
C(43)-C(44)	1.207(3)
C(43)-C(41)	1.439(3)
C(13)-C(14)	1.394(2)
C(13)-C(12)	1.399(3)
C(13)-C(15)	1.438(3)
C(44)-C(45)	1.442(3)
C(17)-C(22)	1.393(2)
C(17)-C(18)	1.398(3)
C(9)-C(14)	1.398(3)
C(9)-C(10)	1.404(3)
C(9)-C(7)	1.487(3)
C(3)-C(8)	1.392(2)
C(3)-C(4)	1.392(3)
C(3)-C(2)	1.443(3)
C(55)-C(56)	1.393(2)
C(55)-C(54)	1.395(3)
C(55)-C(29)	1.438(3)
C(41)-C(42)	1.393(2)
C(41)-C(40)	1.397(3)
C(22)-H(22)	0.9500
C(45)-C(50)	1.395(2)
C(45)-C(46)	1.395(3)
C(8)-C(7)	1.397(3)
C(8)-H(8)	0.9500
C(12)-C(11)	1.388(3)
C(12)-H(12)	0.9500
C(14)-H(14)	0.9500
C(20)-C(19)	1.385(2)

C(20)-H(20)	0.9500
C(56)-C(51)	1.389(3)
C(56)-H(56)	0.9500
C(30)-C(29)	1.209(3)
C(30)-C(31)	1.437(3)
C(25)-C(24)	1.384(3)
C(25)-H(25)	0.9500
C(50)-C(49)	1.396(2)
C(50)-H(50)	0.9500
C(19)-C(18)	1.394(3)
C(19)-H(19)	0.9500
C(7)-C(6)	1.406(3)
C(52)-C(53)	1.384(3)
C(52)-C(51)	1.404(3)
C(52)-H(52)	0.9500
C(24)-H(24)	0.9500
C(27)-C(28)	1.397(2)
C(27)-C(1)	1.441(3)
C(42)-C(37)	1.392(3)
C(42)-H(42)	0.9500
C(28)-H(28)	0.9500
C(4)-C(5)	1.395(3)
C(4)-H(4)	0.9500
C(18)-H(18)	0.9500
C(36)-C(31)	1.393(2)
C(36)-C(35)	1.395(3)
C(36)-H(36)	0.9500
C(10)-C(11)	1.384(3)
C(10)-H(10)	0.9500
C(51)-C(49)	1.489(3)
C(40)-C(39)	1.388(3)
C(40)-H(40)	0.9500
C(49)-C(48)	1.402(3)
C(53)-C(54)	1.388(3)
C(53)-H(53)	0.9500
C(1)-C(2)	1.204(3)
C(31)-C(32)	1.400(3)
C(54)-H(54)	0.9500
C(48)-C(47)	1.380(3)
C(48)-H(48)	0.9500
C(37)-C(38)	1.406(3)
C(37)-C(35)	1.489(3)

C(11)-H(11)	0.9500
C(38)-C(39)	1.390(3)
C(38)-H(38)	0.9500
C(39)-H(39)	0.9500
C(46)-C(47)	1.390(3)
C(46)-H(46)	0.9500
C(6)-C(5)	1.382(3)
C(6)-H(6)	0.9500
C(47)-H(47)	0.9500
C(5)-H(5)	0.9500
C(35)-C(34)	1.403(3)
C(32)-C(33)	1.389(3)
C(32)-H(32)	0.9500
C(34)-C(33)	1.387(3)
C(34)-H(34)	0.9500
C(33)-H(33)	0.9500

C(28)-C(23)-C(24)	117.01(18)
C(28)-C(23)-C(21)	119.05(15)
C(24)-C(23)-C(21)	123.93(16)
C(15)-C(16)-C(17)	159.3(2)
C(22)-C(21)-C(20)	116.76(17)
C(22)-C(21)-C(23)	119.18(15)
C(20)-C(21)-C(23)	124.05(16)
C(25)-C(26)-C(27)	118.98(18)
C(25)-C(26)-H(26)	120.5
C(27)-C(26)-H(26)	120.5
C(44)-C(43)-C(41)	159.9(2)
C(14)-C(13)-C(12)	118.85(17)
C(14)-C(13)-C(15)	113.75(16)
C(12)-C(13)-C(15)	127.37(19)
C(43)-C(44)-C(45)	160.5(2)
C(22)-C(17)-C(18)	119.25(17)
C(22)-C(17)-C(16)	113.71(15)
C(18)-C(17)-C(16)	126.96(18)
C(14)-C(9)-C(10)	116.68(19)
C(14)-C(9)-C(7)	119.13(16)
C(10)-C(9)-C(7)	124.19(16)
C(8)-C(3)-C(4)	118.98(18)
C(8)-C(3)-C(2)	113.69(15)
C(4)-C(3)-C(2)	127.23(19)
C(56)-C(55)-C(54)	119.04(18)

C(56)-C(55)-C(29)	113.60(16)
C(54)-C(55)-C(29)	127.2(2)
C(42)-C(41)-C(40)	118.85(18)
C(42)-C(41)-C(43)	114.08(15)
C(40)-C(41)-C(43)	126.99(19)
C(17)-C(22)-C(21)	123.05(16)
C(17)-C(22)-H(22)	118.5
C(21)-C(22)-H(22)	118.5
C(50)-C(45)-C(46)	118.84(17)
C(50)-C(45)-C(44)	113.34(15)
C(46)-C(45)-C(44)	127.81(18)
C(3)-C(8)-C(7)	123.25(16)
C(3)-C(8)-H(8)	118.4
C(7)-C(8)-H(8)	118.4
C(11)-C(12)-C(13)	118.8(2)
C(11)-C(12)-H(12)	120.6
C(13)-C(12)-H(12)	120.6
C(13)-C(14)-C(9)	123.08(16)
C(13)-C(14)-H(14)	118.5
C(9)-C(14)-H(14)	118.5
C(19)-C(20)-C(21)	120.57(17)
C(19)-C(20)-H(20)	119.7
C(21)-C(20)-H(20)	119.7
C(51)-C(56)-C(55)	123.21(16)
C(51)-C(56)-H(56)	118.4
C(55)-C(56)-H(56)	118.4
C(29)-C(30)-C(31)	160.1(2)
C(24)-C(25)-C(26)	121.68(17)
C(24)-C(25)-H(25)	119.2
C(26)-C(25)-H(25)	119.2
C(45)-C(50)-C(49)	123.07(16)
C(45)-C(50)-H(50)	118.5
C(49)-C(50)-H(50)	118.5
C(16)-C(15)-C(13)	160.9(2)
C(20)-C(19)-C(18)	122.10(17)
C(20)-C(19)-H(19)	119.0
C(18)-C(19)-H(19)	119.0
C(8)-C(7)-C(6)	116.51(19)
C(8)-C(7)-C(9)	119.43(15)
C(6)-C(7)-C(9)	124.06(17)
C(53)-C(52)-C(51)	120.39(19)
C(53)-C(52)-H(52)	119.8

C(51)-C(52)-H(52)	119.8
C(25)-C(24)-C(23)	120.64(17)
C(25)-C(24)-H(24)	119.7
C(23)-C(24)-H(24)	119.7
C(30)-C(29)-C(55)	160.4(2)
C(26)-C(27)-C(28)	118.81(16)
C(26)-C(27)-C(1)	127.50(18)
C(28)-C(27)-C(1)	113.66(16)
C(37)-C(42)-C(41)	123.33(17)
C(37)-C(42)-H(42)	118.3
C(41)-C(42)-H(42)	118.3
C(23)-C(28)-C(27)	122.82(16)
C(23)-C(28)-H(28)	118.6
C(27)-C(28)-H(28)	118.6
C(3)-C(4)-C(5)	118.8(2)
C(3)-C(4)-H(4)	120.6
C(5)-C(4)-H(4)	120.6
C(19)-C(18)-C(17)	118.18(18)
C(19)-C(18)-H(18)	120.9
C(17)-C(18)-H(18)	120.9
C(31)-C(36)-C(35)	123.19(17)
C(31)-C(36)-H(36)	118.4
C(35)-C(36)-H(36)	118.4
C(11)-C(10)-C(9)	120.77(17)
C(11)-C(10)-H(10)	119.6
C(9)-C(10)-H(10)	119.6
C(56)-C(51)-C(52)	116.82(18)
C(56)-C(51)-C(49)	119.27(15)
C(52)-C(51)-C(49)	123.91(17)
C(39)-C(40)-C(41)	118.80(19)
C(39)-C(40)-H(40)	120.6
C(41)-C(40)-H(40)	120.6
C(50)-C(49)-C(48)	116.72(18)
C(50)-C(49)-C(51)	119.16(16)
C(48)-C(49)-C(51)	124.12(16)
C(52)-C(53)-C(54)	122.07(17)
C(52)-C(53)-H(53)	119.0
C(54)-C(53)-H(53)	119.0
C(2)-C(1)-C(27)	160.8(2)
C(36)-C(31)-C(32)	118.72(17)
C(36)-C(31)-C(30)	113.90(16)
C(32)-C(31)-C(30)	127.37(19)

C(1)-C(2)-C(3)	159.2(2)
C(53)-C(54)-C(55)	118.4(2)
C(53)-C(54)-H(54)	120.8
C(55)-C(54)-H(54)	120.8
C(47)-C(48)-C(49)	120.76(17)
C(47)-C(48)-H(48)	119.6
C(49)-C(48)-H(48)	119.6
C(42)-C(37)-C(38)	116.72(19)
C(42)-C(37)-C(35)	119.04(15)
C(38)-C(37)-C(35)	124.24(17)
C(10)-C(11)-C(12)	121.79(18)
C(10)-C(11)-H(11)	119.1
C(12)-C(11)-H(11)	119.1
C(39)-C(38)-C(37)	120.54(18)
C(39)-C(38)-H(38)	119.7
C(37)-C(38)-H(38)	119.7
C(40)-C(39)-C(38)	121.68(17)
C(40)-C(39)-H(39)	119.2
C(38)-C(39)-H(39)	119.2
C(47)-C(46)-C(45)	118.72(19)
C(47)-C(46)-H(46)	120.6
C(45)-C(46)-H(46)	120.6
C(5)-C(6)-C(7)	120.81(19)
C(5)-C(6)-H(6)	119.6
C(7)-C(6)-H(6)	119.6
C(48)-C(47)-C(46)	121.84(17)
C(48)-C(47)-H(47)	119.1
C(46)-C(47)-H(47)	119.1
C(6)-C(5)-C(4)	121.59(17)
C(6)-C(5)-H(5)	119.2
C(4)-C(5)-H(5)	119.2
C(36)-C(35)-C(34)	116.72(19)
C(36)-C(35)-C(37)	119.13(16)
C(34)-C(35)-C(37)	124.14(17)
C(33)-C(32)-C(31)	119.1(2)
C(33)-C(32)-H(32)	120.5
C(31)-C(32)-H(32)	120.5
C(33)-C(34)-C(35)	120.95(18)
C(33)-C(34)-H(34)	119.5
C(35)-C(34)-H(34)	119.5
C(34)-C(33)-C(32)	121.25(18)
C(34)-C(33)-H(33)	119.4

C(32)-C(33)-H(33) 119.4

Table B.45: Anisotropic displacement parameters (Å^2 $\times 10^3$) for **106**. The anisotropic displacement factor exponent takes the form: $-2p^2[h^2a^{*2}U^{11} + ... + 2hka^*b^*U^{12}]$

Atom	U11	U22	U33	U23	U13	U12
C(23)	24(1)	23(1)	28(1)	-1(1)	0(1)	2(1)
C(16)	29(1)	31(1)	23(1)	-1(1)	-6(1)	5(1)
C(21)	24(1)	20(1)	30(1)	-2(1)	-2(1)	2(1)
C(26)	36(1)	32(1)	25(1)	-1(1)	-2(1)	5(1)
C(43)	32(1)	30(1)	27(1)	3(1)	-7(1)	-5(1)
C(13)	29(1)	25(1)	30(1)	1(1)	3(1)	5(1)
C(44)	35(1)	31(1)	23(1)	-1(1)	-5(1)	-6(1)
C(17)	28(1)	23(1)	29(1)	-2(1)	-5(1)	3(1)
C(9)	26(1)	23(1)	36(1)	1(1)	3(1)	2(1)
C(3)	27(1)	23(1)	39(1)	-5(1)	-6(1)	1(1)
C(55)	27(1)	29(1)	31(1)	6(1)	-6(1)	-4(1)
C(41)	27(1)	24(1)	34(1)	5(1)	-6(1)	-5(1)
C(22)	23(1)	24(1)	30(1)	-3(1)	-2(1)	-1(1)
C(45)	29(1)	25(1)	28(1)	-2(1)	0(1)	-6(1)
C(8)	23(1)	25(1)	37(1)	-3(1)	-4(1)	-1(1)
C(12)	37(1)	30(1)	33(1)	5(1)	3(1)	5(1)
C(14)	30(1)	24(1)	29(1)	1(1)	2(1)	2(1)
C(20)	25(1)	24(1)	35(1)	-1(1)	-1(1)	0(1)
C(56)	23(1)	30(1)	32(1)	6(1)	-5(1)	0(1)
C(30)	34(1)	38(1)	23(1)	0(1)	-3(1)	-8(1)
C(25)	36(1)	30(1)	31(1)	4(1)	7(1)	2(1)
C(50)	30(1)	25(1)	26(1)	-3(1)	1(1)	-2(1)
C(15)	32(1)	29(1)	24(1)	-1(1)	-2(1)	3(1)
C(19)	25(1)	26(1)	39(1)	-2(1)	-6(1)	1(1)
C(7)	24(1)	21(1)	39(1)	-1(1)	-1(1)	2(1)
C(52)	26(1)	24(1)	47(1)	1(1)	-5(1)	1(1)
C(24)	31(1)	26(1)	32(1)	1(1)	4(1)	1(1)
C(29)	30(1)	38(1)	24(1)	3(1)	-6(1)	-6(1)
C(27)	30(1)	26(1)	27(1)	-2(1)	-2(1)	4(1)
C(42)	25(1)	24(1)	34(1)	4(1)	-5(1)	-1(1)
C(28)	30(1)	24(1)	26(1)	1(1)	0(1)	1(1)
C(4)	32(1)	27(1)	44(1)	-8(1)	-12(1)	4(1)
C(18)	30(1)	27(1)	32(1)	-6(1)	-7(1)	3(1)
C(36)	28(1)	29(1)	29(1)	-2(1)	0(1)	-2(1)
C(10)	30(1)	24(1)	45(1)	4(1)	4(1)	-1(1)
C(51)	27(1)	22(1)	34(1)	3(1)	-2(1)	-4(1)
C(40)	31(1)	26(1)	41(1)	7(1)	-12(1)	-4(1)

C(49)	27(1)	21(1)	35(1)	1(1)	0(1)	-4(1)
C(53)	30(1)	27(1)	52(1)	4(1)	-13(1)	1(1)
C(1)	33(1)	31(1)	24(1)	-3(1)	-6(1)	3(1)
C(31)	31(1)	30(1)	29(1)	-1(1)	2(1)	-6(1)
C(2)	32(1)	31(1)	29(1)	-3(1)	-9(1)	3(1)
C(54)	34(1)	31(1)	37(1)	8(1)	-12(1)	-3(1)
C(48)	30(1)	26(1)	40(1)	-3(1)	5(1)	-1(1)
C(37)	25(1)	22(1)	38(1)	1(1)	-2(1)	-3(1)
C(11)	38(1)	30(1)	41(1)	9(1)	8(1)	3(1)
C(38)	26(1)	23(1)	48(1)	2(1)	-1(1)	0(1)
C(39)	27(1)	25(1)	54(1)	7(1)	-10(1)	-1(1)
C(46)	41(1)	33(1)	28(1)	-5(1)	-1(1)	-7(1)
C(6)	24(1)	24(1)	53(1)	-1(1)	-1(1)	-1(1)
C(47)	37(1)	31(1)	40(1)	-9(1)	7(1)	-3(1)
C(5)	25(1)	26(1)	58(2)	-5(1)	-9(1)	-2(1)
C(35)	25(1)	25(1)	37(1)	-2(1)	3(1)	-4(1)
C(32)	39(1)	40(1)	31(1)	-5(1)	2(1)	-8(1)
C(34)	32(1)	30(1)	44(1)	-2(1)	7(1)	-1(1)
C(33)	42(1)	36(1)	40(1)	-8(1)	11(1)	-5(1)

Table B.47: Single crystal data and structure refinement for **121•tBuOH**.

Identification code	CCDC 1873211	
Empirical formula	$C_{49}H_{69}MoNO_4$	
Formula weight	831.99	
Temperature	100(2) K	
Wavelength	0.71073 Å	
Crystal system	Monoclinic	
Space group	P 21/c	
Unit cell dimensions	a = 15.9057(6) Å	$\alpha = 90°$
	b = 15.2617(5) Å	$\beta = 93.394(2)°$
	c = 19.1797(7) Å	$\gamma = 90°$
Volume	4647.7(3) $Å^3$	
Z	4	
Density (calculated)	1.189 Mg/m^3	
Absorption coefficient	0.323 mm^{-1}	
F(000)	1776	
Crystal size	0.100 x 0.080 x 0.060 mm^3	
Theta range for data collection	1.282 to 25.422°	
Index ranges	$-19 \leq h \leq 19$, $-18 \leq k \leq 18$, $-23 \leq l \leq 23$	
Reflections collected	147663	
Independent reflections	8575 [R(int) = 0.0376]	
Completeness to theta = 25.000°	100.0 %	
Refinement method	Full-matrix least-squares on F^2	
Data / restraints / parameters	8575 / 18 / 552	
Goodness-of-fit on F^2	1.077	
Final R indices [$I>2\sigma(I)$]	R1 = 0.0382, wR2 = 0.0907	
R indices (all data)	R1 = 0.0450, wR2 = 0.0965	
Extinction coefficient	n/a	
Largest diff. peak and hole	0.991 and –0.529 $e^- Å^{-3}$	

Table B.48: Atomic coordinates ($\times 10^4$) and equivalent isotropic displacement parameters (Å^2 $\times 10^3$) for **121•tBuOH**. U(eq) is defined as one third of the trace of the orthogonalized U^{ij} tensor.

Atom	x	y	z	U(eq)
C(1)	7511(1)	5523(2)	4971(1)	24(1)
C(2)	7761(1)	5256(2)	4288(1)	25(1)
C(3)	7591(2)	5795(2)	3707(1)	36(1)
C(4)	7870(2)	5565(2)	3061(1)	40(1)
C(5)	8314(2)	4803(2)	2963(1)	35(1)
C(6)	8479(2)	4261(2)	3539(1)	30(1)
C(7)	8212(1)	4481(2)	4193(1)	27(1)
C(8)	8629(2)	4572(2)	2257(1)	47(1)
C(9)	7731(1)	3965(2)	5984(1)	24(1)
C(10)	8429(1)	3389(2)	6092(1)	26(1)
C(11)	8410(2)	2613(2)	5710(1)	29(1)
C(12)	7743(2)	2369(2)	5243(1)	28(1)
C(13)	7054(2)	2916(2)	5185(1)	26(1)
C(14)	7015(1)	3701(2)	5568(1)	23(1)
C(15)	6193(1)	4141(1)	5625(1)	22(1)
C(16)	5461(2)	3644(2)	5519(1)	25(1)
C(17)	4688(2)	3998(2)	5647(1)	25(1)
C(18)	4654(1)	4837(2)	5904(1)	25(1)
C(19)	5396(1)	5324(2)	6008(1)	23(1)
C(20)	5325(1)	6225(2)	6278(1)	25(1)
C(21)	4724(2)	6389(2)	6763(1)	28(1)
C(22)	4545(2)	7227(2)	6979(1)	32(1)
C(23)	4958(2)	7909(2)	6660(1)	31(1)
C(24)	5572(2)	7791(2)	6179(1)	28(1)
C(25)	5798(1)	6921(2)	6021(1)	24(1)
C(26)	9162(2)	3609(2)	6620(1)	31(1)
C(27)	9578(2)	4475(2)	6429(2)	36(1)
C(28)	8826(2)	3676(2)	7354(1)	38(1)
C(29)	9848(2)	2903(2)	6645(2)	39(1)
C(30)	7787(2)	1512(2)	4827(1)	33(1)
C(34)	3928(2)	7372(2)	7557(2)	41(1)
C(35)	3088(2)	6902(3)	7355(2)	69(1)
C(36)	4311(2)	6988(2)	8241(2)	50(1)
C(37)	3738(2)	8339(2)	7662(2)	43(1)
C(38)	6006(2)	8579(2)	5857(1)	33(1)
C(39)	5974(2)	8500(2)	5055(1)	41(1)

C(40)	5588(2)	9453(2)	6031(2)	48(1)
C(41)	6921(2)	8609(2)	6156(2)	39(1)
C(42)	8861(2)	7092(2)	5668(1)	33(1)
C(43)	8477(2)	7566(2)	5028(2)	42(1)
C(44)	9507(2)	6433(2)	5448(2)	40(1)
C(45)	9249(2)	7745(2)	6198(2)	54(1)
C(46)	7213(2)	6284(2)	7741(2)	48(1)
N(1)	6154(1)	4989(1)	5845(1)	22(1)
O(1)	7733(1)	4755(1)	6297(1)	24(1)
O(2)	6424(1)	6736(1)	5604(1)	23(1)
O(3)	8214(1)	6647(1)	6027(1)	27(1)
Mo(1)	7314(1)	5835(1)	5824(1)	22(1)
C(31)	8449(3)	1592(2)	4292(2)	50(1)
C(32)	7995(3)	745(2)	5321(2)	47(1)
C(33)	6924(2)	1280(2)	4442(2)	48(1)
C(31A)	8659(9)	976(9)	5044(8)	36(4)
C(32A)	7102(10)	971(11)	5009(9)	47(4)
C(33A)	7846(10)	1766(10)	4060(8)	39(4)
C(47)	8029(5)	6203(7)	8137(4)	76(2)
C(48)	6650(3)	5482(3)	7809(2)	48(1)
C(49)	6692(4)	7081(3)	7995(3)	62(2)
O(4)	7280(2)	6413(2)	7014(1)	37(1)
C(47A)	8284(12)	6092(15)	7882(8)	62(5)
C(48A)	6854(14)	5927(10)	8314(8)	102(7)
C(49A)	7214(15)	7190(9)	7599(8)	99(7)
O(4A)	7082(5)	5804(6)	7100(4)	44(2)

Table B.50: Bond lengths [Å] and angles [°] for **121•tBuOH**.

C(1)-C(2)	1.450(3)
C(1)-Mo(1)	1.749(2)
C(2)-C(3)	1.398(3)
C(2)-C(7)	1.401(3)
C(3)-C(4)	1.386(4)
C(3)-H(3)	0.9500
C(4)-C(5)	1.379(4)
C(4)-H(4)	0.9500
C(5)-C(6)	1.392(4)
C(5)-C(8)	1.513(4)
C(6)-C(7)	1.390(3)
C(6)-H(6)	0.9500
C(7)-H(7)	0.9500
C(8)-H(8A)	0.9800
C(8)-H(8B)	0.9800
C(8)-H(8C)	0.9800
C(8)-H(8D)	0.9800
C(8)-H(8E)	0.9800
C(8)-H(8F)	0.9800
C(9)-O(1)	1.347(3)
C(9)-C(14)	1.410(3)
C(9)-C(10)	1.421(3)
C(10)-C(11)	1.391(3)
C(10)-C(26)	1.537(3)
C(11)-C(12)	1.399(4)
C(11)-H(11)	0.9500
C(12)-C(13)	1.377(3)
C(12)-C(30)	1.535(3)
C(13)-C(14)	1.409(3)
C(13)-H(13)	0.9500
C(14)-C(15)	1.480(3)
C(15)-N(1)	1.365(3)
C(15)-C(16)	1.394(3)
C(16)-C(17)	1.378(3)
C(16)-H(16)	0.9500
C(17)-C(18)	1.375(3)
C(17)-H(17)	0.9500
C(18)-C(19)	1.397(3)

C(18)-H(18)	0.9500
C(19)-N(1)	1.363(3)
C(19)-C(20)	1.476(3)
C(20)-C(21)	1.396(3)
C(20)-C(25)	1.408(3)
C(21)-C(22)	1.380(4)
C(21)-H(21)	0.9500
C(22)-C(23)	1.392(4)
C(22)-C(34)	1.540(3)
C(23)-C(24)	1.394(3)
C(23)-H(23)	0.9500
C(24)-C(25)	1.413(3)
C(24)-C(38)	1.534(3)
C(25)-O(2)	1.344(3)
C(26)-C(29)	1.532(4)
C(26)-C(27)	1.532(4)
C(26)-C(28)	1.538(4)
C(27)-H(27A)	0.9800
C(27)-H(27B)	0.9800
C(27)-H(27C)	0.9800
C(28)-H(28A)	0.9800
C(28)-H(28B)	0.9800
C(28)-H(28C)	0.9800
C(29)-H(29A)	0.9800
C(29)-H(29B)	0.9800
C(29)-H(29C)	0.9800
C(30)-C(32A)	1.425(16)
C(30)-C(31)	1.517(4)
C(30)-C(33A)	1.528(15)
C(30)-C(32)	1.530(4)
C(30)-C(33)	1.559(4)
C(30)-C(31A)	1.643(14)
C(34)-C(37)	1.522(4)
C(34)-C(36)	1.531(4)
C(34)-C(35)	1.545(4)
C(35)-H(35A)	0.9800
C(35)-H(35B)	0.9800
C(35)-H(35C)	0.9800
C(36)-H(36A)	0.9800
C(36)-H(36B)	0.9800
C(36)-H(36C)	0.9800

C(37)-H(37A)	0.9800
C(37)-H(37B)	0.9800
C(37)-H(37C)	0.9800
C(38)-C(41)	1.533(4)
C(38)-C(40)	1.535(4)
C(38)-C(39)	1.542(4)
C(39)-H(39A)	0.9800
C(39)-H(39B)	0.9800
C(39)-H(39C)	0.9800
C(40)-H(40A)	0.9800
C(40)-H(40B)	0.9800
C(40)-H(40C)	0.9800
C(41)-H(41A)	0.9800
C(41)-H(41B)	0.9800
C(41)-H(41C)	0.9800
C(42)-O(3)	1.442(3)
C(42)-C(44)	1.514(4)
C(42)-C(43)	1.521(4)
C(42)-C(45)	1.528(4)
C(43)-H(43A)	0.9800
C(43)-H(43B)	0.9800
C(43)-H(43C)	0.9800
C(44)-H(44A)	0.9800
C(44)-H(44B)	0.9800
C(44)-H(44C)	0.9800
C(45)-H(45A)	0.9800
C(45)-H(45B)	0.9800
C(45)-H(45C)	0.9800
C(46)-C(48A)	1.381(15)
C(46)-C(49A)	1.408(14)
C(46)-O(4)	1.417(4)
C(46)-O(4A)	1.437(8)
C(46)-C(47)	1.470(9)
C(46)-C(48)	1.528(5)
C(46)-C(49)	1.565(6)
C(46)-C(47A)	1.73(2)
N(1)-Mo(1)	2.2548(19)
O(1)-Mo(1)	1.9773(16)
O(2)-Mo(1)	2.0005(16)
O(3)-Mo(1)	1.9157(15)
Mo(1)-O(4)	2.452(3)

Mo(1)-O(4A)	2.496(7)
C(31)-H(31A)	0.9800
C(31)-H(31B)	0.9800
C(31)-H(31C)	0.9800
C(32)-H(32A)	0.9800
C(32)-H(32B)	0.9800
C(32)-H(32C)	0.9800
C(33)-H(33A)	0.9800
C(33)-H(33B)	0.9800
C(33)-H(33C)	0.9800
C(31A)-H(31D)	0.9800
C(31A)-H(31E)	0.9800
C(31A)-H(31F)	0.9800
C(32A)-H(32D)	0.9800
C(32A)-H(32E)	0.9800
C(32A)-H(32F)	0.9800
C(33A)-H(33D)	0.9800
C(33A)-H(33E)	0.9800
C(33A)-H(33F)	0.9800
C(47)-H(47A)	0.9800
C(47)-H(47B)	0.9800
C(47)-H(47C)	0.9800
C(48)-H(48A)	0.9800
C(48)-H(48B)	0.9800
C(48)-H(48C)	0.9800
C(49)-H(49A)	0.9800
C(49)-H(49B)	0.9800
C(49)-H(49C)	0.9800
O(4)-H(4A)	1.13(5)
C(47A)-H(47D)	0.9800
C(47A)-H(47E)	0.9800
C(47A)-H(47F)	0.9800
C(48A)-H(48D)	0.9800
C(48A)-H(48E)	0.9800
C(48A)-H(48F)	0.9800
C(49A)-H(49D)	0.9800
C(49A)-H(49E)	0.9800
C(49A)-H(49F)	0.9800
O(4A)-H(4A1)	1.27(11)
C(2)-C(1)-Mo(1)	174.34(18)

C(3)-C(2)-C(7)	118.0(2)
C(3)-C(2)-C(1)	120.3(2)
C(7)-C(2)-C(1)	121.6(2)
C(4)-C(3)-C(2)	120.4(2)
C(4)-C(3)-H(3)	119.8
C(2)-C(3)-H(3)	119.8
C(5)-C(4)-C(3)	121.9(2)
C(5)-C(4)-H(4)	119.0
C(3)-C(4)-H(4)	119.0
C(4)-C(5)-C(6)	117.9(2)
C(4)-C(5)-C(8)	121.2(3)
C(6)-C(5)-C(8)	121.0(3)
C(7)-C(6)-C(5)	121.3(2)
C(7)-C(6)-H(6)	119.4
C(5)-C(6)-H(6)	119.4
C(6)-C(7)-C(2)	120.5(2)
C(6)-C(7)-H(7)	119.8
C(2)-C(7)-H(7)	119.8
C(5)-C(8)-H(8A)	109.5
C(5)-C(8)-H(8B)	109.5
H(8A)-C(8)-H(8B)	109.5
C(5)-C(8)-H(8C)	109.5
H(8A)-C(8)-H(8C)	109.5
H(8B)-C(8)-H(8C)	109.5
C(5)-C(8)-H(8D)	109.5
H(8A)-C(8)-H(8D)	141.1
H(8B)-C(8)-H(8D)	56.3
H(8C)-C(8)-H(8D)	56.3
C(5)-C(8)-H(8E)	109.5
H(8A)-C(8)-H(8E)	56.3
H(8B)-C(8)-H(8E)	141.1
H(8C)-C(8)-H(8E)	56.3
H(8D)-C(8)-H(8E)	109.5
C(5)-C(8)-H(8F)	109.5
H(8A)-C(8)-H(8F)	56.3
H(8B)-C(8)-H(8F)	56.3
H(8C)-C(8)-H(8F)	141.1
H(8D)-C(8)-H(8F)	109.5
H(8E)-C(8)-H(8F)	109.5
O(1)-C(9)-C(14)	119.2(2)
O(1)-C(9)-C(10)	120.6(2)

C(14)-C(9)-C(10)	120.2(2)
C(11)-C(10)-C(9)	117.2(2)
C(11)-C(10)-C(26)	121.7(2)
C(9)-C(10)-C(26)	121.1(2)
C(10)-C(11)-C(12)	123.8(2)
C(10)-C(11)-H(11)	118.1
C(12)-C(11)-H(11)	118.1
C(13)-C(12)-C(11)	117.3(2)
C(13)-C(12)-C(30)	122.4(2)
C(11)-C(12)-C(30)	120.3(2)
C(12)-C(13)-C(14)	122.2(2)
C(12)-C(13)-H(13)	118.9
C(14)-C(13)-H(13)	118.9
C(13)-C(14)-C(9)	118.6(2)
C(13)-C(14)-C(15)	119.3(2)
C(9)-C(14)-C(15)	121.1(2)
N(1)-C(15)-C(16)	120.5(2)
N(1)-C(15)-C(14)	120.6(2)
C(16)-C(15)-C(14)	118.5(2)
C(17)-C(16)-C(15)	120.5(2)
C(17)-C(16)-H(16)	119.7
C(15)-C(16)-H(16)	119.7
C(18)-C(17)-C(16)	118.9(2)
C(18)-C(17)-H(17)	120.6
C(16)-C(17)-H(17)	120.6
C(17)-C(18)-C(19)	119.7(2)
C(17)-C(18)-H(18)	120.1
C(19)-C(18)-H(18)	120.1
N(1)-C(19)-C(18)	121.3(2)
N(1)-C(19)-C(20)	121.1(2)
C(18)-C(19)-C(20)	117.6(2)
C(21)-C(20)-C(25)	120.0(2)
C(21)-C(20)-C(19)	118.0(2)
C(25)-C(20)-C(19)	121.8(2)
C(22)-C(21)-C(20)	121.8(2)
C(22)-C(21)-H(21)	119.1
C(20)-C(21)-H(21)	119.1
C(21)-C(22)-C(23)	116.8(2)
C(21)-C(22)-C(34)	120.0(2)
C(23)-C(22)-C(34)	123.2(2)
C(22)-C(23)-C(24)	124.2(2)

C(22)-C(23)-H(23)	117.9
C(24)-C(23)-H(23)	117.9
C(23)-C(24)-C(25)	117.4(2)
C(23)-C(24)-C(38)	120.9(2)
C(25)-C(24)-C(38)	121.6(2)
O(2)-C(25)-C(20)	118.7(2)
O(2)-C(25)-C(24)	122.1(2)
C(20)-C(25)-C(24)	119.1(2)
C(29)-C(26)-C(27)	107.3(2)
C(29)-C(26)-C(10)	112.2(2)
C(27)-C(26)-C(10)	110.6(2)
C(29)-C(26)-C(28)	107.7(2)
C(27)-C(26)-C(28)	109.9(2)
C(10)-C(26)-C(28)	109.1(2)
C(26)-C(27)-H(27A)	109.5
C(26)-C(27)-H(27B)	109.5
H(27A)-C(27)-H(27B)	109.5
C(26)-C(27)-H(27C)	109.5
H(27A)-C(27)-H(27C)	109.5
H(27B)-C(27)-H(27C)	109.5
C(26)-C(28)-H(28A)	109.5
C(26)-C(28)-H(28B)	109.5
H(28A)-C(28)-H(28B)	109.5
C(26)-C(28)-H(28C)	109.5
H(28A)-C(28)-H(28C)	109.5
H(28B)-C(28)-H(28C)	109.5
C(26)-C(29)-H(29A)	109.5
C(26)-C(29)-H(29B)	109.5
H(29A)-C(29)-H(29B)	109.5
C(26)-C(29)-H(29C)	109.5
H(29A)-C(29)-H(29C)	109.5
H(29B)-C(29)-H(29C)	109.5
C(32A)-C(30)-C(33A)	118.3(9)
C(31)-C(30)-C(32)	110.3(3)
C(32A)-C(30)-C(12)	107.9(7)
C(31)-C(30)-C(12)	109.7(2)
C(33A)-C(30)-C(12)	106.9(6)
C(32)-C(30)-C(12)	110.2(2)
C(31)-C(30)-C(33)	108.9(3)
C(32)-C(30)-C(33)	105.8(3)
C(12)-C(30)-C(33)	111.9(2)

C(32A)-C(30)-C(31A)	107.2(9)
C(33A)-C(30)-C(31A)	105.7(8)
C(12)-C(30)-C(31A)	110.8(5)
C(37)-C(34)-C(36)	109.3(2)
C(37)-C(34)-C(22)	112.0(2)
C(36)-C(34)-C(22)	108.9(2)
C(37)-C(34)-C(35)	108.0(3)
C(36)-C(34)-C(35)	109.3(3)
C(22)-C(34)-C(35)	109.4(2)
C(34)-C(35)-H(35A)	109.5
C(34)-C(35)-H(35B)	109.5
H(35A)-C(35)-H(35B)	109.5
C(34)-C(35)-H(35C)	109.5
H(35A)-C(35)-H(35C)	109.5
H(35B)-C(35)-H(35C)	109.5
C(34)-C(36)-H(36A)	109.5
C(34)-C(36)-H(36B)	109.5
H(36A)-C(36)-H(36B)	109.5
C(34)-C(36)-H(36C)	109.5
H(36A)-C(36)-H(36C)	109.5
H(36B)-C(36)-H(36C)	109.5
C(34)-C(37)-H(37A)	109.5
C(34)-C(37)-H(37B)	109.5
H(37A)-C(37)-H(37B)	109.5
C(34)-C(37)-H(37C)	109.5
H(37A)-C(37)-H(37C)	109.5
H(37B)-C(37)-H(37C)	109.5
C(41)-C(38)-C(24)	108.2(2)
C(41)-C(38)-C(40)	107.9(2)
C(24)-C(38)-C(40)	112.5(2)
C(41)-C(38)-C(39)	110.5(2)
C(24)-C(38)-C(39)	110.6(2)
C(40)-C(38)-C(39)	107.2(2)
C(38)-C(39)-H(39A)	109.5
C(38)-C(39)-H(39B)	109.5
H(39A)-C(39)-H(39B)	109.5
C(38)-C(39)-H(39C)	109.5
H(39A)-C(39)-H(39C)	109.5
H(39B)-C(39)-H(39C)	109.5
C(38)-C(40)-H(40A)	109.5
C(38)-C(40)-H(40B)	109.5

H(40A)-C(40)-H(40B)	109.5
C(38)-C(40)-H(40C)	109.5
H(40A)-C(40)-H(40C)	109.5
H(40B)-C(40)-H(40C)	109.5
C(38)-C(41)-H(41A)	109.5
C(38)-C(41)-H(41B)	109.5
H(41A)-C(41)-H(41B)	109.5
C(38)-C(41)-H(41C)	109.5
H(41A)-C(41)-H(41C)	109.5
H(41B)-C(41)-H(41C)	109.5
O(3)-C(42)-C(44)	109.6(2)
O(3)-C(42)-C(43)	110.2(2)
C(44)-C(42)-C(43)	109.8(2)
O(3)-C(42)-C(45)	105.1(2)
C(44)-C(42)-C(45)	111.4(2)
C(43)-C(42)-C(45)	110.7(2)
C(42)-C(43)-H(43A)	109.5
C(42)-C(43)-H(43B)	109.5
H(43A)-C(43)-H(43B)	109.5
C(42)-C(43)-H(43C)	109.5
H(43A)-C(43)-H(43C)	109.5
H(43B)-C(43)-H(43C)	109.5
C(42)-C(44)-H(44A)	109.5
C(42)-C(44)-H(44B)	109.5
H(44A)-C(44)-H(44B)	109.5
C(42)-C(44)-H(44C)	109.5
H(44A)-C(44)-H(44C)	109.5
H(44B)-C(44)-H(44C)	109.5
C(42)-C(45)-H(45A)	109.5
C(42)-C(45)-H(45B)	109.5
H(45A)-C(45)-H(45B)	109.5
C(42)-C(45)-H(45C)	109.5
H(45A)-C(45)-H(45C)	109.5
H(45B)-C(45)-H(45C)	109.5
C(48A)-C(46)-C(49A)	123.1(11)
C(48A)-C(46)-O(4A)	115.7(7)
C(49A)-C(46)-O(4A)	109.7(7)
O(4)-C(46)-C(47)	113.9(4)
O(4)-C(46)-C(48)	105.9(3)
C(47)-C(46)-C(48)	113.1(5)
O(4)-C(46)-C(49)	105.7(3)

C(47)-C(46)-C(49)	111.9(5)
C(48)-C(46)-C(49)	105.7(4)
C(48A)-C(46)-C(47A)	105.0(11)
C(49A)-C(46)-C(47A)	100.6(12)
O(4A)-C(46)-C(47A)	98.0(6)
C(19)-N(1)-C(15)	118.90(19)
C(19)-N(1)-Mo(1)	121.75(15)
C(15)-N(1)-Mo(1)	119.06(15)
C(9)-O(1)-Mo(1)	123.44(13)
C(25)-O(2)-Mo(1)	124.01(14)
C(42)-O(3)-Mo(1)	138.84(15)
C(1)-Mo(1)-O(3)	101.17(9)
C(1)-Mo(1)-O(1)	97.31(9)
O(3)-Mo(1)-O(1)	102.63(7)
C(1)-Mo(1)-O(2)	98.87(9)
O(3)-Mo(1)-O(2)	96.29(7)
O(1)-Mo(1)-O(2)	152.14(6)
C(1)-Mo(1)-N(1)	93.00(9)
O(3)-Mo(1)-N(1)	165.77(7)
O(1)-Mo(1)-N(1)	76.59(6)
O(2)-Mo(1)-N(1)	80.06(7)
C(1)-Mo(1)-O(4)	169.72(10)
O(3)-Mo(1)-O(4)	68.62(9)
O(1)-Mo(1)-O(4)	84.13(9)
O(2)-Mo(1)-O(4)	83.95(8)
N(1)-Mo(1)-O(4)	97.24(9)
C(1)-Mo(1)-O(4A)	162.9(2)
O(3)-Mo(1)-O(4A)	87.99(19)
O(1)-Mo(1)-O(4A)	66.41(19)
O(2)-Mo(1)-O(4A)	94.34(18)
N(1)-Mo(1)-O(4A)	78.64(19)
C(30)-C(31)-H(31A)	109.5
C(30)-C(31)-H(31B)	109.5
H(31A)-C(31)-H(31B)	109.5
C(30)-C(31)-H(31C)	109.5
H(31A)-C(31)-H(31C)	109.5
H(31B)-C(31)-H(31C)	109.5
C(30)-C(32)-H(32A)	109.5
C(30)-C(32)-H(32B)	109.5
H(32A)-C(32)-H(32B)	109.5
C(30)-C(32)-H(32C)	109.5

H(32A)-C(32)-H(32C)	109.5
H(32B)-C(32)-H(32C)	109.5
C(30)-C(33)-H(33A)	109.5
C(30)-C(33)-H(33B)	109.5
H(33A)-C(33)-H(33B)	109.5
C(30)-C(33)-H(33C)	109.5
H(33A)-C(33)-H(33C)	109.5
H(33B)-C(33)-H(33C)	109.5
C(30)-C(31A)-H(31D)	109.5
C(30)-C(31A)-H(31E)	109.5
H(31D)-C(31A)-H(31E)	109.5
C(30)-C(31A)-H(31F)	109.5
H(31D)-C(31A)-H(31F)	109.5
H(31E)-C(31A)-H(31F)	109.5
C(30)-C(32A)-H(32D)	109.5
C(30)-C(32A)-H(32E)	109.5
H(32D)-C(32A)-H(32E)	109.5
C(30)-C(32A)-H(32F)	109.5
H(32D)-C(32A)-H(32F)	109.5
H(32E)-C(32A)-H(32F)	109.5
C(30)-C(33A)-H(33D)	109.5
C(30)-C(33A)-H(33E)	109.5
H(33D)-C(33A)-H(33E)	109.5
C(30)-C(33A)-H(33F)	109.5
H(33D)-C(33A)-H(33F)	109.5
H(33E)-C(33A)-H(33F)	109.5
C(46)-C(47)-H(47A)	109.5
C(46)-C(47)-H(47B)	109.5
H(47A)-C(47)-H(47B)	109.5
C(46)-C(47)-H(47C)	109.5
H(47A)-C(47)-H(47C)	109.5
H(47B)-C(47)-H(47C)	109.5
C(46)-C(48)-H(48A)	109.5
C(46)-C(48)-H(48B)	109.5
H(48A)-C(48)-H(48B)	109.5
C(46)-C(48)-H(48C)	109.5
H(48A)-C(48)-H(48C)	109.5
H(48B)-C(48)-H(48C)	109.5
C(46)-C(49)-H(49A)	109.5
C(46)-C(49)-H(49B)	109.5
H(49A)-C(49)-H(49B)	109.5

C(46)-C(49)-H(49C)	109.5
H(49A)-C(49)-H(49C)	109.5
H(49B)-C(49)-H(49C)	109.5
C(46)-O(4)-Mo(1)	150.8(2)
C(46)-O(4)-H(4A)	112(2)
Mo(1)-O(4)-H(4A)	84(2)
C(46)-C(47A)-H(47D)	109.5
C(46)-C(47A)-H(47E)	109.5
H(47D)-C(47A)-H(47E)	109.5
C(46)-C(47A)-H(47F)	109.5
H(47D)-C(47A)-H(47F)	109.5
H(47E)-C(47A)-H(47F)	109.5
C(46)-C(48A)-H(48D)	109.5
C(46)-C(48A)-H(48E)	109.5
H(48D)-C(48A)-H(48E)	109.5
C(46)-C(48A)-H(48F)	109.5
H(48D)-C(48A)-H(48F)	109.5
H(48E)-C(48A)-H(48F)	109.5
C(46)-C(49A)-H(49D)	109.5
C(46)-C(49A)-H(49E)	109.5
H(49D)-C(49A)-H(49E)	109.5
C(46)-C(49A)-H(49F)	109.5
H(49D)-C(49A)-H(49F)	109.5
H(49E)-C(49A)-H(49F)	109.5
C(46)-O(4A)-Mo(1)	143.8(5)
C(46)-O(4A)-H(4A1)	123(5)
Mo(1)-O(4A)-H(4A1)	80(5)

Table B.52: Anisotropic displacement parameters (Å^2 $\times 10^3$) for **121•tBuOH**. The anisotropic displacement factor exponent takes the form: $-2p^2[h^2a^{*2}U^{11} + ... + 2hka^*b^*U^{12}]$

Atom	U11	U22	U33	U23	U13	U12
C(1)	24(1)	23(1)	26(1)	4(1)	0(1)	-2(1)
C(2)	24(1)	30(1)	21(1)	-1(1)	2(1)	-2(1)
C(3)	40(1)	42(2)	26(1)	5(1)	2(1)	11(1)
C(4)	45(2)	57(2)	19(1)	9(1)	3(1)	7(1)
C(5)	31(1)	49(2)	24(1)	-7(1)	4(1)	-7(1)
C(6)	27(1)	33(1)	29(1)	-7(1)	6(1)	-3(1)
C(7)	27(1)	29(1)	24(1)	1(1)	2(1)	-4(1)
C(8)	50(2)	65(2)	27(1)	-10(1)	10(1)	-6(2)
C(9)	28(1)	27(1)	17(1)	2(1)	4(1)	-4(1)
C(10)	24(1)	31(1)	23(1)	7(1)	3(1)	-4(1)
C(11)	30(1)	29(1)	29(1)	6(1)	7(1)	2(1)
C(12)	36(1)	25(1)	24(1)	2(1)	8(1)	-3(1)
C(13)	31(1)	26(1)	21(1)	1(1)	3(1)	-5(1)
C(14)	29(1)	23(1)	19(1)	4(1)	3(1)	-4(1)
C(15)	28(1)	24(1)	13(1)	2(1)	-1(1)	-2(1)
C(16)	31(1)	24(1)	20(1)	0(1)	-2(1)	-4(1)
C(17)	28(1)	28(1)	19(1)	2(1)	-3(1)	-6(1)
C(18)	25(1)	29(1)	21(1)	0(1)	0(1)	-2(1)
C(19)	28(1)	26(1)	16(1)	1(1)	0(1)	-3(1)
C(20)	27(1)	27(1)	20(1)	-5(1)	0(1)	-4(1)
C(21)	30(1)	32(1)	23(1)	-5(1)	3(1)	-7(1)
C(22)	30(1)	39(1)	26(1)	-12(1)	3(1)	-4(1)
C(23)	34(1)	29(1)	30(1)	-11(1)	1(1)	0(1)
C(24)	31(1)	27(1)	24(1)	-4(1)	-2(1)	-2(1)
C(25)	25(1)	29(1)	17(1)	-4(1)	-2(1)	-3(1)
C(26)	26(1)	37(1)	30(1)	7(1)	0(1)	-2(1)
C(27)	27(1)	40(2)	41(2)	5(1)	-1(1)	-7(1)
C(28)	36(1)	53(2)	26(1)	6(1)	-4(1)	-3(1)
C(29)	32(1)	44(2)	41(2)	8(1)	-2(1)	1(1)
C(30)	39(1)	27(1)	33(1)	-2(1)	7(1)	1(1)
C(34)	40(2)	46(2)	38(2)	-17(1)	14(1)	-7(1)
C(35)	43(2)	84(3)	83(3)	-45(2)	34(2)	-22(2)
C(36)	80(2)	38(2)	34(2)	-6(1)	29(2)	-2(2)
C(37)	43(2)	54(2)	32(1)	-14(1)	8(1)	5(1)
C(38)	42(1)	24(1)	33(1)	-2(1)	4(1)	0(1)
C(39)	60(2)	30(1)	33(2)	6(1)	4(1)	2(1)

C(40)	62(2)	27(1)	58(2)	-4(1)	16(2)	2(1)
C(41)	45(2)	31(1)	42(2)	-4(1)	4(1)	-11(1)
C(42)	32(1)	32(1)	36(1)	1(1)	6(1)	-10(1)
C(43)	43(2)	39(2)	44(2)	10(1)	12(1)	-4(1)
C(44)	32(1)	43(2)	46(2)	10(1)	10(1)	-5(1)
C(45)	50(2)	56(2)	56(2)	-12(2)	8(2)	-29(2)
C(46)	77(2)	41(2)	26(1)	-1(1)	-6(1)	-10(2)
N(1)	28(1)	22(1)	16(1)	1(1)	-2(1)	-2(1)
O(1)	26(1)	27(1)	19(1)	1(1)	0(1)	-5(1)
O(2)	27(1)	22(1)	19(1)	-2(1)	2(1)	-2(1)
O(3)	28(1)	29(1)	24(1)	0(1)	2(1)	-7(1)
Mo(1)	25(1)	23(1)	18(1)	0(1)	2(1)	-4(1)
C(31)	63(3)	40(2)	48(2)	-9(2)	25(2)	-4(2)
C(32)	66(3)	29(2)	47(2)	-2(2)	3(2)	-3(2)
C(33)	49(2)	38(2)	56(2)	-23(2)	-5(2)	2(2)
C(47)	71(5)	102(6)	52(5)	-6(4)	-10(4)	-22(4)
C(48)	62(3)	45(2)	38(2)	5(2)	4(2)	-8(2)
C(49)	101(4)	52(3)	36(3)	-8(2)	24(3)	-7(3)
O(4)	43(2)	38(2)	29(1)	-3(1)	4(1)	-9(1)
C(47A)	63(11)	93(10)	29(8)	-22(8)	-10(6)	-11(9)
C(48A)	180(20)	69(10)	53(9)	-12(7)	22(10)	-27(11)
C(49A)	190(20)	41(7)	61(10)	-8(7)	-29(11)	11(10)
O(4A)	48(4)	43(5)	39(4)	0(3)	1(3)	-4(4)

Bibliography

(1) Pennella, F.; Banks, R. L.; Bailey, G. C. *Chem. Commun. (London)* **1968**, 1548–1549.

(2) Mortreux, A.; Blanchard, M. *Bull. Soc. Chim. Fr.* **1972**, 1641.

(3) Mortreux, A.; Blanchard, M. *J. Chem. Soc., Chem. Commun.* **1974**, 786–787.

(4) Mortreux, A.; Petit, F.; Blanchard, M. *Tetrahedron Lett.* **1978**, *19*, 4967–4968.

(5) Woodward, R. B.; Hoffmann, R. *Angew. Chem. Int. Ed. Engl.* **1969**, *8*, 781–853.

(6) Mortreux, A.; Delgrange, J. C.; Blanchard, M.; Lubochinsky, B. *J. Mol. Catal.* **1977**, *2*, 73–82.

(7) Mortreux, A.; Dy, N.; Blanchard, M. *J. Mol. Catal.* **1976**, *1*, 101–109.

(8) Fischer, E. O.; Kreis, G.; Kreiter, C. G.; Mülle, J.; Huttner, G.; Lorenz, H. *Angew. Chem.* **1973**, *85*, 618–620.

(9) Katz, T. J.; McGinnis, J. *J. Am. Chem. Soc.* **1975**, *97*, 1592–1594.

(10) Devarajan, S.; Walton, D. R. M.; Leigh, G. J. *J. Organomet. Chem.* **1979**, *181*, 99–104.

(11) Fritch, J. R.; Vollhardt, K. P. C. *Angew. Chem. Int. Ed. Engl.* **1979**, *18*, 409–411.

(12) Wengrovius, J. H.; Sancho, J.; Schrock, R. R. *J. Am. Chem. Soc.* **1981**, *103*, 3932–3934.

(13) Clark, D. N.; Schrock, R. R. *J. Am. Chem. Soc.* **1978**, *100*, 6774–6776.

(14) McCullough, L. G.; Schrock, R. R. *J. Am. Chem. Soc.* **1984**, *106*, 4067–4068.

(15) Strutz, H.; Schrock, R. R. *Organometallics* **1984**, *3*, 1600–1601.

(16) Schrock, R. R.; Listemann, M. L.; Sturgeoff, L. G. *J. Am. Chem. Soc.* **1982**, *104*, 4291–4293.

(17) Listemann, M. L.; Schrock, R. R. *Organometallics* **1985**, *4*, 74–83.

(18) Latham, I. A.; Sita, L. R.; Schrock, R. R. *Organometallics* **1986**, *5*, 1508–1510.

(19) Edwards, D. S.; Schrock, R. R. *J. Am. Chem. Soc.* **1982**, *104*, 6806–6808.

(20) Edwards, D. S.; Biondi, L. V.; Zillen, J. W.; Churchill, M. R.; Schrock, R. R. *Organometallics* **1983**, *2*, 1505–1513.

(21) Toreki, R.; Schrock, R. R.; Davis, W. M. *J. Am. Chem. Soc.* **1992**, *114*, 3367–3380.

(22) Williams, D. S.; Schrock, R. R. *Organometallics* **1994**, *13*, 2101–2104.

(23) LaPointe, A. M.; Schrock, R. R. *Organometallics* **1995**, *14*, 1875–1884.

(24) Freudenberger, J. H.; Schrock, R. R.; Churchill, M. R.; Rheingold, A. L.; Ziller, J. W. *Organometallics* **1984**, *3*, 1563–1573.

(25) Sancho, J.; Schrock, R. R. *J. Mol. Catal.* **1982**, *15*, 75–79.

(26) Murdzek, J. S.; Blum, L.; Schrock, R. R. *Organometallics* **1988**, *7*, 436–441.

(27) Schrock, R. R.; Pedersen, S. F.; Churchill, M. R.; Ziller, J. W. *Organometallics* **1984**, *3*, 1574–1583.

(28) Schrock, R. R.; Murdzek, J. S.; Freudenberger, J. H.; Churchill, M. R.; Ziller, J. W. *Organometallics* **1986**, *5*, 25–33.

(29) McCullough, L. G.; Schrock, R. R.; Dewan, J. C.; Murdzek, J. C. *J. Am. Chem. Soc.* **1985**, *107*, 5987–5998.

(30) McCullough, L. G.; Listemann, M. L.; Schrock, R. R.; Churchill, M. R.; Ziller, J. W. *J. Am. Chem. Soc.* **1983**, *105*, 6729–6730.

(31) Freudenberger, J. H.; Schrock, R. R. *Organometallics* **1986**, *5*, 1411–1417.

(32) Chisholm, M. H.; Folting, K.; Huffman, J. C.; Rothwell, I. P. *J. Am. Chem. Soc.* **1982**, *104*, 4389–4399.

(33) Chisholm, M. H.; Folting, K.; Hoffman, D. M.; Huffman, J. C. *J. Am. Chem. Soc.* **1984**, *106*, 6794–6805.

(34) Churchill, M. R.; Ziller, J. W.; Pedersen, S. F.; Schrock, R. R. *J. Chem. Soc., Chem. Commun.* **1984**, 485–486.

(35) Pedersen, S. F.; Schrock, R. R.; Churchill, M. R.; Wasserman, H. J. *J. Am. Chem. Soc.* **1982**, *104*, 6808–6809.

(36) Churchill, M. R.; Ziller, J. W.; McCullough, L.; Pedersen, S. F.; Schrock, R. R. *Organometallics* **1983**, *2*, 1046–1048.

(37) Churchill, M. R.; Ziller, J. W.; Freudenberger, J. H.; Schrock, R. R. *Organometallics* **1984**, *3*, 1554–1562.

(38) Krouse, S. A.; Schrock, R. R. *Macromolecules* **1989**, *22*, 2569–2576.

(39) Bittner, C.; Ehrhorn, H.; Bockfeld, D.; Brandhorst, K.; Tamm, M. *Organometallics* **2017**, *36*, 3398–3406.

(40) Strutz, H.; Dewan, J. C.; Schrock, R. R. *J. Am. Chem. Soc.* **1985**, *107*, 5999–6005.

(41) Schrock, R. R.; Weinstock, I. A.; Horton, A. D.; Liu, A. H.; Schofield, M. H. *J. Am. Chem. Soc.* **1988**, *110*, 2686–2687.

(42) Weinstock, I. A.; Schrock, R. R.; Davis, W. M. *J. Am. Chem. Soc.* **1991**, *113*, 135–144.

(43) Fürstner, A.; Seidel, G. *Angew. Chem. Int. Ed.* **1998**, *37*, 1734–1736.

(44) Weiss, K.; Michel, A.; Auth, E.-M.; Bunz, U. H. F.; Mangel, T.; Müllen, K. *Angew. Chem. Int. Ed. Engl.* **1997**, *36*, 506–509.

(45) Fürstner, A.; Davies, P. W. *Chem. Commun.* **2005**, 2307–2320.

(46) Bunz, U. H. F. *Acc. Chem. Res.* **2001**, *34*, 998–1010.

(47) Tsai, Y.-C.; Johnson, M. J. A.; Mindiola, D. J.; Cummins, C. C.; Klooster, W. T.; Koetzle, T. F. *J. Am. Chem. Soc.* **1999**, *121*, 10426–10427.

(48) Tsai, Y.-C.; Diaconescu, P. L.; Cummins, C. C. *Organometallics* **2000**, *19*, 5260–5262.

(49) Blackwell, J. M.; Figueroa, J. S.; Stephens, F. H.; Cummins, C. C. *Organometallics* **2003**, *22*, 3351–3353.

(50) Laplaza, C. E.; Johnson, M. J. A.; Peters, J. C.; Odom, A. L.; Kim, E.; Cummins, C. C.; George, G. N.; Pickering, I. J. *J. Am. Chem. Soc.* **1996**, *118*, 8623–8638.

(51) Fürstner, A.; Mathes, C.; Lehmann, C. W. *J. Am. Chem. Soc.* **1999**, *121*, 9453–9454.

(52) Fürstner, A.; Mathes, C.; Lehmann, C. W. *Chem. Eur. J.* **2001**, *7*, 5299–5317.

(53) Schrock, R. R. *Acc. Chem. Res.* **1986**, *19*, 342–348.

(54) Zhang, W.; Kraft, S.; S. Moore, J. *Chem. Commun.* **2003**, 832–833.

(55) Zhang, W.; Kraft, S.; Moore, J. S. *J. Am. Chem. Soc.* **2004**, *126*, 329–335.

(56) Jyothish, K.; Zhang, W. *Angew. Chem. Int. Ed.* **2011**, *50*, 3435–3438.

(57) Schaubach, S.; Gebauer, K.; Ungeheuer, F.; Hoffmeister, L.; Ilg, M. K.; Wirtz, C.; Fürstner, A. *Chem. Eur. J.* **2016**, *22*, 8494–8507.

(58) Jyothish, K.; Wang, Q.; Zhang, W. *Adv. Synth. Catal.* **2012**, *354*, 2073–2078.

(59) Yang, H.; Liu, Z.; Zhang, W. *Adv. Synth. Catal.* **2013**, *355*, 885–890.

(60) Gdula, R. L.; Johnson, M. J. A. *J. Am. Chem. Soc.* **2006**, *128*, 9614–9615.

(61) Geyer, A. M.; Wiedner, E. S.; Gary, J. B.; Gdula, R. L.; Kuhlmann, N. C.; Johnson, M. J. A.; Dunietz, B. D.; Kampf, J. W. *J. Am. Chem. Soc.* **2008**, *130*, 8984–8999.

(62) Finke, A. D.; Moore, J. S. *Chem. Commun.* **2010**, *46*, 7939–7941.

(63) Geyer, A. M.; Holland, M. J.; Gdula, R. L.; Goodman, J. E.; Johnson, M. J. A.; Kampf, J. W. *J. Organomet. Chem.* **2012**, *708–709*, 1–9.

(64) Geyer, A. M.; Gdula, R. L.; Wiedner, E. S.; Johnson, M. J. A. *J. Am. Chem. Soc.* **2007**, *129*, 3800–3801.

(65) Bindl, M.; Stade, R.; Heilmann, E. K.; Picot, A.; Goddard, R.; Fürstner, A. *J. Am. Chem. Soc.* **2009**, *131*, 9468–9470.

(66) Beer, S.; Hrib, C. G.; Jones, P. G.; Brandhorst, K.; Grunenberg, J.; Tamm, M. *Angew. Chem. Int. Ed.* **2007**, *46*, 8890–8894.

(67) Beer, S.; Brandhorst, K.; Hrib, C. G.; Wu, X.; Haberlag, B.; Grunenberg, J.; Jones, P. G.; Tamm, M. *Organometallics* **2009**, *28*, 1534–1545.

(68) Mayr, A.; McDermott, G. A. *J. Am. Chem. Soc.* **1986**, *108*, 548–549.

(69) McDermott, G. A.; Dorries, A. M.; Mayr, A. *Organometallics* **1987**, *6*, 925–931.

(70) Heppekausen, J.; Stade, R.; Kondoh, A.; Seidel, G.; Goddard, R.; Fürstner, A. *Chem. Eur. J.* **2012**, *18*, 10281–10299.

(71) Krouse, S. A.; Schrock, R. R.; Cohen, R. E. *Macromolecules* **1987**, *20*, 903–904.

(72) Jacobson, H.; Stockmayer, W. H. *J. Chem. Phys.* **1950**, *18*, 1600–1606.

(73) Carnes, M.; Buccella, D.; Siegrist, T.; Steigerwald, M. L.; Nuckolls, C. *J. Am. Chem. Soc.* **2008**, *130*, 14078–14079.

(74) Lysenko, S.; Haberlag, B.; Wu, X.; Tamm, M. *Macromol. Symp.* **2010**, *293*, 20–23.

(75) Zhang, W.; Moore, J. S. *J. Am. Chem. Soc.* **2005**, *127*, 11863–11870.

(76) Miljanić, O. Š.; Vollhardt, K. P. C.; Whitener, G. D. *Synlett* **2003**, *2003*, 0029–0034.

(77) Lhermet, R.; Fürstner, A. *Chem. Eur. J.* **2014**, *20*, 13188–13193.

(78) Fischer, F. R.; Nuckolls, C. *Angew. Chem. Int. Ed.* **2010**, *49*, 7257–7260.

(79) Sedbrook, D. F.; Paley, D. W.; Steigerwald, M. L.; Nuckolls, C.; Fischer, F. R. *Macromolecules* **2012**, *45*, 5040–5044.

(80) Bunz, U. H. F. *Chem. Rev.* **2000**, *100*, 1605–1644.

(81) Bunz, U. H. F. *Macromol. Rapid Commun.* **2009**, *30*, 772–805.

(82) Weder, C.; Blankenburg, L.; Bunz, U. H. F.; Klemm, E.; Moore, J.; Pautzsch, T.; Ray, C. R.; Swager, T. M.; Voskerician, G.; Weder, C.; Yamaguchi, I.; Yamamoto, T.; Yasuda, T.; Zheng, J., *Poly(Arylene Ethynylene)s: From Synthesis to Application.* OCLC: 858881947; Springer London, Limited: Guildford, 2010.

(83) Lahiri, S.; Thompson, J. L.; Moore, J. S. *J. Am. Chem. Soc.* **2000**, *122*, 11315–11319.

(84) Blatchly, R. A.; Tew, G. N. *J. Org. Chem.* **2003**, *68*, 8780–8785.

(85) Lee, O.-S.; Saven, J. G. *J. Phys. Chem. B* **2004**, *108*, 11988–11994.

(86) Jones, T. V.; Slutsky, M. M.; Laos, R.; de Greef, T. F. A.; Tew, G. N. *J. Am. Chem. Soc.* **2005**, *127*, 17235–17240.

(87) Jones, T. V.; Slutsky, M. M.; Tew, G. N. *New J. Chem.* **2008**, *32*, 676–679.

(88) Stone, M. T.; Moore, J. S. *Org. Lett.* **2004**, *6*, 469–472.

(89) Khan, A.; Hecht, S. *J. Polym. Sci. A Polym. Chem.* **2006**, *44*, 1619–1627.

(90) Bellone, D. E.; Bours, J.; Menke, E. H.; Fischer, F. R. *J. Am. Chem. Soc.* **2015**, *137*, 850–856.

(91) Kawase, T.; Nishiyama, Y.; Nakamura, T.; Ebi, T.; Matsumoto, K.; Kurata, H.; Oda, M. *Angew. Chem. Int. Ed.* **2007**, *46*, 1086–1088.

(92) Kawase, T.; Darabi, H. R.; Oda, M. *Angew. Chem. Int. Ed. Engl.* **1996**, *35*, 2664–2666.

(93) Kawase, T.; Ueda, N.; Oda, M. *Tetrahedron Lett.* **1997**, *38*, 6681–6684.

(94) Wong, H. N. C.; Garratt, P. J.; Sondheimer, F. *J. Am. Chem. Soc.* **1974**, *96*, 5604–5605.

(95) Chaffins, S.; Brettreich, M.; Wudl, F. *Synthesis* **2002**, *2002*, 1191–1194.

(96) Orita, A.; Hasegawa, D.; Nakano, T.; Otera, J. *Chem. Eur. J.* **2002**, *8*, 2000–2004.

(97) Zhang, X.-X.; Lippard, S. J. *J. Org. Chem.* **2000**, *65*, 5298–5305.

(98) Müller, M.; Iyer, V. S.; Kübel, C.; Enkelmann, V.; Müllen, K. *Angew. Chem. Int. Ed. Engl.* **1997**, *36*, 1607–1610.

(99) Schrock, R. R.; Jamieson, J. Y.; Araujo, J. P.; Bonitatebus Jr., P. J.; Sinha, A.; Lopez, L. P. H. *J. Organomet. Chem.* **2003**, *684*, 56–67.

(100) Walborsky, E. C.; Wigley, D. E.; Roland, E.; Dewan, J. C.; Schrock, R. R. *Inorg. Chem.* **1987**, *26*, 1615–1621.

(101) Stoebenau, E. J.; Jordan, R. F. *J. Am. Chem. Soc.* **2004**, *126*, 11170–11171.

(102) Stoebenau, E. J.; Jordan, R. F. *J. Am. Chem. Soc.* **2006**, *128*, 8638–8650.

(103) Solooki, D.; Ferrara, J. D.; Malaba, D.; Bradshaw, J. D.; Tessier, C. A.; Youngs, W. J.; John, J. A.; Tour, J. M. In *Inorganic Syntheses*, Cowley, A. H., Ed.; John Wiley & Sons, Inc.: 1996, pp 122–128.

(104) Solooki, D.; Bradshaw, J. D.; Tessier, C. A.; Youngs, W. J.; See, R. F.; Churchill, M.; Ferrara, J. D. *J. Organomet. Chem.* **1994**, *470*, 231–236.

(105) Baldwin, K. P.; Bradshaw, J. D.; Tessier, C. A.; Youngs, W. J. *Synlett* **1993**, 853–855.

(106) Drew, M. G. B.; Brisdon, B. J.; Day, A. *J. Chem. Soc., Dalton Trans.* **1981**, 1310–1316.

(107) Bielawski, C. W.; Grubbs, R. H. *Prog. Polym. Sci.* **2007**, *32*, 1–29.

(108) Schrock, R. R. *Acc. Chem. Res.* **2014**, *47*, 2457–2466.

(109) Crowe, W. E.; Mitchell, J. P.; Gibson, V. C.; Schrock, R. R. *Macromolecules* **1990**, *23*, 3534–3536.

(110) Ulman, M.; Grubbs, R. H. *Organometallics* **1998**, *17*, 2484–2489.

(111) Love, J. A.; Morgan, J. P.; Trnka, T. M.; Grubbs, R. H. *Angew. Chem. Int. Ed. Engl.* **2002**, *41*, 4035–4037.

(112) Romero, P. E.; Piers, W. E.; McDonald, R. *Angew. Chem. Int. Ed.* **2004**, *43*, 6161–6165.

(113) Xia, Y.; Olsen, B. D.; Kornfield, J. A.; Grubbs, R. H. *J. Am. Chem. Soc.* **2009**, *131*, 18525–18532.

(114) Elling, B. R.; Xia, Y. *J. Am. Chem. Soc.* **2015**, *137*, 9922–9926.

(115) Hilf, S.; Kilbinger, A. F. M. *Nat. Chem.* **2009**, *1*, 537–546.

(116) Jeong, H.; John, J. M.; Schrock, R. R.; Hoveyda, A. H. *J. Am. Chem. Soc.* **2015**, *137*, 2239–2242.

(117) Chen, P. *Acc. Chem. Res.* **2016**, *49*, 1052–1060.

(118) Schwab, P.; Grubbs, R. H.; Ziller, J. W. *J. Am. Chem. Soc.* **1996**, *118*, 100–110.

(119) Lane, D. R.; Beavers, C. M.; Olmstead, M. M.; Schore, N. E. *Organometallics* **2009**, *28*, 6789–6797.

(120) Walsh, D. J.; Lau, S. H.; Hyatt, M. G.; Guironnet, D. *J. Am. Chem. Soc.* **2017**, *139*, 13644–13647.

(121) Nagarkar, A. A.; Yasir, M.; Crochet, A.; Fromm, K. M.; Kilbinger, A. F. M. *Angew. Chem. Int. Ed.* **2016**, *55*, 12343–12346.

(122) Zhang, T.; Fu, L.; Gutekunst, W. R. *Macromolecules* **2018**, *51*, 6497–6503.

(123) Chu, L.; Qing, F.-L. *J. Am. Chem. Soc.* **2010**, *132*, 7262–7263.

(124) Reed, A. E.; Weinstock, R. B.; Weinhold, F. *J. Chem. Phys.* **1985**, *83*, 735–746.

(125) Tang, W.; Kwak, Y.; Braunecker, W.; Tsarevsky, N. V.; Coote, M. L.; Matyjaszewski, K. *J. Am. Chem. Soc.* **2008**, *130*, 10702–10713.

(126) Wang, Y.; Zhang, Y.; Parker, B.; Matyjaszewski, K. *Macromolecules* **2011**, *44*, 4022–4025.

(127) Wang, X.-Y.; Narita, A.; Müllen, K. *Nat. Rev. Chem.* **2018**, *2*, 0100.

(128) Müllen, K. In *Hierarchical Macromolecular Structures: 60 Years after the Staudinger Nobel Prize II*, Percec, V., Ed.; Advances in Polymer Science 262; Springer International Publishing: 2013, pp 61–92.

(129) Yang, L.; Park, C.-H.; Son, Y.-W.; Cohen, M. L.; Louie, S. G. *Phys. Rev. Lett.* **2007**, *99*, 186801.

(130) Chen, Y.-C.; de Oteyza, D. G.; Pedramrazi, Z.; Chen, C.; Fischer, F. R.; Crommie, M. F. *ACS Nano* **2013**, *7*, 6123–6128.

(131) Chen, Z.; Wang, H. I.; Bilbao, N.; Teyssandier, J.; Prechtl, T.; Cavani, N.; Tries, A.; Biagi, R.; De Renzi, V.; Feng, X.; Kläui, M.; De Feyter, S.; Bonn, M.; Narita, A.; Müllen, K. *J. Am. Chem. Soc.* **2017**, *139*, 9483–9486.

(132) Bronner, C.; Stremlau, S.; Gille, M.; Brauße, F.; Haase, A.; Hecht, S.; Tegeder, P. *Angew. Chem. Int. Ed.* **2013**, *52*, 4422–4425.

(133) Vo, T. H.; Shekhirev, M.; Kunkel, D. A.; Orange, F.; Guinel, M. J.-F.; Enders, A.; Sinitskii, A. *Chem. Commun.* **2014**, *50*, 4172–4174.

(134) Cloke, R. R.; Marangoni, T.; Nguyen, G. D.; Joshi, T.; Rizzo, D. J.; Bronner, C.; Cao, T.; Louie, S. G.; Crommie, M. F.; Fischer, F. R. *J. Am. Chem. Soc.* **2015**, *137*, 8872–8875.

(135) Durr, R. A.; Haberer, D.; Lee, Y.-L.; Blackwell, R.; Kalayjian, A. M.; Marangoni, T.; Ihm, J.; Louie, S. G.; Fischer, F. R. *J. Am. Chem. Soc.* **2018**, *140*, 807–813.

(136) Ruffieux, P.; Wang, S.; Yang, B.; Sánchez-Sánchez, C.; Liu, J.; Dienel, T.; Talirz, L.; Shinde, P.; Pignedoli, C. A.; Passerone, D.; Dumslaff, T.; Feng, X.; Müllen, K.; Fasel, R. *Nature* **2016**, *531*, 489–492.

(137) De Oteyza, D. G.; García-Lekue, A.; Vilas-Varela, M.; Merino-Díez, N.; Carbonell-Sanromà, E.; Corso, M.; Vasseur, G.; Rogero, C.; Guitián, E.; Pascual, J. I.; Ortega, J. E.; Wakayama, Y.; Peña, D. *ACS Nano* **2016**, *10*, 9000–9008.

(138) Rizzo, D. J.; Veber, G.; Cao, T.; Bronner, C.; Chen, T.; Zhao, F.; Rodriguez, H.; Louie, S. G.; Crommie, M. F.; Fischer, F. R. *Nature* **2018**, *560*, 204–208.

(139) Gröning, O.; Wang, S.; Yao, X.; Pignedoli, C. A.; Barin, G. B.; Daniels, C.; Cupo, A.; Meunier, V.; Feng, X.; Narita, A.; Müllen, K.; Ruffieux, P.; Fasel, R. *Nature* **2018**, *560*, 209–213.

(140) Talirz, L.; Ruffieux, P.; Fasel, R. *Advanced Materials* **2016**, *28*, 6222–6231.

(141) Narita, A. et al. *Nat. Chem.* **2014**, *6*, 126–132.

(142) Goldhaber-Gordon, D.; Montemerlo, M. S.; Love, J. C.; Opiteck, G. J.; Ellenbogen, J. C. *Proc. IEEE* **1997**, *85*, 521–540.

(143) Zhao, P.; Chauhan, J.; Guo, J. *Nano Lett.* **2009**, *9*, 684–688.

(144) Nguyen, G. D. et al. *Nature Nanotechnol.* **2017**, *12*, 1077–1082.

(145) Bronner, C.; Durr, R. A.; Rizzo, D. J.; Lee, Y.-L.; Marangoni, T.; Kalayjian, A. M.; Rodriguez, H.; Zhao, W.; Louie, S. G.; Fischer, F. R.; Crommie, M. F. *ACS Nano* **2018**, *12*, 2193–2200.

(146) Shekhirev, M.; Sinitskii, A. In *Chemistry of Carbon Nanostructures*; De Gruyter: Berlin, Boston, 2017, pp 194–225.

(147) Bielawski, C. W.; Benitez, D.; Grubbs, R. H. *Science* **2002**, *297*, 2041–2044.

(148) Wright, D. B.; Touve, M. A.; Adamiak, L.; Gianneschi, N. C. *ACS Macro Lett.* **2017**, *6*, 925–929.

(149) Boyd, T. J.; Schrock, R. R. *Macromolecules* **1999**, *32*, 6608–6618.

(150) Meier, S.; Reisinger, H.; Haag, R.; Mecking, S.; Mülhaupt, R.; Stelzer, F. *Chem. Commun.* **2001**, 855–856.

(151) Van Hensbergen, J. A.; Burford, R. P.; Lowe, A. B. *J. Polym. Sci. A Polym. Chem.* **2012**, *51*, 487–492.

(152) Jordan, R. S.; Wang, Y.; McCurdy, R. D.; Yeung, M. T.; Marsh, K. L.; Khan, S. I.; Kaner, R. B.; Rubin, Y. *Chem* **2016**, *1*, 78–90.

(153) Jordan, R. S.; Li, Y. L.; Lin, C.-W.; McCurdy, R. D.; Lin, J. B.; Brosmer, J. L.; Marsh, K. L.; Khan, S. I.; Houk, K. N.; Kaner, R. B.; Rubin, Y. *J. Am. Chem. Soc.* **2017**, *139*, 15878–15890.

(154) Hein, S. J.; Lehnherr, D.; Arslan, H.; J. Uribe-Romo, F.; Dichtel, W. R. *Acc. Chem. Res.* **2017**, *50*, 2776–2788.

(155) Hou, I. C.-Y.; Hu, Y.; Narita, A.; Müllen, K. *Polym. J.* **2018**, *50*, 3–20.

(156) Alabugin, I. V.; Gonzalez-Rodriguez, E. *Acc. Chem. Res.* **2018**, *51*, 1206–1219.

(157) Utsumi, K.; Kawase, T.; Oda, M. *Chem. Lett.* **2003**, *32*, 412–413.

(158) Nasielski, J.; Hadei, N.; Achonduh, G.; Kantchev, E. A. B.; O'Brien, C. J.; Lough, A.; Organ, M. G. *Chem. Eur. J.* **2010**, *16*, 10844–10853.

(159) Agapie, T.; Henling, L. M.; DiPasquale, A. G.; Rheingold, A. L.; Bercaw, J. E. *Organometallics* **2008**, *27*, 6245–6256.

(160) Schrauzer, G. N.; Hughes, L. A.; Strampach, N. *Z. Naturforsch. B* **2014**, *37*, 380–385.

(161) Jeong, H.; von Kugelgen, S.; Bellone, D.; Fischer, F. R. *J. Am. Chem. Soc.* **2017**, *139*, 15509–15514.

(162) Àrias, Ò.; Brandhorst, K.; Baabe, D.; Freytag, M.; Jones, P. G.; Tamm, M. *Dalton Trans.* **2017**, *46*, 4737–4748.

(163) Nielsen, K. T.; Bechgaard, K.; Krebs, F. C. *Macromolecules* **2005**, *38*, 658–659.

(164) Sedláček, J.; Sokol, J.; Zedník, J.; Faukner, T.; Kubů, M.; Brus, J.; Trhlíková, O. *Macromol. Rapid Commun.* **2017**, *39*, 1700518.

(165) Vo, T. H.; Shekhirev, M.; Kunkel, D. A.; Morton, M. D.; Berglund, E.; Kong, L.; Wilson, P. M.; Dowben, P. A.; Enders, A.; Sinitskii, A. *Nat. Commun.* **2014**, *5*, 3189.

(166) Katritzky, A. R.; Abdel-Fattah, A. A. A.; Wang, M. *J. Org. Chem.* **2003**, *68*, 1443–1446.

(167) Akoka, S.; Barantin, L.; Trierweiler, M. *Anal. Chem.* **1999**, *71*, 2554–2557.

(168) Lakowicz, J. R., *Principles of Fluorescence Spectroscopy (2nd) Second Edition*, First Printing edition; Kluwer Acacemic Publishers: 1999.

(169) Chai, J.-D.; Head-Gordon, M. *Phys. Chem. Chem. Phys.* **2008**, *10*, 6615–6620.

(170) Frisch, M. J. et al. Gaussian 09, Revision D.01., Wallingford CT: Gaussian, Inc., 2016.

(171) Dilworth, J. R.; Richards, R. L.; Chen, G. J.-J.; Mcdonald, J. W. In *Inorganic Syntheses*; John Wiley & Sons, Ltd: 2007, pp 33–43.

(172) Haberlag, B.; Freytag, M.; Daniliuc, C. G.; Jones, P. G.; Tamm, M. *Angew. Chem. Int. Ed.* **2012**, *51*, 13019–13022.

(173) Cloke, R. R. Synthesis of Doped Graphene Nanoribbons from Molecular and Polymeric Precursors., Ph.D. United States – California: University of California, Berkeley, 2015, 226 pp.

(174) Chuentragool, P.; Vongnam, K.; Rashatasakhon, P.; Sukwattanasinitt, M.; Wacharasindhu, S. *Tetrahedron* **2011**, *67*, 8177–8182.

(175) Sundholm, E. G. *Tetrahedron* **1977**, *33*, 991–994.

(176) Ogawa, T.; Ohta, K.; Iijima, T.; Suzuki, T.; Ohta, S.; Endo, Y. *Bioorganic & Medicinal Chemistry* **2009**, *17*, 1109–1117.

(177) Snégaroff, K.; Komagawa, S.; Chevallier, F.; Gros, P. C.; Golhen, S.; Roisnel, T.; Uchiyama, M.; Mongin, F. *Chem. Eur. J.* **2010**, *16*, 8191–8201.

(178) Belardi, B.; O'Donoghue, G. P.; Smith, A. W.; Groves, J. T.; Bertozzi, C. R. *J. Am. Chem. Soc.* **2012**, *134*, 9549–9552.

(179) Slocum, D. W.; Tekin, K. C.; Nguyen, Q.; Whitley, P. E.; Reinscheld, T. K.; Fouzia, B. *Tetrahedron Letters* **2011**, *52*, 7141–7145.

(180) Monnereau, C.; Blart, E.; Odobel, F. *Tetrahedron Lett.* **2005**, *46*, 5421–5423.

(181) Zhou, Z.-L.; Keana, J. F. W. *J. Org. Chem.* **1999**, *64*, 3763–3766.

(182) Tresse, C.; Guissart, C.; Schweizer, S.; Bouhoute, Y.; Chany, A.-C.; Goddard, M.-L.; Blanchard, N.; Evano, G. *Adv. Synth. Catal.* **2014**, *356*, 2051–2060.

(183) Kobayashi, Y.; Yamashita, T.; Takahashi, K.; Kuroda, H.; Kumadaki, I. *Tetrahedron Lett.* **1982**, *23*, 343–344.

(184) Konno, T.; Chae, J.; Kanda, M.; Nagai, G.; Tamura, K.; Ishihara, T.; Yamanaka, H. *Tetrahedron* **2003**, *59*, 7571–7580.

(185) Benoit, D.; Chaplinski, V.; Braslau, R.; Hawker, C. J. *J. Am. Chem. Soc.* **1999**, *121*, 3904–3920.

(186) Holton, R. A.; Crouse, D. J.; Williams, A. D.; Kennedy, R. M. *J. Org. Chem.* **1987**, *52*, 2317–2318.

(187) Orita, A.; An, D. L.; Nakano, T.; Yaruva, J.; Ma, N.; Otera, J. *Chem. Eur. J.* **2002**, *8*, 2005–2010.

(188) Gröber, S.; Görls, H.; Weigand, W. *European Journal of Inorganic Chemistry* **2015**, *2015*, 149–155.

(189) Klet, R. C.; VanderVelde, D. G.; Labinger, J. A.; Bercaw, J. E. *Chem. Commun.* **2012**, *48*, 6657–6659.

(190) Morri, A. K.; Thummala, Y.; Doddi, V. R. *Org. Lett.* **2015**, *17*, 4640–4643.

(191) Mueller-Westerhoff, U. T.; Zhou, M. *J. Org. Chem.* **1994**, *59*, 4988–4992.

(192) Ito, S.; Wehmeier, M.; Brand, J. D.; Kübel, C.; Epsch, R.; Rabe, J. P.; Müllen, K. *Chem. Eur. J.* **2000**, *6*, 4327–4342.

(193) *Organic Syntheses* **1992**, *70*, 246.

(194) Tikhomirov, D. A.; Eremeev, A. V. *Chem Heterocycl Compd* **1987**, *23*, 30–34.

(195) Jonathan, P. H.; Fukushima, T.; Kin, T.; Ogawa, A.; Aida, T. (Japan Science & Technology Agency). Amphipathic Hexa-Peri-Hexabenzocoronene Derivative. pat., JP4005571, CIB: B82B1/00; C07C43/205; (IPC1-7): B82B1/00; C07C43/205, 2007.

(196) Thompson, W. J.; Gaudino, J. *J. Org. Chem.* **1984**, *49*, 5237–5243.

(197) Hemel, J. V.; Esmans, E. L.; Alderweireldt, F. C.; Dommisse, R. A.; Groot, A. D.; Balzarini, J.; Clercq, E. D. *Nucleosides and Nucleotides* **1994**, *13*, 2345–2366.

(198) Felpin, F.-X.; Bertrand, M.-J.; Lebreton, J. *Tetrahedron* **2002**, *58*, 7381–7389.